2012

Challenges in the Discovery and Characterization of Magnetic Intermetallics

William A. Phelan
Louisiana State University and Agricultural and Mechanical College

CHALLENGES IN THE DISCOVERY AND CHARACTERIZATION OF MAGNETIC INTERMETALLICS

A Dissertation

Submitted to the Graduate Faculty of the
Louisiana State University and
Agricultural and Mechanical College
In partial fulfillment of the
Requirements for the degree of
Doctor of Philosophy

in

The Department of Chemistry

by
William Adam Phelan
B.S., University of Central Arkansas, 2007
May 2012

Dedication

To Caitlin for always giving me better than what I thought was the best, To Jaxsen for all those late nights, To my brother for giving me the best advice I have ever received, To my father who always jokingly offers a helping hand, To my mother who finally understood the purpose of my research, To Roy and Cheryl for always providing motivation, To Giang for his hard work and patience, To Mike the Tiger for luck, To my collaborators for their time, money, and fruitful discussions, To my teachers for their knowledge and support, To Julia Y. Chan who would never let me quit

and

To my friends

Acknowledgements

Preparing this document was a milestone that I found challenging, difficult, and often times unrewarding. The fact that a dissertation containing the name "W. Adam Phelan", where the name actually refers to me; William Adam Phelan is astonishing. And even though writing an *Acknowledgements* section for a monograph, thesis, or dissertation is optional according to the *Electronic Thesis and Dissertation Guidelines* as set forth by the Graduate School of Louisiana State University, I feel it is mandatory. Without my friends, family, and teachers I am nothing and this document would never exist.

Firstly, I would like to acknowledge the loves of my life, my spouse Sarah Caitlin Phelan and my puppy Jaxsen. Caitlin, you have seen and unlocked more potential in me than any other. Without your persistent reassurance with regard to by academic abilities there would have been no Due Amiche in Conway, there would have never been any cultural experiences in Baton Rouge, and there would be no future adventures in Maryland. We are truly on the exciting path that your Gigi and Papa took as young couple. We may not get to experience every site, restaurant, and museum wherever we live, but at least we will get to experience a select few together. I love you very much. Jaxsen, we first became acquainted the weekend of Andrew and Christina's wedding in Fort Smith. I knew then that would not be our final interaction. You have been nothing but joy since arriving to Caitlin and my home on October 27, 2010. Thank you for always being exited to see me when I awake up in the morning and when I return home from work in the evening. I love you and you are a good boy.

Secondly, I would like acknowledge my family. Mother and Father, your jokes about magnets, late evening phone conversations, love, and support truly kept me motivated when courses were tough, research was slow, and when I wanted to quit graduate school. I am very

happy and grateful that I can count on you both to give me the same support and advice that you gave me as a child, in which a large part of my success is based upon. Hunter, you gave me the best advice I have ever received. One late night before a final exam my senior year of College, you told me to just, "Give it hell.". Every time I need motivation, I always think about this moment. Grandpa Jack and Nana your phone conversations during my return trips home from work always took away a lot of stress. Even though I am far away from Fayetteville, I feel that we have become closer through these conversations. Richard, your support for me was never more obvious until last Christmas. I appreciate the "unofficial hell yes [whiskey] shot", upon hearing the news of my unofficial Johns Hopkins postdoctoral offer. Roy and Cheryl, until only recently have I looked to each of you for the same forms of advice and support to which my parents provide. I am very grateful that you never relinquished your arms, even though mine were not always extended. I also appreciate the little tastes of home you brought to Caitlin and I during your visits. The Fat Tire beer, Pizza Parlor pizza, Paul's Meat Market beef jerky, and McClard's BBQ sauce were wonderful treats for this home sick graduate student. I love you all.

Next, I would like to acknowledge the members of my committee. Dr. George Stanley, Dr. Andrew Maverick, and Dr. David Young thank you for all the great advice and knowledge each of you shared with me during my many office visits. I really appreciate that. Special thanks to my collaborators: Dr. David Young, Dr. Amar B. Karki, Neel Haldolaarachchige, Dr. Emila Morosan, Jiakui Wang, Liang Zhao, Dr. Frank Fronczek, Dr. Steve Watkins, Dr. Xiaoping Wang, Dr. Christina Hoffmann, Dr. Shane Stadler, Gregory McCandless, and last but certainly not least Dr. John DiTusa.

I would also like to acknowledge all of Dr. Julia Y. Chan's current and former graduate students. A special thanks is extended to Giang V. Nguyen, Brenton L. Drake, Michael

J. Kangas, and Devin Schmitt. I could have gotten out of graduate school without you. I just doubt I would have earned a Ph.D. (Crosses Fingers!)

I would like to thank Dr. Julia Y. Chan for taking time on a December afternoon in 2009 to have the following conversation with me.

Me: "I am thinking about leaving with my Master's [degree]."
Dr. Chan: "No!"
Me: "What you mean, 'NO!'? This is my choice."
Dr. Chan: "I do not believe you ever gave research a shot."

Well I am still here, and I have accepted a postdoctoral position at the Johns Hopkins University, which is contingent upon the fulfillment of the degree requirements for a Doctorate of Philosophy degree. Thank you for everything.

Lastly, I would like acknowledge the funding agencies who have graciously supported my research: Louisiana State University – Board of Regents Fellowship, National Science Foundation – Division of Materials Research (DMR–0756281 and DMR–1063735), and the Alfred P. Sloan Fellowship.

Table of Contents

List of Tables

List of Figures

Abstract

The crystal growth and characterization of four families of compounds, $LnFeSb_3$ (Ln = Pr, Nd, Sm, Gd, and Tb) and $CeCo(Sb, Sn)_3$, $Ln_2Fe_4Sb_5$ (Ln = La – Nd and Sm), $LnCu_2(Al,Si)_5$ (Ln = La and Ce), and $Ln(Cu,Al,Ga)_{13}$ (Ln = La – Pr and Eu), are presented in this dissertation. Special emphasis is placed on describing their structure-magnetic properties correlations. Discoveries and studies of these systems were motivated by their structurally related predecessors, which are comprised of complex structural subunits and exhibit unusual physical properties. The magnetic behaviors exhibited by a selection of these intermetallics include the large magnetoresistances and varying degrees of magnetic anisotropy displayed by $PrFeSb_3$ and $NdFeSb_3$, spin glass behavior observed in the low temperature magnetic susceptibility measurements of $La_2Fe_4Sb_5$, and the ferromagnetic and moderate magnetocaloric effects observed for $Eu(Cu,Al,Ga)_{13}$ and $Eu(Cu,Al)_{13}$. These materials are diverse and beautifully illustrate the complexity of the field of magnetism.

Chapter 1 describes the motivations behind the explorations of the abovementioned phase spaces. X-ray and neutron scattering, magnetism, the magnetocaloric effect, and the origins of enhanced electron mass behavior will be reviewed. Additionally, this chapter serves to link these projects. Subsequent chapters provide an in-depth analysis of the structure-property correlations for each system which have been elucidated by their synthesis, structural determinations, and physical properties measurements.

Chapter 1. Introduction*

1.1 Motivation and Challenges

One of the key challenges in the research of materials physics and chemistry is the discovery and growth of materials in large single crystal form. The premise of a recent article in *Physics Today* was to highlight the fact that in the last two decades the United States has fallen by the wayside when it comes to the discovery and growth of materials in large single crystal form.[1] More recently, the National Research Council of the National Academic Press released a report entitled *Frontiers in Crystalline Matter: From Discovery to Technology*.[2] The central emphasis of this report concerned the growth of large, robust, and defect free single crystals or thin-films for the development of the next generation of crystalline materials and the creation of new materials for energy production and conversion. This report continually reiterates the importance of how the discovery, growth, and the optimization of old and new crystalline materials will impact the US economy.

The central motivation of our research group has and continues to be the discovery of novel, highly correlated intermetallic compounds in single crystal form.[3] Intermetallic compounds and other forms of solid-state matter comprise an interesting class of materials where electron-electron or electron-lattice interactions give rise to fascinating and unusual phenomena. In our research group special attention has been placed on the synthesis of intermetallic compounds comprised of lanthanides, transition metals, and metalloids. These strongly correlated electron materials can exhibit interesting physical properties such as unusual forms of magnetism,[4] unconventional superconductivity,[5] and peculiar phase transitions which are not influenced by common external variables such as temperature, pressure, and external fields but

rather quantum fluctuations.[6] The interesting physical properties of correlated materials, optimized existing correlated materials, and newly undiscovered correlated materials are now and will continue to shape the demands of the planet, reform the theories of chemistry and physics, and influence the economies of countries both large and small.[2] Moreover, we employ the flux-growth method to discover and grow large single crystalline materials so that we may accurately determine their structure-physical property relationships.

The flux-growth procedure can be advantageous compared to traditional solid state techniques. These advantages include kinetic control of product formation where typically the most thermodynamically favorable product is yielded when conventional arc-melting techniques are employed, faster diffusion rates compared to traditional "heat and beat" techniques, and perhaps the most exciting advantage are the large single crystals which can be prepared using the flux-growth procedure.[7] The intricate details concerning the flux-growth procedure as it is employed in our laboratory are provided in the following section.

High quality, large single crystals of a particular phase must be grown to accurately characterize the structure and measure the physical properties of that phase. Only then are we able to elucidate the crystal structure-physical property relationships. However, growing large single crystals of a desired phase can present many challenges including limited temperature ranges,[8] competing phases,[9] and homogeneity ranges.[10] Solutions to a number of challenges are described along with the compounds studied, where appropriate.

1.2 Experimental

A broad range of knowledge concerning a variety of experimental techniques is required in order to accurately and reliably derive correlations between the structure and the physical properties of materials. This section serves to highlight the experimental techniques commonly

employed in our laboratory. Brief reviews of the flux-growth procedure, descriptions of the various X-ray and neutron sources, elementary X-ray and neutron diffraction theory, and the basics of magnetism and the heat capacity of solids are given.

1.2.1 Flux-Growth Procedure

As stated in the section above, the interesting physical properties and chemical structures inherent to known intermetallic compounds comprised of lanthanides, transition metals, and metalloids fuel our to desire to seek-out and discover new intermetallic compounds in single crystal form, so that we may derive correlations with respect to their chemical structures and physical properties. Targeting interesting phases which contain metalloids is advantageous from a crystal grower's perspective. Metalloids such as Al, Ga, In, Sn, Pb, Sb, and Bi have considerably lower melting points compared to lanthanides and transition metals.[3, 7, 11] This allows the crystal grower to take advantage of a procedure known as *flux-growth* in order to prepare single crystals of intermetallic compounds comprised of lanthanides, transition metals, and metalloids. Slow diffusion rates and small reaction surface areas are kinetic limiting factors which accompany the growth of crystals *via* solid state reactions. These limiting factors can be overcome if the higher melting lanthanides and transition metals are allowed to react with a metalloid flux, molten metalloid. An excess molten metalloid reacts with the lanthanide and transition metal by acting as a dissolving agent. At high enough temperatures all elements have formed a molten solution and diffusion takes place more rapidly compared to solid state reactions. After the appropriate amount of time has passed to allow for proper diffusion, a slow cooling step is initiated to allow nucleation and eventually crystal growth to proceed. References three, seven, and eleven should be consulted if information regarding more detailed

descriptions of the flux-growth procedure is of interest.[3, 7, 11] A more in-depth experimental description of the flux-growth procedure applied in our laboratory is described below.

The desired amounts of lanthanide, transition metal, and low melting metalloid are weighed out using an analytical balance and carefully placed into an alumina crucible. The crucible is then topped with quartz wool, which acts as a filtering media during a later step of the reaction procedure. Next, the reaction vessel is sealed into an evacuated silica fused tube to ensure minimal oxidation and placed into a high temperature furnace. The reaction ampoule is then subjected to a predetermined temperature profile similar to that shown in Figure 1.1. Upon completion, the synthesized crystals are separated from the excess flux *via* centrifugation. Any remaining flux wetting the crystal surfaces can be removed mechanically or by the use of chemical etchants.

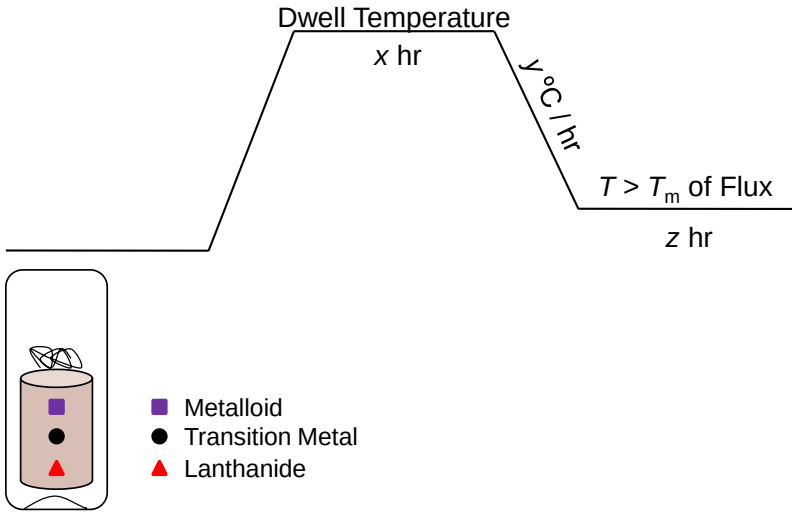

Figure 1.1 A general schematic of a reaction and temperature profile employed during flux-growth synthesis.

Binary and ternary phase diagrams should be consulted when mapping reaction and temperature profiles. By aiding in the determination of starting reactants, heating and cooling reaction rates, and dwell temperatures, these diagrams can serve as valuable tools for the

avoidance of thermodynamically stable "line" compounds. A few words of caution should be mentioned with respect to both the binary and ternary phase diagrams. Ternary phase diagrams offer insight into the stability of compounds at *only* one particular temperature. While binary phase diagrams offer limited predictability with regard to the alteration of reaction chemistry upon the addition of a third element. These factors and the experimentalist's experience should be considered when preparing reactions containing three or more elements which will be subjected to variety of varying temperature conditions.

1.2.2 X-ray and Neutron Sources

X-rays and neutrons can be generated using a variety of sources. A majority of the X-ray diffraction experiments presented in this dissertation were conducted using a Nonius KappaCCD single crystal X-ray diffractometer equipped with a Mo K_α source ($\lambda = 0.71073$ Å) and a Bruker D8 Advance powder X-ray diffractometer equipped with Cu K_α source ($\lambda = 1.54056$ Å). These instruments are housed on the 6th floor of Choppin Hall at Louisiana State University. However, the X-rays and neutrons used for the diffraction experiments as described in Chapter 5 and 6 were generated using synchrotron and spallation sources, respectively. The experimental motives for the use of each source are provided in the respective sections. A discussion about how X-rays and neutrons are generated using different sources is provided below.

• X-ray Generation from Coolidge Tubes

The Nonius KappaCCD and Bruker D8 Advance instruments described above use Coolidge sealed tubes to produce X-rays. These tubes, also known as standard X-ray tubes, are named after their inventor, William Coolidge. A general schematic of a Coolidge tube is shown below in Figure 1.2.[12] The deceleration of energetic electrons by a metal target produces the X-rays which emanate from Coolidge tubes. The filament, typically a tungsten cathode, is heated

by the application of an electric current and emits electrons which are quickly drawn to the anode, Mo and Cu targets in the Nonius KappaCCD and D8 Advance, *via* a high voltage which is applied across the tube. The negative voltage maintained at the cathode repels the electrons and focuses them onto a narrow region of the anode known as the focal spot. X-rays are emitted from this spot in all directions and escape through transparent beryllium windows.

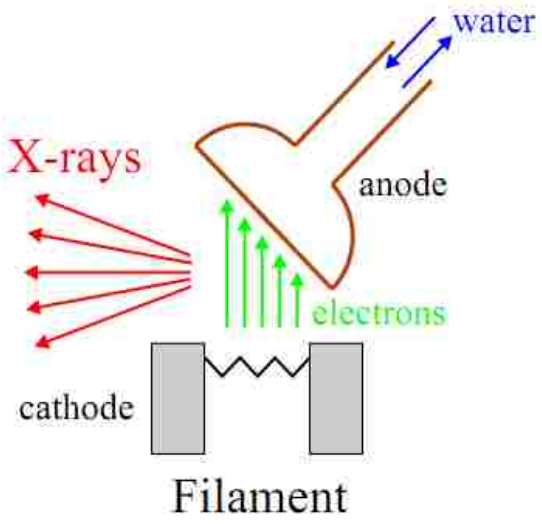

Figure 1.2 A general schematic of a Coolidge tube used for X-ray production. This figure was obtained from Reference 12.[12]

Monochromators, collimators, and other optical elements can then be used to focus the generated X-rays onto a sample. The target atoms which comprise the anode (Mo, Cu, Ag…) determine the characteristic X-ray wavelengths emitted, and the spectrum of emitted wavelengths can be described by the Bohr model.[12-13]

• X-ray Generation from Synchrotron Sources

After the invention of the Coolidge tube in 1912, progress in the experimental exploitation of X-ray intensities essentially remained unchanged. In the 1970's it was realized that the synchrotron radiation emitted from charged particles in accelerators was a potential

source for more intense and brilliant X-rays. Today's third generation synchrotrons are brighter than standard laboratory based X-ray sources by approximately a factor of 10^{12}.[12]

Figure 1.3 shows a schematic of an experimental beamline at a third generation synchrotron source. The charged particles orbiting the storage ring (1) are made to traverse circular and straight sections of the ring. In the straight sections insertion devices (2), made up of a lattice of magnets, force the charged particles to undergo small-amplitude oscillations.

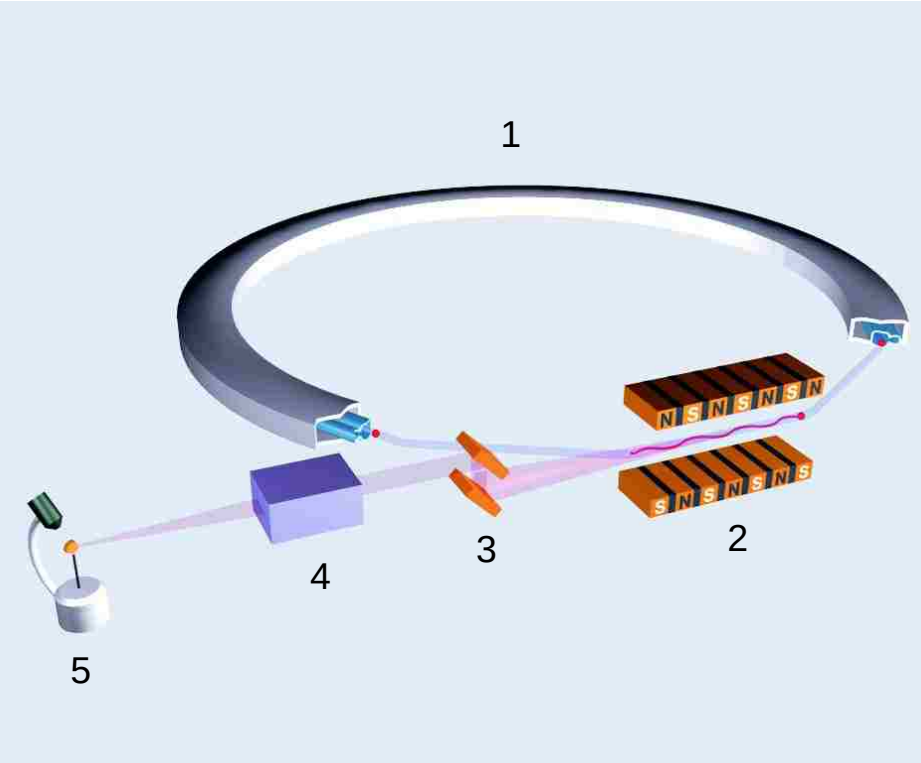

Figure 1.3 A schematic of an X-ray beamline located at a third generation synchrotron source. The key components which make up a third generation synchrotron source are a storage ring (1), an insertion device (2), a monochromator (3), focusing optics (4), and an experimental hutch (5). This schematic was obtained from Reference 12.[12]

X-rays are emitted when charged particles oscillate, and if the amplitude of the oscillations are small the emitted X-rays add coherently resulting in a very intense beam of X-rays. A monochromator (3) is used to select a specific X-ray wavelength, and this wavelength is focused onto sample (5) using focusing optics (4).[12]

• Neutron Generation from Nuclear Reactor Sources

Nuclear reactors operate on the principles of nuclear fission chain reactions. Most nuclear reactors generate neutrons by the fission of Uranium atoms, the reactor fuel. A schematic of this process is shown in Figure 1.4. When a neutron (^{1}n) collides and is absorbed

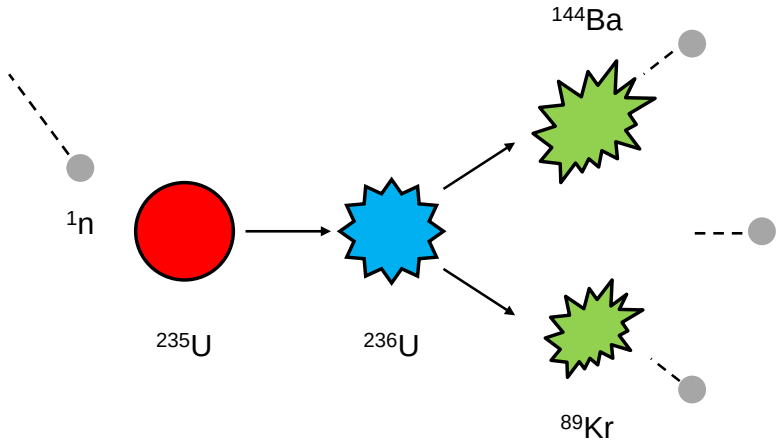

Figure 1.4 A schematic of the nuclear fission process. Adapted from reference 14.[14]

by a ^{235}U nucleus, a large amount of energy is transferred into the system, and an excited ^{236}U nucleus is formed. This excited nucleus begins to oscillate until the repelling Coulomb force drives it to separate into a ^{89}Kr nucleus, a ^{144}Ba nucleus, and three neutrons. At least one neutron is required to maintain the chain reaction, and trigger a subsequent fission reaction. The remaining neutrons can be used for neutron scattering experiments.[14]

The design of the High Flux Isotope Reactor (HFIR) located at Oak Ridge National Laboratory (ORNL) is shown below. The reactor core, or fuel region, contains a group of fuel rods in a large pool of water or heavy water (D_2O). The water or heavy water moderates (decelerates) the neutrons and helps to cool the reactor, while the beryllium reflectors help to maintain the fission reaction by reflecting neutrons back to the reactor core. The beam tubes inserted in the walls of the pool deliver neutrons to the scattering instruments. The emerging

neutrons are collimated in beam tubes, and a single crystal monochromator is used to select a specific neutron wavelength. The monochromatic neutrons are allowed to impinge upon a sample. The sample then elastically and inelastically scatters neutrons. Additional monochromators and analyzer crystals select neutrons of a specific energy. These neutrons are then scattered into a bank of detectors.[14-15]

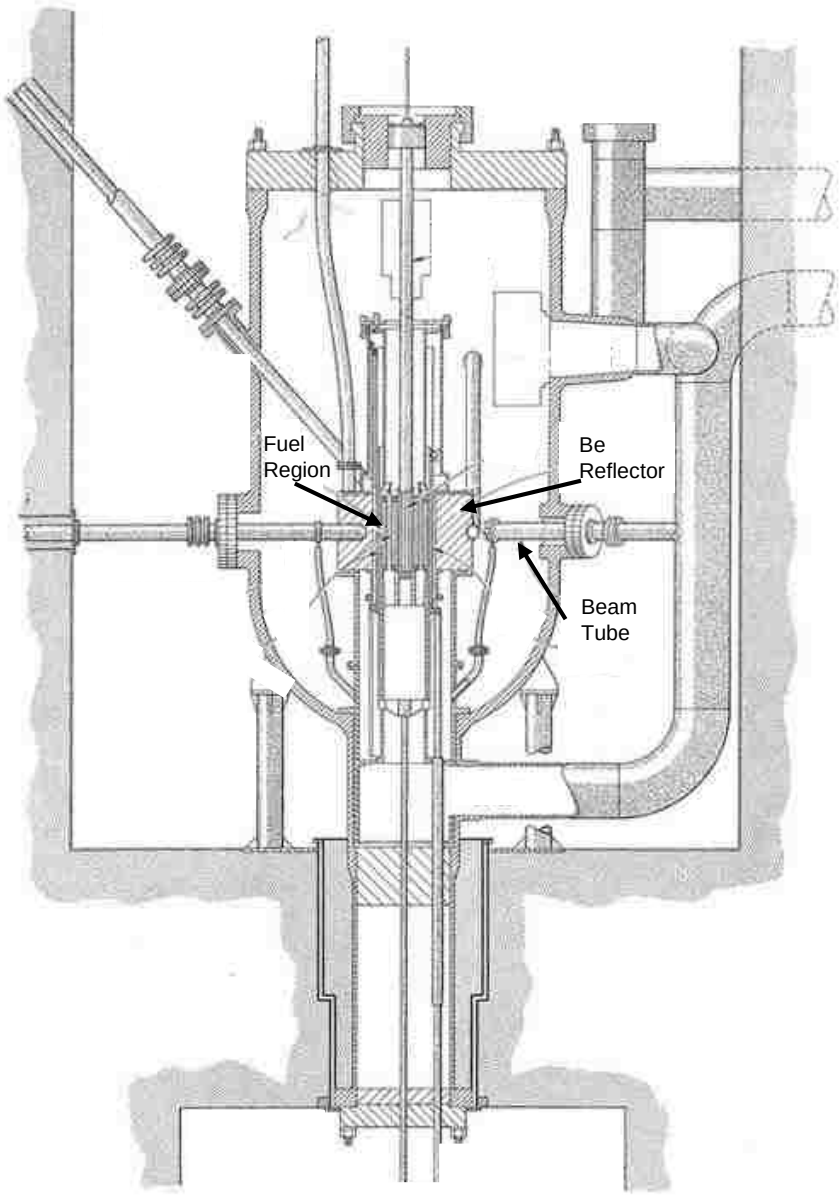

Figure 1.5 This design was obtained from reference 15.[15]

• **Neutron Generation from Spallation Sources**

Spallation neutron sources generate neutrons by allowing high energy proton bursts, produced by ion sources and accelerators, to collide with heavy metal targets, such as tungsten or mercury. These collisions produce bursts of neutrons by driving neutrons from the nuclei of the heavy metal targets. The high energy neutron bursts are then moderated before entering the experimental area.[14, 16] A schematic of an experiment employing neutrons generated by spallation is shown in Figure 1.6.

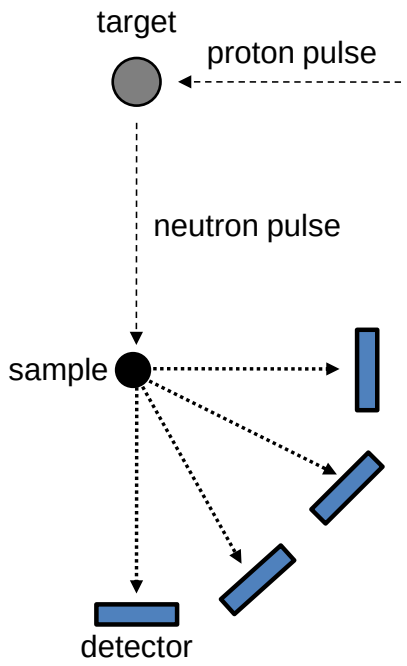

Figure 1.6 A schematic of a neutron scattering experiment at a spallation source. Figure was adapted from reference 17.[17]

Neutrons generated from spallation sources arrive in pulses, unlike the continuous beam of neutrons produced by reactor sources. Therefore, the monochromator crystals needed at reactor sources are not used at spallation sources. Furthermore, all the moderated neutrons can be used. The fact that all neutrons from a spallation source can be used relies on the measurement of the time it takes for each detected neutron to traverse the distance between the moderator and the

detector, time of flight (TOF). From the measured time of flight, the neutron velocity and thus the neutron wavelength can be determined.[14, 16]

1.2.3 Basic X-ray and Neutron Diffraction Theory

X-ray and neutron diffraction experiments can be used as complementary techniques to probe the internal structures of materials. The angular positions and the intensities of the diffraction peaks measured using a detector can be used to deduce the unit cell dimensions (periodicity) and the atom types and atom positions within the unit cell, respectively.[13] Before examining the principles of nuclear and magnetic scattering, a discussion about the principles of form factors, structure factors, and Fourier transform as it relates to both X-ray and neutron scattering will provide a useful foundation for the subsequent discussions.

Form factors, $f(\boldsymbol{Q})$, provide a measure of the scattering amplitude of a wave by an isolated atom. The description of form factors can be discussed in terms of Fourier transform. Fourier transform can be used to describe the spatial density distributions of a scattering object, electrons or nuclei. This spatial density distribution as related to the form factor can be seen in Equation 1.1:

$$f(\vec{Q}) = \int \rho(\vec{r}) e^{i\vec{Q}\cdot\vec{r}} dr \qquad (1.1)$$

where $\rho(r)$ is the spatial density distribution of the scattering object and $\boldsymbol{Q}$ is the momentum transfer vector. It should be noted that the values of form factors vary from atom to atom because the spatial density distribution of electrons of an atom change across the periodic table.[13, 18]

Matter consists of many electrons from which X-rays may scatter. The scattering of X-rays by matter can thus be described by the summation of all of these individual scatterers and is given by the structure factor, $F(\boldsymbol{Q})$:

$$F(\vec{Q}) = \sum_{j}^{N} f_j(\vec{Q}) e^{i\vec{Q}\cdot\vec{r}_j} \qquad (1.2)$$

where $f_j(\boldsymbol{Q})$ is the form factor for the j^{th} atom in the unit cell, $\boldsymbol{r}_j$ is the position of j^{th} atom in the unit cell, N is the sum over all unit cells in the material. Since $F(\boldsymbol{Q})$ is a measure of the scattering amplitude of all the j^{th} atoms in the unit cell, the intensity contributed by these atoms to the diffraction peaks in a spectrum is given by $I(\boldsymbol{Q}) = F(\boldsymbol{Q})F^*(\boldsymbol{Q})$.[18] A material's composition can thus be deduced by applying reverse Fourier transforms to the intensities of the diffraction peaks.

From the discussion above, nuclear neutron scattering can be easily understood if the scattering of a neutron from a single, fixed nucleus is first examined. The incident neutron can be represented as a plane wave by $\psi_i = e^{i\boldsymbol{k}\cdot\boldsymbol{r}}$ where $\boldsymbol{k} = 2\pi m\boldsymbol{v}/h$ is the neutron wavevector which points along the neutron's trajectory. The amplitude of the scattered neutron wave depends on the strength of the interaction between the neutron and the nucleus. From scattering theory, the resultant wave will be spherically symmetric and can be represented by $\psi_{sc} = (-b/\boldsymbol{r})e^{i\boldsymbol{k}\cdot\boldsymbol{r}}$. Here the constant b, the scattering amplitude or scattering length, is a measure of the strength of the interaction between the neutron and the nucleus and takes the place of $f(\boldsymbol{Q})$ in Equations 1.1 and 1.2. The 1/r prefactor is in keeping with the inverse square law that applies to all wave motions and states that the intensity of a wave, given by the square of its wave function, decreases as the inverse square from the scatterer to the observer.[16, 19-21]

In order to understand how neutrons are scattered by matter, a description for the summation of all the scattering events from the individual nuclei are needed. From the above assumption that the nucleus was fixed and given that the wavevector, a measure of momentum, is unchanged between the incident and scattering neutron, the scattering of a neutron from a fixed nucleus can be regarded as elastic. However, atoms in matter are free to move and can

ultimately absorb energy from or impart energy to an outgoing neutron wave. In this case the scattering is not necessarily elastic, and the incident and scattered neutron wavefunctions become $\psi_i = e^{i\boldsymbol{k}\cdot\boldsymbol{r}}$ and $\psi_{sc} = (-b/\boldsymbol{r})e^{\boldsymbol{k}'\cdot\boldsymbol{r}}$. Since the total energy and momentum in a collision must be conserved, the overall momentum transfer is given by the equality:

$$\frac{h(\vec{k}-\vec{k}')}{2\pi} = \frac{h(\vec{Q})}{2\pi} = m\Delta\vec{v} = \Delta\vec{p} \qquad (1.3)$$

where $\boldsymbol{Q}$ is the scattering vector. $\boldsymbol{k}$ and $\boldsymbol{k}'$ are the wavevectors for the incident neutrons and scattered neutrons, respectively.[16, 20]

As mentioned above, the measured intensities of the scattered neutrons are directly correlated to the types of atoms and the atomic positions within the unit cell. Van Hove showed that the scattered intensity as a function of $\boldsymbol{Q}$ and energy (E) is proportional to the Fourier transform as a function of the scattering amplitudes of the atoms in a materials.[22] Van Hove's equation is shown below and closely resembles the complex conjugate shown above.

$$I(\vec{Q},E) = \frac{1}{h}\frac{\vec{k}'}{\vec{k}}\sum_{i,j} b_i b_j \int_{-\infty}^{\infty} \left\langle e^{-i\vec{Q}\cdot\vec{r}_i(0)} e^{i\vec{Q}\cdot\vec{r}_j(t)} \right\rangle e^{-i(E/\hbar)t}\, dt \qquad (1.4)$$

Here $\boldsymbol{r}_i$ is the position of the i^{th} nucleus at time zero, $\boldsymbol{r}_j$ is the position of the j^{th} nucleus at time t, b_i is the scattering amplitude of nucleus i and, b_j is the scattering amplitude of nucleus j. This equation and manipulations thereof provide scattering information about the equilibrium structure of matter and how the structures of matter evolve with time.[21]

Equation 1.4 can be further broken down to describe coherent scattering, incident neutron waves interact with all of the sample nuclei in a coordinated fashion thus producing interference effects, and incoherent scattering, incident neutron waves interact independently and randomly with each sample nucleus thus producing no interference effects. Coherent scattering processes can be either elastic or inelastic. Elastic coherent scattering provides information about the

equilibrium structure of matter, whereas, inelastic coherent scattering provides information about how the structure of matter evolves with time. Thus inelastic coherent scattering events can provide information about quantized lattice thermal vibrations (phonons) and quantized spin thermal excitations (magnons). Incoherent scattering processes can also be elastic or inelastic. Incoherent elastic scattering usually appears as unwanted background scattering, and incoherent inelastic scattering provides information about atomic diffusion. For the sake of brevity, the succeeding discussions will be limited to coherent elastic scattering.[19-21]

Coherent elastic scattering is usually discussed in terms of diffraction. Diffraction occurs because the incident X-ray and neutron waves interact with a sample's electrons and nuclei, respectively, in a coordinated fashion, coherence. As the incident X-ray or neutron waves arrive at the electrons or nuclei, these electrons or nuclei become the centers of scattered spherical waves. If these scattered rays have the same relative phases, they will interfere constructively. These waves are commonly referred to as "in phase". Constructive interference will only occur in particular directions relative to the incident and scattered waves that are related to the symmetry and the lattice spacings of a given unit cell. In all other directions the scattered beams will be "out of phase" and will completely annul one another.[13, 18] Constructive interference will give rise to waves of a particular intensity. For coherent elastic scattering ($\Delta E = 0$), Van Hoves equation reduces to[21-22]:

$$I(\vec{Q}) = \sum_{i,j} b_{coh}^2 e^{i\vec{Q}\cdot(\vec{r}_i - \vec{r}_j)} \tag{1.5}$$

Since materials are composed of many atoms and since each atom is responsible for contributing a relative phase to a scattered wave, it seems astonishing that the intensity given in Equation 1.5 could equal anything but zero. W.H. Bragg and his son W.L. Bragg were able to

mathematically express the conditions necessary for diffraction and these conditions are illustrated in Figure 1.7.

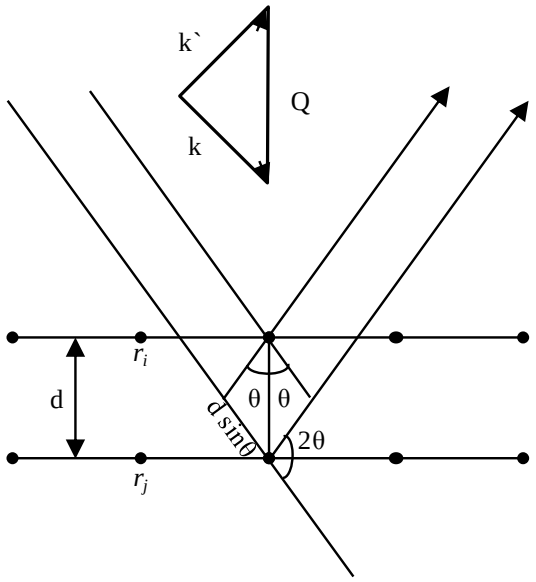

Figure 1.7 Schematic illustration for the necessary conditions for constructive interference of diffraction. Adapted from reference 16.[16]

Suppose that ***Q*** is perpendicular to the parallel planes of atoms as illustrated in Figure 1.7. If ***Q*** is an intergral multiple of 2π/d (n2π/d), where d (r_i-r_j) is the distance between the parallel planes, then ***Q***·(r_i-r_j) is a multiple of 2π and I(***Q***) is non-zero because of the exponential term in Equation 5. Using these relationships, Bragg's Law can be written as $n\lambda = 2d\sin\theta$. Thus Bragg scattering may occur for a set of planes with spacing d, such that the X-ray or neutron wavelength and the scattering angle (2θ) satisfy the Bragg law.[13, 18, 21]

In order to obtain diffraction from a particular set of planes, the crystal must be rotated about the incident X-ray or neutron beam to the correct orientation so that ***Q*** is perpendicular to the Bragg planes. Sharp peaks or Bragg peaks as a function of the scattering angle are measured at a detector, since the scattering for a particular set of Bragg planes will only occur when the crystal is oriented perpendicular to ***Q***. The intensities of these Bragg peaks are given by Equation 1.5.

Before discussing magnetic neutron scattering, a distinction should be made regarding the differences between X-ray form factors ($f(\boldsymbol{Q})$) and nuclear neutron scattering amplitudes (b). As mentioned above X-rays are scattered by the electrons of an atom. Because the electron clouds of atoms and the X-ray wavelengths are comparable in size, the form factor decreases with increasing 2θ. By contrast, the neutron wavelengths are much larger than the sizes of the atomic nuclei and as a consequence the neutron scattering amplitudes remain constant as a function of 2θ. Values of the nuclear neutron scattering amplitudes and the X-ray form factors have been experimentally determined and can be found in references twenty-three and twenty-four.[23-24]

As mentioned above, the magnetic moment of a neutron can also interact with the magnetic moments of atoms containing unpaired electrons. Halpern and Johnson devised an expression to describe the amplitudes for magnetic neutron scattering.[25] This amplitude is represented as $\alpha_M(\boldsymbol{Q}) = pf(\boldsymbol{Q})\mu_\perp$ where $p = 0.2696\times10^{-12}$ cm, $f(\boldsymbol{Q})$ is the form factor of the unpaired electrons, and $\mu_\perp$ is the component of the atomic magnetic moment perpendicular to $\boldsymbol{Q}$. Magnetic neutron scattering is sensitive only to $\mu_\perp$, and the magnetic contribution to the Bragg peaks will be zero if the moments are parallel to $\boldsymbol{Q}$.[14]

The magnetic structure factor takes the following form:

$$M(Q) = p\sum_{j}^{N_m} f_j(Q)\mu_j e^{iQ\cdot r_j} \qquad (1.6)$$

where N_m is the total number of magnetic atoms, and the intensity of the magnetic Bragg peaks are given by $I_M(\mathbf{Q}) = M_\perp(\boldsymbol{Q})M_\perp(\boldsymbol{Q})^*$.[14, 20, 26] Similar to the X-ray form factor, the magnetic form factor decreases with increasing 2θ because the neutrons wavelengths are on the same order as the dimensions of the unpaired electron orbits. However, the magnetic form factor is in general different from the X-ray form factor since it depends only on the unpaired electrons.[14, 19] Some

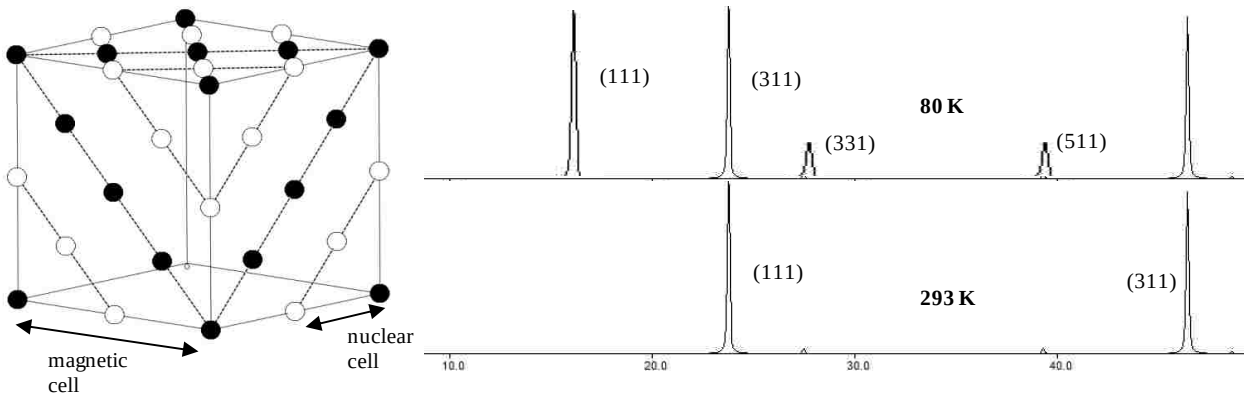

Figure 1.8 The magnetic and nuclear unit cells for MnO (left). The black and white atoms correspond to spins which point up and down, respectively. Neutron diffraction patterns for MnO above (bottom right) and below (top right) the ordering temperature can be viewed above. The oxygens have been omitted for clarity. The figure to the right was simulated using *Poudrix*.

values for the magnetic form factors of particular atoms and ions can be found in reference fourteen.[14]

The periodicity of the magnetic structure can differ from that of the nuclear structure. For magnetically ordered materials this periodicity is described by a propagation vector. Shull and Smart were the first to successfully solve a magnetic structure and showed that MnO ordered antiferromagnetically.[27-28] MnO orders antiferromagnetically below 120 K *via* the superexchange mechanism. The magnetic structure of MnO can be viewed in Figure 1.8. The spins are aligned parallel with respect to one another within a single (111) plane, but are aligned antiparallel between planes. The magnetic cell is thus a supercell, which is twice as large as the original nuclear cell, and can be described as having a propagation vector of $2a \times 2b \times 2c$. The difference in periodicity and symmetry between the nuclear and magnetic cell alters the observed diffraction patterns. The observed diffraction pattern in Figure 1.8 for MnO below the ordering temperature (top) contains more peaks relative to the observed diffraction pattern above the ordering temperature (bottom). This is typical when the magnetic unit cell is a supercell of the nuclear unit cell. In reality, the identification of the appropriate propagation vector and the

structure solution of a magnetic material are more complicated than that described above. The magnetic symmetry of a material is governed by the principles of Group Theory which are beyond the scope of this dissertation. References fourteen, twenty, and twenty-six should be consulted as good reviews for the principles which govern the possible allowed magnetic symmetries.[14, 20, 26]

1.2.4 Physical Properties

Precise details regarding the exact experimental conditions such as: the type of instruments used, sample manipulations, and data acquisition procedures with respect to any measured physical properties are provided where appropriate within each chapter. The following subsections were written to provide the interested reader with the *basic* theoretical knowledge of the physical properties measured by the Chan Group and our collaborators. More specifically, the rudimentary fundamentals of magnetism, the magnetocaloric effect, and the specific heat treatment of solids are presented.

1.2.4.1 Magnetism

The close proximity of atoms or ions in a solid allows them to interact in such a way that can led to the occurrence of cooperative phenomena which are usually not observed in gasses or liquids. The magnetic interactions of atoms or ions in a solid can lead to cooperative phenomena.[29] The origins of magnetism, my favorite subject, are derived from the spin (S) and/or orbital (L) motions, magnetic moments, of electrons comprising the individual atoms or ions in a solid. The nuclei of these atoms or ions may also possess magnetic moments, but the contributions of these magnetic effects to the total magnetism of a solid are usually only observed – if at all – at very low temperatures (T ~ 1 K).[17, 29-30] Reviews of the magnetic interactions described in later chapters of this dissertation are provided in the sub-sections below.

The simplest forms of magnetism, diamagnetism and paramagnetism, are described first. The most commonly observed cooperative magnetic phenomena, ferromagnetism and antiferromagnetism, are then reviewed. Finally, this section will conclude with a brief summary of a few special cases of antiferromagnetism, geometric and spin glasses frustration.

• Behaviour of Magnetic Materials in the Presence of an Applied Magnetic Field

Regardless of the particular types of magnetic interactions inherent to a material, its macroscopic response to an applied magnetic field (H) can be characterized by the resulting magnetic flux or magnetic induction (B) of the material. In a vacuum, H and B are related by the permeability of free space (μ_o).

$$B = \mu_o H \tag{1.7}$$

When a material is placed inside an applied magnetic field (H), the magnetic flux or induction (B) within the material can increase or decrease. Whether the magnetic flux density (B) increases or decreases within a sample upon the application of an applied magnetic field (H) depends on the sample's magnetization (M), and its relation to the magnetic flux density (B) is given by Equation 1.8.

$$B = \mu_o H + \mu_o M \tag{1.8}$$

Therefore, $\mu_o H$ and $\mu_o M$ are the magnetic induction generated by the applied magnetic field (H) and the additional induction contributed by the material (M), respectively.[17, 29-30]

A material's magnetization (M) or magnetic moment per unit volume is typically discussed in terms of magnetic susceptibility (χ). The equality provided in Equation 1.9 shows how the magnetization (M) of a material is related to its magnetic susceptibility (χ).

$$\chi = \frac{M}{H} \tag{1.9}$$

A material's magnetic susceptibility (χ) provides a measure of the response of the material to an applied magnetic field (H).[17, 29-30]

The different forms of magnetic behavior can be distinguished by the magnitudes and directions of χ. χ is very small and negative for diamagnetic materials. Whereas, paramagnetic materials exhibit small positive values of magnetic susceptibility (χ). Therefore, when a diamagnetic (paramagnetic) material is placed into an applied magnetic field (H), the magnetic flux density (B) is less (greater) than the magnetic flux density (B) that would pass through a vacuum. Thus, diamagnetic (paramagnetic) materials are repelled by (attracted to) an applied magnetic field (H).[17, 29-30]

Ferromagnetic materials are strongly attracted to a magnetic field and $\chi \gg 1$. For antiferromagnetic materials the direction and magnitude of χ are positive and slightly less than that of paramagnetic substances, respectively.[17, 29-30] More thorough treatments of diamagnetism, paramagnetism, ferromagnetism, and antiferromagnetism are provided below. Additionally, an interesting and special class of antiferromagnetic materials, frustrated materials, is briefly discussed.

• Diamagnetism

The simplest form of magnetism will be considered first. Larmor or Langevin diamagnetism results from the spin angular momentum (S) and orbital angular (L) momentum of electrons in filled atomic shells. Therefore diamagnetism is present in all materials. (Expect of course for hydrogen-like atoms.) Since the spin angular momentum (S) and orbital angular momentum (L); and thus, the total angular momentum (J) resulting from electrons in filled shells is zero, diamagnetic effects do not contribute to any *well-defined* magnetic response of the atoms or ions that make-up a magnetic material.[17, 29-30]

• Paramagnetism

Materials in which no net magnetization (M) exists in zero applied magnetic field (H) are said to be paramagnetic. The simplest form of paramagnetism occurs in materials where the magnetic moments are well separated from one another. In this case, the moments do not interact with one another and only respond to thermal fluctuations and applied magnetic fields (H). Paramagnetism can also exist in materials where the magnetic moments do interact weakly. However, these interactions must be so weak, that no net magnetization (M) appears in these materials in the absence of an applied magnetic field (H). This type of paramagnetic behavior occurs in both ferromagnetic and antiferromagnetic materials slightly above their ordering or critical temperatures.[17, 29-30]

The magnetic susceptibility (χ) of many paramagnetic materials can be described by the Curie law. The Curie law states that the magnetic susceptibility (χ) is inversely proportional to the temperature (T) and takes the form:

$$\chi = \frac{C}{T} \tag{1.10}$$

where C is known as the Curie constant. As stated above, this response occurs when there is no magnetic interaction between the magnetic moments of a material. The magnetic moments tend to align with an applied magnetic field (H), but this alignment is opposed by thermal fluctuations. The Curie constant has units of temperature and can be written as:

$$C = \frac{\mu_o n g^2 \mu_B^2 J(J+1)}{2k_B} \tag{1.11}$$

where n is the concentration of free spins, μ_B is the effective Bohr magneton, and k_B is Boltzmann's constant. The Landé g factor for a particular atom or ion is given by:

$$g = 1 + \frac{J(J+1) + S(S+1) - L(L+1)}{2J(J+1)} \qquad (1.12)$$

where S, L, and J correspond to the spin, orbital, and total angular momentum of the unpaired electrons. The Landé g factor is a multiplicative constant needed to describe the magnetic energy levels separated by an applied magnetic field.[17, 29-30]

The Curie law behavior exhibited by most paramagnetic materials is shown schematically in Figure 1.9. In this schematic both $\chi = C/T$ and $1/\chi = T/C$ are shown plotted as a function of temperature (T). The χ vs. T plot clearly shows that χ diverges in the as limit of T = 0 K, thus demonstrating that as the thermal fluctuations decrease, the magnetic moments align with the applied magnetic field and both the magnetization (M) and the magnetic susceptibility (χ) increase.

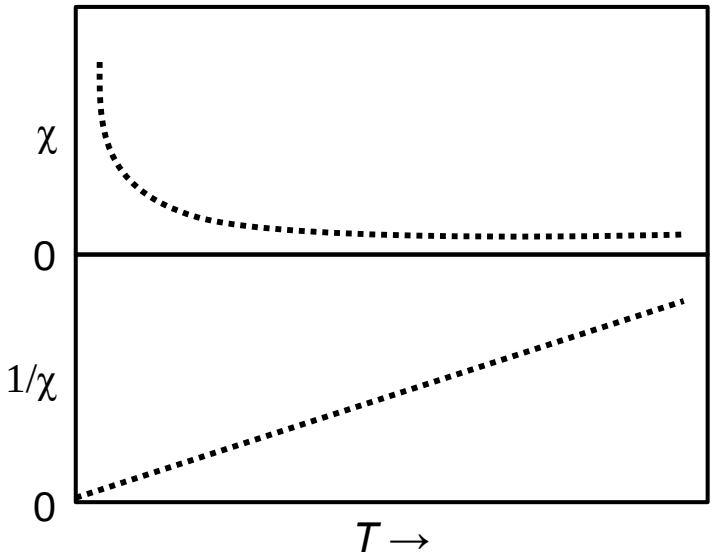

Figure 1.9 Curie law behavior of the magnetic susceptibility (χ) vs. T as expressed in Equation 1.10. This figure was adapted from reference 30.[30]

A plot of the $1/\chi$ vs. T data measured for paramagnetic materials allows for both a test of the validity of the Curie law and the determination of the Curie constant (C) from the reciprocal slope of a linear plot. The effective magneton number (p_{eff}) can be calculated from the Curie

constant (C) if the concentration of free spins (n) in the paramagnetic material is known using Equation 1.13.

$$p_{\text{eff}} = \text{g}\sqrt{\text{J}(\text{J}+1)} = \sqrt{\frac{3k_{\text{B}}\text{C}}{\mu_{\text{o}}\text{n}\mu_{\text{B}}^2}} \qquad (1.13)$$

The effective magneton number is a measure of the magnetic moment of an atom or ion, and a theoretical value for this number can also be calculated (p_{calc}) easily using the predictions of Hund's rules. If the effective magneton number (p_{eff}) determined from the Curie constant (C) and the p_{calc} calculated using the predictions of Hund's rules are in good agreement, then the paramagnetic material in question is said to follow Curie law behavior. (It is assumed that the reader is familiar with Hund's rules.)[17, 29-30]

• Ferromagnetism and Antiferromagnetism

When a paramagnetic material is cooled, the energy of the magnetic interactions between the magnetic moments increase while the energy of the thermal fluctuations decrease. For some paramagnetic materials, there exists a critical temperature such that when the material is cooled below this critical temperature, the energy of the magnetic interactions exceeds that of the thermal fluctuations. These conditions typically result in a magnetically ordered state (cooperative phenomena).

Ferromagnetically and antiferromagnetically ordered states are the most commonly observed magnetically ordered states. The adjacent magnetic moments in a ferromagnetically ordered state are all aligned parallel, while the adjacent magnetic moments in an antiferromagnetically ordered state are aligned antiparallel. Depictions of these magnetically ordered states are shown schematically for an arbitrary cubic rare-earth (RE) system in Figure 1.10a and 1.10b.[17, 29-30]

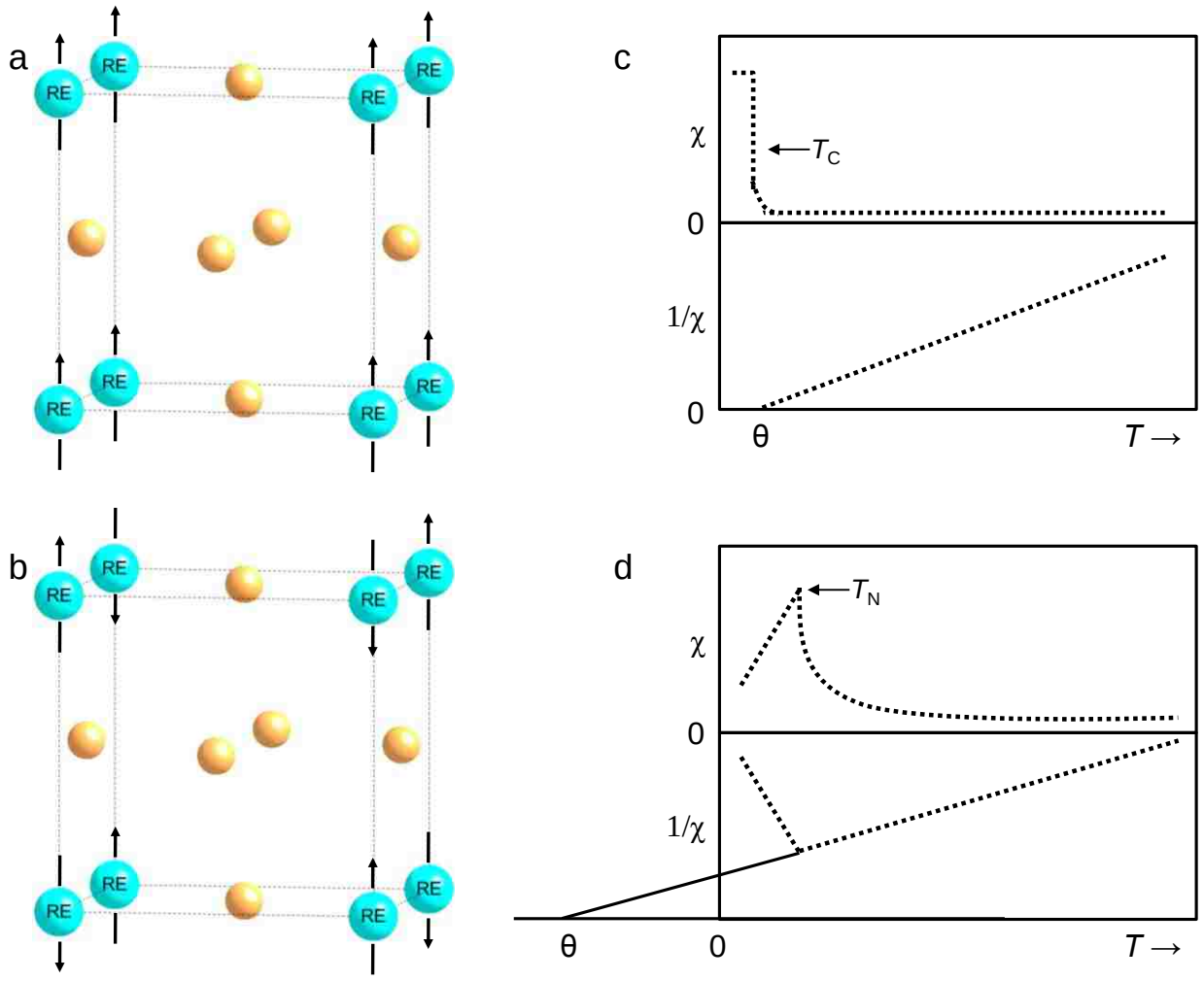

Figure 1.10 A ferromagnetic **(a)** and antiferromagnetic **(b)** state for an arbitrary cubic rare earth (RE) system. A schematic of the magnetic susceptibility and reciprocal magnetic susceptibility as a function of temperature for a ferromagnetic **(c)** and antiferromagnetic material **(d)**.

If spontaneous magnetic coupling exists between adjacent magnetic moments, which may order ferromagnetically or antiferromagnetically at temperatures below the critical temperature, a better fit to the high temperature magnetic susceptibility (paramagnetic regime) is provided by the Curie-Weiss law:

$$\chi = \frac{C}{T - \theta} \tag{1.14}$$

where θ is the Weiss constant and has the same units as temperature. This constant provides a measure of the magnitude and direction of the coupling strength between adjacent magnetic moments.[17, 29-30]

A basic schematic of the magnetic susceptibility (χ) and reciprocal magnetic susceptibility (1/χ) for the ferromagnetic and antiferromagnetic ground states of the arbitrary cubic rare-earth (RE) system are shown in Figure 1.10c and 1.10d, respectively. In paramagnetic materials that display a propensity to order ferromagnetically, there exist short range magnetic correlations slightly above the critical temperature. In this situation the adjacent magnetic moments over a very short correlation length are aligned parallel with respect to one another (short range order). The tiny magnetic fields generated by individual magnetic moments will reinforce one another, and this has the effect of increasing the material's magnetization, and thus, its magnetic susceptibility (Equation 1.9). The magnetic susceptibility values for materials that show a propensity to order ferromagnetically are typically larger compared to the magnetic susceptibility values for the simple paramagnetic case. The Weiss temperature can be determined by fits of the reciprocal magnetic susceptibility (1/χ) vs. T in the paramagnetic regime using Equation 1.14. Since the magnetic susceptibility values of ferromagnetic materials are larger compared to paramagnetic materials, the extrapolated intercept (Weiss temperature) will be nonzero and positive. The determined positive Weiss temperature value usually coincides with the ferromagnetic ordering temperature or Curie temperature (T_C) of the material where T_C is the maximum temperature value of $-(dM/dH)_T$ vs. T curve. Below the Curie temperature (T_C) a long range ferromagnetically ordered ground state dominates, and this is signaled by a monotonic increase in the magnetic susceptibility (Figure 1.10c). Eventually all of

the magnetic moments will align parallel, and a saturation limit will be reached as the temperature is lowered even further.[17, 29-30]

In paramagnetic materials that display a propensity to order antiferromagnetically, there exist short range antiferromagnetic correlations slightly above the critical temperature. In this situation the adjacent magnetic moments over a very short correlation length are aligned antiparallel with respect to one another (short range order). The tiny magnetic fields generated by individual magnetic moments will cancel one another, and this has the effect of slightly decreasing the material's magnetization, and thus, its magnetic susceptibility compared to paramagnetic materials (Equation 1.9). Again, the Weiss temperature can be determined by fits of the reciprocal magnetic susceptibility ($1/\chi$) vs. T in the paramagnetic regime using Equation 1.14. Since the magnetic susceptibility values of antiferromagnetic materials are slightly smaller compared to paramagnetic materials, the extrapolated intercept (Weiss temperature) will be nonzero and negative. The determined negative Weiss temperature value usually coincides with the antiferromagnetic ordering temperature or Néel temperature (T_N) of the material where T_N is the maximum temperature value of $-(dM/dH)_T$ vs. T curve. Below the Néel temperature (T_N) a long range antiferromagnetically ordered ground state dominates, and this is signaled by a decrease in the magnetic susceptibility (Figure 1.10d).[17, 29-30]

• Geometrical and Spin Glass Frustration – Special Cases of Antiferromagnetism

For some systems it is not possible to minimize the energy of all the magnetic interactions to find a lowest energy, unique ground state. This often leads to many degenerate or nearly degenerate ground states separated by small energy quantities. Under these conditions a system is said to be *frustrated*. The two most common types of frustration, geometrical and spin glass frustration, are summarized below.[17, 31-33]

The concepts of geometrical frustration will be presented first. Consider the lattices in Figure 1.11a and 1.11b, in which nearest-neighbor (NN) antiferromagnetic (AFM) interactions are energetically favorable. This condition is easily satisfied for the square lattice and one low

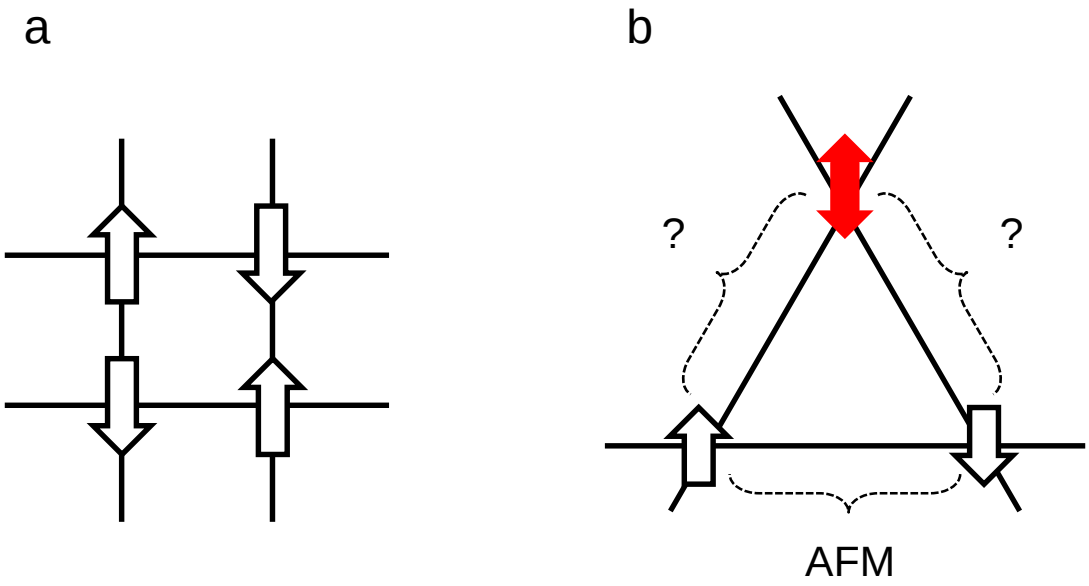

Figure 1.11 Antiferromagnetic (AFM) nearest-neighbor interactions on a square **(a)** and triangular lattice **(b)**. This figure was adapted from reference 32.[32]

energy, unique ground state is dominant. However, complications arise when the magnetic moments are confined to the corners of a triangular lattice. As shown in Figure 1.11b, if two adjacent magnetic moments are aligned antiparallel, the placement of a third magnetic moment onto the triangular lattice cannot be accomplished in such a way to satisfy the conditions of energetically favorable nearest-neighbor (NN) antiferromagnetic (AFM) interactions. Thus, the origins of *geometrical frustration* arise from the particular lattice-type in question. The third magnetic moment will have to ferromagnetically align with one of the nearest-neighbors (NN), and these circumstances will result in the formation of three degenerate ground states. Now imagine a solid composed of an infinite amount of triangular lattices where nearest-neighbor

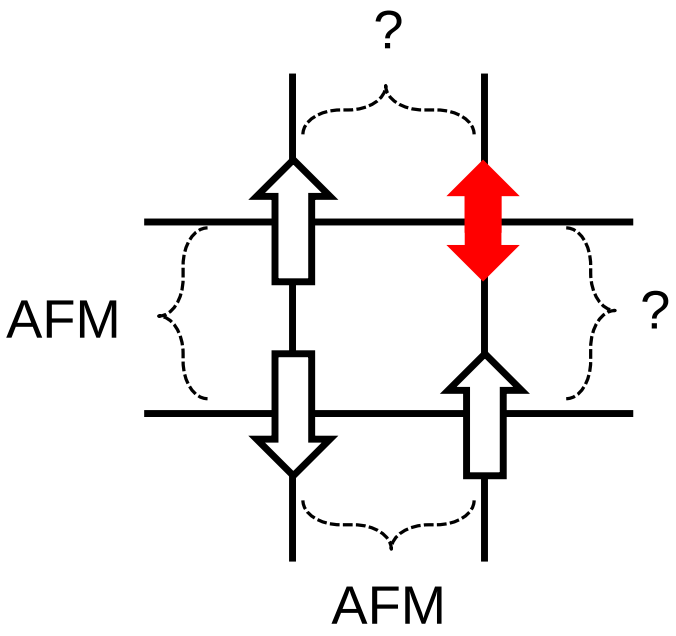

Figure 1.12 Magnetic frustration induced my site disorder. This figure was adapted from reference 32.[32]

(NN) antiferromagnetic interactions (AFM) are energetically favorable. An infinite amount of ground states will be formed under these conditions, and one can only imagine the complex magnetic behaviors possible. (In reality a single ground state will dominate depending of the particular experimental conditions. However, complex magnetic behaviors are usually associated with geometrically frustrated materials.)[17, 32-33]

The second most common form of magnetic frustration is known as spin glass frustration. Here the origins of magnetic frustrations are derived from lattice site disorder and/or geometric frustration. Therefore, the same magnetic behaviors observed in geometrically frustrated systems may or *may not* result from the lattice geometry. A schematic of the magnetic frustration induced by site disorder is shown in Figure 1.12.

A good example of spin glass behavior can be found in a system where a small amount of magnetic atoms (Mn) are doped onto random lattices sites of a nonmagnetic host (Cu). Since the

types of magnetic interactions (ferromagnetic and antiferromagnetic) between randomly placed Mn atoms will depend on their separation distances, competing ferromagnetic and antiferromagnetic Mn – Mn interactions will lead to frustration. Given that Mn magnetic moments are randomly scattered throughout the Cu host and lack periodicity, similar to the random placement of atoms and lack of periodicity in glasses, this system is termed a *spin glass*. This is illustrated in Figure 1.12 where the Mn atoms are randomly scattered throughout the Cu host (Cu atoms not shown), thus leading to frustration where competing magnetic interactions exist due to differing Mn – Mn separation distances.[17, 31-33]

1.2.4.2 The Magnetocaloric Effect

Modern civilization depends heavily on refrigeration for preserving food-goods and climate controlled living spaces. Current conventional refrigeration and heat pump systems are disadvantageous from both a physics and a chemistry perspective. Today's most efficient refrigeration units operate well below the theoretical Carnot efficiency, and it seems very unlikely that further improvements can be made to the existing vapor compression/decompression technology. Additionally, current refrigerators employ hydrofluorocarbons (HFCs), hydrochlorofluorocarbons (HCFCs) as replacements for chlorofluorocarbons (CFCs), and ammonia, all of which are common greenhouse gases that deplete the ozone layer to various degrees, and are health hazards.[34-36]

Magnetic refrigeration devices that employ ferromagnetic materials may be used to supersede the inefficient vapor compression/decompression technology by making use of the magnetocaloric effect (MCE), a property which is inherent to a magnetic material. The magnetocaloric properties of a magnetic material can be manipulated as follows: When a material becomes magnetized by the adiabatic application of a magnetic field, the magnetic

entropy of the material is reduced. Since a closed system has been defined, the temperature of the material increases as a result of the increase in the lattice entropy. This portion of the cycle is analogous to the isothermal compression of a gas employed in the current vapor cycle. In the reverse process, adiabatic demagnetization of the material will increase the magnetic entropy of the material, thus leading to a decrease in the lattice entropy. The magnetic material then cools and this final loop in the closed cycle corresponds to the isothermal expansion of a gas used in the current vapor cycle.[34-36] This process is shown schematically in Figure 1.13.

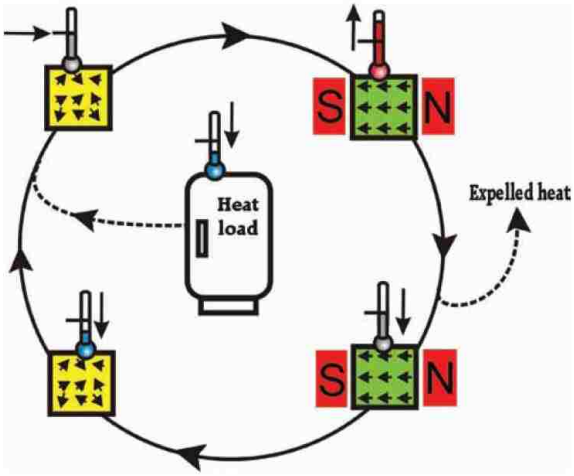

Figure 1.13 Schematic diagram of the described magnetic-refrigeration cycle. This figure was obtained from reference 36.[36]

The magnetocaloric properties of a magnetic material originate from the coupling of a magnetic field with its magnetic moments, and can be fully characterized in terms of two measurable quantities: the magnetic entropy change (ΔS_M) and the adiabatic temperature change (ΔT_{ad}). These quantities can be related to the magnetic properties of a material using the following Maxwell relations:

$$\left(\Delta S_{\mathrm{M}}\right)_T = \mu_0 \int_{\mathrm{H}_i}^{\mathrm{H}_f} \left(\frac{\partial \mathrm{M}}{\partial T}\right)_{\mathrm{H}} d\mathrm{H} \qquad (1.14)$$

$$(\Delta T_{ad}) = -\mu_0 \int_{H_i}^{H_f} \frac{T}{C_H} \left(\frac{\partial M}{\partial T} \right)_H dH \qquad (1.15)$$

A third quantity known as the refrigerant capacity (RC) has also been used to characterize the magnetocaloric properties of a material. More specifically, the RC quantifies the amount of heat that a magnetic material can absorb or dissipate during the closed loop refrigeration cycle. The RC is commonly defined in three different ways: RC can be calculated using the equality $RC = \left|\Delta S_M^{max}\right|(H) \times \delta T_{FWHM}(H)$, approximated as the area under the $\left|\Delta S_M\right|(T)$ curve between $T - \delta T_{FWHM}$ and $T + \delta T_{FWHM}$, and the RC can also be defined as the maximum value of $\left|\Delta S_M\right| \times \Delta T$ below the $\left|\Delta S_M(T)\right|$ curve. More detailed descriptions of these quantities can be found in references thirty-seven and thirty-eight.[37-38] Generally, larger magnitudes of these quantities correspond to greater cooling capacities of materials. From Equations 1.14 and 1.15 it is obvious that a material's MCE will peak near the ferromagnetic Curie temperature (T_C), decreasing below T_C because the magnetization becomes saturated, and decreasing above T_C since the susceptibility of the material decreases with increasing temperature in the paramagnetic regime.[34-36]

As far as the practical applications of magnetic refrigeration are concerned, increasing ΔH much further beyond 2 T to achieve larger ΔS_M and ΔT_{ad} values is currently unrealistic given today's state-of-the-art permanent magnets, the materials used to induce field changes in magnetocaloric materials. Therefore, current research efforts are aimed at optimizing the $(\partial M/\partial T)_H$ of existing materials and discovering new materials which exhibit a large $(\partial M/\partial T)_H$.[34-36] An ideal, commercially viable magnetocaloric material would function at ambient temperatures and exhibit a ΔT_{ad} between 40 K and 50 K.

1.2.4.3 Specific Heat Capacity, the Single Ion Kondo Effect, and the Origins of Heavy-Fermion Behavior

• Specific Heat Capacity

When a solid absorbs a small amount of heat (dQ), its temperature rises by dT. The ratio of the incremental heat (dQ) absorbed by the incremental rise in temperature (dT) is termed the *specific heat capacity*. The specific heat capacity at constant volume (V) can be mathematically expressed as follows:

$$C_V = \frac{1}{n}\frac{dQ}{dT} \tag{1.16}$$

where C_v is the specific heat capacity at constant volume, $n = N/N_A$ is the number of moles, and N_A is Avogadro's number.[30]

The molar specific heat capacity at constant volume (C_v) and low temperatures for a simple metals can be expressed by the following form:

$$C_V \approx \gamma T + \beta T^3 \tag{1.17}$$

At low temperatures, C_v is dominated by a free electron contribution (γ) which is linear in temperature (T), and a lattice or phonon contribution which is proportional to T^3. The Sommerfeld coefficient (γ) and the phonon contribution (β) can easily be determined by plotting the molar specific heat capacity at constant volume divided by temperature (C_v/T) as a function of temperature squared (T^2). If linear fits to the low temperature portion of this curve are performed, the resulting values of the intercept and slope correspond to the Sommerfeld coefficient (γ) and the phonon contribution (β), respectively.[30]

• The Single Ion Kondo Effect

The resistivity (ρ), the inverse of conductivity (σ), of metals decreases with decreasing temperature. This behavior can be explained by the reduction of populated phonon modes

(lattice vibrations) at lower temperatures. At high temperatures, higher frequency phonon modes (lattice vibrations) are populated; therefore, the free conduction electrons mean free path through a crystal lattice is perturbed as the free electrons are easily scattered at high temperatures. The number of phonon modes (lattice vibrations) populated decreases with decreasing temperature; as a result, the free electrons travel through the crystal lattice more easily. A typical resistivity (ρ) vs. temperature (T) curve for a metal is shown in Figure 1.14.[17, 30]

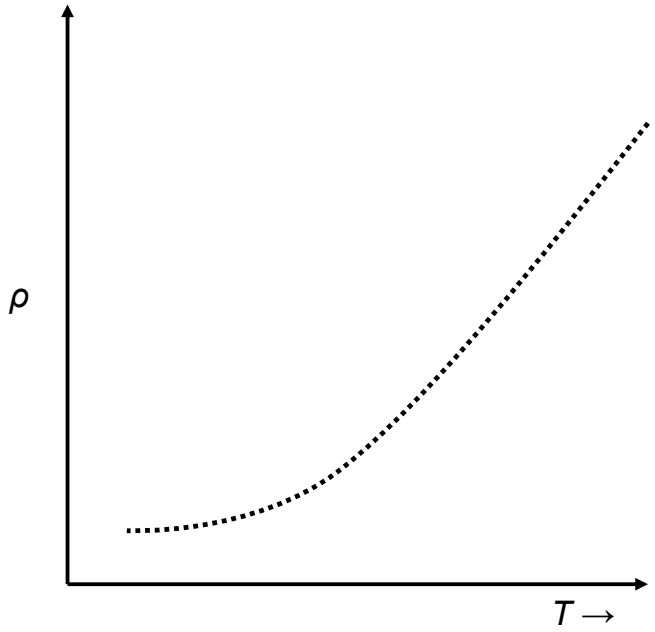

Figure 1.14 Schematic of a typical resistivity (ρ) vs. temperature (T) curve for a metal.

The magnetic interactions of dilute magnetic ions (Mn, Fe, Co…) in a non-magnetic host (Cu, Ag, Au…) can be considered negligible. Therefore, the only remaining interactions in such a system involve the magnetic moments of the magnetic ions and the free conduction electron spins. At high temperatures the magnetic moments behave similarly to free paramagnetic moments described above. Below a characteristic temperature, the Kondo temperature (T_K), the interaction between the magnetic moments and the free conduction electrons leads to the compensation or screening of the dilute magnetic moments. The compensation of the dilute

magnetic moments results from the free conduction electrons which have formed a cloud of opposite spin-polarization around each dilute magnetic moment resulting in a quasi-bound, singlet state. The compensation or screening of the dilute magnetic moments by the conduction electron is known as the *Kondo effect*. The effect has profound experimental consequences. First, the magnetic susceptibility will deviate from Curie-Weiss behavior below the Kondo temperature (T_K). Second, a local minimum in will appear in the resistivity (ρ) at low temperatures, below which the resistivity increases. A typical resistivity (ρ) vs. temperature (T) curve for a magnetically dilute alloy exhibiting the Kondo effect at low temperatures is shown in Figure 1.15.[17]

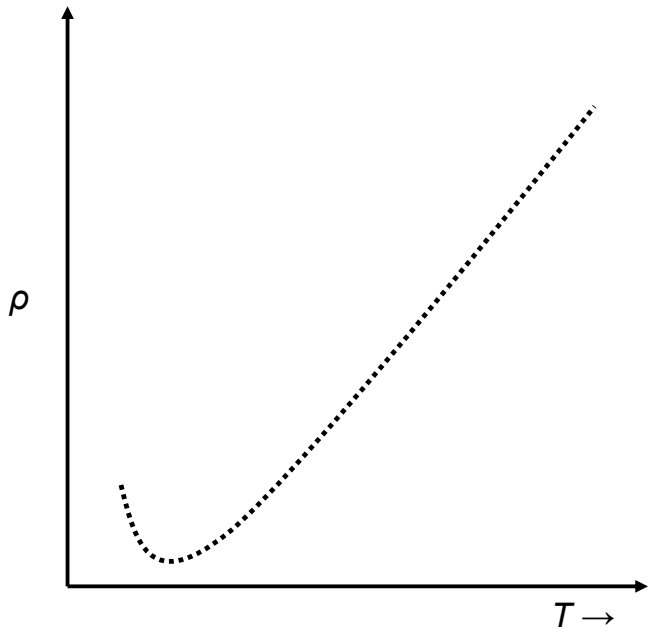

Figure 1.15 Schematic of a typical resistivity (ρ) vs. temperature (T) curve for a magnetically dilute alloy exhibiting the Kondo effect at low temperatures. Adapted from reference 17.[17]

The upturn in the resistivity (ρ) at low temperatures is a consequence of the quasi-bound state formed by the free conduction electrons. Since the spin of the free conduction electrons are quasi-bound to the spin of the dilute magnetic atoms, their movement through the crystal lattice is impeded.[17, 30] Therefore, an increase in the ρ vs. T is observed.

• The Origins of Heavy-Fermion Behavior

The occurrence of enhanced mass or heavy-fermion behavior is nearly limited to a subset of *f*-electron materials which contain the elements Ce, Yb, and U.[39-41] The "traditional mechanism" leading to the origin of heavy-fermion behavior in these systems will be discussed below. Heavy-fermion behavior has also been observed in a handful of Pr-containing intermetallics[42-43] and certain magnetically frustrated systems which are not comprised of rare-earth elements.[44] However, the origins leading to enhanced mass behavior in these systems are still under debate and will not be described here.

A visual approach is first taken to describe heavy-fermion physics. The phenomenon will be treated mathematically in the subsequent paragraph. At high temperatures the *f*-electron magnetic moments of intermetallic compounds containing Ce, Yb, and U are essentially localized.[45] This has been shown to be true time-and-time again, as heavy-fermion materials in their "normal" state exhibit Curie-Weiss magnetism.[39-41] As these materials are cooled, the localized moments are screened by the spins of the free conduction electron forming a singlet state known as an *incoherent Kondo state*.[45] A visual representation of the formation of low temperature incoherent Kondo state from the cooling of an arbitrary rare-earth (Ce or Yb) cubic system in its "normal" state is depicted below. This incoherent Kondo state is a manifestation of the Single Ion Kondo model onto a periodic lattice and is often referred to as the *Kondo Lattice Model*. The resistivity curves of magnetically dilute alloys which exhibit the Kondo effect (Figure 1.15) and heavy-fermion materials (Figure 1.18) display similar features. As the heavy-fermion materials are cooled even further, the *f*-electrons screened by the conduction electron clouds become itinerant (delocalized), and these singlet states travel through the lattice coherently.[45] A monotonic decrease in the resistivity (ρ) versus temperature (T) curve is

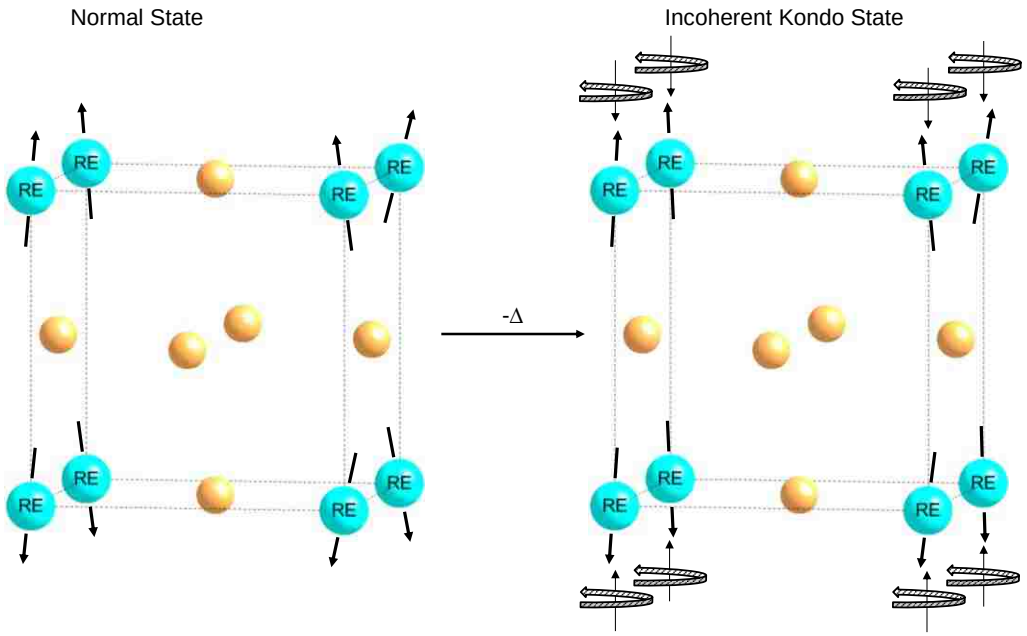

Figure 1.16 The "normal" high-temperature state (left) and the low temperature incoherent Kondo state (right) is shown above. The spins of the free conduction electrons screen the local rare-earth magnetic moments, which result in the formation of an incoherent Kondo state as the heavy-fermion material is cooled.

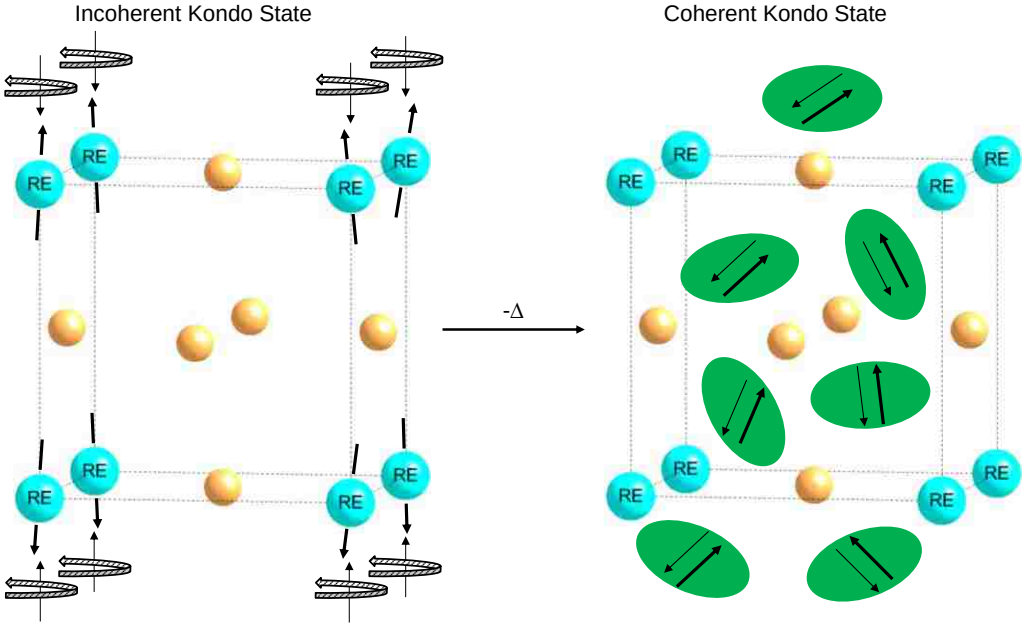

Figure 1.17 The incoherent Kondo state (left) and coherent Kondo state (right) is shown above. As the heavy-fermion materials are cooled, the *f*-electrons screened by the conduction electron clouds become itinerant (delocalized), and these singlet states travel through the lattice coherently. The figure to the right is adapted from artist renderings by Piers Coleman.[46]

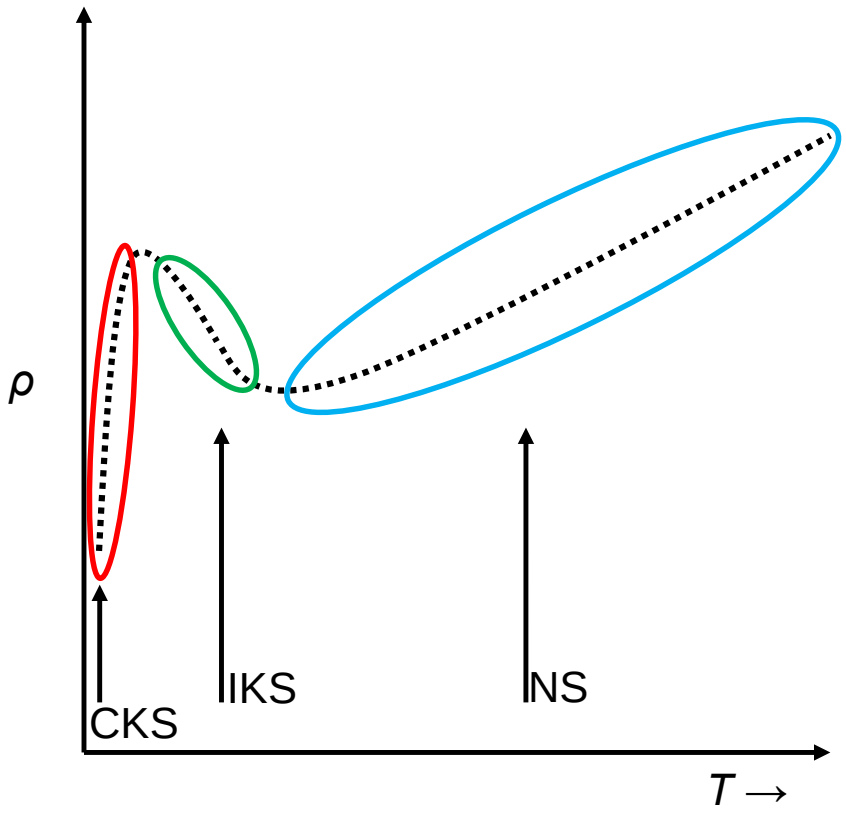

Figure 1.18 A typical resistivity curve for a heavy-fermion intermetallic material illustrating the features of the normal state (NS), incoherent Kondo state (IKS), and coherent Kondo state (CKS) is shown above.

observed below coherence temperature (T^*), and this state is called a *Kondo coherent state*. The formation of a Kondo coherent state is shown schematically in Figure 1.17. The conduction electrons behave as if their masses are greatly enhanced upon the formation of a coherent Kondo state. A typical resistivity curve for a heavy-fermion intermetallic material illustrating the features of the normal state (NS), incoherent Kondo state (IKS), and coherent Kondo state (CKS) is shown above.

Let us now examine the mathematics of heavy-fermion physics, relying on the above illustrations when needed. The mathematical expression for the energy of a free electron can be

found by solving the Schrödinger equation, and this expression is given in the following equation.

$$\varepsilon(\vec{k}) = \frac{\hbar^2 \vec{k}^2}{2\mathrm{m}^*} \tag{1.18}$$

Here $\hbar$ is Planck's constant divided by 2π, $\vec{k}$ is the wavevector of the electron, and m^* is the effective mass of the electron. When the singlet states become delocalized upon the formation of a coherent Kondo state, a narrow conduction band is formed at the Fermi level (ε_f); thus, giving rise to a large density of states (DOS) at the Fermi level. Since the DOS of states can be loosely defined as the number of states (N) per ε_f; the effective electron mass will be proportional to the DOS.

$$\mathrm{DOS}[\varepsilon(\vec{k}_f)] \approx \frac{\mathrm{N}}{\varepsilon(\vec{k}_f)} \approx \frac{\mathrm{N}2\mathrm{m}^*}{\hbar^2 \vec{k}_f^2} \tag{1.19}$$

From Equation 1.17, its was shown that the low temperature specific heat capacity at constant volume (C_v) could be described in terms of an electronic contribution (γ) and a lattice contribution (β). The Sommerfeld coefficient (γ) is proportional to the electronic DOS at the Fermi level (ε_f); and thus, is proportional to the effective electron mass.

$$\gamma \propto \mathrm{DOS}[\varepsilon(\vec{k}_f)] \approx \frac{\mathrm{N}}{\varepsilon(\vec{k}_f)} \approx \frac{\mathrm{N}2\mathrm{m}^*}{\hbar^2 \vec{k}_f^2} \tag{1.20}$$

As described above, if linear fits to the low temperature portion of the C_v/T vs. T are performed, the resulting values of the intercept and slope correspond to the Sommerfeld coefficient (γ) and the phonon contribution (β), respectively. The Sommerfeld coefficients for simple metals such as Cu are typically on the order of 1 mJ/mol K^2. Therefore, heavy-fermion materials are characterized by their large Sommerfeld coefficients which are on the order of 100 – 1000 mJ/mol K^2.[39-41]

1.3. Research Projects Summary

1.3.1. $LnFeSb_3$ (Ln = Pr, Nd, Sm, Gd, and Tb)

The low-dimensional layered $LnTSb_3$ (T = V, Cr, and Ni) phases display interesting anisotropic magnetic behavior.[47-55] To further study the magnetic properties of the $LnTSb_3$ family, single crystals of $LnFeSb_3$ (Ln = Pr, Nd, Sm, Gd, and Tb) were prepared *via* the flux-growth method. $LnFeSb_3$ (Ln = Pr, Nd, Sm, Gd, and Tb) crystallizes in the $LaPdSb_3$ structure-type with lattice parameters of $a \sim 12$ Å, $b \sim 6$ Å, and $c \sim 12$ Å.[56]

Similar to $LnTSb_3$ (T = V, Cr, and Ni), the $LnFeSb_3$ compounds display varying degrees of magnetic anisotropy. $PrFeSb_3$ and $NdFeSb_3$ are paramagnetic down to 3 K, while the rest of the analogues order antiferromagnetically at this temperature when the applied field is oriented parallel to the *a*-axis of these orthorhombic structures. When the field is applied along the *bc*-plane, antiferromagnetic order emerges around 5 K for the Pr and Nd analogues. Only weak magnetic order was observed for the Sm and Gd analogues along this field orientation. Curie-Weiss fits determined that the magnetic behavior of these compounds derives from within the Ln sublattice. It is interesting to note that the Fe-sublattice does not contribute to the magnetism.[56] The synthesis, structure, and physical properties of the $LnFeSb_3$ (Ln = Pr, Nd, Sm, Gd, and Tb) compounds will be discussed in more detail in Chapter 2.

1.3.2. $CeCo(Sb, Sn)_3$

An interesting class of Sb-containing phases is the Ce – Ni – Sb ternary intermetallics. α-$CeNiSb_3$ and β-$CeNiSb_3$ both display Kondo lattice behavior around 25 K and order ferromagnetically with $T_c \sim 6$ K.[51, 54] These properties are interesting because the occurrence of ferromagnetism in Ce-containing compounds, which display features of Kondo screening at higher temperatures may be indicative of an undercompensated or underscreened Kondo lattice.

These conditions have been predicted and experimentally shown to result in the formation of a singular Fermi liquid. [57] Additionally, the ferromagnetic transition temperature of α-$CeNiSb_3$ was found to increase under applied pressures up to 25 kbar, decrease for applied pressure greater than 25 kbar, and a second ferromagnetic ordered phase emerged between pressures of 35 kbar and 55 kbar. The existence of a quantum critical point (QCP) at $P \sim 60$ kbar was suggested due to the nearly complete suppression of the first magnetic phase and an increase in the T^2 coefficient and ρ_0 observed from fits to electrical resistivity at this pressure.[58]

More recently, $CeCoSb_3$, which adopts the $LaPdSb_3$ structure-type and is isostructural to β-$CeNiSb_3$, was prepared using a Sn flux.[59] Theoretical band-structure calculations performed by Cai *et. al.* lead the authors to conclude that the magnetic and electrical properties of $CeCoSb_3$ would be nearly identical to β-$CeNiSb_3$.[54, 59] To further extend the studies of Ce – Transition Metal – Sb phases, and having the desire to target the interesting physical properties mentioned above, we have grown this phase using a Sn flux. The synthesis, structure, and physical properties of the $CeCo(Sb, Sn)_3$ compounds will be discussed in more detail in Chapter 3.

1.3.3. $Ln_2Fe_4Sb_5$ (Ln = La – Nd, Sm)

Understanding that the Fe and Co-sublattices of the abovementioned $LnFeSb_3$ (Ln = Pr, Nd, Sm, Gd, and Tb) and $CeCo(Sb, Sn)_3$ compounds did not magnetically order even down to low temperatures was quite surprising. Using Fe, Ni, or Co to synthesize magnetic intermetallic compounds would seem to be a nontrivial task as they are ferromagnetic in there elemental states. However, the very electronegative late transition metals (T) of Ln – T – M containing compounds often become reduced by the very electropositive lanthanide, thus quenching the transition metal's magnetic moment.[60-61] Thus it stands to reason that if the transition metal units

are present in abundance with respect to the lanthanide units per given compound, then the transition metal will not contribute diamagnetically to overall magnetization.

Initially small single crystals of $Ln_2Fe_4Sb_5$ (Ln = La, Ce, Pr, Nd, and Sm) were grown from a stoichiometric melt of their constituent elements. The structures of these crystals were verified *via* single crystal X-ray diffraction. However, the small sizes of the single crystals made it impossible to measure the physical properties of these systems; thus, making it impossible to derive structure-physical property correlations. Binary phase diagrams were then studied to find an inert flux that would not react with Ln, Fe, or Sb. At high temperatures Bi does not react with these elements and reactions were conducted using the melts of Ln, Fe, Sb, and Bi from two, four, five, and ten equivalents, respectively. These reactions yielded single crystals of $Ln_2Fe_4Sb_5$ (Ln = La, Ce, Pr, Nd, and Sm) which were adequate for physical property measurements. The data obtained from the physical properties measurements for each analogue suggest spin glass behavior. The synthesis, structure, and physical properties of the $Ln_2Fe_4Sb_5$ (Ln = La, Ce, Pr, Nd, and Sm) compounds will be discussed in more detail in Chapter 4.

1.3.4. $LnCu_2(Al,Si)_5$ (Ln = La and Ce)

While exploring the Ln-Cu-Al phase space, small single crystals of $LnCu_2(Al,Si)_5$ (Ln = La and Ce) were serendipitously grown *via* the flux-growth method. The silica wool, normally used for excess flux filtration, incorporated into the structures. X-ray diffraction and Energy-Dispersive Spectroscopic (EDS) measurements revealed that these single crystals nucleate from the surfaces of $Ln(Cu,Al,Si)_4$ (Ln = La and Ce) impurities. Similar to $CePd_{1+x}Ga_{6-x}$, these phases crystallize in the $SrAu_2Ga_5$ structure-type. Knowing that $CePd_{1+x}Ga_{6-x}$ exhibited heavy-fermion behavior, attempts to prepare the nearly isovalent $LnCu_2(Al,Si)_5$ (Ln = La and Ce) compounds on a larger scale for physical properties measurements were undertaken.[62]

Buttons of $LnCu_2(Al,Si)_5$ (Ln = La and Ce) were prepared *via* arc-melting. These buttons were subsequently annealed at 750ºC for three weeks. Rietveld refinements were employed to model the X-ray powder diffraction. Physical property measurements were conducted on the remaining portions of the buttons. No Magnetic ordering was observed for $CeCu_2(Al,Si)_5$ down to 2.25 K. Fits to the heat capacity of $CeCu_2(Al,Si)_5$ did not provide evidence for enhanced electron mass behavior. The synthesis, structure, and physical properties of the $LnCu_2(Al,Si)_5$ (Ln = La and Ce) compounds will be discussed in more detail in Chapter 5.

1.3.5. $Ln(Cu,Al,Ga)_{13}$ (Ln = La, Ce, Pr, and Eu)

The large sizes of single crystals of $Ln(Cu,Al,Ga)_{13}$ (Ln = La, Ce, Pr, and Eu) synthesized using both Al and Ga as metallic fluxes were adequate for single-crystal neutron diffraction experiments. These diffraction experiments were performed using the TOPAZ beamline at the Spallation Neutron Source (SNS) located at Oak Ridge National Laboratory (ORNL). The disorder of the 8*b* and 96*i* Wyckoff sites of $Ln(Cu,Al,Ga)_{13}$ (Ln = La, Ce, Pr, and Eu) could not fully elucidated due do the similar X-ray form factors and small differences of the neutron scattering lengths of Cu and Ga.

$Eu(Cu,Al,Ga)_{13}$ and $Eu(Cu,Al)_{13}$ order ferromagnetically at ~6 K and ~8 K, respectively. Since $La(Fe,Si)_{13}$ orders ferromagnetically, exhibits a giant magnetocaloric effect close to room temperature, and is isostructural to $Eu(Cu,Al,Ga)_{13}$ and $Eu(Cu,Al)_{13}$; the magnetocaloric properties of $Eu(Cu,Al,Ga)_{13}$ and $Eu(Cu,Al)_{13}$ were studied.[63] The thermodynamic properties of $Pr(Cu,Al,Ga)_{13}$ are very interesting. The Sommerfeld coefficient for $Pr(Cu,Al,Ga)_{13}$ (γ ~ 350 mJ/mol-K^2) is large compared to simple metals like Cu. Only a handful of Pr compounds are known to exhibit heavy-fermion behavior.[64] The synthesis, structure, and physical properties of

the $Ln(Cu,Al,Ga)_{13}$ (Ln = La, Ce, Pr, and Eu) compounds will be discussed in more detail in Chapter 6.

1.4 References

1. Feder, T., US Condensed-Matter Community Grapples with Availability of Crystalline Samples. *Phys. Today* **2007**, *60*, 26-28.

2. The National Academies Press: Washington, D. C., Frontiers in Crystalline Matter: from Discovery to Technology, Commitee for an Assesment and Outlook for New Materials Synthesis and Crystal Growth. National Academies Press: Washington, D.C., 2009.

3. Phelan, W. A.; Menard, M. C.; Kangas, M. J.; McCandless, G. T.; Drake, B. L.; Chan, J. Y., Adventures in Crystal Growth: Synthesis and Characterization of Single Crystals of Complex Intermetallic Compounds. *Chem. Mater.* **2012**, *24*, 409-420.

4. Nakatsuji, S.; Nambu, Y.; Tonomura, H.; Sakai, O.; Jonas, S.; Broholm, C.; Tsunetsugu, H.; Qiu, Y. M.; Maeno, Y., Spin Disorder on a Triangular Lattice. *Science* **2005**, *309*, 1697-1700.

5. Kamihara, Y.; Hiramatsu, H.; Hirano, M.; Kawamura, R.; Yanagi, H.; Kamiya, T.; Hosono, H., Iron-Based Layered Superconductor: LaOFeP. *J. Am. Chem. Soc.* **2006**, *128*, 10012-10013.

6. Coleman, P.; Schofield, A. J., Quantum Criticality. *Nature* **2005**, *433*, 226-229.

7. Canfield, P. C.; Fisk, Z., Growth of Single Crystals from Metallic Fluxes. *Philos. Mag. B.* **1992**, *65*, 1117-1123.

8. Janssen, Y.; Angst, M.; Dennis, K. W.; McCallum, R. W.; Canfield, P. C., Differential Thermal Analysis and Solution Growth of Intermetallic Compounds. *J. Cryst. Growth* **2005**, *285*, 670-680.

9. Phelan, W. A.; Kangas, M. J.; Drake, B. L.; Zhao, L. L.; Wang, J. K.; DiTusa, J. F.; Morosan, E.; Chan, J. Y., Crystal Growth, Structure, and Physical Properties of $LnCu_2(Al,Si)_5$ (Ln = La and Ce). *Inorg. Chem.* **2011**, *51*, 920-927.

10. Drake, B. L.; Kangas, M. J.; Capan, C.; Haldolaarachchige, N.; Xiong, Y.; Adams, P. W.; Young, D. P.; Chan, J. Y., Crystal Growth, Structure, and Physical Properties of Ln(Ag, Al, Si)$_2$ (Ln = Ce and Gd). *J. Phys.: Condens. Matter* **2010**, *22*, 426002.

11. Kanatzidis, M. G.; Pottgen, R.; Jeitschko, W., The Metal Flux: A PreparativeTool for the Exploration of Intermetallic Compounds. *Angew. Chem. Int. Ed.* **2005**, *44*, 6996-7023.

12. Als-Nielsen, J.; McMorrow, D., *Elements of Modern X-ray Physics*. Wiley: New York, 2001.

13. Cullity, B. D., *Elements of X-ray Diffraction*. 2d ed.; Addison-Wesley Pub. Co.: Reading, Mass., 1978.

14. Wenk, H.-R., *Neutron Scattering in Earth Sciences*. Mineralogical Society of America: Chantilly, Va., 2006.

15. http://neutrons.ornl.gov/facilities/HFIR/techparameters.shtml.

16. Pynn, R., Neutron Scattering: A Primer. Los Almos National Laboratory: 1989.

17. Blundell, S., *Magnetism in Condensed Matter*. Oxford University Press: Oxford ; New York, 2001.

18. Stout, G. H.; Jensen, L. H., *X-ray Structure Determination: A Practical Guide*. Macmillan: New York, 1968.

19. Bacon, G. E.; Lonsdale, K., *Neutron Diffraction*. *Rep. Prog. Phys* **1953**, *16*, 1-61.

20. Chatterji, T., *Neutron Scattering from Magnetic Materials*. 1st ed.; Elsevier: Amsterdam ; Boston, 2006; p xi, 559 p.

21. Liang, L.; Rinaldi, R.; Schober, H., Neutron Applications in Earth, Energy and Environmental sciences. In *Neutron Scattering Applications and Techniques.* [Online] Springer: New York, NY, 2009.

22. Van Hove, L., Correlations in Space and Time and Born Approximation Scattering in Systems of Interacting Particles. *Phys. Rev.* **1954**, *95*, 249.

23. International Union of Crystallography., *International Tables for X-ray Crystallography*. Kynoch Press: Birmingham, Eng.,, 1968.

24. http://www.ncnr.nist.gov/resources/n-lengths/.

25. Halpern, O.; Johnson, M. H., On the Magnetic Scattering of Neutrons. *Phys. Rev.* **1939**, *55*, 0898-0923.

26. Izyumov, Y. A., The Neutron-Diffraction Analysis of the Crystal Magnetic Structures. *Uspekhi Fizicheskikh Nauk* **1980**, *131*, 387-422.

27. Shull, C. G.; Smart, J. S., Detection of Antiferromagnetism by Neutron Diffraction. *Phys. Rev.* **1949**, *76*, 1256-1257.

28. Shull, C. G.; Strauser, W. A.; Wollan, E. O., Neutron Diffraction by Paramagnetic and Antiferromagnetic Substances. *Phys. Rev.* **1951**, *83*, 333-345.

29. West, A. R., *Basic Solid State Chemistry*. 2nd ed.; John Wiley & Sons: New York, 1999.

30. Gersten, J. I.; Smith, F. W., *The Physics and Chemistry of Materials*. John Wiley: New York, 2001.

31. Moessner, R.; Ramirez, A. R., Geometrical Frustration. *Phys. Today* **2006**, *59*, 24-29.

32. Ramirez, A. P., Strongly Geometrically Frustrated Magnets. *Ann. Rev. Mater. Sci.* **1994**, *24*, 453-480.

33. Greedan, J. E., Geometrically Frustrated Magnetic Materials. *J. Mater. Chem* **2001**, *11*, 37-53.

34. Gschneidner, K. A.; Pecharsky, V. K., Magnetocaloric Materials. *Annu. Rev. Mater. Sci.* **2000**, *30*, 387-429.

35. Pecharsky, V. K.; Gschneidner, K. A., Advanced Magnetocaloric Materials: What Does the Future Hold? *Int. J. Refrig.* **2006**, *29*, 1239-1249.

36. Gutfleisch, O.; Willard, M. A.; Bruck, E.; Chen, C. H.; Sankar, S. G.; Liu, J. P., Magnetic Materials and Devices for the 21st Century: Stronger, Lighter, and More Energy Efficient. *Adv. Mater.* **2011**, *23*, 821-842.

37. Gorria, P.; Llamazares, J. L. S.; Alvarez, P.; Perez, M. J.; Marcos, J. S.; Blanco, J. A., Relative Cooling Power Enhancement in Magneto-Caloric Nanostructured Pr_2Fe_{17}. *J. Phys. D: Appl. Phys.* **2008**, *41*.

38. Alvarez, P.; Gorria, P.; Sanchez Llamazares, J. L.; Perez, M. J.; Franco, V.; Reiffers, M.; Curlik, I.; Gazo, E.; Kovac, J.; Blanco, J. A., Magnetic Properties and Magneto-Caloric Effect in Pseudo-Binary Intermetallic $(Ce,R)_2Fe_{17}$ compounds (R = Y, Pr and Dy). *Intermetallics* **2011**, *19*, 982-987.

39. Fisk, Z.; Hess, D. W.; Pethick, C. J.; Pines, D.; Smith, J. L.; Thompson, J. D.; Willis, J. O., Heavy-Electron Metal - New Highly Correlated States of Matter. *Science* **1988**, *239*, 33-42.

40. Fisk, Z.; Ott, H. R.; Rice, T. M.; Smith, J. L., Heavy-Electron Metals. *Nature* **1986**, *320*, 124-129.

41. Fisk, Z.; Sarrao, J. L.; Smith, J. L.; Thompson, J. D., The Physics and Chemistry of Heavy Fermions. *Proc. Natl. Acad. Sci. U.S.A.* **1995**, *92*, 6663-6667.

42. Yatskar, A.; Beyermann, W. P.; Movshovich, R.; Canfield, P. C., Possible Correlated-Electron Behavior from Quadrupolar Fluctuations in $PrInAg_2$. *Phys. Rev. Lett.* **1996**, *77*, 3637-3640.

43. Bauer, E. D.; Frederick, N. A.; Ho, P. C.; Zapf, V. S.; Maple, M. B., Superconductivity and Heavy Fermion Behavior in $PrOs_4Sb_{12}$. *Phys. Rev. B* **2002**, *65*, 100506.

44. D.C, J., Heavy fermion behaviors in LiV_2O_4. *Physica B* **2000**, *281-282*, 21-25.

45. Shishido, H.; Shibauchi, T.; Yasu, K.; Kato, T.; Kontani, H.; Terashima, T.; Matsuda, Y., Tuning the Dimensionality of the Heavy Fermion Compound $CeIn_3$. *Science* **2010**, *327*, 980-983.

46. http://www.physics.rutgers.edu/~coleman/.

47. Hartjes, K.; Jeitschko, W.; Brylak, M., Magnetic Properties of the Rare-Earth Transition Metal Antimonides $LnVSb_3$ and $LnCrSb_3$ (Ln=La-Nd, Sm). *J. Magn. Magn. Mater.* **1997**, *173*, 109-116.

48. Jackson, D. D.; Torelli, M.; Fisk, Z., Anisotropy in Magnetic and Transport Properties of $LaTSb_3$ (T = Cr, V). *Phys. Rev. B* **2002**, *65*, 014421.

49. Jackson, D. D.; Fisk, Z., Anisotropy in Magnetic and Transport Properties of $SmTSb_3$ (T = Cr, V). *J. Magn. Magn. Mater.* **2003**, *256*, 106-116.

50. Jackson, D. D.; Fisk, Z., Anisotropy in Magnetic and Transport Properties of $GdCrSb_3$. *J. Alloys Compd.* **2004**, *377*, 243-247.

51. Macaluso, R. T.; Wells, D. M.; Sykora, R. E.; Albrecht-Schmitt, T. E.; Mar, A.; Nakatsuji, S.; Lee, H.; Fisk, Z.; Chan, J. Y., Structure and electrical resistivity of $CeNiSb_3$. *J. Solid State Chem.* **2004**, *177*, 293-298.

52. Crerar, S. J.; Deakin, L.; Mar, A., Structure and Physical Properties of Ternary Antimonide $YbCrSb_3$. *Chem. Mater.* **2005**, *17*, 2780-2784.

53. Thomas, E. L.; Macaluso, R. T.; Lee, H. O.; Fisk, Z.; Chan, J. Y., Crystal Growth, Characterization, and Physical Properties of $PrNiSb_3$, $NdNiSb_3$, and $SmNiSb_3$. *J. Solid State Chem.* **2004**, *177*, 4228-4236.

54. Thomas, E. L.; Gautreaux, D. P.; Lee, H. O.; Fisk, Z.; Chan, J. Y., Discovery of β-$LnNiSb_3$ (Ln = La, Ce): Crystal Growth, Structure, and Magnetic and Transport Behavior. *Inorg. Chem.* **2007**, *46*, 3010-3016.

55. Sefat, A. S.; Bud'ko, S. L.; Canfield, P. C., Magnetization, Resistivity, and Heat Capacity of the Anisotropic $RVSb_3$ Crystals (R=La-Nd, Sm, Gd-Dy). *J. Magn. Magn. Mater.* **2008**, *320*, 120-141.

56. Phelan, W. A.; Nguyen, G. V.; Karki, A. B.; Young, D. P.; Chan, J. Y., Synthesis, Structure, Magnetic and Transport Properties of $LnFeSb_3$ (Ln = Pr, Nd, Sm, Gd, and Tb) -Tuning of Anisotropic Long-Range Magnetic Order as a Function of Ln. *Dalton Trans.* **2010**, *39*, 6403-6409.

57. Perkins, N. B.; Iglesias, J. R.; Nunez-Regueiro, M. D.; Coqblin, B., Coexistence of Ferromagnetism and Kondo Effect in the Underscreened Kondo Lattice. *EPL-Europhys. Lett.* **2007**, *79*, 57006.

58. Sidorov, V. A.; Bauer, E. D.; Lee, H.; Nakatsuji, S.; Thompson, J. D.; Fisk, Z., Complex Magnetic Phase Diagram of Ferromagnetic $CeNiSb_3$. *Phys. Rev. B* **2005**, *71*, 094422.

59. Cai, W.-Z.; Wu, L.-M.; Li, L.-H.; Chen, L., Syntheses, Structures, and Theoretical Studies of New Ternary Antimonides β-*RE*$CoSb_3$ (*RE* = La-Nd, Sm). *Eur. J. Inorg. Chem.* **2009**, *2009*, 230-237.

60. Francisco, M. C.; Malliakas, C. D.; Piccoli, P. M. B.; Gutmann, M. J.; Schultz, A. J.; Kanatzidis, M. G., Development and Loss of Ferromagnetism Controlled by the Interplay of Ge Concentration and Mn Vacancies in Structurally Modulated $Y_4Mn_{1-x}Ga_{12-y}Ge_y$. *J. Am. Chem. Soc.* **2010**, *132*, 8998-9006.

61. Papoian, G. A.; Hoffmann, R., Hypervalent Bonding in One, Two, and Three Dimensions: Extending the Zintl-Klemm Concept to Nonclassical Electron-Rich Networks. *Angew. Chem. Int. Ed.* **2000**, *39*, 2409-2448.

62. Tobash, P. H.; Ronning, F.; Thompson, J. D.; Bobev, S.; Bauer, E. D., Magnetic Order and Heavy Fermion Behavior in $CePd_{1+x}Al_{6-x}$: Synthesis, Structure, and Physical Properties. *J. Solid State Chem.* **2010**, *183*, 707-711.

63. Jia, L.; Sun, J. R.; Shen, J.; Gao, B.; Zhao, T. Y.; Zhang, H. W.; Hu, F. X.; Shen, B. G., Influence of Interstitial and Substitutional Atoms on the Crystal Structure of $La(FeSi)_{13}$. *J. Alloys Compd.* **2011**, *509*, 5804-5809.

64. Cho, J. Y.; Thomas, E. L.; Nambu, Y.; Capan, C.; Karki, A. B.; Young, D. P.; Kuga, K.; Nakatsuji, S.; Chan, J. Y., Crystal Growth, Structure, and Physical Properties of $Ln(Cu,Ga)_{13-x}$ (Ln = La-Nd, Eu; $x \approx 0.2$). *Chem. Mater.* **2009**, *21*, 3072-3078.

Chapter 2. Synthesis, Structure, Magnetic and Transport Properties of $LnFeSb_3$ (Ln = Pr, Nd, Sm, Gd, and Tb) –Tuning of Anisotropic Long-Range Magnetic Order as a Function of Ln*

2.1 Introduction

Lanthanide transition metal antimonides, Ln-T-Sb, display a wide variety of interesting geometric bonding networks and physical properties. For example, the Zintl phases $Eu_{14}MnSb_{11}$ and $Yb_{14}MnSb_{11}$ exhibit colossal magnetoresistance and a high thermoelectric figure of merit, *ZT*, at high temperature, respectively.[1-2] $PrOs_4Sb_{12}$, the first Pr-based heavy-fermion intermetallic, was found to be superconducting with T_c = 1.85 K.[3]

The layered $LnTSb_3$ (T = V, Cr, and Ni) family of compounds display interesting anisotropic magnetic behavior. Compounds crystallizing in the $CeCrSb_3$ structure type, $LnCrSb_3$ (Ln = La-Nd, Sm), [a ~ 13, b ~ 6, c ~ 6 Å, Z = 4] have moderate ferromagnetic ordering temperatures (Curie temperatures), T_C ~ 105-125 K, which result from the ordering of the Cr sublattice. Susceptibility data for the Ce, Pr, Nd, and Sm analogues show an additional antiferromagnetic transition, $T_N \leq 30$ K, due to the Ln^{3+} ions.[4-6] The Tb and Dy analogues exhibit only antiferromagnetic ordering below 17 K, while the Gd analogue shows antiferromagnetic and ferrimagnetic transitions at T_N = 26 K and T_C ~ 90 K, respectively.[7-9] The lanthanide contraction presumably leads to the shift from ferromagnetic to antiferromagnetic ordering.[5, 7] However, $YbCrSb_3$ has the highest ferromagnetic ordering temperature within this family of compounds (T_C ~ 280 K), where the Yb ions are in their nonmagnetic divalent (Yb^{2+}) state.[10]

The replacement of Cr with Ni led to the discovery of two new related polymorphs. α-$CeNiSb_3$ [a = 12.6340(7), b = 6.2037(3), c = 18.3698(9) Å, and Z = 12] and β-$CeNiSb_3$ [a = 12.9170(2), b = 6.1210(5), c = 12.0930(6) Å, and Z = 8] both display Kondo lattice behavior and

*Apapted with permission of The Royal Society of Chemistry: Phelan, W. A.; Nguyen, G. V.; Karki, A. B.; Young, D. P.; Chan, J. Y., Synthesis, Structure, Magnetic and Transport Properties of $LnFeSb_3$ (Ln = Pr, Nd, Sm, Gd, and Tb) -Tuning of Anisotropic Long-Range Magnetic Order as a Function of Ln. *Dalton Trans.* **2010**, *39*, 6403-6409.

ferromagnetic order *ca*. T_C ~ 6 K.[11-13] Flux-growth synthesis methods using Sb and Sn were used to prepare both α-$CeNiSb_3$ and β-$CeNiSb_3$, respectively.[11, 13] The α-$CeNiSb_3$ structure type is known to exist for Ln = La, Ce, Pr, Nd, and Sm, whereas, the β-$CeNiSb_3$ structure, which adopts the $LaPdSb_3$ structure type, exists for Ln = La, Ce, Pr, Nd, Sm, Gd, and Tb.[12-15] The Ln^{3+} sublattice orders antiferromagnetically below 5 K in α-$LnNiSb_3$ (Ln = Pr, Nd, and Sm) compounds, however, β-$LnNi(Sn,Sb)_3$ (Ln = Pr, Nd, Sm, Gd, and Tb) compounds do not magnetically order down to 2 K.[12, 15]

To further study the magnetic properties of the $LnTSb_3$ family, the growth of single crystals of $LnFeSb_3$ was performed *via* the flux growth method. Iron was the chosen transition metal, because we wanted to study the role of Fe in an intermetallic system with a lanthanide sublattice. Furthermore, metallic iron is a known ferromagnet, and these magnetic properties can extend to intermetallics composed of iron. Using the flux growth method, single crystals of $LnFeSb_3$ (Ln = Pr, Nd, Sm, Gd, and Tb) were prepared. Herein, we report the synthesis, structure, magnetic, and transport properties of these intermetallic compounds.

2.2 Experimental

2.2.1 Synthesis

Single crystals of $LnFeSb_3$ (Ln = Pr, Nd, Sm, Gd, and Tb) were synthesized *via* the flux-growth method from excess Sb. These phases were prepared by placing Pr-Tb (99.9%), along with Fe powder (99.998%), and Sb shot (99.9999%) (all purchased from Alfa Aesar) into 2-mL alumina crucibles in a 1:2:20 molar ratio of Ln:Fe:Sb. The crucibles were topped with quartz wool, and the reaction vessels were sealed into separate evacuated fused-silica tubes. The ampoules were heated to 1373 K and held constant for 12 h and then cooled at a rate of 5 K h^{-1} to 913 K. After dwelling at 913 K for 12 h, the excess Sb was separated from single crystals by

Table 2.1 Crystallographic data for $LnFeSb_3$ (Ln = Pr, Nd, Sm, Gd, and Tb)

	$PrFeSb_3$	$NdFeSb_3$	$SmFeSb_3$	$GdFeSb_3$	$TbFeSb_3$
formula weight	562.01	565.34	571.45	578.35	580.02
space group	*Pbcm*	*Pbcm*	*Pbcm*	*Pbcm*	*Pbcm*
crystal system	orthorhombic	orthorhombic	orthorhombic	orthorhombic	orthorhombic
a (Å)	12.7490(2)	12.6790(2)	12.54900(10)	12.4700(2)	12.3920(2)
b (Å)	6.1730(4)	6.1630(3)	6.1440(4)	6.1350(4)	6.1220(4)
c (Å)	12.1590(5)	12.1370(3)	12.0910(4)	12.0640(4)	12.0230(4)
V (Å^3)	956.91(7)	948.39(5)	932.23(7)	922.94(7)	912.11(7)
Z	8	8	8	8	8
Temperature/K	298(5)	298(5)	298(5)	298(5)	298(5)
coll. reflections	2532	3918	2511	2531	2496
ind. reflections	1433	2157	1417	1409	1400
goodness of fit on F_o^2	1.25	1.12	1.19	1.16	1.13
R_{int}	0.025	0.035	0.019	0.037	0.037
$R_1(F)$ for $F_o^2 > 2\sigma(F_o^2)$[a]	0.035	0.038	0.030	0.029	0.058
$R_w(F_o^2)$[b]	0.104	0.113	0.082	0.071	0.163
$\Delta\rho_{max}$ (e Å^3)	2.219	3.922	3.595	1.821	4.899
$\Delta\rho_{min}$ (e Å^3)	-2.824	-3.653	-3.493	-2.841	-8.530

[a] $R_1(F) = \sum ||F_o| - |F_c|| / \sum |F_o|$
[b] $R_w(F_o^2) = [\sum[w(F_o^2 - F_c^2]^2] / \sum w(F_o^2)^2]^{1/2}$

centrifugation. Thin, shiny, black plate-like crystals with dimensions up to 0.10 x 0.20 x 4.5 mm^3 were mechanically extracted. The surfaces of all the crystals were observed to be clean with little evidence of flux contamination. No signs of surface oxidation were observed when the crystals were exposed to air and moisture over a period of months. Attempts to prepare a nonmagnetic analogue, $LnFeSb_3$ (Ln = La and Y), and smaller lanthanide analogues, $LnFeSb_3$ (Ln = Eu and Dy-Yb), proved unsuccessful.

2.2.2 Single – Crystal X-ray Diffraction

Plate-shaped single crystals of $PrFeSb_3$, $NdFeSb_3$, $SmFeSb_3$, $GdFeSb_3$, and $TbFeSb_3$ were each mounted onto separate glass fiber tips of a goniometer with epoxy and placed on a Nonius

Table 2.2 Atomic positions, Wyckoff sites, and U_{eq} for $LnFeSb_3$ (Ln = Pr, Nd, Gd, and Tb)

Atom	Wyckoff Site	x	y	z	U_{eq}[a]
Pr1	4*c*	0.69967(5)	¼	0	0.00728(18)
Pr2	4*d*	0.30688(5)	0.27533(10)	¾	0.00710(18)
Fe1	8*e*	0.10037(9)	0.03820(19)	0.86031(9)	0.0092(3)
Sb1	4*c*	0.97171(6)	¼	0	0.0085(2)
Sb2	4*d*	0.78166(6)	0.26514(11)	¾	0.0079(2)
Sb3	8*e*	0.50269(4)	0.51195(8)	0.87671(4)	0.00806(18)
Sb4	4*c*	0.22097(6)	¼	0	0.0077(2)
Sb5	4*d*	0.93925(5)	0.89587(11)	¾	0.0085(2)
Nd1	4*c*	0.69957(4)	¼	0	0.00772(12)
Nd2	4*d*	0.30703(4)	0.27582(8)	¾	0.00757(12)
Fe1	8*e*	0.10107(7)	0.03803(15)	0.86044(7)	0.00936(17)
Sb1	4*c*	0.97164(5)	¼	0	0.00897(14)
Sb2	4*d*	0.78036(5)	0.26467(9)	¾	0.00830(13)
Sb3	8*e*	0.50275(3)	0.51211(7)	0.87662(3)	0.00848(12)
Sb4	4*c*	0.22219(5)	¼	0	0.00809(13)
Sb5	4*d*	0.93923(4)	0.89557(9)	¾	0.00888(13)
Sm1	4*c*	0.69930(4)	¼	0	0.00576(14)
Sm2	4*d*	0.30726(4)	0.27661(9)	¾	0.00569(14)
Fe1	8*e*	0.10261(8)	0.03777(17)	0.86050(9)	0.0085(2)
Sb1	4*c*	0.97152(5)	¼	0	0.00695(17)
Sb2	4*d*	0.77789(5)	0.26395(10)	¾	0.00601(16)
Sb3	8*e*	0.50292(3)	0.51195(7)	0.87647(3)	0.00609(15)
Sb4	4*c*	0.22480(5)	¼	0	0.00588(16)
Sb5	4*d*	0.93895(5)	0.89540(10)	¾	0.00688(17)
Gd1	4*c*	0.69917(4)	¼	0	0.00822(13)
Gd2	4*d*	0.30761(4)	0.27811(9)	¾	0.00822(13)
Fe1	8*e*	0.10361(9)	0.03721(18)	0.86072(9)	0.0115(2)
Sb1	4*c*	0.97146(5)	¼	0	0.00932(17)
Sb2	4*d*	0.77617(6)	0.26331(11)	¾	0.00852(16)
Sb3	8*e*	0.50319(4)	0.51259(8)	0.87641(4)	0.00842(14)
Sb4	4*c*	0.22661(6)	¼	0	0.00832(16)
Sb5	4*d*	0.93905(5)	0.89508(11)	¾	0.00939(17)
Tb1	4*c*	0.69903(7)	¼	0	0.0081(3)
Tb2	4*d*	0.30763(7)	0.27854(14)	¾	0.0083(3)
Fe1	8*e*	0.10468(14)	0.0375(3)	0.86064(14)	0.0113(4)
Sb1	4*c*	0.97121(9)	¼	0	0.0095(3)
Sb2	4*d*	0.77482(10)	0.26277(17)	¾	0.0087(3)
Sb3	8*e*	0.50330(6)	0.51265(13)	0.87632(5)	0.0086(3)
Sb4	4*c*	0.22806(10)	¼	0	0.0088(3)

[a]U_{eq} is defined as one-third of the trace of the orthogonalized Uij tensor.

Table 2.3 Selected interatomic distances (Å) and angles (º) for $LnFeSb_3$ (Ln = Pr, Nd, Sm, Gd, and Tb)

	PrFeSb3	NdFeSb3	SmFeSb3	$GdFeSb_3$	$TbFeSb_3$
Bond					
Ln1-Sb1	3.4683(9)	3.4496(7)	3.4161(8)	3.3955(8)	3.3728(13)
Ln1-Sb2 (x 2)	3.2158(3)	3.2038(3)	3.1807(3)	3.1662(3)	3.1500(5)
Ln1-Sb3 (x 2)	3.3259(7)	3.3125(5)	3.2878(6)	3.2729(6)	3.2571(10)
Ln1-Sb3 (x 2)	3.3420(7)	3.3285(5)	3.3007(6)	3.2849(6)	3.2680(9)
Ln1-Sb4 (x 2)	3.2481(4)	3.2372(3)	3.2163(3)	3.2041(3)	3.1916(5)
Ln2-Sb2	3.2274(9)	3.2101(7)	3.1792(8)	3.1548(9)	3.1356(13)
Ln2-Sb2	3.3456(9)	3.3394(7)	3.3261(8)	3.3266(9)	3.3188(13)
Ln2-Sb3 (x 2)	3.2771(7)	3.2620(5)	3.2338(6)	3.2160(6)	3.1999(10)
Ln2-Sb3 (x 2)	3.3033(7)	3.2893(6)	3.2644(6)	3.2474(7)	3.2320(10)
Ln2-Sb4 (x 2)	3.2348(4)	3.2232(3)	3.1992(3)	3.1853(3)	3.1682(5)
Ln2-Sb5	3.2249(9)	3.2084(7)	3.1747(8)	3.1586(8)	3.1342(13)
Sb3-Sb3	3.0024(9)	2.9995(7)	2.9917(8)	2.9870(9)	2.9791(13)
Sb3-Sb3	3.0815(9)	3.0735(7)	3.0583(8)	3.0501(9)	3.0375(13)
Sb3-Sb3	3.0873(2)	3.08227(15)	3.0729(2)	3.0685(2)	3.0621(2)
Fe-Sb1	2.6257(12)	2.6211(10)	2.6146(11)	2.6085(12)	2.6059(19)
Fe-Sb1	2.6990(12)	2.6960(9)	2.6928(11)	2.6913(12)	2.6898(18)
Fe-Sb2	2.6272(13)	2.6259(10)	2.6199(12)	2.6182(12)	2.613(2)
Fe-Sb4	2.6379(12)	2.6333(9)	2.6261(11)	2.6230(12)	2.6147(18)
Fe-Sb5	2.6058(12)	2.6034(10)	2.6016(12)	2.5991(12)	2.6007(19)
Fe-Sb5	2.6323(13)	2.6293(11)	2.6239(12)	2.6245(13)	2.617(2)
Fe-Fe	2.683(2)	2.6809(18)	2.672(2)	2.672(2)	2.660(3)
Angle					
Sb3-Sb3-Sb3	87.15(2)	87.117(16)	87.153(17)	86.997(18)	86.98(3)
Sb3-Sb3-Sb3	90.0	90.0	90.0	90.0	90.0
Sb3-Sb3-Sb3	90.0	90.0	90.0	90.0	90.0
Sb3-Sb3-Sb3	92.79(2)	92.822(16)	92.779(17)	92.924(18)	92.94(3)
Sb5-Fe-Sb1	80.13(4)	80.05(3)	79.81(3)	79.69(3)	79.44(6)
Sb5-Fe-Sb5	82.49(3)	82.36(3)	82.14(3)	81.90(3)	81.85(5)
Sb5-Fe-Sb2	88.41(4)	88.40(3)	88.51(4)	88.54(4)	88.61(6)
Sb5-Fe-Sb4	91.39(4)	91.46(3)	91.56(3)	91.62(4)	91.70(6)
Sb1-Fe-Sb2	95.50(4)	95.55(3)	95.65(4)	95.77(4)	95.66(7)
Sb1-Fe-Sb4	97.08(4)	97.21(3)	97.42(4)	97.67(4)	97.76(6)
Sb2-Fe-Sb4	108.24(5)	108.22(4)	108.19(4)	108.15(4)	108.20(7)
Sb2-Fe-Sb5	112.82(4)	112.87(3)	113.07(4)	113.16(4)	113.38(7)
Sb1-Fe-Sb5	146.18(5)	145.96(4)	145.49(5)	145.10(5)	144.86(8)
Sb5-Fe-Sb4	163.34(5)	163.36(4)	163.28(5)	163.31(5)	163.18(8)

Kappa CCD X-ray diffractometer (Mo Kα radiation, λ = 0.71073 Å). Data collections for all compounds were performed at room temperature and the crystallographic parameters are listed in Table 2.1. The orthorhombic Laue symmetry *mmm* and the systematic absences obtained led to the initial space group selection of *Pbma*, which transformed to the standard setting of *Pbcm* (No. 57). The generation of the initial structural model and further refinement were conducted using SIR97 and SHELX97, respectively.[16-17] After the refinement of all the atomic positions, the collected data were corrected for absorption, and the displacement parameters were refined as anisotropic. Weighting and extinction schemes were applied during the final stages of refinement. Atomic coordinates and anisotropic displacements are provided in Table 2.2. Selected interatomic distances and angles for $PrFeSb_3$, $NdFeSb_3$, $SmFeSb_3$, $GdFeSb_3$, and $TbFeSb_3$ are provided in Table 2.3.

2.2.3 Physical Properties Measurements

Magnetization data for all compounds were obtained using a 9-Tesla Quantum Design Physical Property Measurement System (PPMS). The temperature-dependent magnetization data for $PrFeSb_3$, $NdFeSb_3$, $GdFeSb_3$ and $TbFeSb_3$ were obtained under zero-field cooled (ZFC) conditions from T = 2 to 280 K and from T = 3 to 50 K with an applied field of 0.1 T parallel to the *a*-axis and the *bc*-plane, respectively. Temperature-dependent magnetization data for $SmFeSb_3$ were obtained under zero-field cooled conditions over the same temperature ranges but with an applied field of 1 T. Field-dependent measurements for all analogues were collected at T = 3 K for fields between 0 and 9 T oriented parallel to the *a*-axis. The temperature-dependent electrical resistivity (T = 2 to 290 K) and magnetoresistance (MR) (at T = 3 K and up to H = 9 T) were measured by a standard four-probe ac-technique using the PPMS. Pt wires with a diameter of 1 mil were attached to each sample with silver epoxy.

2.3 Results and Discussion

2.3.1 Structure and Synthesis

$LnFeSb_3$ (Ln = Pr, Nd, Sm, Gd, and Tb) adopts the $LaPdSb_3$ structure type with lattice parameters *a*~12 Å, *b*~6 Å, and *c*~12 Å.[14] The $LaPdSb_3$ structure type is similar to the $CeCrSb_3$ and α-$CeNiSb_3$ structure types.[11, 18] As shown in Figure 2.1, $PrFeSb_3$ can be viewed as being built up by inserting Pr atoms between a layer of Fe-centered octahedra, $^2_\infty[FeSb_2]$, and a distorted square net composed of Sb atoms, $^2_\infty[Sb]$. A host of Sb-Sb interactions within the $^2_\infty[FeSb_2]$ layers have been omitted for clarity.

$PrFeSb_3$ contains two crystallographically inequivalent Pr atoms with slightly different coordination environments. The Pr1 atoms are surrounded by 8 Sb atoms, adopting a square antiprismatic geometry, where 4 atoms of the $^2_\infty[Sb]$ layer form a square base, and 4 Sb atoms from the $^2_\infty[FeSb_2]$ layer form a square directly above, but twisted 45° with respect to the square of the $^2_\infty[Sb]$ layer. The Pr2 atoms are surrounded by 9 Sb atoms and adopt a monocapped square antiprismatic geometry with an additional Sb5 atom capping a second square formed by the $^2_\infty[FeSb_2]$ layer. The Sb1 atom in the capping position of Pr1 is considered too far from the Pr1 atom for any considerable bonding interactions.

The two crystallographically inequivalent Pr atoms in α-$PrNiSb_3$ have identical coordination geometries with Pr1 being bonded to 4 Sb1, 2 Sb2, 2 Sb4, and 1 Sb6 atoms and Pr2 being bonded to 2 Sb1, 1 Sb2, 2 Sb3, 3 Sb4, and 1 Sb5 atoms.[12] $PrVSb_3$ and $PrCrSb_3$ contain one crystallographically equivalent Pr atom surrounded by 9 Sb atoms and adopt a monocapped square antiprism.[18] In $PrFeSb_3$, the Pr1-Sb distances of 3.2158(3)-3.3420(7) Å and the Pr2-Sb distances of 3.2249(9)-3.3456(9) Å are within the range of the Pr1-Sb distances of 3.2141(8)-

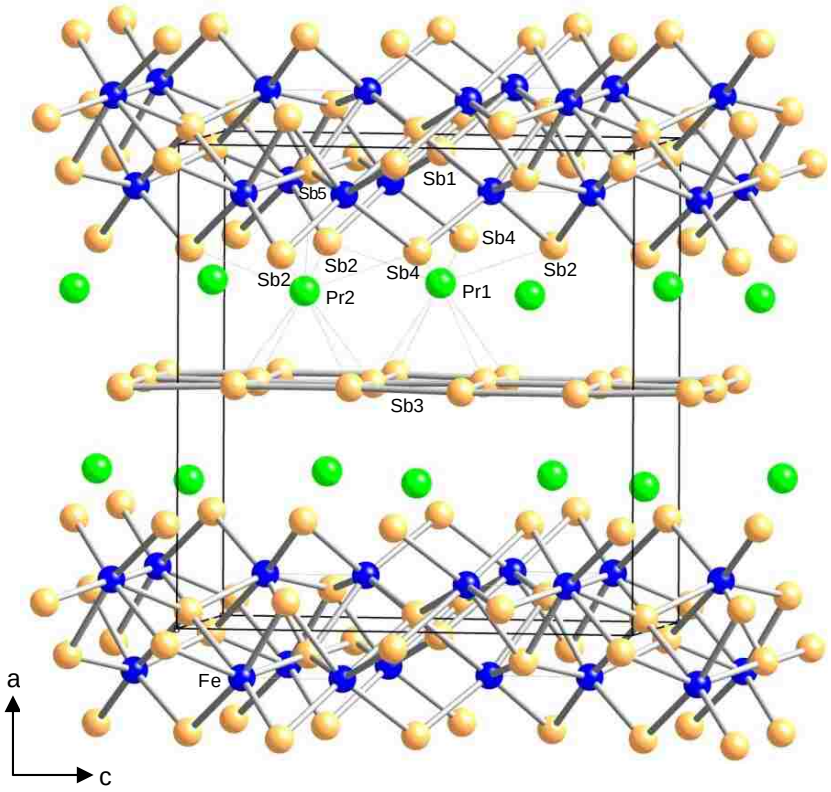

Figure 2.1 Crystal structure of $PrFeSb_3$.

3.309(1) Å and Pr2-Sb distances of 3.2174(7)-3.4384(9) Å in α-$PrNiSb_3$, and to the Pr1-(Sn,Sb) distances of 3.2074(3)-3.3408(15) Å and Pr2-(Sn,Sb) distances of 3.198(4)-3.326(4) Å in $PrNi(Sn,Sb)_3$.[12, 15]

The $^2_\infty[FeSb_2]$ octahedra are edge-sharing in the [010] and edge- and face-sharing in the [001] directions. The Fe-Sb distances of $PrFeSb_3$ range from 2.6058(12)-2.6990(12) Å which are slightly longer but comparable to the Fe-Sb distances of the $FeSb_6$ octahedra in $FeSb_2$, which range from 2.5762(6)-2.6164(11) Å.[19-20]

The main structural distinction between $PrCrSb_3$, α-$PrNiSb_3$, and $PrFeSb_3$ lies in the packing of the $^2_\infty[TSb_2]$ octahedral layer along the *c*-axis. The $^2_\infty[CrSb_2]$ octahedra in $PrCrSb_3$ are edge-sharing in the [010] direction and face-sharing in the [001].[18] The $^2_\infty[NiSb_2]$ octahedra in α-$PrNiSb_3$ are edge-sharing in the [010] direction and both edge- and face-sharing in the [001]

direction, with two distinct types of edge-sharing in [001], resulting in an approximate tripling of its *c*-lattice parameter, 18.36706(6) Å, compared to 6.0738(7) Å in $PrCrSb_3$.[12, 18] The $^2_\infty[FeSb_2]$ octahedra in $PrFeSb_3$ are edge-sharing in [010], whereas they are face-sharing, with every other octahedron sharing edges in [001]. This gives rise to an approximate doubling of the *c*-lattice parameter, 12.1590(5)Å, compared to $PrCrSb_3$. The angles between the Fe and Sb atoms diverge considerably from the ideal 90°. Furthermore, Fe-Fe interactions are present at the adjourning octahedral faces with a distance of 2.683(2) Å.

The Sb3 atoms in $PrFeSb_3$ form the $^2_\infty[Sb]$ nets, while both Sb1 and Sb3 atoms interact to form the $^2_\infty[Sb]$ nets in α-$PrNiSb_3$. The Sb-Sb distances in $PrFeSb_3$ range from 3.0024(9)-3.0873(2) Å and are shorter in comparison to the Sb-Sb distance in α-$PrNiSb_3$, which range from 3.0606(7)-3.1021(2) Å.[12] These distances are comparable to the Sb-Sb distance of 2.908-3.355 Å in elemental antimony.[21] Note the distortion of the $^2_\infty[Sb]$ is more pronounced in α-$PrNiSb_3$ with bond angles ranging from 84.945(13)°-94.953(13)° in comparison to the bond angles of $PrFeSb_3$, which range from 87.15(2)°-92.79(2)°.

As mentioned above, attempts to prepare nonmagnetic or smaller lanthanide analogues proved unsuccessful, yielding only $FeSb_2$ and LnSb (Ln = Y, Dy, Ho, Er, Tm, and Yb) binaries. It is again worth noting that β-$LnNi(Sn,Sb)_3$ structures only exist when Ln = La, Ce, Pr, Nd, Sm, Gd, and Tb.[15] It is interesting to note the Tb analogue is the end member for the isostructural β-$LnNi(Sn,Sb)_3$ and $LnFeSb_3$ (Ln = Pr, Nd, Sm, Gd, and Tb) compounds. This suggests that Tb is the lower limit of stability for this structure type. A decrease in the lattice volume consistent with the lanthanide contraction is observed within each series of compounds. Ln1-Sb3 (Ln = Pr, Nd, Sm, Gd, and Tb) and Ln1-(Sn,Sb)3 distances as a function of Ln^{3+} ionic radii are plotted in Figure 2.2. The same trend is observed in both series of compounds, where the distances

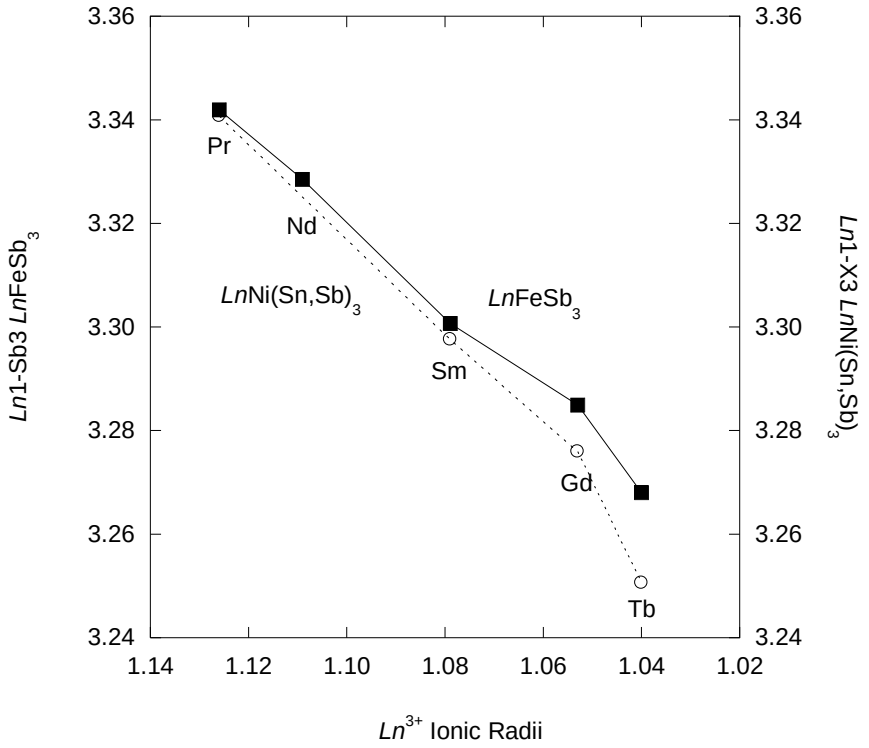

Figure 2.2 Ln1-Sb3 (Ln = Pr, Nd, Sm, Gd, and Tb) and Ln1-(Sn, Sb)3 distances plotted as a function of Ln^{3+} ionic radii for $LnFeSb_3$ and β-$LnNi(Sn,Sb)_3$.

between the Ln1 atoms and the Sb or (Sn,Sb) nets decrease with decreasing ionic radii. It has been proposed that the substitution of smaller lanthanides within the β-$LnNi(Sn,Sb)_3$ series leads to the destabilization of the structure due to the increasing strain and angle distortion as a result of the decreasing Ln1-(Sn,Sb)3 and (Sn,Sb)3-(Sn,Sb)3 distances.[15] Furthermore, physical property measurements for $TbNi(Sn,Sb)_3$ were not conducted because of low product yield. Table 2.3 and Figure 2.2 illustrate that the Ln1-Sb3 and Sb3-Sb3 distances across the series for $LnFeSb_3$ are correspondingly longer than the Ln1-(Sn,Sb)3 and (Sn,Sb)3-(Sn,Sb)3 distances for β-$LnNi(Sn,Sb)_3$. These longer distances could help stabilize $TbFeSb_3$, ultimately leading to a greater yield and adequate crystal sizes needed for physical property measurements.

The stability of the $LnTSb_3$ (T = V, Cr, Fe, and Ni) structures may also be rationalized based on the preparation procedure and the given transition metal. For example experiments

were undertaken to convert α-$CeNiSb_3$ to β-$CeNiSb_3$. This conversion was successful when crystals of α-$CeNiSb_3$ (initially grown from an antimony flux.) were seeded with Sn flux and spun at 573 K. Furthermore, arc-melting elemental Ce, Ni, and Sb using the proper ratios yielded α-$CeNiSb_3$. These results seem to suggest that the α-$CeNiSb_3$ and β-$CeNiSb_3$ phases are thermodynamically and kinetically stable phases, respectively.[13] While the title compounds were grown using an Sb flux, the α-$PrFeSb_3$ and α-$NdFeSb_3$ phases were originally prepared via arc-melting.[22-24] These results also suggest that the alpha and beta polymorphs are dependent on the synthetic methods, and the transition metal determines the structural adoption.

2.3.2 Physical Properties

As stated above, magnetic anisotropy is a common theme within the $LnTSb_3$ (T = V, Cr, and Ni) family of compounds.[6, 9, 12, 25] Figure 2.3a and 2.3b show the temperature-dependent magnetic susceptibility with the applied magnetic field parallel to the *a*-axis and the *bc*-plane for crystals of $LnFeSb_3$ (Ln = Pr, Nd, Sm, Gd, and Tb), respectively. The magnetic susceptibility data in Figure 2.3a were collected over a complete temperature range (2 – 280 K) in order to accurately calculate the magnetic moments recovered *via* Curie-Weiss fitting in the paramagnetic region. The magnetic susceptibility data in Figure 2.3b, with the field applied parallel to the *bc*-plane, were collected from 2 – 50 K in order to check for magnetic anisotropy.

$PrFeSb_3$ and $NdFeSb_3$ do not appear to order down to 2 and 3 K, respectively, when the field is oriented parallel to the *a*-axis. Cusps in the susceptibility data where the magnetic field is applied along the *a*-axis indicate antiferromagnetic transitions with corresponding Néel temperatures of 3.1, 7.3, and 8.6 K for $SmFeSb_3$, $GdFeSb_3$ and $TbFeSb_3$, respectively. The effective magnetic moments from high-temperature modified Curie-Weiss fitting, $\chi = \chi_o + C/(T + \theta)$, are 3.37, 3.45, 0.71, 8.24, and 9.78 μ_B for $PrFeSb_3$, $NdFeSb_3$, $SmFeSb_3$, $GdFeSb_3$, and

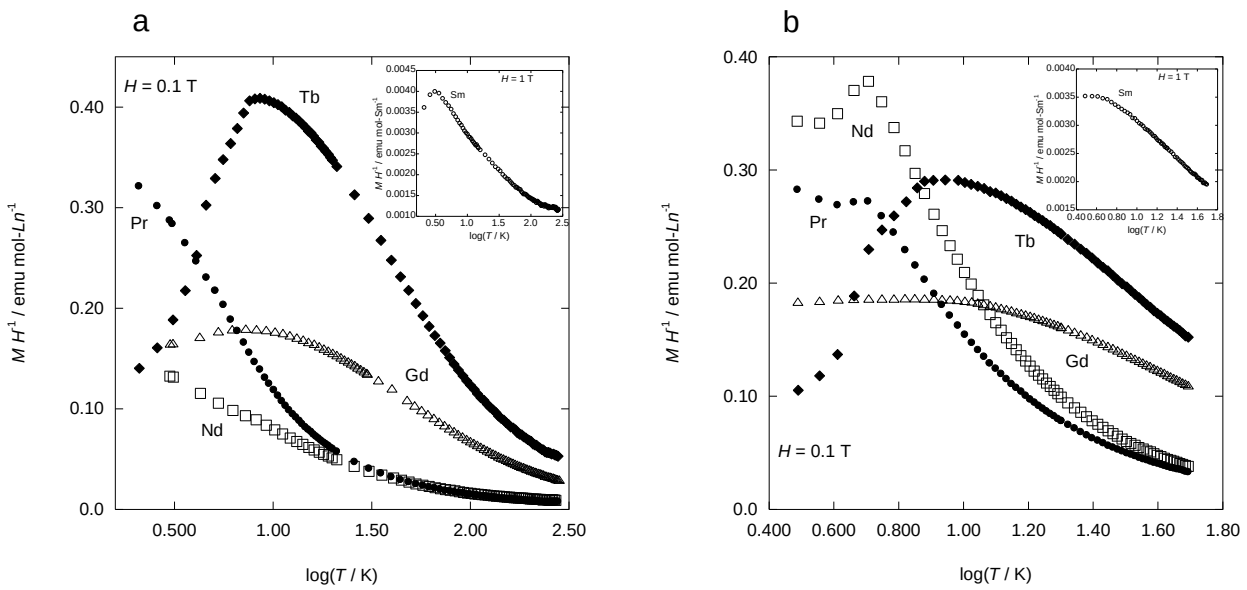

Figure 2.3 (a) Zero field-cooled magnetic susceptibility vs. log(*T* / K) for crystals of $LnFeSb_3$ (Ln = Pr, Nd, Sm, Gd, and Tb), where the field is applied parallel to the *a*-axis. **(b)** Zero field-cooled magnetic susceptibility vs. log(*T* / K) for crystals of $LnFeSb_3$ (Ln = Pr, Nd, Sm, Gd, and Tb), where the field is applied parallel to the *bc*-plane.

$TbFeSb_3$, respectively. These experimental effective magnetic moments differ slightly from, but are close to the Pr^{3+}, Nd^{3+}, Sm^{3+}, Gd^{3+}, and Tb^{3+} free ion values, as shown in Table 2.4. The negative Weiss constants, θ, for $SmFeSb_3$, $GdFeSb_3$, and $TbFeSb_3$ are suggestive of antiferromagnetic correlations. The negative Weiss constants for $PrFeSb_3$ and $NdFeSb_3$ suggest that antiferromagnetic correlations exist in these compounds as well, and they may order magnetically below the base temperature of the magnetometer. It should be noted that the large positive χ_o terms obtained from the high-temperature modified Curie-Weiss fitting are consistent for metallic, magnetic systems.

Figure 2.3b highlights the magnetic anisotropy in this system, as antiferromagnetic ordering *ca.* 5 K is observed for $PrFeSb_3$ and $NdFeSb_3$ when the field is oriented parallel to the *bc*-plane. Weak or partial ordering in $SmFeSb_3$ and $GdFeSb_3$ is evidenced by the broad maximum in the data at low temperature. This is in stark contrast to the obvious Néel transitions

Table 2.4 Summary of the magnetic properties of $LnFeSb_3$ (Ln = Pr, Nd, Sm, Gd, and Tb) where the magnetic field was oriented parallel to the *a*-axis

	$PrFeSb_3$	$NdFeSb_3$	$SmFeSb_3$	$GdFeSb_3$	$TbFeSb_3$
H / T	0.1	0.1	1	0.1	0.1
Fit Region	53 - 240 K	83 - 223 K	41 - 159 K	151 - 282 K	104 - 278 K
μ_{calc} / μ_B	3.58	3.62	0.84	7.94	9.72
μ_{exp} / μ_B	3.37(0.10)	3.45(0.49)	0.71(0.02)	8.24(0.55)	9.78(1.32)
Ms_{calc} / μ_B	3.2	3.3	2.1	7.0	9.0
Ms / μ_B	1.3	1.4	-	-	-
χ_0	0.00181(14)	0.00385(56)	0.00091(27)	0.00242(41)	0.00951(14)
T_N / K	-	-	3.1	7.3	8.6
θ	-7.77(1.40)	-18.52(8.68)	-20.27(4.61)	-29.09(2.64)	-4.26(3.19)
dG	0.8	1.84	4.46	15.75	10.50

observed in Figure 2.3a, where the magnetic field was applied along the *a*-axis. Magnetic anisotropy is not observed for $TbFeSb_3$, where the Néel temperature of 8.8 K is almost identical to that found in Figure 2.3a.

Figure 2.4 shows the magnetization data with respect to the applied magnetic field parallel to the *a*-axis for all analogues. The *M* vs. *H* curves for $PrFeSb_3$ and $NdFeSb_3$ are linear up to about 1 T and start to saturate at higher fields, indicative of paramagnetic behavior. The magnetization of $SmFeSb_3$ and $GdFeSb_3$ correspond to antiferromagnetic behavior and do not saturate up to 9 T. For $TbFeSb_3$ the magnetization with the applied magnetic field is linear with the field up to about 1.5 T. Above this field, the magnetization deviates from linearity and increases rapidly, typical of a metamagnetic transition, but does not saturate up to 9 T. This behavior resembles that of a spin-flop transition, where the antiferromagnetic alignment is partially broken under the applied magnetic field.

Lanthanide magnetic interactions are often described by the Ruderman-Kittel-Kasuaya-Yosida (RKKY) mechanism. This indirect magnetic interaction allows the localized lanthanide *f*-electrons to magnetically couple via the conduction electrons. Table 2.4 and Figure 2.5 show

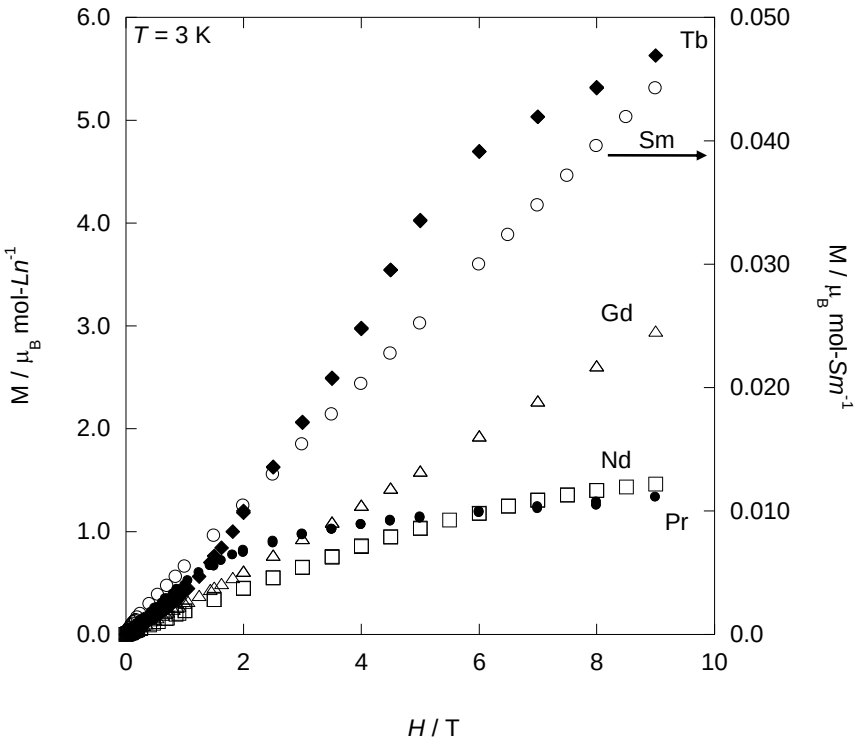

Figure 2.4 Magnetization (*M*) vs. applied Field (*H*) for crystals of $PrFeSb_3$, $NdFeSb_3$, $SmFeSb_3$, $GdFeSb_3$, and $TbFeSb_3$ at $T = 3$ K parallel to the *a*-axis.

that the Weiss constants for $LnFeSb_3$ (Ln = Pr, Nd, Sm, Gd, and Tb) scale with the de Gennes factor, $dG = (g_j - 1)^2 J(J + 1)$, which indicates that the magnetic interactions between these 4*f* moments can be attributed to the RKKY mechanism. RKKY exchange accounted for the magnetic interactions of La^{3+}- and Gd^{3+}-doped samples of $LnCrSb_3$ (Ln = La, Pr, Sm, and Gd), where the ordering temperatures of the Ln sublattice scaled with the de Gennes factor.[26]

The resistivity as a function of temperature for $LnFeSb_3$ (Ln = Pr, Nd, Sm, Gd, and Tb) is shown in Figure 2.6. The electric current was applied parallel to the *bc*-plane of the crystals. All analogues display metallic behavior. $PrFeSb_3$, $NdFeSb_3$, and $TbFeSb_3$ show kinks near their Néel temperatures. These kinks correspond to the antiferromagnetic order observed for these analogues when the applied magnetic field is oriented parallel to the *bc*-plane, whereby the onset of ordering reduces the spin-disorder scattering of electrons, which causes a drop in the

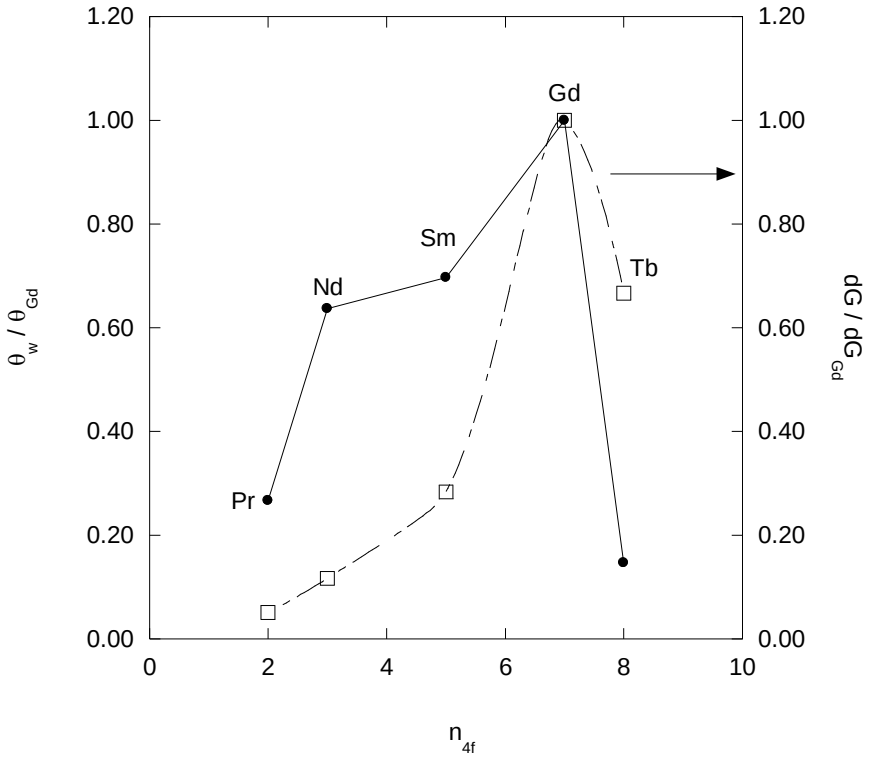

Figure 2.5 Normalized Weiss constants (Solid line) and de Gennes factor (dash line) as a function of the number of 4f electrons.

resistance. The small maximum observed in the resistivity of $PrFeSb_3$ near 80 K was reproducible, but its origin is unknown.

The magnetoresistance (MR) as a function of field for $LnFeSb_3$ (Ln = Pr, Nd, Sm, Gd, and Tb) is shown in Figure 2.7. The electric current and the magnetic field were applied parallel to the *bc*-plane and the *a*-axis of the crystals, respectively. $SmFeSb_3$ and $TbFeSb_3$ exhibit small positive MR that saturates in a field below 2 T. $PrFeSb_3$, $NdFeSb_3$ and $GdFeSb_3$ exhibit large positive MR. The MR for $GdFeSb_3$ starts to saturate in a field above 2 T, reaching a maximum value *ca.* 30%. The MR for $NdFeSb_3$ and $PrFeSb_3$ appear not to completely saturate up to a field of 9 T reaching a maximum value *ca.* 70% and 160%, respectively. The MR is not proportional to H^2, suggesting nonclassical behavior. The larger positive non-saturating MR of $PrFeSb_3$ and $NdFeSb_3$ can be attributed to the weaker magnetic spin-interactions of the local 4*f* moments

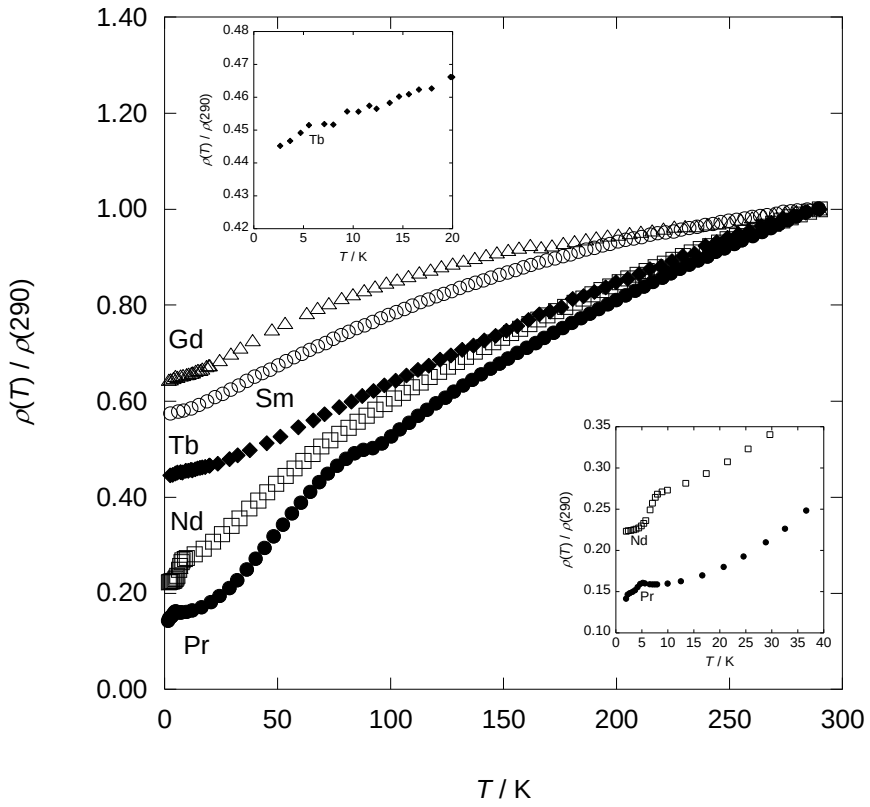

Figure 2.6 Temperature-dependent resistivity for crystals of $PrFeSb_3$, $NdFeSb_3$, $SmFeSb_3$, $GdFeSb_3$, and $TbFeSb_3$.

along the *a*-axis compared to $SmFeSb_3$, $GdFeSb_3$ and $TbFeSb_3$. The disordered spins of the local 4*f* moments tend to act as scattering centers and will impede the flow of the conduction electrons. Since $SmFeSb_3$, $GdFeSb_3$ and $TbFeSb_3$ order at $T \geq 3$ K the ordered local 4*f* moments tend to impede the flow of conduction electrons to a lesser extent, consequently resulting in lower MR values compared to $PrFeSb_3$ and $NdFeSb_3$. Large positive non-saturating MR has been observed in other antimonide compounds which contain similar structural networks, such as $LnSb_2$ (Ln = La, Pr, Sm, Nd).[27-28]

2.4 Conclusions

In summary, five new compounds of the composition $LnFeSb_3$ (Ln = Pr, Nd, Sm, Gd, and Tb) have been synthesized via the flux-growth method. All five compounds are isostructural to

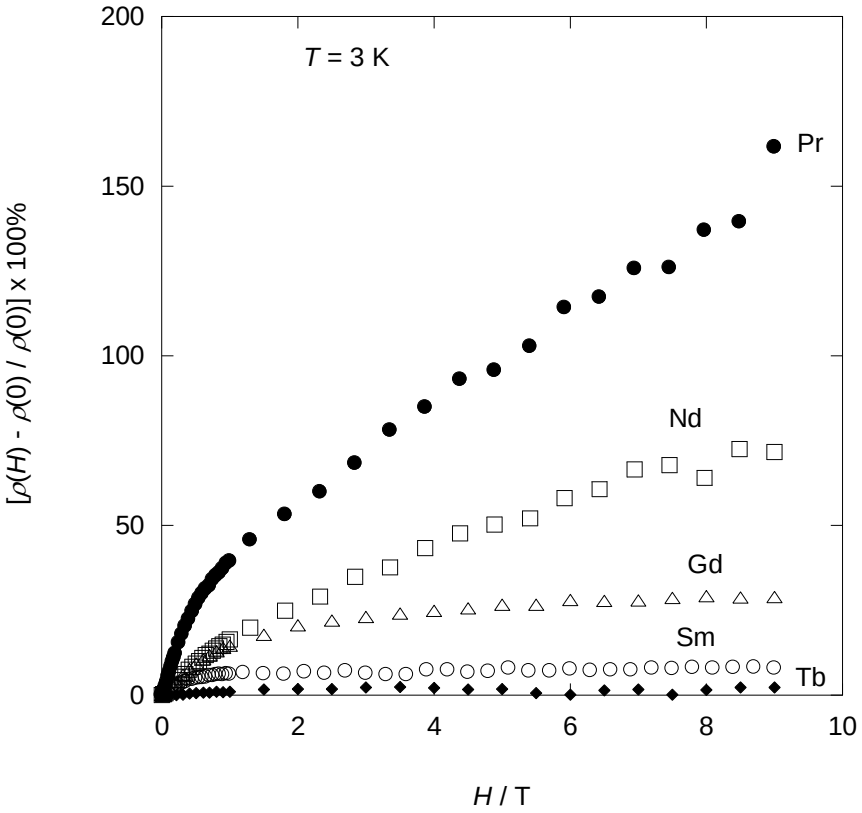

Figure 2.7 Magnetoresistance vs. H / T for crystals of $PrFeSb_3$, $NdFeSb_3$, $SmFeSb_3$, $GdFeSb_3$, and $TbFeSb_3$. The magnetic field was applied parallel to the *a*-axis.

$LaPdSb_3$ with the Ln^{3+} interleaved between Fe-centered octahedra, $^{2}_{\infty}[FeSb_2]$, and a nearly square net composed of Sb atoms, $^{2}_{\infty}[Sb]$. The lanthanide contraction is observed in the lattice parameters and the bond distances for Ln = Pr, Nd, Sm, Gd, and Tb, are as expected.

With the exception of $TbFeSb_3$, all analogues exhibit magnetic anisotropy. The fitted lanthanide effective moments are close to those expected for their free ion values. The magnetic anisotropy exhibited by these analogues accounts for the observed transport properties. The resistivity as a function of temperature indicates that all analogues exhibit metallic behavior. Perhaps one of the more notable features is the large positive non-saturating MR for the $PrFeSb_3$, $GdFeSb_3$, and $NdFeSb_3$.

The magnetic structures of these compounds are unknown at this time. The negative Weiss constants suggest that antiferromagnetic order occurs between the nearest-neighbors within a single plane of lanthanide ions. Elastic neutron scattering experiments would be interesting to perform in order to determine how the magnetic structure varies across this series of compounds.

2.5 References

1. Chan, J. Y.; Kauzlarich, S. M.; Klavins, P.; Shelton, R. N.; Webb, D. J., Colossal Magnetoresistance in the Transition-Metal Zintl Compound $Eu_{14}MnSb_{11}$. *Chem. Mater.* **1997**, *9*, 3132-3135.

2. Kauzlarich, S. M.; Brown, S. R.; Snyder, G. J., Zintl Phases for Thermoelectric Devices. *Dalton Transactions* **2007**, 2099-2107.

3. Bauer, E. D.; Frederick, N. A.; Ho, P. C.; Zapf, V. S.; Maple, M. B., Superconductivity and Heavy Fermion Behavior in $PrOs_4Sb_{12}$. *Phys. Rev. B* **2002**, *65*, 1-5.

4. Raju, N. P.; Greedan, J. E.; Ferguson, M. J.; Mar, A., $LaCrSb_3$: A New Itinerant Electron Ferromagnet with a Layered Structure. *Chem. Mater.* **1998**, *10*, 3630-3635.

5. Hartjes, K.; Jeitschko, W.; Brylak, M., Magnetic Properties of the Rare-Earth Transition Metal Antimonides $LnVSb_3$ and $LnCrSb_3$ (Ln=La-Nd, Sm). *J. Magn. Magn. Mater.* **1997**, *173*, 109-116.

6. Jackson, D. D.; Fisk, Z., Anisotropy in Magnetic and Transport Properties of $SmTSb_3$ (T = Cr, V). *J. Magn. Magn. Mater.* **2003**, *256*, 106-116.

7. Leonard, M.; Saha, S.; Ali, N., Magnetic Properties of $RTSb_3$. *J. Appl. Phys* **1999**, *85*, 4759-4761.

8. Deakin, L.; Mar, A., Magnetic Properties and Magnetoresistance of $GdCrSb_3$. *Chem. Mater.* **2003**, *15*, 3343-3346.

9. Jackson, D. D.; Fisk, Z., Anisotropy in Magnetic and Transport Properties of $GdCrSb_3$. *J. Alloys Compd.* **2004**, *377*, 243-247.

10. Crerar, S. J.; Deakin, L.; Mar, A., Structure and Physical Properties of Ternary Antimonide $YbCrSb_3$. *Chem. Mater.* **2005**, *17*, 2780-2784.

11. Macaluso, R. T.; Wells, D. M.; Sykora, R. E.; Albrecht-Schmitt, T. E.; Mar, A.; Nakatsuji, S.; Lee, H.; Fisk, Z.; Chan, J. Y., Structure and Electrical Resistivity of $CeNiSb_3$. *J. Solid State Chem.* **2004**, *177*, 293-298.

12. Thomas, E. L.; Macaluso, R. T.; Lee, H. O.; Fisk, Z.; Chan, J. Y., Crystal Growth, Characterization and Physical Properties of $PrNiSb_3$, $NdNiSb_3$, and $SmNiSb_3$. *J. Solid State Chem.* **2004**, *177*, 4228-4236.

13. Thomas, E. L.; Gautreaux, D. P.; Lee, H. O.; Fisk, Z.; Chan, J. Y., Discovery of β-$LnNiSb_3$ (Ln = La, Ce): Crystal Growth, Structure, and Magnetic and Transport Behavior. *Inorg. Chem.* **2007**, *46*, 3010-3016.

14. Thomas, E. L.; Gautreaux, D. P.; Chan, J. Y., The Layered Intermetallic Compound $LaPdSb_3$. *Acta Crystallogr. Sect. E. Struct. Rep. Online* **2006**, *62*, I96-I98.

15. Gautreaux, D. P.; Capan, C.; DiTusa, J. F.; Young, D. P.; Chan, J. Y., Synthesis, Structure and Physical Properties of $LnNi(Sn,Sb)_3$ (Ln = Pr, Nd, Sm, Gd, Tb). *J. Solid State Chem.* **2008**, *181*, 1977-1982.

16. Altomare, A.; Burla, M. C.; Camalli, M.; Cascarano, G. L.; Giacovazzo, C.; Guagliardi, A.; Moliterni, A. G. G.; Polidori, G.; Spagna, R., SIR97: A New Tool for Crystal Structure Determination and Refinement. *J. Appl. Crystallogr.* **1999**, *32*, 115-119.

17. Sheldrick, G. M., *In SHELXL-97, Program for Refinement of Crystal Structures*. University of Göttingen: Göttingen, Germany: 1997.

18. Brylak, M.; Jeitschko, W., Ternary Antimonides $LnTSb_3$ with Ln = La-Nd, Sm and T=V,Cr. *Naturforsch., B* **1995**, *50*, 899-904.

19. Holseth, H.; Kjekshus, A., Compound with Marcasite Type Crystal Structure .4. Crystal Structure of $FeSb_2$. *Acta Chem Scand* **1969**, *23*, 3043-3050.

20. Holseth, H.; Kjekshus, A.; Andresen, A. F., Compounds with Marcasite Type Crystal Structure .6. Neutron Diffraction Studies of $CrSb_2$ and $FeSb_2$. *Acta Chem Scand* **1970**, *24*, 3309-3316.

21. Donohue, J., *The Structures of the Elements*. Wiley: New York,, 1974; p xi, 436 p.

22. Chykhrij, S.; Smetana, V., Phase Relations in the Pr-Fe-Sb and Pr-Co-Sb Systems. *Inorg. Mater.* **2006**, *42*, 503-507.

23. Liu, J.; Liu, W.; Zong, B.; Wang, L.; Cui, X.; Li, J., Phase Relationships in the Pr-Fe-Sb System at 773 K. *J. Alloys Compd.* **2008**, *456*, 101-104.

24. Zeng, L. M.; Qin, P. L.; Nong, L. Q.; Zhang, J. L.; Liao, J. P., The 773 K Isothermal Section of the Nd-Fe-Sb Ternary System. *J. Alloys Compd.* **2007**, *437*, 84-86.

25. Jackson, D. D.; Torelli, M.; Fisk, Z., Anisotropy in Magnetic and Transport Properties of $LaTSb_3$ (T = Cr, V). *Phys. Rev. B.* **2002**, *65*, 014421.

26. Jackson, D. D.; Fisk, Z., Effect of Rare-Earth Doping in $RCrSb_3$ (R = La, Pr, Sm, and Gd). *Phys. Rev. B* **2006**, *73*, 024421-7.

27. Young, D. P.; Goodrich, R. G.; Ditusa, J. F.; Guo, S.; Adams, P. W.; Chan, J. Y.; Hall, D., High Magnetic Field Sensor Using $LaSb_2$. *Appl. Phys. Lett.* **2003**, *82*, 3713-3715.

28. Bud'ko, S. L.; Canfield, P. C.; Mielke, C. H.; Lacerda, A. H., Anisotropic Magnetic Properties of Light Rare-Earth Diantimonides. *Phys. Rev. B* **1998**, *57*, 13624-13638.

Chapter 3. Synthesis, Magnetic, Transport, and Thermodynamic Investigation of $CeCo(Sb, Sn)_3$*

3.1 Introduction

Ternary lanthanide – transition metal – antimonide systems display unusual geometric networks and bonding patterns.[1-3] Additionally, these systems are known to exhibit a wide variety of interesting physical properties.[4] For example, the highly correlated skutterudite $CeFe_4Sb_{12}$ exhibits a thermoelectric efficiency (zT) greater than 1.0 in a high temperature region.[5-7] Another interesting class of Sb-containing phases is the Ce – Ni – Sb ternary intermetallics. α-$CeNiSb_3$ and β-$CeNiSb_3$ both display Kondo lattice behavior around 25 K and order ferromagnetically with $T_c \sim 6$ K.[8-9] These properties are interesting because the occurrence of ferromagnetism in Ce-containing compounds, which display features of Kondo screening at higher temperatures may be indicative of an undercompensated or underscreened Kondo lattice. These conditions have been predicted and experimentally shown to result in the formation of a singular Fermi liquid.[10] Additionally, the ferromagnetic transition temperature of α-$CeNiSb_3$ was found to increase under applied pressures up to 25 kbar, decrease for applied pressure greater than 25 kbar, and a second ferromagnetic ordered phase emerged between pressures of 35 kbar and 55 kbar. The existence of a quantum critical point (QCP) at $P \sim 60$ kbar was suggested due to the nearly complete suppression of the first magnetic phase and an increase in the T^2 coefficient and ρ_0 observed from fits to electrical resistivity at this pressure.[11]

More recently, $CeCoSb_3$, which adopts the $LaPdSb_3$ structure-type and is isostructural to β-$CeNiSb_3$, was prepared using Sn flux.[12] Theoretical band-structure calculations performed by Cai *et. al.* lead the authors to conclude that the magnetic and electrical properties of $CeCoSb_3$ would be nearly identical to β-$CeNiSb_3$.[9, 12] However, the magnetic, transport, and

*Adapted with Permission from Elsevier: Phelan, W. A.; Nguyen, G. V.; DiTusa, J. F.; Chan, J. Y., Synthesis, Magnetic, Transport, and Thermodynamic Investigation of $CeCo(Sb, Sn)_3$. *J. Alloys Compd.* **2012**, 523, 171-181.

thermodynamic properties of $CeCoSb_3$ remain uncharacterized. To further extend the study of Ce – Transition Metal – Sb phases and having the desire to target the interesting physical properties mentioned above, we have grown this phase employing a synthetic procedure similar to that previously described and this will be further elaborated in the *Materials and Methods* section.[12] In this manuscript we present the synthesis, structural characterization, and physical properties for $CeCo(Sn,Sb)_3$.

3.2 Materials and Methods

3.2.1 Synthesis

Single crystals of $CeCo(Sb, Sn)_3$ were synthesized via the flux-growth method from excess Sn as previously reported.[12] This phase was prepared by placing Ce (99.9%), along with Co powder (99.998%), Sb shot (99.9999%), and Sn shot (99.99+%) into a 2-mL alumina crucible in a 5:5:15 mmolar ratio of Ce:Co:Sb with 3 grams of Sn. The crucible was sealed into an evacuated fused-silica tube and was heated to 913 K for 1 day and then heated to 1323 K at a rate of 100 K/h for 3 days. After dwelling at 1323 K for 3 days, the ampoules were cooled to room temperature at a rate of 5.3 K/h. The excess Sn flux was etched using dilute hydrochloric acid and thin, shiny, black plate-like crystals were mechanically extracted. The average crystal dimensions for the length, width, and height correspond to ~ 0.5 mm, ~ 1 mm, and 3 mm, respectively. The surfaces of all the crystals were observed to be clean with little evidence of flux contamination. No signs of surface oxidation were observed when the crystals were exposed to air and moisture over a period of months.

3.2.2 Single-Crystal X-ray Diffraction

Plate-shaped single crystals of $CeCo(Sb, Sn)_3$ were mounted onto glass fiber tips of a goniometer with epoxy and placed on a Nonius Kappa CCD X-ray diffractometer (Mo Kα

Table 3.1 Crystallographic Parameters for $CeCo(Sb, Sn)_3$

Formula	$CeCo(Sb, Sn)_3$
a (Å)	12.8400(5)
b (Å)	6.1340(5)
c (Å)	12.1060(15)
V (Å^3)	953.48(15)
Z	8
Crystal system	Orthorhombic
Space group	*Pbcm*
θ range (°)	2.6-33.1
μ (mm^{-1})	29.34
Data collection	
Crystal Size	0.10 mm x 0.13 mm x 0.22 mm
Measured reflections	11660
Independent reflections	1779
Reflections with $I>2\sigma(I)$	1728
R_{int}	0.037
h	-19 – 19
k	-8 – 8
l	-18– 17
Refinement	
$^aR_1[F^2>2\sigma(F^2)]$	0.048
$^bwR_2(F^2)$	0.148
Parameters	53
GOOF	1.22
$\Delta\rho_{max}$ (e Å^{-3})	4.94
$\Delta\rho_{min}$ (e Å^{-3})	-3.96

$^aR_1=\sum \| F_o | - | F_c \| / \sum | F_o |$, $^bwR_2 = [\sum[w(F_o^2 - F_c^2)]/\sum[w(F_o^2)^2]]^{1/2}$

radiation, λ = 0.71073 Å). A data collection was performed at room temperature and the crystallographic parameters for $CeCo(Sb, Sn)_3$ are listed in Table 3.1. The orthorhombic Laue symmetry *mmm* and the systematic absences observed led to the initial space group selection of *Pbma*, which transformed to the standard setting of *Pbcm* (No. 57). Direct methods were used to generate the initial structural model using SIR97 and further refinement was conducted using SHELX97.[13-14] After the refinement of all the atomic positions, the collected data were corrected

Table 3.2 Atomic Positions and Anisotropic Displacement Parameters for $CeCo(Sb, Sn)_3$ where X = Sb and Sn

Atom	x	y	z	$U_{eq}(Å^2)^a$
Ce1	0.70043(5)	¼	0	0.01009(19)
Ce2	0.30495(5)	0.26645(10)	¾	0.00990(18)
Co1	0.10242(8)	0.03361(17)	0.86220(8)	0.0110(2)
X1	0.97323(6)	¼	0	0.0119(2)
X2	0.78703(6)	0.25615(10)	¾	0.0107(2)
X3	0.50181(3)	0.50911(8)	0.87653(5)	0.01127(19)
X4	0.21706(6)	¼	0	0.0107(2)
X5	0.94442(5)	0.88482(11)	¾	0.0117(2)

[a] U_{eq} is defined as 1/3 of the trace of the orthogonalized U_{ij} tensor.

for absorption and the displacement parameters were refined as anisotropic. Weighting schemes and extinction corrections were applied during the final stages of refinement. The atomic coordinates and anisotropic displacements are provided in Table 3.2. Selected interatomic distances and angles for $CeCo(Sb, Sn)_3$ are provided in Table 3.3. It should be noted that attempts to refine the occupancies of both Sn and Sb for a given Wyckoff site simultaneously were unsuccessful, as the X-ray scattering amplitudes for Sn and Sb are very similar. Therefore all positions were refined as pure Sb. (The $LnCo(Sb, Sn)_3$ (Ln = La, Pr, Nd, and Sm) phases were grown under similar synthetic conditions described in Section 3.2.1. and their structures were characterized using X-ray diffraction as described here. The crystallographic parameters for these phases can be viewed in the supplemental tables which are provided in Appendix 3.)

3.2.3 Elemental Analysis

Since X-ray diffraction cannot reliably resolve Sb from Sn, the chemical composition of a clean single crystal of $CeCo(Sb, Sn)_3$ was determined by energy dispersive spectroscopy (EDS) using a Hitachi S-3600N scanning electron microscope (SEM). A total of seven scans were performed using an accelerating voltage of 15 keV with a beam to sample distance of 20 mm.

Table 3.3 Selected Interatomic Distances and Angles for $CeCo(Sb, Sn)_3$ where X = Sb and Sn

Interatomic Distances (Å)	
Ce1 – X1	3.5027(9)
Ce1 – X2 (x 2)	3.2245(5)
Ce1 – X3 (x 2)	3.3408(7)
Ce1 – X3 (x 2)	3.3563(6)
Ce1 – X4 (x 2)	3.2448(4)
Ce2 – X2	3.2277(9)
Ce2 – X2	3.3456(9)
Ce2 – X3 (x 2)	3.3092(7)
Ce2 – X3 (x 2)	3.3158(7)
Ce2 – X4 (x 2)	3.2316(5)
Ce2 – X5	3.2832(9)
X3 – X3	2.9920(10)
X3 – X3	3.0635(10)
X3 – X3	3.0674(3)
Co – X1	2.5986(11)
Co – X1	2.7011(11)
Co – X2	2.5993(11)
Co – X4	2.5906(11)
Co – X5	2.6064(11)
Co – X5	2.6168(12)
Co – Co	2.717(2)
Angles (º)	
X3 – X3 – X3	87.847(19)
X3 – X3 – X3	90
X3 – X3 – X3	90
X3 – X3 – X3	92.126(19)
X5 – Co – X1	79.00(3)
X5 – Co – X5	80.73(3)
X5 – Co – X2	85.61(4)
X5 – Co – X4	92.47(7)
X1 – Co – X2	95.81(4)
X1 – Co – X4	98.16(4)
X2 – Co – X4	111.20(4)
X2 – Co – X5	113.16(4)
X1 – Co – X5	142.98(4)
X5 – Co – X4	163.18(5)

The composition obtained by normalizing all elements to the Ce composition was found to be $CeCo_{0.95(3)}Sn_{0.57(5)}Sb_{2.6(1)}$. The incorporation of Sn for Sb was observed in the structures of $LnNi(Sn,Sb)_3$ (Ln = Pr, Nd, Sm, Gd, and Tb), which were synthesized using a similar strategy as described above.[15]

3.2.4 Physical Properties

Magnetic data for $CeCo(Sb, Sn)_3$ were collected using a Quantum Design Magnetic Property Measurement System (MPMS). The temperature-dependent magnetic susceptibility data were measured under zero field cooled (ZFC) conditions between 2.25 K and 300 K under an applied magnetic field of 100 Oe. Field dependent magnetization data were measured between 5 K and 200 K with magnetic fields up to 5 T. The electrical resistivity and specific heat capacity data were collected using a Quantum Design Physical Property Measurement System (PPMS). The magnetic fields and the electrical currents were both applied parallel to the height (long direction) of these thin plates.

3.3 Results and Discussion

3.3.1 Structure

$CeCo(Sb, Sn)_3$ adopts the $LaPdSb_3$ structure-type with lattice parameters *a*~12 Å, *b*~6 Å, and *c*~12 Å.[16] Detailed descriptions of compounds adopting the $LaPdSb_3$ have been provided elsewhere.[9, 12, 15-17] Therefore, only a brief structural description of $CeCo(Sb, Sn)_3$ is provided below. The $LaPdSb_3$ structure-type is similar to the $CeCrSb_3$ and α-$CeNiSb_3$ structure types.[8, 18] As shown in Figure 3.1, $CeCo(Sb, Sn)_3$ can be viewed as being built up by inserting Ce atoms between a layer of Co-centered octahedra, $^2_\infty[CoX_2]$ where X = Sb and Sn, and a distorted square net composed of X atoms, $^2_\infty[X]$. A host of X-X interactions within the $^2_\infty[CoX_2]$ layers have been omitted for clarity.

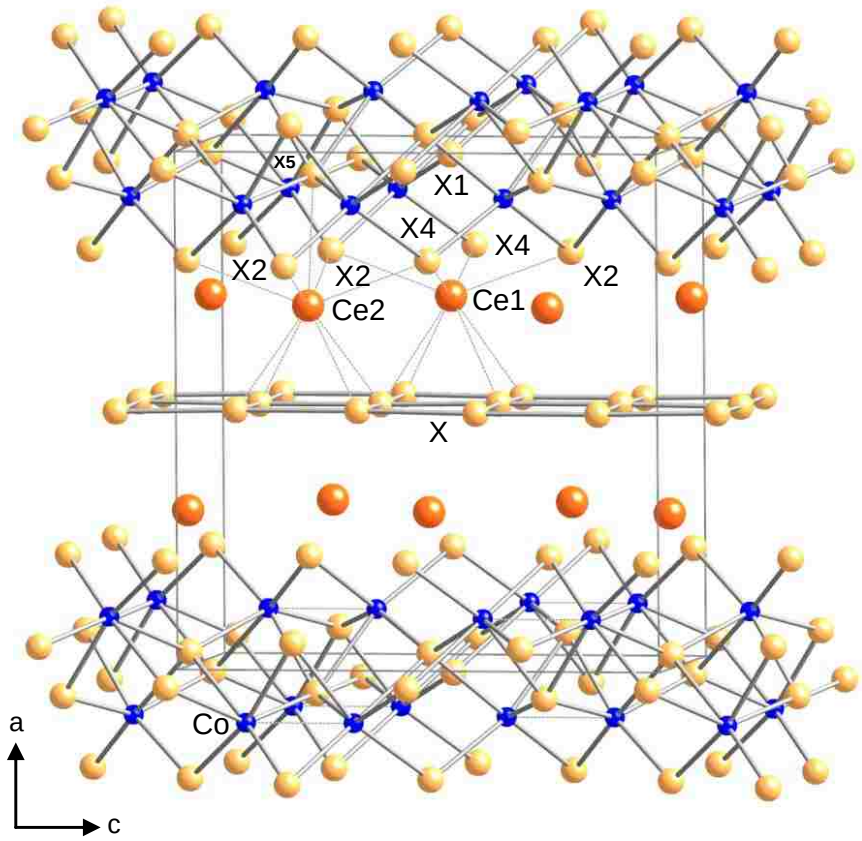

Figure 3.1 Crystal structure of $CeCo(Sb,Sb)_3$ where X = Sb and Sn.

$CeCo(Sb, Sn)_3$ contains two crystallographically inequivalent Ce sites with slightly different coordination environments. The Ce1 atoms are surrounded by 8 X atoms, adopting a square antiprismatic geometry, where 4 atoms of the $^2_\infty[X]$ layer form a square base, and 4 X atoms from the $^2_\infty[CoX_2]$ layer form a square directly above, but twisted 45° with respect to the square of the $^2_\infty[X]$ layer. The Ce2 atoms are surrounded by 9 X atoms and adopt a monocapped square antiprismatic geometry with an additional X5 atom capping the second square formed by the $^2_\infty[XSb_2]$ layer. The X1 atom in the capping position of Ce1 is considered too far from the Ce1 atom for any considerable bonding interactions. The main structural distinction between $CeCrSb_3$, α-$CeNiSb_3$, and $CeCo(Sb, Sn)_3$ lies in the packing of the $^2_\infty[TSb_2]$ octahedral layer

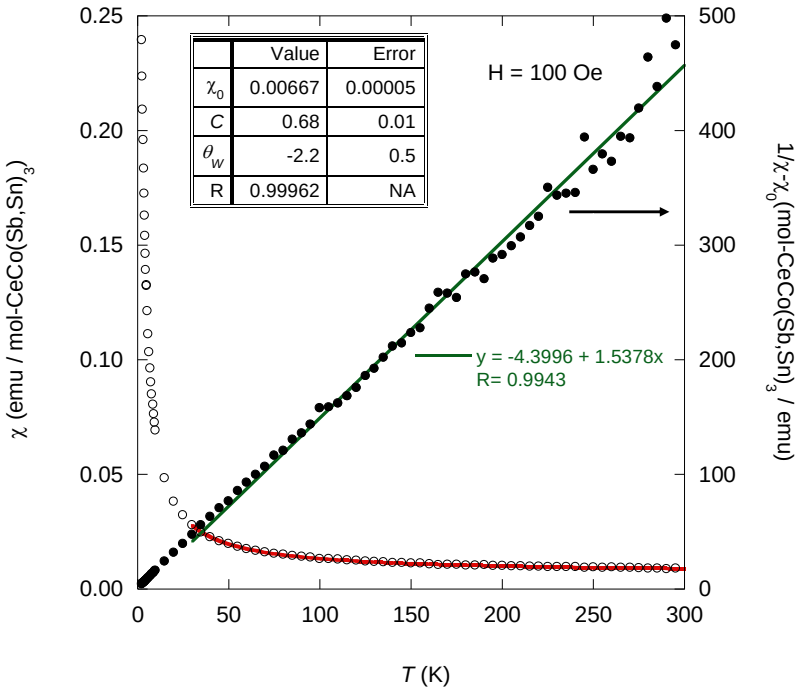

Figure 3.2 Temperature dependent magnetic susceptibility, $\chi = M/H$, of $CeCo(Sb, Sn)_3$ under an applied field of 100 Oe is shown on the left axis, and the inverse magnetic susceptibility, $1/\chi-\chi_0$, as a function of temperature is shown on the right axis. The χ_0, C, and θ_W parameters which were obtained from a modified Curie-Weiss fit to the magnetic susceptibility can be viewed in the inset table of this figure.

along the [001] direction.[8, 18] The $^2_\infty[CoX_2]$ octahedra in $CeCo(Sb, Sn)_3$ are edge-sharing in [010], whereas they are face-sharing, with every other octahedron sharing edges in [001]. The angles between the Co and X atoms diverge considerably from the ideal 90°. Furthermore, Co-Co interactions are present at the adjourning octahedral faces with a distance of 2.717(2) Å.

3.3.2 Physical Properties

The temperature-dependent magnetic susceptibility of $CeCo(Sb, Sn)_3$ in a field of 100 Oe is shown in Figure 3.2. The modified Curie-Weiss form, $\chi(T) = \chi_0 + C/(T - \theta_W)$, where C is the Curie constant, θ_W represents the Weiss temperature, and χ_0 accounts for the temperature

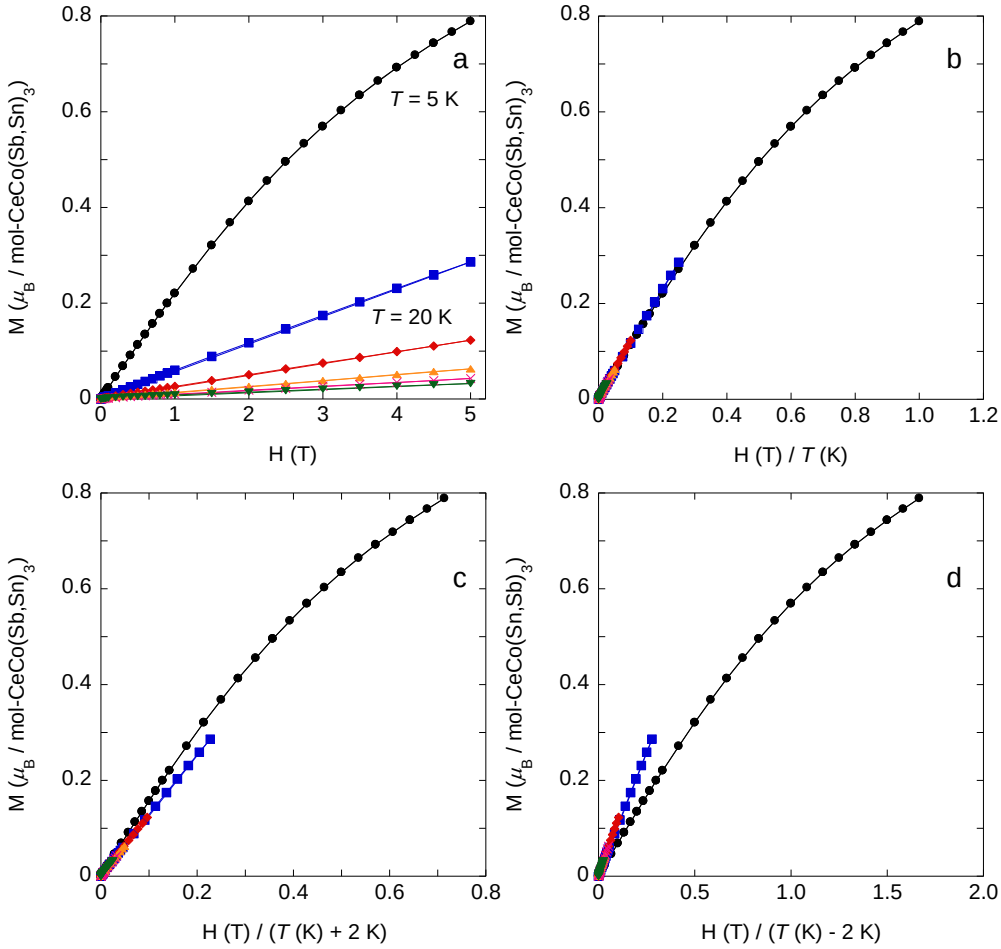

Figure 3.3a-d. (a) Magnetization (M) of $CeCo(Sb, Sn)_3$ as a function of applied field (H) at 5 K, 20 K, 50 K, 100 K, 150 K, and 200 K, (b) Magnetization vs. field divided by temperature (H/*T*), (c) Magnetization vs. H/*T* + 2 K, (d) Magnetization vs. H/*T* – 2 K. The circles, squares, diamonds, triangles, crosses, and upside down triangles represent the magnetic isotherms at *T* = 5 K, 20 K, 50 K, 100 K, 150 K, and 200 K, respectively.

independent contributions to the magnetic susceptibility due to Pauli paramagnetism and Larmor diamagnetism, was used to fit the magnetic susceptibility data from 30 K – 300 K. The values and errors for the parameters obtained from the fit of the modified Curie-Weiss form to the data are displayed in the inset table of Figure 3.2. The value of χ_0 thus obtained was subtracted from χ, and the inverse of $\chi - \chi_0$ is plotted on the right axis of Figure 3.2. A linear fit to these data from 30 – 300 K was performed to attempt to extract more accurate values for *C* and θ_W. The

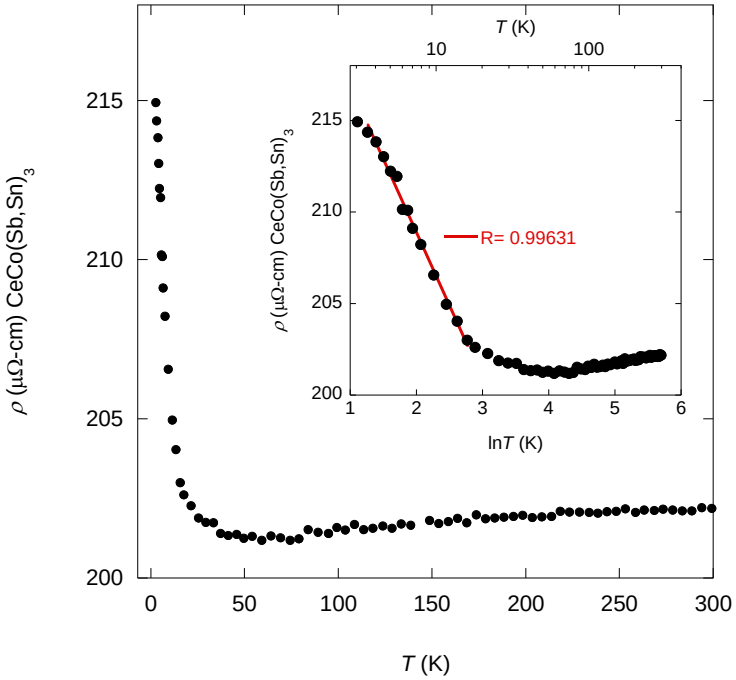

Figure 3.4 Temperature-dependent electrical resistivity (ρ) for CeCo(Sb, Sn)$_3$. The inset shows a linear fit of ρ vs. ln$T$ for CeCo(Sb, Sn)$_3$ from 3 K to 10 K.

effective moment obtained from C, 2.28 μ_B/mol-Ce, was compared to the calculated value using $\mu_{eff} = g_J[J(J+1)]^{1/2}\ \mu_B$ or 2.54μ_B/mol-Ce for a free Ce^{3+} ion. Similar to what was observed for isostructural β-CeNiSb$_3$ the effective moment in CeCo(Sb, Sn)$_3$ is somewhat smaller than the expected value for a Ce^{3+} ion indicating that there is likely no magnetic moment associated with the transition metal site (Co).[9] In addition, a small negative Weiss temperature of -2.2 K was obtained from fits to the magnetic susceptibility using the modified Curie-Weiss equation, while a small positive Weiss temperature of 2.9 K was obtained from linear fits to the inverse $\chi - \chi_0$ data. These data indicate a small Weiss temperature, however, the variation in the values obtained indicate that there may be systematic error of order a few kelvin in our method for determining θ_W.

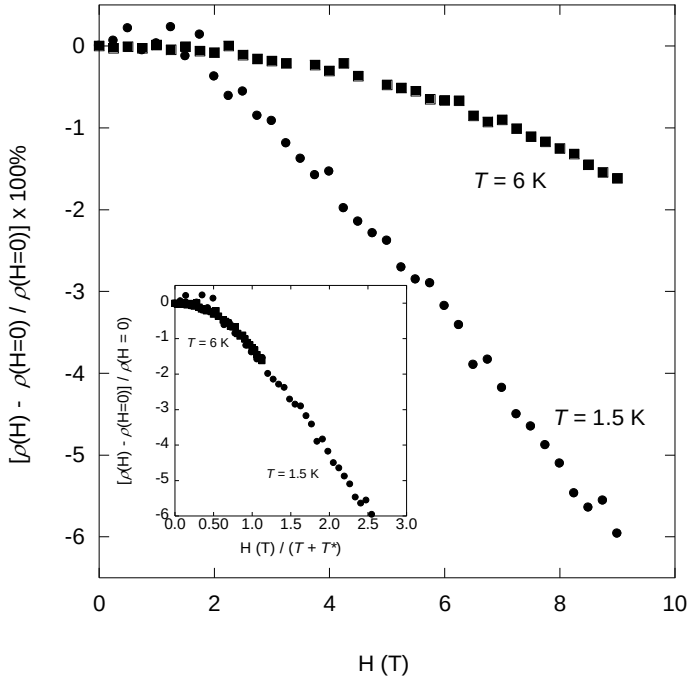

Figure 3.5. Magnetoresistance, [ρ(H) – ρ(H=0) / ρ(H=0)] x 100%, as a function of applied field at T = 1.5 (circles) and (squares) K and T = 6 K. The inset shows magnetoresistances at T = 1.5 K (circles) and T = 6 K (squares) as a function of H(T)/(T-T*).

The magnetic properties of this system were further probed by measuring the field-dependent magnetization for fields of up to 5 T at temperatures between 5 and 200 K (Fig. 3a). The magnetization data above 5 K is linear and shows no sign of saturation, whereas the data at 5 K show a tendency towards saturation at high fields as expected for a paramagnet. Figure 3.3b, 3.3c, and 3.3d display the field-dependent magnetization curves vs. H/T – θ for θ = 0 K, +2 K, and -2 K to explore the sign and magnitude of the magnetic exchange interaction between the Ce magnetic moments. As can be seen in Figure 3.3b, the data scale best when plotted against H/T suggestive of weak correlations on the order of magnitude of 1 K. The quality of the scaling is visibly reduced when we include a small ferromagnetic coupling, as shown in Figure 3.3d, so

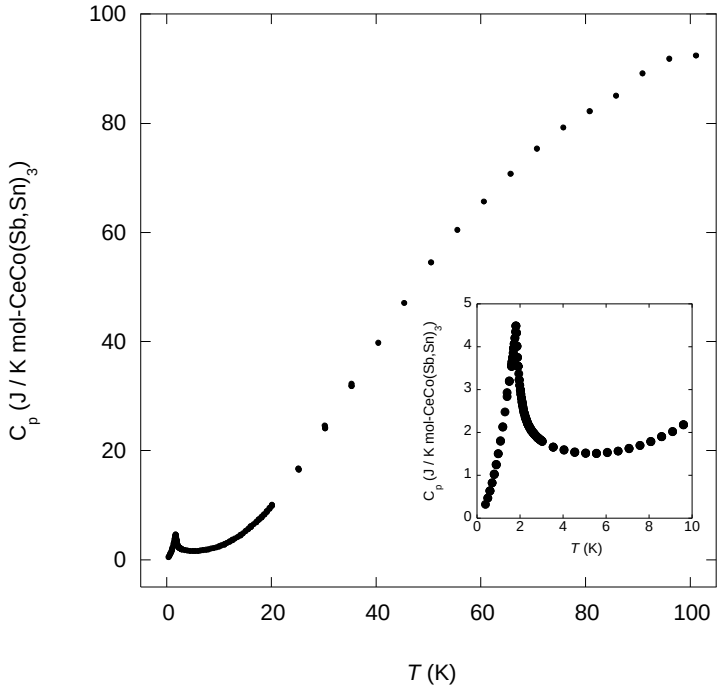

Figure 3.6 Specific heat capacity (C_p) for $CeCo(Sb, Sn)_3$ as a function of temperature. The inset serves to highlight the thermodynamic phase transition.

that we conclude that our magnetization data does not support ferromagnetic correlations between the magnetic ions.

The electrical resistivity as a function of temperature for $CeCo(Sb, Sn)_3$ is displayed in Figure 3.4. The resistivity is nearly temperature independent below room temperature with a value above 200 μΩcm indicating disordered metallic transport as would perhaps be expected for a material with partial Sn occupation of the X site. Below 10 K a decreasing ρ with T is observed. Because we suspect Kondo lattice behavior for this Ce compound, we plot ρ as a function of ln$T$ in the inset of Figure 3.4 where linearity is apparent, although the T-range is limited. Our identification of the upturn in the resistivity at low temperatures as a Kondo feature is further supported by the negative magnetoresistance, ρ (H) – ρ (H=0) / ρ (H=0), that we

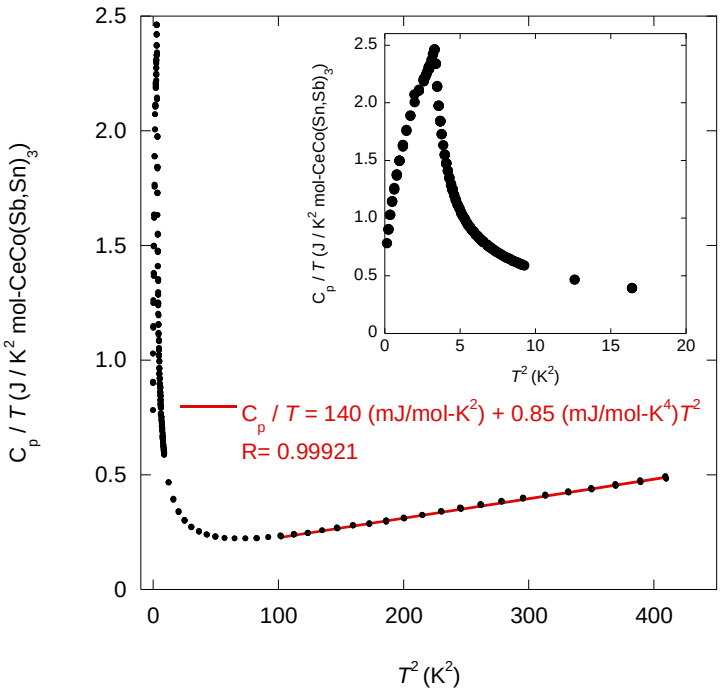

Figure 3.7 A plot of C_p/T vs. T^2 for CeCo(Sb, Sn)$_3$. The inset serves to highlight the thermodynamic phase transition.

observe at T = 1.5 K and T = 6 K as shown in Figure 3.5. A negative magnetoresistance that increases in magnitude with decreasing temperature is expected in the incoherent magnetic scattering regime.[19] Additionally, the inset of Figure 3.5 shows that the isothermal curves scale well when the magnetic field values are normalized by (T + T*) where T* = 2 K. The nice overlap between the two isothermal magnetoresistance curves shown in the inset of Figure 3.5 by a 2 K scaling factor is suggestive of a low Kondo temperature for CeCo(Sb, Sn)$_3$.

Perhaps more informative is the specific heat capacity (C_p) displayed as a function of temperature for CeCo(Sb, Sn)$_3$ in Figure 3.6. We observe a phase transition at T ~ 2 K which is more apparent in the inset of Figure 3.6 where the low temperature data is presented on a finer

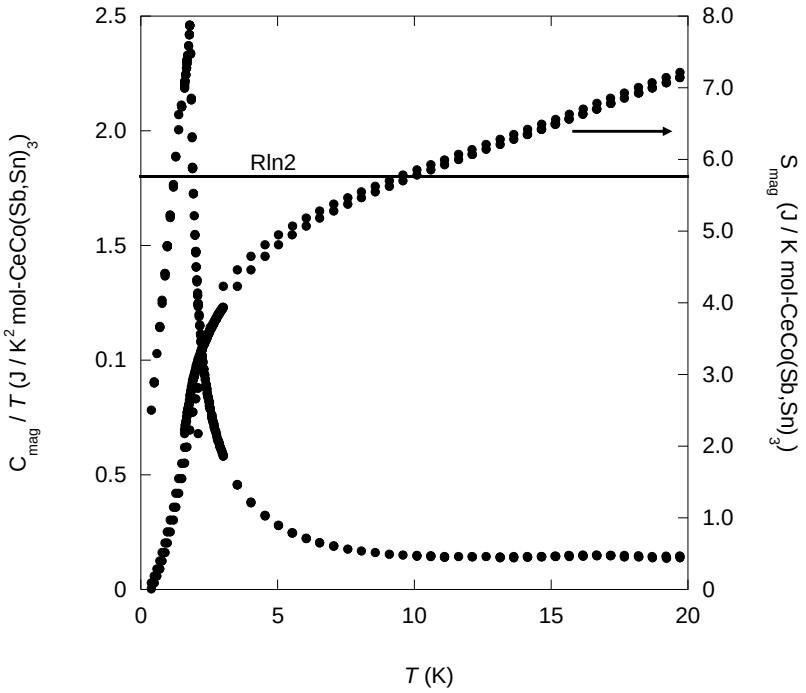

Figure 3.8 Magnetic heat capacity divided by temperature (C_{mag}/T) and magnetic entropy (S_{mag}) as a function of temperature. Rln2 is indicated by the line.

scale. This sharp peak found at a low temperature is likely a magnetic phase transition which is not inconsistent with the small θ_W values obtained from the susceptibility and our scaling of the magnetization data (Figure 3.3). Fits of the standard metallic form, $C_p/T = \gamma + \beta T^2$, to our C_p/T vs. T^2 data from 100 K^2 to 400 K^2 for $CeCo(Sb, Sn)_3$ were performed to extract the β and γ coefficients shown in Figure 3.7. The best fit values for β and γ obtained from this procedure were 0.85mJ/mol-K^4 and 140 mJ/mol-K^2, respectively. The value of γ indicated by our fitting procedure is considerable larger than that found in simple metals such as Cu ($\gamma \sim 1$ mJ/mol-K^2), and would imply the formation of a heavy Fermion metallic state.[20-23] To further assess this possibility we estimated the magnetic heat capacity (C_{mag}) by subtracting βT^3 from the specific heat capacity (C_p). The magnetic heat capacity divided by temperature (C_{mag}/T) and the

magnetic entropy (S_{mag}) determined by integrating C_{mag}/T are shown on the left and right axes of Figure 3.8, respectively. Here, we observe that the entropy increases sharply from our lowest temperatures up to 5 K while it continues to increase with *T* at a smaller rate above 5 K. The entropy expected for a S = ½, magnetic moment is exceeded above 10 K confirming that the phase transition observed at 2 K is likely magnetic in origin.

3.4 Conclusions

Single crystals of $CeCo(Sb, Sn)_3$ where grown via the flux-growth method using excess Sn. These crystals were characterized by single crystal X-ray diffraction and a more accurate composition of these crystals was determined by EDS. We have shown that the magnetic susceptibility of $CeCo(Sb, Sn)_3$ is paramagnetic down to the lowest temperature measured. The Curie-Weiss analysis and magnetization scaling suggest weak magnetic correlations become relevant on the order of magnitude 1 K. This is further supported by our analysis of the heat capacity data which indicate a magnetic transition near 2 K. Additionally, the low temperature resistivity and MR% behavior of $CeCo(Sb, Sn)_3$ are consistent with incoherent Kondo scattering of the conducting electrons.[19] A standard analysis of the heat capacity data indicates that $CeCo(Sb, Sn)_3$ has enhanced charge carries mass, γ = 140 mJ/mol-K^2. However, this is inconsistent with a low Kondo temperature and the absence of a coherence observed in the resistivity. Furthermore, the negative magnetoresistance values at low temperatures for $CeCo(Sb, Sn)_3$ are also not consistent with a coherent heavy Fermion metallic state where a positive magnetoresistance has been observed in a number heavy-fermion compounds.[19, 24] Gschneidner *et. al.* [25] have proposed that large, nearly linear, contributions to the specific heat occur as a result of low lying crystal field levels. In this case a large γ is confused with the tail of a higher temperature Schottky peak which results from the crystal field splitting of the Ce *f*-

levels. Low lying crystal field levels have been observed in $CeCd_{11}$ (3 doublets – 0K, 17.5 K, and 80 K) and $CeGa_2$ (3 doublets – 0 K, 62.5 K and 310 K) which give rise to erroneously large Sommerfeld coefficients (γ).[25-27] That our magnetic entropy for $CeCo(Sb, Sn)_3$ displays a continuously increase beyond Rln2 may be indicative of contributions from low lying crystal field levels similar to what has been observed in $CeMg_3$.[28] In view of both our resistivity and magnetoresistance data which indicate an absence of a coherent heavy Fermion state, we conclude that the enhanced Sommerfeld coefficient, γ = 140 mJ/mol-K^2, indicated from the standard analysis of the specific heat data for $CeCo(Sb, Sn)_3$ is likely a result of low lying crystal field levels rather than the formation of heavy quasiparticles.

3.5 References

1. Kleinke, H., From Molecular Sb Units to Infinite Chains, Layers, and Networks: Sb-Sb Interactions in Metal-Rich Antimonides. *Chem. Soc. Rev.* **2000**, *29*, 411-418.

2. Mills, A. M.; Lam, R.; Ferguson, M. J.; Deakin, L.; Mar, A., Chains, Planes, and Antimonides. *Coordin. Chen. Rev.* **2002**, *233-234*, 207-222.

3. Papoian, G. A.; Hoffmann, R., Hypervalent Bonding in One, Two, and Three Dimensions: Extending the Zintl-Klemm Concept to Nonclassical Electron-Rich Networks. *Angew. Chem. Int. Ed.* **2000**, *39*, 2409-2448.

4. Thomas, E. L.; Millican, J. N.; Okudzeto, E. K.; Chan, J. Y., Crystal Growth and the Search for Highly Correlated Intermetallics. *Comments Inorg. Chem.* **2006**, *27*, 1-39.

5. Kauzlarich, S. M.; Brown, S. R.; Snyder, G. J., Zintl Phases for Thermoelectric Devices. *Dalton Trans.* **2007**, 2099-2107.

6. Phelan, W. A.; Menard, M. C.; Kangas, M. J.; McCandless, G. T.; Drake, B. L.; Chan, J. Y., Adventures in Crystal Growth: Synthesis and Characterization of Single Crystals of Complex Intermetallic Compounds. *Chem. Mater.* **2012**, *24*, 409-420.

7. Sefat, A. S.; Bud'ko, S. L.; Canfield, P. C., Magnetization, Resistivity and Heat Capacity of the Anisotropic $RVSb_3$ Crystals (R=La-Nd, Sm, Gd-Dy). *J. Magn. Magn. Mater.* **2008**, *320*, 120-141.

8. Macaluso, R. T.; Wells, D. M.; Sykora, R. E.; Albrecht-Schmitt, T. E.; Mar, A.; Nakatsuji, S.; Lee, H.; Fisk, Z.; Chan, J. Y., Structure and Electrical Resistivity of $CeNiSb_3$. *J. Solid State Chem.* **2004**, *177*, 293-298.

9. Thomas, E. L.; Gautreaux, D. P.; Lee, H. O.; Fisk, Z.; Chan, J. Y., Discovery of β-$LnNiSb_3$ (Ln = La, Ce): Crystal Growth, Structure, and Magnetic and Transport Behavior. *Inorg. Chem.* **2007**, *46*, 3010-3016.

10. Perkins, N. B.; Iglesias, J. R.; Nunez-Regueiro, M. D.; Coqblin, B., Coexistence of Ferromagnetism and Kondo Effect in theUnderscreened Kondo Lattice. *EPL-Europhys. Lett.* **2007**, *79*, 57006.

11. Sidorov, V. A.; Bauer, E. D.; Lee, H.; Nakatsuji, S.; Thompson, J. D.; Fisk, Z., Complex Magnetic Phase Diagram of Ferromagnetic $CeNiSb_3$. *Phys. Rev. B* **2005**, *71*, 094422.

12. Cai, W.-Z.; Wu, L.-M.; Li, L.-H.; Chen, L., Syntheses, Structures, and Theoretical Studies of New Ternary Antimonides β-*RE*CoSb3 (*RE*= La-Nd, Sm). *Eur. J. Inorg. Chem.* **2009**, *2009*, 230-237.

13. Altomare, A.; Burla, M. C.; Camalli, M.; Cascarano, G. L.; Giacovazzo, C.; Guagliardi, A.; Moliterni, A. G. G.; Polidori, G.; Spagna, R., SIR97: A New Tool for Crystal Structure Determination and Refinement. *J. Appl. Crystallogr.* **1999**, *32*, 115-119.

14. Sheldrick, G. M., A Short History of SHELX. *Acta Crystallogr., A* **2008**, *64*, 112-122.

15. Gautreaux, D. P.; Capan, C.; DiTusa, J. F.; Young, D. P.; Chan, J. Y., Synthesis, Structure and Physical Properties of $LnNi(Sn,Sb)_3$ (Ln = Pr, Nd, Sm, Gd, Tb). *J. Solid State Chem.* **2008**, *181*, 1977-1982.

16. Thomas, E. L.; Gautreaux, D. P.; Chan, J. Y., The Layered Intermetallic Compound $LaPdSb_3$. *Acta Crystallogr. Sect. E. Struct. Rep. E* **2006**, *62*, I96-I98.

17. Phelan, W. A.; Nguyen, G. V.; Karki, A. B.; Young, D. P.; Chan, J. Y., Synthesis, Structure, Magnetic and Transport Properties of $LnFeSb_3$ (Ln = Pr, Nd, Sm, Gd, and Tb)

- Tuning of Anisotropic Long-Range Magnetic Order as a Function of Ln. *Dalton Trans.* **2010**, *39*, 6403-6409.

18. Brylak, M.; Jeitschko, W., Ternary Antimonides $LnTSb_3$ with Ln=La-Nd, Sm and T=V,Cr. *Naturforsch., B* **1995**, *50*, 899-904.

19. Rauchschwalbe, U.; Steglich, F.; Rietschel, H., Magnetoresistance of Heavy-Fermion Compounds. *Physica B & C* **1987**, *148*, 33-36.

20. Fisk, Z.; Hess, D. W.; Pethick, C. J.; Pines, D.; Smith, J. L.; Thompson, J. D.; Willis, J. O., Heavy-Electron Metals - New Highly Correlated States of Matter. *Science* **1988**, *239*, 33-42.

21. Fisk, Z.; Ott, H. R.; Rice, T. M.; Smith, J. L., Heavy-Electron Metals. *Nature* **1986**, *320*, 124-129.

22. Fisk, Z.; Sarrao, J. L.; Smith, J. L.; Thompson, J. D., The Physics and Chemistry of Heavy Fermions. *Proc. Natl. Acad. Sci. U.S.A.* **1995**, *92*, 6663-6667.

23. Fisk, Z.; Sarrao, J. L.; Thompson, J. D., Heavy Fermions. *Curr. Opin. Solid State Mater. Sci.* **1996**, *1*, 42-46.

24. Oomi, G.; Kagayama, T., Effect of Pressure on the Magnetoresistance and Magnetostriction of Heavy-Fermion Materials. *Physica B* **1994**, *201*, 235-238.

25. Gschneidner, K. A.; Tang, J.; Dhar, S. K.; Goldman, A., False Heavy Fermions. *Physica B* **1990**, *163*, 507-510.

26. Tang, J.; Gschneidner, K. A., The Influence of Crystalline Electric-Field on the Low-Temperature Properties of $CeCd_{11}$. *J. Magn. Magn. Mater.* **1988**, *75*, 355-360.

27. Burlet, P.; Fremy, M. A.; Gignoux, D.; Lapertot, G.; Quezel, S.; Regnault, L. P.; Rossatmignod, J.; Roudaut, E., Magnetic-Properties of the Kondo Lattice $CeGa_2$. *J. Magn. Magn. Mater.* **1987**, *63-4*, 34-36.

28. Das, P. K.; Kumar, N.; Kulkarni, R.; Thamizhavel, A., Magnetic Properties of the Heavy-Fermion Antiferromagnet $CeMg_3$. *Phys. Rev. B* **2011**, *83*, 134416.

Chapter 4. Discovery of Spin Glass Behavior in $Ln_2Fe_4Sb_5$ (Ln = La – Nd and Sm)

4.1Introduction

Motivated by the diverse physical properties of ternary intermetallics with Group 15 elements such as As, Sb, and Bi, our research group and others have been involved in the discovery, synthesis, and structure determination of lanthanide-transition metal-pnictide compounds, such as the $LnTSb_3$ (Ln = early lanthanides; T = Ni, Fe, Co) phases.[1-8] These compounds are of particular interest because the number of transition metal analogues that can be synthesized allowing for the study of the interplay of magnetism in both the lanthanide and transition metal sublattices. Many of these analogues display local moment magnetism due to lanthanide ordering with no contribution from the transitional metal to the overall effective moment.[1-8] Similar behavior is also found in isostructural analogues of Ln_4FeGa_{12} (Ln = Tb, Dy, Ho, and Er) where the magnetic lanthanides order antiferromagnetically at temperatures below 25 K.[9] However, the Y_4FeGa_{12} analogue orders ferromagnetically at 36 K with no localized magnetic moment on the Fe site, where the magnetism was attributed to the polarized itinerant electrons.[9]

Fe-containing intermetallics are well known to exhibit interesting physical properties. For example, the new families of iron-based superconductors exhibit subtle structural transitions and antiferromagnetism as well as high superconducting transition temperatures. The superconductivity mechanism is not known but likely involves magnetic degrees of freedom for this family of compounds.[10-11] More recently, a new iron pnictide compound, $CaFe_4As_3$, was reported, and unlike the layered, low-dimensional iron pnictide superconductors, the structure of $CaFe_4As_3$ is more 3-dimensional.[12-14] A second order incommensurate spin density wave transition at 88 K was observed for $CaFe_4As_3$, while a first order incommensurate to

commensurate spin density wave transition was observed at lower temperatures.[12, 15-16] The higher temperature spin density wave order was shown to be very robust as chemical dopants and hydrostatic pressure had little effect on the ordering temperature. However, the lower temperature first order incommensurate to commensurate spin density wave transition of $CaFe_4As_3$ was shown to be greatly influenced by these tuning parameters.[17]

More recently and inspired by the first reported example of a low-spin quasi-two-dimensional system in $NiGa_2S_4$ ($FeGa_2S_4$-type),[18] we investigated a family of sulfides exhibiting magnetic frustration as a result of an ordered triangular magnetic lattice. Studies of the isostructural analogues, MAl_2S_4 (M = Mn, Fe, and Co), led us to attribute the magnetic frustration observed in these compounds to a combination of geometric lattice frustration and magnetic site disorder.[19] Notably, the frustration factors (θ_w/T^*) for both $FeGa_2S_4$[20] and $FeAl_2S_4$[19] were determined to be 10 (θ_w ~ -160 K) and 21.4 (θ_w ~ -225 K), respectively, indicative of moderate degrees of magnetic frustration.

With the goal of discovering compounds with the magnetism associated with the Fe-sublattice rather than simply from the lanthanide moments, we chose to grow single crystals of $Ln_2Fe_4Sb_5$ (Ln = La – Nd and Sm) for these investigations.[21] The synthesis and structure of $Ln_2Fe_4Sb_5$ (Ln = La – Nd) was first reported by P. Woll[22] and are structurally similar to the $LnTSb_3$ (Ln = early lanthanides; T = Ni, Fe, Co) phases.[1-8] However the physical properties of $Ln_2Fe_4Sb_5$ (Ln = La – Nd and Sm) remain uncharacterized. We have prepared single crystals of $Ln_2Fe_4Sb_5$ (Ln = La – Nd and Sm) in two ways; by direct reactions of the constituent elements as well as by way of an inert Bi-flux. Spin glass features can be observed in the physical property data of $Ln_2Fe_4Sb_5$ (Ln = La – Nd and Sm). Because of the similarity of the magnetic susceptibility and magnetization of the La analogue to the other lanthanide containing analogues,

we conclude that the spin glass state in associated with the Fe-sublattice. Herein, we report the synthesis, structure, physical properties, and structure-property relationships of $Ln_2Fe_4Sb_5$ (Ln = La – Nd and Sm).

4.2 Experimental

4.2.1 Synthesis

Small single crystals of $Ln_2Fe_4Sb_5$ (Ln = La – Nd and Sm) were first grown from a stoichiometric melt of the constituent elements. Ln = La – Nd, or Sm (3N), Fe (4N), and Sb (5N) were placed in separate 2 mL alumina crucibles in a 2:4:5 molar ratio of Ln : Fe : Sb. The crucibles were then sealed in separate evacuated fused-silica tubes and placed into a high temperature furnace. These reaction ampoules were heated to 1200ºC for 24 hours at a rate of 100ºC /h. The ampoules were then cooled to 720ºC at a rate of 5ºC /h. Upon reaching 720ºC, the reaction ampoules were taken from the furnace and allowed to cool on a bench top. Small plate-like crystals adequate for single crystal X-ray diffraction experiments were observed to grow in the shape of plates; however, larger crystals were needed for physical property measurements.

Larger, plate-like, single crystals (~ 3 mm) of $Ln_2Fe_4Sb_5$ (Ln = La – Nd and Sm) were grown *via* an inert Bi flux. Ln = La – Nd, and Sm (3N), Fe (4N), Sb (5N), and Bi (5N) were placed into separate 2 mL alumina crucibles in a 2:4:5:10 molar ratio of Ln : Fe : Sb: Bi. Each crucible was then topped with silica wool and sealed in separate evacuated fused-silica tubes and placed in a high temperature furnace. These reaction ampoules were heated to 1200ºC K for 72 hours at a rate of 100ºC /h. The ampoules were cooled to 825ºC at a rate of 5ºC /h, and the excess molten Bi-flux was then separated from the plated-shaped single crystals *via* centrifugation.

Table 4.1 Crystallographic Parameters for $Ln_2Fe_4Sb_5$ (Ln = La – Nd And Sm)

Formula	$La_2Fe_{4.03}Sb_{4.94}$	$Ce_2Fe_{3.98}Sb_{4.93}$	$Pr_2Fe_{4.02}Sb_{4.93}$	$Nd_2Fe_{3.96}Sb_{4.91}$	$Sm_2Fe_{3.95}Sb_{4.93}$
a (Å)	4.3522(15)	4.3237(15)	4.3133(15)	4.3051(15)	4.2723(15)
c (Å)	26.201(8)	25.998(2)	25.976(15)	25.9080 (15)	25.558(9)
V (Å^3)	496.3(3)	486.0(2)	483.3(4)	480.2(2)	466.5(3)
Z	2	2	2	2	2
Crystal system	Tetragonal	Tetragonal	Tetragonal	Tetragonal	Tetragonal
Space group	*I*4/*mmm*	*I*4/*mmm*	*I*4/*mmm*	*I*4/*mmm*	*I*4/*mmm*
θ range (°)	3.1 – 36.5	2.6 – 37.0	2.6 – 37.0	2.6 – 33.1	2.6 – 37.0
μ (mm^{-1})	27.24	28.26	29.15	29.87	32.23
Data collection					
Crystal Size (mm)	0.01 x 0.08 x 0.10	0.03 x 0.05 x 0.08	0.03 x 0.08 x 0.10	0.01 x 0.08 x 0.13	0.03 x 0.10 x 0.13
Measured reflections	6672	6745	6743	5198	6413
Independent reflections	424	418	422	311	401
Reflections with $I>2\sigma(I)$	398	375	392	298	384
R_{int}	0.028	0.025	0.030	0.026	0.031
h	0 - 7	0 - 7	0 - 7	0 - 6	0 - 7
k	-4 - 5	-4 - 5	-4 - 5	-3 - 4	-4 - 5
l	0 - 42	0 - 43	0 - 43	0 - 38	0 - 42
Refinement					
$^aR_1[F^2>2\sigma(F^2)]$	0.046	0.038	0.049	0.044	0.040
$^bwR_2(F^2)$	0.121	0.104	0.149	0.118	0.111
Parameters	22	21	21	21	21
GOOF	1.14	1.16	1.15	1.21	1.20
$\Delta\rho_{max}$ (e Å^{-3})	6.32	5.45	5.11	3.91	4.48
$\Delta\rho_{min}$ (e Å^{-3})	-2.71	-3.99	-3.28	-2.64	-5.70

$^aR_1=\sum \| F_o | - | F_c \| / \sum | F_o |$, $^bwR_2 = [\sum[w(F_o^2 - F_c^2)]/\sum[w(F_o^2)^2]]^{1/2}$

4.2.2 Single-Crystal X-ray Diffraction

Single crystals of $Ln_2Fe_4Sb_5$ (Ln = La – Nd and Sm) were mounted onto separate glass fiber tips of a goniometer using epoxy and placed on a Nonius KappaCCD X-ray diffractometer equipped with Mo Kα radiation (λ = 0.71073 Å). The crystallographic parameters for all

Table 4.2 Atomic Coordinates, Anisotropic Displacement Parameters, and Occupancies for $Ln_2Fe_4Sb_5$ (Ln = La – Nd and Sm)

Atom	Wyckoff Site	x	y	z	$U_{eq}(Å^2)^a$	Occ.
La1	4*e*	0	0	0.34800(4)	0.0102(3)	1
Fe1	2*a*	0	0	0	0.0150(7)	1
Fe2	8*g*	0	½	0.45039(10)	0.0291(12)	0.759(14)
Sb1	4*d*	0	½	¼	0.0088(3)	1
Sb2	4*e*	0	0	0.10768(4)	0.0104(3)	1
Sb3	8*j*	0	0.0788(11)	½	0.0298(17)	0.235(5)
Ce1	4*e*	0	0	0.34751(3)	0.0090(2)	1
Fe1	2*a*	0	0	0	0.0129(6)	1
Fe2	8*g*	0	½	0.44922(10)	0.0316(12)	0.744(12)
Sb1	4*d*	0	½	¼	0.0070(2)	1
Sb2	4*e*	0	0	0.10983(4)	0.0091(2)	1
Sb3	4*e*	0	0	0.48595(15)	0.0412(13)	0.462(8)
Pr1	4*e*	0	0	0.34716(4)	0.0104(3)	1
Fe1	2*a*	0	0	0	0.0146(8)	1
Fe2	8*g*	0	½	0.44894(13)	0.0344(16)	0.755(19)
Sb1	4*d*	0	½	¼	0.0085(3)	1
Sb2	4*e*	0	0	0.11072(5)	0.0100(4)	1
Sb3	4*e*	0	0	0.48405(18)	0.0318(13)	0.464(11)
Nd1	4*e*	0	0	0.34686(4)	0.0103(4)	1
Fe1	2*a*	0	0	0	0.0177(9)	1
Fe2	8*g*	0	½	0.44849(13)	0.0328(17)	0.739(17)
Sb1	4*d*	0	½	¼	0.0080(4)	1
Sb2	4*e*	0	0	0.11160(5)	0.0100(4)	1
Sb3	4*e*	0	0	0.48338(16)	0.0247(13)	0.456(10)
Sm1	4*e*	0	0	0.34659(3)	0.0113(2)	1
Fe1	2*a*	0	0	0	0.0145(6)	1
Fe2	8*g*	0	½	0.44755(10)	0.0338(13)	0.737(13)
Sb1	4*d*	0	½	¼	0.0097(2)	1
Sb2	4*e*	0	0	0.11287(4)	0.0109(3)	1
Sb3	4*e*	0	0	0.48335(12)	0.0240(9)	0.461(8)

[a]U_{eq} is defined as 1/3 of the trace of the orthogonalized U_{ij} tensor.

Table 4.3 Selected Interatomic Distances and Angles for $Ln_2Fe_4Sb_5$ (Ln = La – Nd and Sm)

	$La_2Fe_4Sb_5$	$Ce_2Fe_4Sb_5$	$Pr_2Fe_4Sb_5$	$Nd_2Fe_4Sb_5$	$Sm_2Fe_4Sb_5$
Distance (Å)					
Ln–Sb1 (x4)	3.3657(10)	3.3318(8)	3.3197(15)	3.3062(10)	3.2645(10)
Ln–Sb2 (x4)	3.2893(11)	3.2522(11)	3.2403(12)	3.2288(12)	3.1937(11)
Fe1–Fe2 (x2)	2.5348(15)	2.5331(15)	2.5318(19)	2.5326(18)	2.5219(15)
Fe2–Fe2 (x1)	2.600(5)	2.641(5)	2.652(7)	2.669(6)	2.681(5)
Fe2-Sb2 (x2)	2.6553(18)	2.6514(18)	2.656(2)	2.657(2)	2.6360(17)
Fe2-Sb3 (x2)	2.247(4)-2.5579(17)	2.3634(19)	2.342(2)	2.335(2)	2.3239(17)
Sb1-Sb1 (x2)	3.0775(11)	3.0573(11)	3.0500(11)	3.0442(11)	3.0210(11)
angle (º)					
Fe2-Fe1-Fe2	61.71(10)	62.83(10)	63.18(13)	63.59(13)	64.22(10)
Fe1-Fe2-Fe2	59.15(5)	58.59(5)	58.41(7)	58.20(6)	57.89(5)
Fe1-Fe2-Fe2	59.15(5)	58.59(5)	58.41(7)	58.20(6)	57.89(5)
Sb1-Sb1-Sb1	90.0	90.0	90.0	90.0	90.0

compounds obtained from room temperature data collections are listed in Table 4.1. The tetragonal Laue symmetry 4/*mmm* and systematic absences led to the space group selection of *I*4/*mmm*. The generation of the initial models and structure refinement were conducted using SIR97 and SHELX97, respectively.[23-24] After the refinement of all atomic positions, the collected data were corrected for extinction and absorption. The displacement parameters were then refined as anisotropic and weighting schemes were applied during the final stages of refinement. The atomic coordinates, displacement parameters, and occupancies are listed in Table 4.2. Selected interatomic distances and angles for all analogues are provided in Table 4.3.

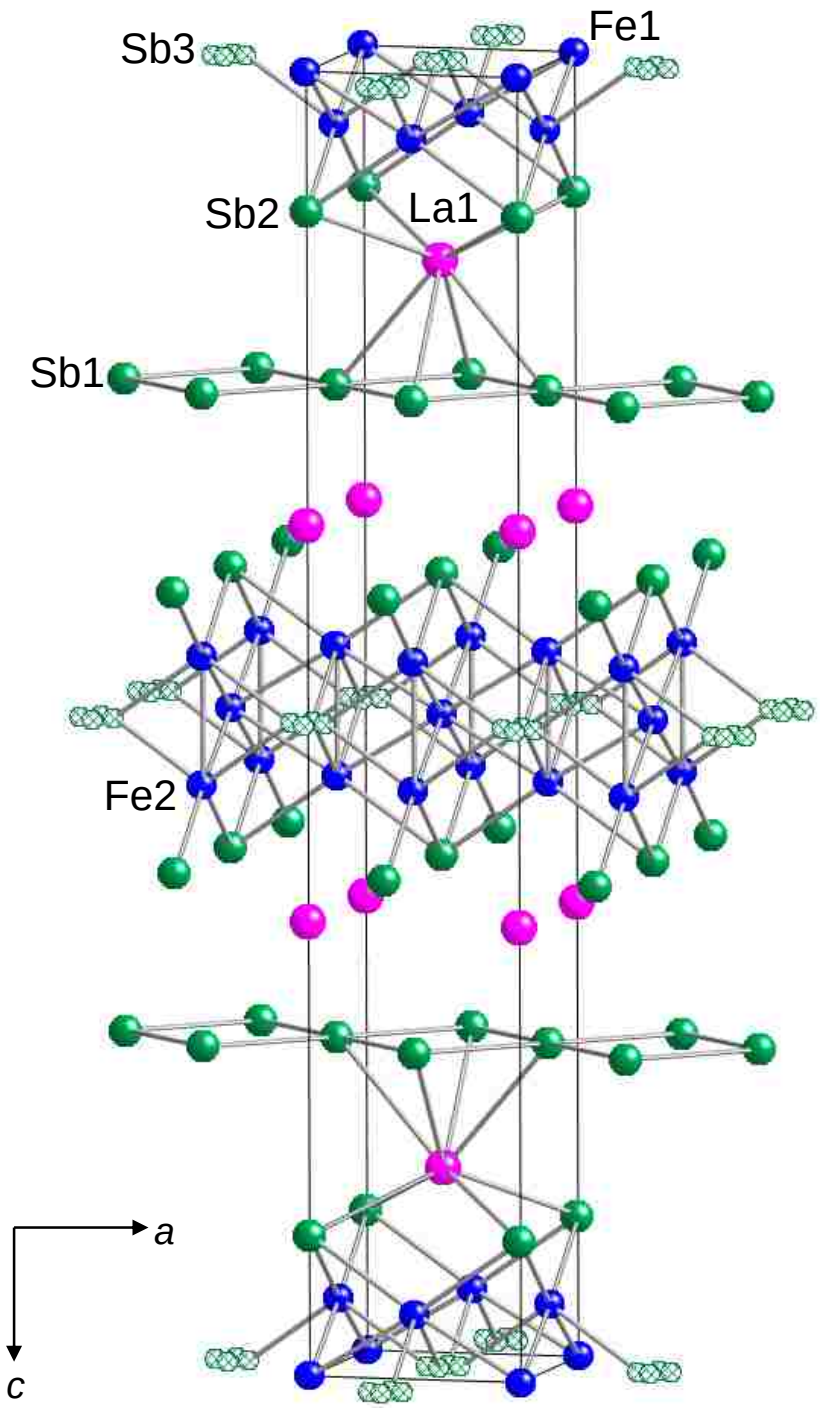

Figure 4.1 Crystal structure of $La_2Fe_4Sb_5$.

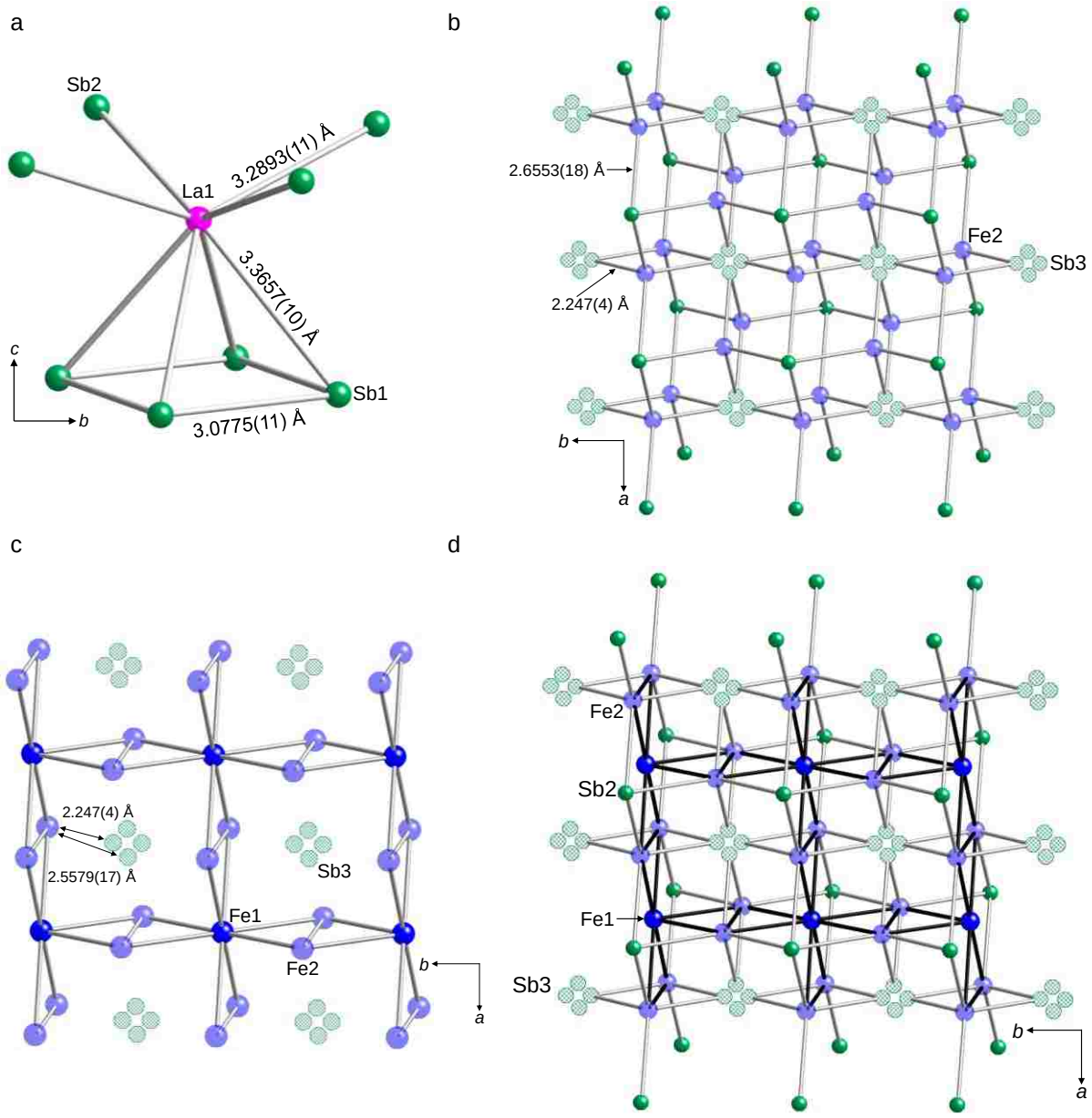

Figure 4.2a-d The structural subunits comprising $La_2Fe_4Sb_5$.

Since the reported compositions in Table 4.1 are very close to $Ln_2Fe_4Sb_5$ (Ln = La – Nd and Sm), the compounds hereafter will be referred to as $Ln_2Fe_4Sb_5$ (Ln = La – Nd and Sm).

4.2.3 Physical Properties

Magnetic data were collected using a Quantum Design Magnetic Property Measurement System (MPMS). The temperature-dependent magnetic susceptibility data were measured along

the *a*- and *c*-axis of each crystal under an applied magnetic field of 1000 Oe under both zero-field cooled (ZFC) and field cooled (FC) conditions between 2.25 and 400 K for all analogues. Field-dependent magnetization data were collected at 5 K with applied magnetic fields up to 5 T. The temperature dependent electrical resistivity and isothermal transverse magnetoresistance (MR) for $La_2Fe_4Sb_5$ and $Ce_2Fe_4Sb_5$ were measured by the standard four-probe ac-technique using the MPMS. The frequency and current employed for these experiments were 17 Hz and 1 mA, respectively. The specific heat capacity data for $La_2Fe_4Sb_5$ and $Ce_2Fe_4Sb_5$ were collected using a Quantum Design Physical Property Measurement System (PPMS).

4.3 Results and Discussion

4.3.1 Structure

The crystal structure of $La_2Fe_4Sb_5$ is shown in Figure 4.1. $La_2Fe_4Sb_5$ can be envisioned as being partially built from La1[$Sb1_4Sb2_4$] square antiprisms.[25] This geometric network can be viewed in Figure 4.2a, and this network is also present in $LaSb_2$[26-27] and $LnTSb_3$ (Ln = early lanthanides; T =Cr, Ni, Fe, Co).[1-5, 7-8, 28-29] The La1 atoms are surrounded by 8 Sb atoms and adopt a square antiprismatic geometry. Four Sb1 atoms form a perfect square net and are situated directly above or below the La1 atoms, while four Sb2 atoms form a square directly below or above the La1 atoms but twisted 45º with respect to the perfect square net. These planar square Sb sheets are commonly observed geometric networks for Sb-containing compounds.[30-31] The La – Sb bond distances of $La_2Fe_4Sb_5$ range from 3.2893(11) Å – 3.3657(10) Å and are comparable to the La – Sb bond distances reported for $LaPdSb_3$ which also form square antiprisms (3.2850(5) Å – 3.4252(17) Å).[3]

An expanded view of the Fe-sublattice for $La_2Fe_4Sb_5$ is shown in Figure 4.2b-d. The bonding interactions of Fe-sublattice can be partitioned into two parts (Fe – Sb and Fe – Fe

bonds) which are shown in Figure 4.2b-c. The occupationally disordered Fe2 atoms (translucent blue spheres) are bonded to the Sb2 and Sb3 atoms in a tetrahedral arrangement as shown in Figure 4.2b. This arrangement is similar to the tetrahedral Fe – Pn coordination found in the new classes of iron pnictide superconductors[32-33] and the tetrahedral arrangement of the Ni – Sb bonds in $LnNi_{1-x}Sb_2$ (Ln = Y, Gd-Er).[34] Fe2 – Sb2 and Fe2 – Sb3 bond distances correspond to 2.6553(18) Å and 2.247(7) Å – 2.5579(17) Å, respectively. These Fe2 – Sb3 bond distance are smaller than the Fe – Sb bond distances of $FeSb_2$, which range from 2.5762(6) Å – 2.6164(11) Å.[35-36] Similar short interatomic distances were observed for $La_2Fe_{5-x}Sb_{10-y}$ (x = 1.12, y = 5.08) and were attributed to the occupational disorder of the Fe2 position.[25] The positional disorder of the Sb3 position for $La_2Fe_4Sb_5$ also influences the short Fe2 – Sb3 interatomic distances. The Fe – Fe contacts within the Fe-sublattice of $La_2Fe_4Sb_5$ are shown in Figure 4.2c and form a 2-dimensional bowtie network of Fe – Fe bonds composed of nearly equilateral triangles. The triangles are comprised of Fe1 atoms (blue spheres) bonded to two Fe2 atoms (translucent blue spheres) at a distance of 2.5348(15) Å, and an Fe2 – Fe2 bond at a distance of 2.600(5) Å. These Fe – Fe bond distances are slightly smaller than the Fe – Fe bond distances reported for the $LnFeSb_3$ (Ln = Pr, Nd, Sm, Gd, and Tb) compounds.[7] The nearly equilateral triangles of Fe and the occupational disorder modeled for the Fe2 site present the possibility for geometric magnetic frustration and associated spin glass ordering in $Ln_2Fe_4Sb_5$ (Ln = La – Nd and Sm).[37] The physical properties presented below do indeed exhibit features inherent to many spin-glass systems. Figure 4.2d shows the complete bond arrangement of the Fe-sublattice of $La_2Fe_4Sb_5$.

It is worth noting that the positional disorder for Sb3 varies from $La_2Fe_4Sb_5$ compared to $Ln_2Fe_4Sb_5$ (Ln = Ce – Nd and Sm), as this position is slightly shifted from the 2*b* Wyckoff position which has the Wyckoff site symmetry of 4/*mmm*. A large, unrealistic U_{eq} value for Sb3

Table 4.4 Magnetic Parameters for $La_2Fe_4Sb_5$

	$La_2Fe_4Sb_5$
Fe^{3+} Fit	
Fit Region	70 K – 400 K
χ_0	0.00539(4)
C (cm^3 K/mol)	17.638
θ_w (K)	-147.8(2)
R^2	0.99986
Fe^{2+} Fit	
Fit Region	70 K – 400 K
χ_0	0.01422(2)
C (cm^3 K/mol)	12.094
θ_w (K)	-92.7(9)
R^2	0.99716

Table 4.5 Magnetic Parameters for $Ln_2Fe_4Sb_5$ (Ln = Ce – Nd and Sm)

	$Ce_2Fe_4Sb_5$	$Pr_2Fe_4Sb_5$	$Nd_2Fe_4Sb_5$	$Sm_2Fe_4Sb_5$
Fit Region	45 K – 400 K	37 K – 400 K	40 K – 400 K	60 K – 400 K
χ_0	-0.0114(2)	0.0272(2)	0.00212(2)	0.0062(2)
C_{Fe3+} (cm^3 K/mol)	17.418	17.594	17.331	17.491
C_{Ln3+} (cm^3 K/mol)	1.599	3.201	3.271	12.04
θ_{Fe3+} (K)	-146(1)	-98.2(7)	-149(1)	-155(2)
θ_{Ln3+} (K)	19.8(3)	17.1(1)	14.5(2)	10(3)
R^2	0.99935	0.99984	0.9964	0.99848

in all analogue models results when this atom is left on the 2*b* Wyckoff position. The Sb3 position for $La_2Fe_4Sb_5$ is positionally disordered around a 4-fold axis of rotation whereas, the Sb3 position for $Ln_2Fe_4Sb_5$ (Ln = Ce – Nd and Sm) is positionally disordered around a mirror plane. P. Woll also observed that the Sb3 position of $Ce_2Fe_4Sb_5$ and $Pr_2Fe_4Sb_5$ were positionally disordered around a mirror plane; however, no positional disorder was modeled for the Sb3 position of $La_2Fe_4Sb_5$ or $Nd_2Fe_4Sb_5$.[22] However, modeling the positional disorder of the Sb3 for $La_2Fe_4Sb_5$ and $Nd_2Fe_4Sb_5$ as described above is more suitable.

The Sb2 atoms which form the square nets in $La_2Fe_4Sb_5$ are separated by a distance of 3.0775(11) Å. This bond distance is slightly larger but comparable to the Sb – Sb bond distances reported for $LnFeSb_3$ (Ln = Pr, Nd, Sm, Gd, and Tb) (~3.00 Å)[7] and those reported for the Zintl phase Sr_2Sb_3 (2.887 Å – 2.922 Å).[38] However, these Sb-Sb distances are shorter than those reported for $Eu_{14}MnSb_{11}$ (3.258(2) Å).[39]

4.3.2 Physical Properties

The temperature-dependent magnetic susceptibility of $La_2Fe_4Sb_5$ is shown in Figure 4.3a-b where a magnetic field of 1kOe was applied along the *a*-axis of the crystal. When the fits of modified Curie-Weiss equation; $\chi(T) = \chi_0 + C/(T - \theta_w)$, where C represents the Curie constant, θ_w denotes the Weiss temperature, and χ_0 represents the temperature-independent contributions to the magnetic susceptibility due to Larmor diamagnetism and Pauli paramagnetism, to the data were performed taking the Curie constant as a free parameter we find that C is not well constrained by the data above 70 K. Therefore, to get an impression of the size of the magnetic moment associated with the Fe atoms we performed fits with the Curie constant fixed at the expected values for Fe^{3+} and Fe^{2+}. The usual form, Equation 4.1, was used to calculate the expected Curie constant for both an Fe^{3+} and Fe^{2+}-sublattice in $La_2Fe_4Sb_5$:

$$C = \frac{N_A \cdot g^2 \cdot \mu_B{}^2 \cdot J(J+1)}{3k_B} = \frac{N_A \cdot p_{eff}^2}{3k_B} \qquad 4.1$$

where N_A is Avogadro's number, g is the Landé g-factor, μ_B is the Bohr magneton, J is the total angular momentum as predicted by Hund's rules, and k_B is Boltzmann's constant.[40] The Curie constant values which correspond to an Fe^{3+} and Fe^{2+}-sublattice for $La_2Fe_4Sb_5$ were calculated to be 17.638 cm^3 K/mol and 12.094 cm^3 K/mol, respectively. The magnetic susceptibility data for $La_2Fe_4Sb_5$ were fit from 70 K – 400 K by setting the Curie constant equal to the calculated values and allowing the θ_w and χ_0 parameters to float. The best fit magnetic parameters obtained this procedure are listed in Table 4.4 and the resulting fits are shown in Figure 4.3a-b. From Figure 4.3 and Table 4.4, it can be clearly seen that the model fit the data somewhat better assuming that the iron magnetic ions are present in a Fe^{3+} oxidation state. Additionally, the divergence of the field cooled (FC) and zero-field cooled (ZFC) magnetic susceptibility around 30 K (T^* ~ 30 K) and the large Weiss temperature (θ_w ~ -150 K) inferred from the fit support the notion of a low temperature spin glass state in $La_2Fe_4Sb_5$ originating in the Fe-sublattice. This magnetic behavior correlates well with the structural motif shown in Figure 4.2c, where the nearly equilateral triangles composed of magnetic Fe-ions combined with the occupational disorder of the Fe2 and the positional disorder of the Sb3 site can most certainly lead to spin glass behavior.[37] Similar to the spin glass materials MAl_2S_4 (M = Mn, Fe, and Co),[19] the spin glass behavior of $Ln_2Fe_4Sb_5$ (Ln = La – Nd and Sm) results from the magnetic interactions of an occupationally disordered transition metal sublattice.

After characterizing the La compound, we explored the changes that occur upon substituting Ln elements on the La site expecting more complex magnetic behavior. However, the magnetic susceptibility is not vastly different across the series as can be seen in Figure 4.4a-d where the data for $Ln_2Fe_4Sb_5$ (Ln = Ce – Nd and Sm) in a magnetic field of 1kOe applied along

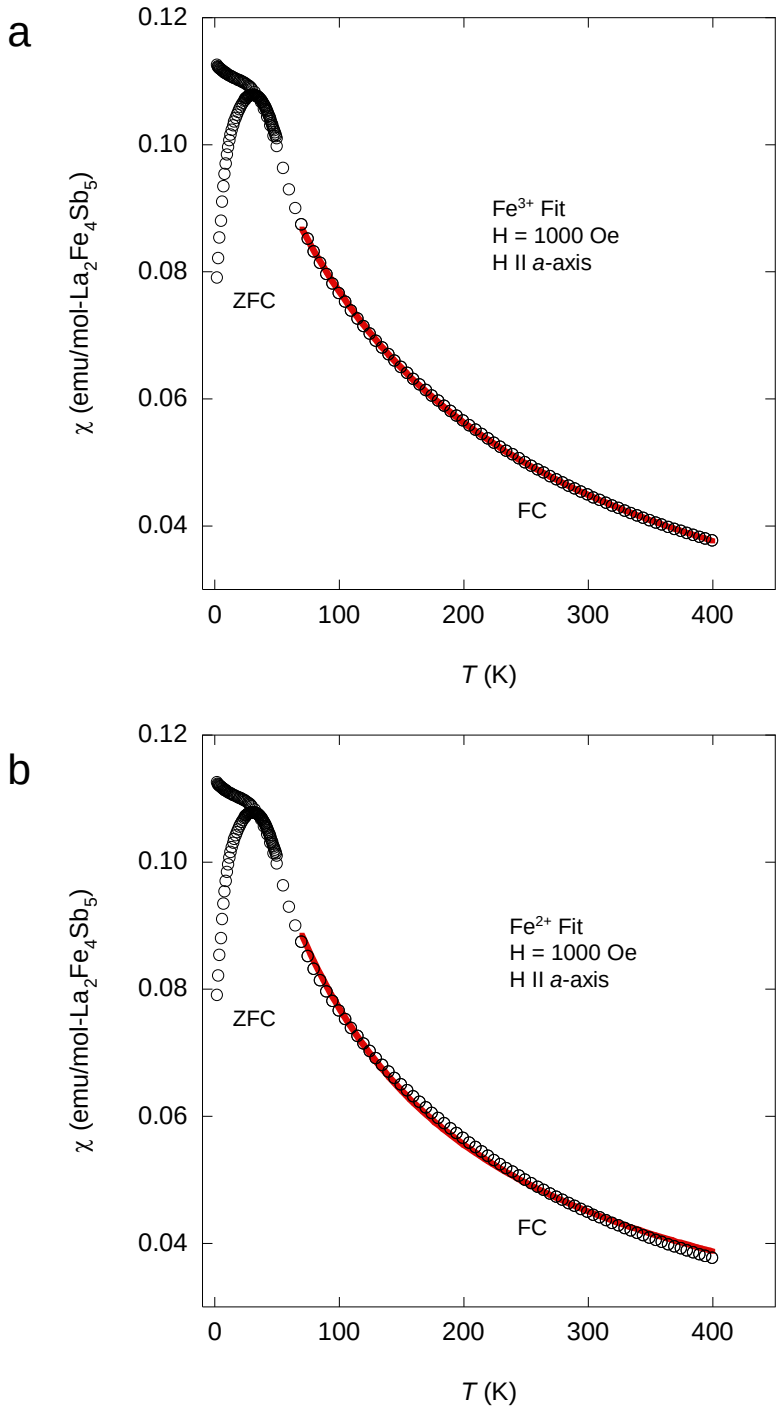

Figure 4.3a-b The temperature dependent magnetic susceptibility (χ) of $La_2Fe_4Sb_5$ where a magnetic field (H) of 1kOe was applied along the *a*-axis of the crystal structure.

the *a*-axis of the crystals are displayed. When a similar fitting procedure to that described above was employed to fit these magnetic data, we did not find satisfactory convergence of Equation

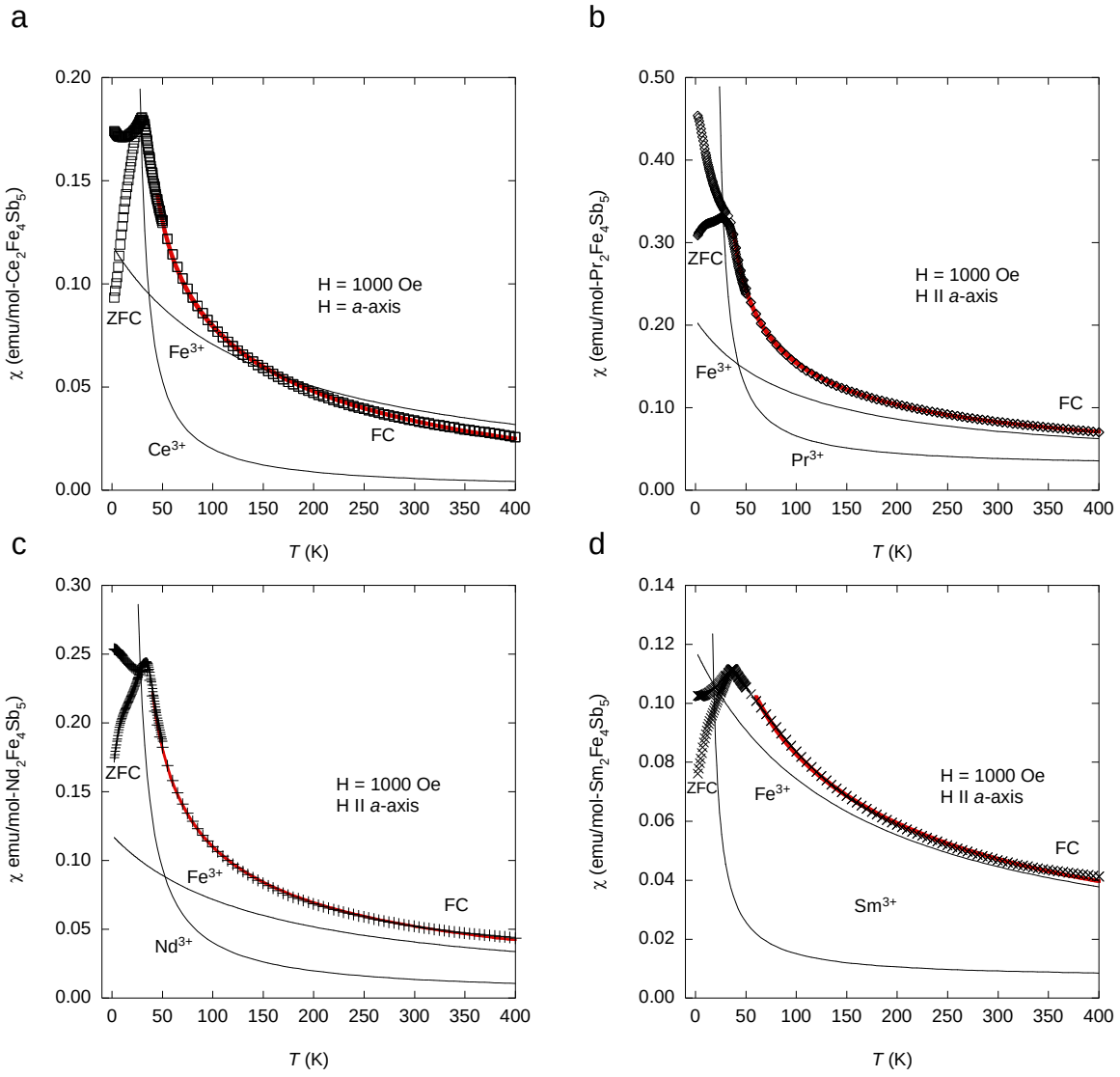

Figure 4.4a-d The temperature dependent magnetic susceptibility (χ) of $Ln_2Fe_4Sb_5$ (Ln = Ce – Nd, and Sm) where a magnetic field (H) of 1kOe was applied along the *a*-axis of the crystal structure.

4.1 to the data. This model assumes a single magnetic moment results from both the Ln and the Fe sublattices. Thus the data forced us to consider a slightly more complex model where the Fe and Ln ions formed two non-interacting magnetic sublattices. Here we used a modified Curie-Weiss equation with the inclusion of a second Curie-Weiss term, $\chi(T) = \chi_0 + C_{Fe3+}/(T - \theta_{Fe3+}) + C_{Ln3+}/(T - \theta_{Ln3+})$. The expected Curie constant for an independent Fe^{3+}-sublattices and Ln^{3+}

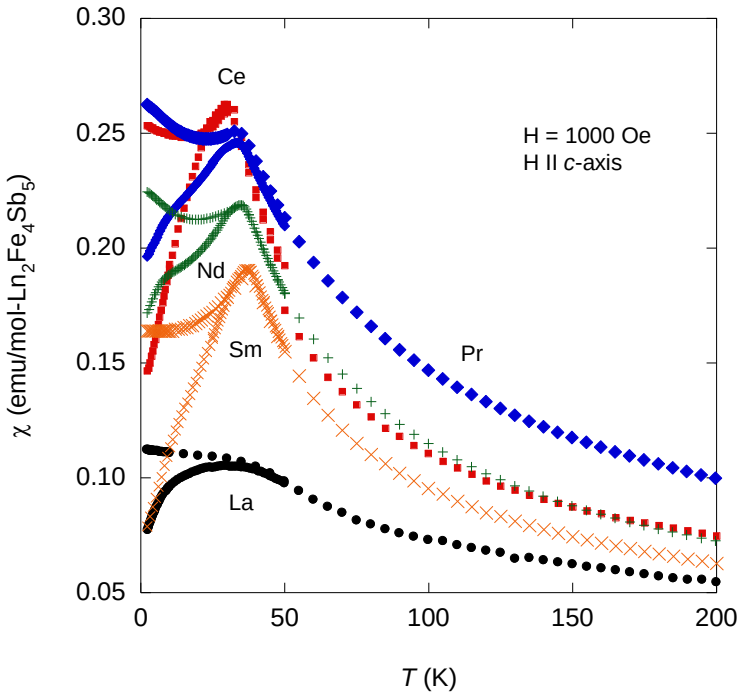

Figure 4.5 The temperature dependent magnetic susceptibility (χ) of $Ln_2Fe_4Sb_5$ (Ln = La – Nd, and Sm) where a magnetic field (H) of 1kOe was applied along the *c*-axis of the crystal.

(Ln^{3+} = Ce^{3+} – Nd^{3+} and Sm^{3+}) sublattices were calculated using Equation 4.1 and are displayed in Table 4.5. It was assumed that the Fe ions in $Ln_2Fe_4Sb_5$ (Ln = Ce – Nd and Sm) adopt a 3^+ oxidation state based on the fitting results for $La_2Fe_4Sb_5$ (Figure 4.3a-b). The magnetic susceptibility data for $Ln_2Fe_4Sb_5$ (Ln = Ce – Nd and Sm) were fit by setting the two Curie constants equal to the calculated values Fe^{3+} and Ln^{3+} (Ln^{3+} = Ce^{3+} – Nd^{3+} and Sm^{3+}) and allowing the θ_w and χ_0 parameters to float. The results of these fits are shown in Figure 4.4a-d and all magnetic parameters obtained from the fits are provided in Table 4.5. Curves which correspond to the calculated magnetic susceptibility based on these parameters for the individual Ln^{3+} and Fe^{3+}-sublattice contributions for $Ln_2Fe_4Sb_5$ (Ln = Ce – Nd and Sm) are included in Figure 4.4. Our best fits that result from the procedure described above are dominated above 100 K by the contribution from the Fe-sublattice which is very similar in magnitude to that found in the La compound. An additional contribution dominates in a narrow temperature range above

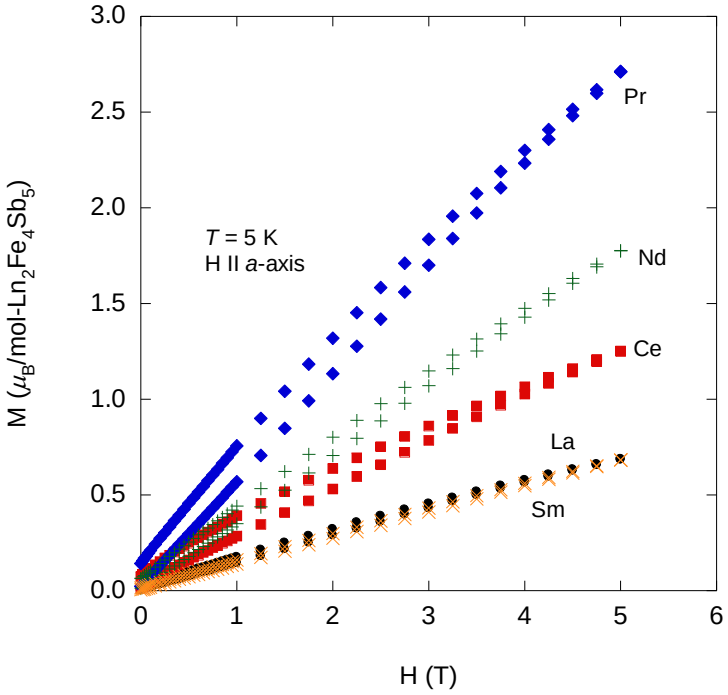

Figure 4.6 The field dependent magnetization (M) of $Ln_2Fe_4Sb_5$ (Ln = La – Nd, and Sm) where a magnetic fields up to 5 T were applied along the *a*-axis of the crystal at 5 K.

*T**. The observed large increase in $\chi(T)$ at temperatures above *T** result in positive Weiss temperatures ($\theta_{Ln3+} > 0$) corresponding to ferromagnetic interactions in the Ln-sublattice. The small changes in the magnetic susceptibility for $T > 100$ K along with the quality of the fits of this simple model to the data further support the notion that the Ln^{3+} and Fe^{3+}-sublattices are not well coupled to one another in this *T*-range. Additionally, the divergence of the field cooled (FC) and zero-field cooled (ZFC) magnetic susceptibility around 30 K (*T** ~ 30 K) and the large negative θ_{Fe3+} evidence low temperature spin glass behavior for all $Ln_2Fe_4Sb_5$ (Ln = Ce – Nd and Sm) crystals investigated.[37]

The temperature-dependent magnetic susceptibility from 2 K – 200 K for $Ln_2Fe_4Sb_5$ (Ln = La – Nd and Sm) is shown Figure 4.5 where a magnetic field of 1kOe was applied along the *c*-axis of the crystals. Similar to the H ∥ *a*-axis data, bifurcations in the field cooled (FC) and zero-

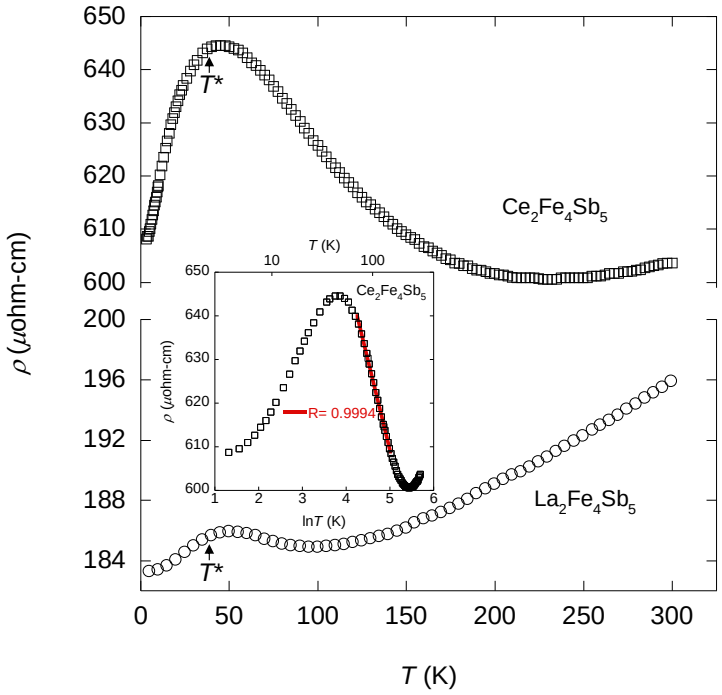

Figure 4.7 Temperature dependent electrical resistivity (ρ) for $La_2Fe_4Sb_5$ and $Ce_2Fe_4Sb_5$. The inset shows a liner fit to the resistivity (ρ) vs. ln$T$ of $Ce_2Fe_4Sb_5$ from 70 K – 150 K.

field cooled (ZFC) magnetic susceptibility for each analogue are observed between 25 and 40 K. Little to no magnetic anisotropy is observed in the magnetic data when the susceptibilities for $Ln_2Fe_4Sb_5$ (Ln = La – Nd and Sm) are compared along the different axial directions. The field-dependent magnetization up to 5 T at 5 K is presented in Figure 4.6 for $Ln_2Fe_4Sb_5$ (Ln = La – Nd and Sm) with the magnetic field applied along the *a*-axis of these crystals. Small hysteresis effects are observed for each analogue indicative of spin glass behavior. Spin glass materials are characterized by their large number of nearly degenerate states, therefore, the exact ground states occupied at low temperatures is determined by the history of the experimental conditions and thus irreversible magnetic behavior is observed.[37]

The electrical resistivity versus temperature for $La_2Fe_4Sb_5$ and $Ce_2Fe_4Sb_5$ is shown in Figure 4.7. Both analogues display metallic behavior down to 3 K. $La_2Fe_4Sb_5$ and $Ce_2Fe_4Sb_5$ both display a wide range of temperatures where ρ decreases with T, between 50 and 100 K for

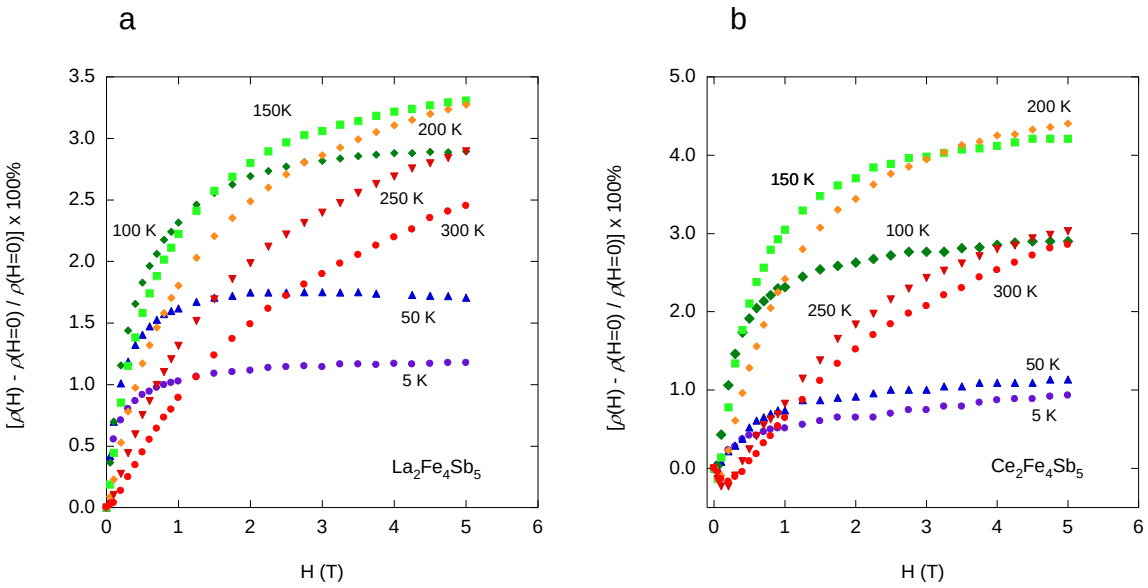

Figure 4.8 Field dependent magnetoresistance [(ρ(H) – ρ(H=0) / ρ(H=0)) x 100%] for **a** $La_2Fe_4Sb_5$ and **b** $Ce_2Fe_4Sb_5$ at various temperatures.

$La_2Fe_5Sb_5$ and between 50 and 225 K for $Ce_2Fe_4Sb_5$. A Kondo mechanism is usually suspected when $d\rho/dT < 0$ over wide ranges of temperature in metallic systems containing magnetic moments, and a plot of ρ as a function of ln$T$ for $Ce_2Fe_4Sb_5$ is included in the inset of Figure 4.7 for a comparison to the usual Kondo form. A similar linear fit ρ vs. ln$T$ curve in the region of the upturn for $La_2Fe_4Sb_5$ is not displayed due to the limited temperature range where $d\rho/dT < 0$. In addition, the resistivity maxima are observed close to T^* ($T^* \sim 30$ K) was observed as the bifurcations in the ZFC and FC magnetic susceptibility data for $La_2Fe_4Sb_5$ and $Ce_2Fe_4Sb_5$.) for both $La_2Fe_4Sb_5$ and $Ce_2Fe_4Sb_5$. Below T^* the resistivity decreases slightly so that these curves resemble traditional spin glass systems where an incoherent Kondo regime is present above a glassy freezing temperature (T^*). Below (T^*) the Ruderman-Kittel-Kasuya-Yosida (RKKY)

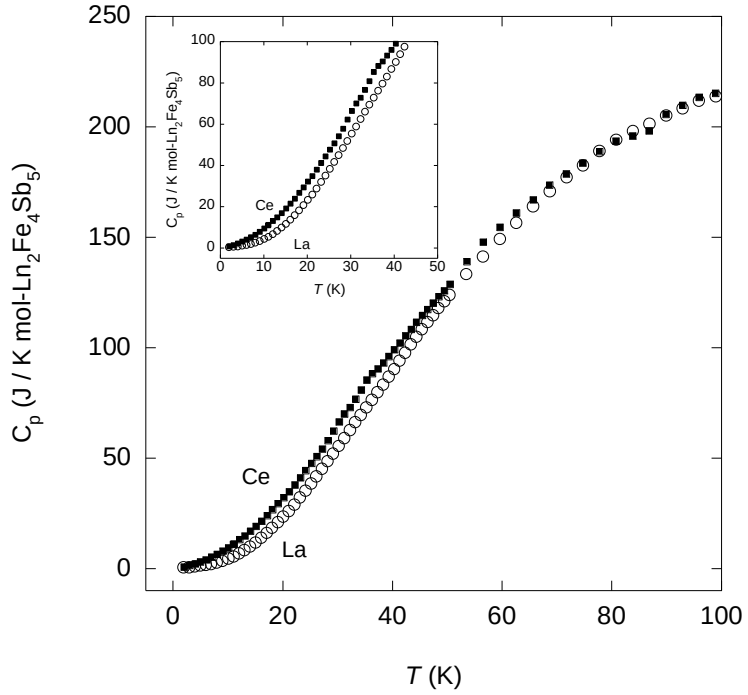

Figure 4.9 Specific heat capacity (C_p) for $La_2Fe_4Sb_5$ and $Ce_2Fe_4Sb_5$ as a function of temperature.

interactions become important and serve to "freeze out" the spins fluctuations reducing the spin disorder scattering.[41]

The magnetoresistance as a function of an applied magnetic field at various temperatures for $La_2Fe_4Sb_5$ and $Ce_2Fe_4Sb_5$ is shown in Figure 4.8a-b. The magnetoresistance for both compounds is small and positive over all values of temperature and field with the exception of the low field values at T = 250 K and 300 K for $Ce_2Fe_4Sb_5$. The origin of this positive magnetoresistance is unknown, as Kondo systems typically exhibit negative magnetoresistances.[42] However, the structurally related $LnNi(Sn,Sb)_3$ (Ln = Pr, Sm, Gd, and Nd) compounds also exhibit small positive magnetoresistance values at 3 K.[5]

The specific heat of $Ln_2Fe_4Sb_5$ (Ln = La and Ce) is shown in Figure 4.9. From the inset of this figure, it can be observed that no thermodynamic phase transitions are present down to the lowest temperatures measured, although a small anomaly can be observed near T* for $Ce_2Fe_4Sb_5$.

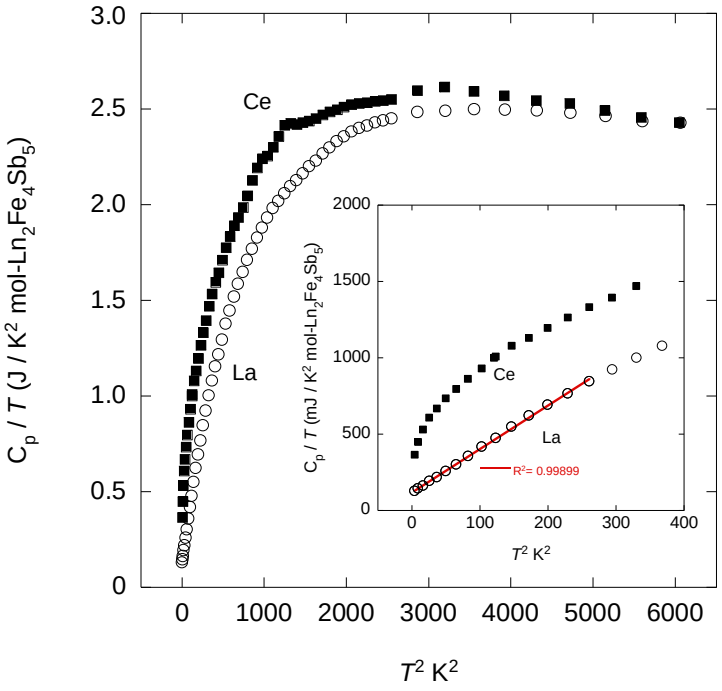

Figure 4.10 Specific heat capacity divided by temperature (C_p/T) of $La_2Fe_4Sb_5$ and $Ce_2Fe_4Sb_5$ as a function of temperature squared (T^2).

The simultaneous occurrence of sharp ordering features in the magnetic response and the absence of a response in the thermal properties is a clear indication of glassy order.[37] A plot of the specific heat divided by temperature (C_p/T) as a function of T^2 for $Ln_2Fe_4Sb_5$ (Ln = La and Ce) is shown in Figure 4.10. Again, no thermodynamic phase transitions are visible in this plot, although the small anomaly around 35 K observed for the Ce compound suggests a small gain in the magnetic entropy near T*. Fits of the C_p/T vs. T^2 data to the standard metallic form ($C_p = \gamma T + \beta T^3$) were performed in order to determine the γ and β coefficients for $La_2Fe_4Sb_5$. The values for the γ and β coefficients for the best fits to our $La_2Fe_4Sb_5$ data were found to be 118 mJ/mol-$La_2Fe_4Sb_5$ K^2 and 2.85 mJ/mol-$La_2Fe_4Sb_5$ K^4, respectively. The Sommerfeld coefficient (γ) for each Fe unit in $La_2Fe_4Sb_5$ is γ ~ 30 mJ/ mol-Fe K^2. This value of the Sommerfeld coefficient is approximately a factor of 30 greater than that of simple metals like Cu, which has a γ ~ 0.7 mJ/mol K^2.[43] A similar fit to the C_p/T vs. T^2 data for $Ce_2Fe_4Sb_5$ appears not to be appropriate

since the data do not resemble this simple form. We believe that contributions from the magnetic degrees of freedom associated with the Ce *f*-electrons is significant in this *T*-range and an accurate separation of magnetic, electronic, and phonon contributions was not deemed possible.

4.4 Conclusion

Single crystals of $Ln_2Fe_4Sb_5$ (Ln = La – Nd and Sm) were grown using an inert Bi flux. Single crystal X-ray diffraction experiments revealed Fe – Sb bonds that form a tetrahedral arrangement similar to that found in the new classes of iron pnictide superconductors.[32-33] This tetrahedral PbO-type slab is not seen in the early lanthanide-transition metal-antimonides previously studied (e.g. $LnTSb_3$ (Ln = early lanthanides; T = Ni, Fe, Co)[1-8]) but, instead observed in the late lanthanide-transition metal-antimonides (e.g. $LnNi_{1-x}Sb_2$ (Ln = late lanthanide)).[8, 34] We have shown by way of the similarity in the magnetic response of the La compared to the Ce – Nd and Sm compounds that the spin-glass behavior of $Ln_2Fe_4Sb_5$ (Ln = La – Nd and Sm) results from magnetic correlations within the Fe-sublattices. The Fe – Fe bonding structural motif of the Fe-sublattices correlates well with the glassy magnetic properties presented for each analogue. The resistivity and heat capacity measurements of $La_2Fe_4Sb_5$ and $Ce_2Fe_4Sb_5$ further support the spin glass behavior in these compounds. The origin of the large Sommerfeld (γ = 118 mJ/mol-$La_2Fe_4Sb_5$ K^2) coefficient determined from fits to the heat capacity of $La_2Fe_4Sb_5$ is unknown. A similar but larger effect in the geometrically frustrated spinel, LiV_2O_4, has been attributed to heavy-fermion behavior.[44] The origins of enhanced mass behavior in LiV_2O_4 is thought to be different from the traditional heavy-fermion mechanism in Ce, Yb, and U-containing compounds. Instead, the origins of heavy-fermion behavior in LiV_2O_4 has been attributed to geometric frustration.[44] We cannot rule out such a mechanism in $La_2Fe_4Sb_5$ as it is

similarly characterized by geometric frustration in the Fe-sublattice and a large γ. However, here we observe a spin glass like ordering unlike what was observed in LiV_2O_4 making the mechanism for the large linear-in-*T* contribution to C(*T*) more likely to be magnetic in origin. The anomalously large linear-in-*T* C(*T*) observed in some spin glass materials is thought to arise from the disruptions of RKKY magnetic interactions between magnetic atoms by a nonmagnetic atom disorder. It is plausible that the enhanced γ that we infer for $La_2Fe_4Sb_5$ results from the disruption of the magnetic interactions within the Fe-sublattice by the Fe2 positional disorder and occupational disorder of the nonmagnetic Sb3 atoms.[45]

4.5 References

1. Macaluso, R. T.; Wells, D. M.; Sykora, R. E.; Albrecht-Schmitt, T. E.; Mar, A.; Nakatsuji, S.; Lee, H.; Fisk, Z.; Chan, J. Y., Structure and Electrical Resistivity of $CeNiSb_3$. *J. Solid State Chem.* **2004**, *177*, 293-298.

2. Thomas, E. L.; Macaluso, R. T.; Lee, H. O.; Fisk, Z.; Chan, J. Y., Crystal Growth, Characterization, and Physical Properties of $PrNiSb_3$, $NdNiSb_3$, and $SmNiSb_3$. *J. Solid State Chem.* **2004**, *177*, 4228-4236.

3. Thomas, E. L.; Gautreaux, D. P.; Chan, J. Y., The Layered Intermetallic Compound $LaPdSb_3$. *Acta Crystallogr. Sect. E. Struct. Rep. E* **2006**, *62*, I96-I98.

4. Thomas, E. L.; Gautreaux, D. P.; Lee, H. O.; Fisk, Z.; Chan, J. Y., Discovery of β-$LnNiSb_3$ (Ln = La, Ce): Crystal Growth, Structure, and Magnetic and Transport Behavior. *Inorg. Chem.* **2007**, *46*, 3010-3016.

5. Gautreaux, D. P.; Capan, C.; DiTusa, J. F.; Young, D. P.; Chan, J. Y., Synthesis, Structure and Physical Properties of $LnNi(Sn,Sb)_3$ (Ln = Pr, Nd, Sm, Gd, Tb). *J. Solid State Chem.* **2008**, *181*, 1977-1982.

6. Gautreaux, D. P.; Parent, M.; Moldovan, M.; Young, D. P.; Chan, J. Y., Magnetization and Transport Properties of α-$CeNi_{0.78}Co_{0.22}Sb_3$. *Physica B.* **2008**, *403*, 1005-1006.

7. Phelan, W. A.; Nguyen, G. V.; Karki, A. B.; Young, D. P.; Chan, J. Y., Synthesis, Structure, Magnetic and Transport Properties of $LnFeSb_3$ (Ln = Pr, Nd, Sm, Gd, and Tb)

-Tuning of Anisotropic Long-Range Magnetic Order as a Function of Ln. *Dalton Trans.* **2010**, *39*, 6403-6409.

8. Phelan, W. A.; Menard, M. C.; Kangas, M. J.; McCandless, G. T.; Drake, B. L.; Chan, J. Y., Adventures in Crystal Growth: Synthesis and Characterization of Single Crystals of Complex Intermetallic Compounds. *Chem. Mater.* **2012**, *24*, 409-420.

9. Drake, B. L.; Grandjean, F.; Kangas, M. J.; Okudzeto, E. K.; Karki, A. B.; Sougrati, M. T.; Young, D. P.; Long, G. J.; Chan, J. Y., Crystal Growth, Transport, and the Structural and Magnetic Properties of Ln_4FeGa_{12} with Ln = Y, Tb, Dy, Ho, and Er. *Inorg. Chem.* **2010**, *49*, 445-456.

10. Lynn, J. W.; Dai, P., Neutron Studies of the Iron-Based Family of High T_C Magnetic Superconductors. *Physica C* **2009**, *469*, 469-476.

11. Canfield, P. C., Still Alluring and Hard to Predict at 100. *Nat. Mater.* **2011**, *10*, 259-261.

12. Zhao, L. L.; Yi, T.; Fettinger, J. C.; Kauzlarich, S. M.; Morosan, E., Fermi-Liquid State and Enhanced Electron Correlations in the Iron Pnictide $CaFe_4As_3$. *Phys. Rev. B* **2009**, *80*, 020404(R).

13. Todorov, I.; Chung, D. Y.; Malliakas, C. D.; Li, Q. a.; Bakas, T.; Douvalis, A.; Trimarchi, G.; Gray, K.; Mitchell, J. F.; Freeman, A. J.; Kanatzidis, M. G., $CaFe_4As_3$: A Metallic Iron Arsenide with Anisotropic Magnetic and Charge-Transport Properties. *J. Am. Chem. Soc.* **2009**, *131*, 5405-5407.

14. Yi, T.; Dioguardi, A. P.; Klavins, P.; Curro, N. J.; Zhao, L. L.; Morosan, E.; Kauzlarich, S. M., Synthesis and Thermal Stability Studies of $CaFe_4As_3$. *Eur. J. Inorg. Chem.* **2011**, 3920-3925.

15. Nambu, Y.; Zhao, L. L.; Morosan, E.; Kim, K.; Kotliar, G.; Zajdel, P.; Green, M. A.; Ratcliff, W.; Rodriguez-Rivera, J. A.; Broholm, C., Incommensurate Magnetism in FeAs Strips: Neutron Scattering from $CaFe_4As_3$. *Phys. Rev. Lett.* **2011**, *106*, 037201.

16. Manuel, P.; Chapon, L. C.; Todorov, I. S.; Chung, D. Y.; Castellan, J. P.; Rosenkranz, S.; Osborn, R.; Toledano, P.; Kanatzidis, M. G., Incommensurate Spin-Density Wave and Magnetic Lock-in Transition in $CaFe_4As_3$. *Phys. Rev. B* **2010**, *81*, 184402.

17. Zhao, L. L.; Kim, S. K.; McCandless, G. T.; Torikachvili, M. S.; Canfield, P. C.; Chan, J. Y.; Morosan, E., Effects of Chemical Doping and Pressure on $CaFe_4As_3$. *Phys. Rev. B* **2011**, *84*, 104444.

18. Nakatsuji, S.; Nambu, Y.; Tonomura, H.; Sakai, O.; Jonas, S.; Broholm, C.; Tsunetsugu, H.; Qiu, Y. M.; Maeno, Y., Spin Disorder on a Triangular Lattice. *Science* **2005**, *309*, 1697-1700.

19. Menard, M. C.; Ishii, R.; Higo, T.; Nishibori, E.; Sawa, H.; Nakatsuji, S.; Chan, J. Y., High-Resolution Synchrotron Studies and Magnetic Properties of Frustrated Antiferromagnets MAl_2S_4 ($M = Mn^{2+}$, Fe^{2+}, Co^{2+}). *Chem. Mater.* **2011**, *23*, 3086-3094.

20. Nakatsuji, S.; Tonomura, H.; Onuma, K.; Nambu, Y.; Sakai, O.; Maeno, Y.; Macaluso, R. T.; Chan, J. Y., Spin Disorder and Order in Quasi-2D Triangular Heisenberg Antiferromagnets: Comparative Study of $FeGa_2S_4$, $Fe_2Ga_2S_5$, and $NiGa_2S_4$. *Phys. Rev. Lett.* **2007**, *99*, 157203.

21. Cordier, G.; Schafer, H.; Woll, P., New Compounds with the $CaMnBi_2$ Structure – on $LaZn_{0.5}Sb_2$, $LaCo_{0.6}Sb_2$, $LaMn_xSb_2$ ($0.65 \leq x \leq 0.76$ and $LaCu_XSb_2$ ($0.82 \leq x \leq 0.87$). *Z. Naturforsch. B* **1985**, *40*, 1097-1099.

22. Woll, P., Zur Darstellung und Strukturchemie von Erdalkali- bzw. Seltenerd-Ubergangsmetall- Element IV bzw. Element-V-Verbindugen. Ph.D. Dissertation. Technischen Hochschule Darmstadt; 1987.

23. Altomare, A.; Burla, M. C.; Camalli, M.; Cascarano, G. L.; Giacovazzo, C.; Guagliardi, A.; Moliterni, A. G. G.; Polidori, G.; Spagna, R., SIR97: A New Tool for Crystal Structure Determination and Refinement. *J. Appl. Crystallogr.* **1999**, *32*, 115-119.

24. Sheldrick, G. M., A Short History of SHELX. *Acta Crystallogr., A* **2008**, *64*, 112-122.

25. Nasir, N.; Grytsiv, A.; Rogl, P.; Kaczorowski, D.; Effenberger, H. S., The System Nd-Fe-Sb: Phase Equilibria, Crystal Structures and Physical Properties. *Intermetallics* **2010**, *18*, 2361-2376.

26. Acatrinei, A. I.; Browne, D.; Losovyj, Y. B.; Young, D. P.; Moldovan, M.; Chan, J. Y.; Sprunger, P. T.; Kurtz, R. L., Angle-Resolved Photoemission Study and First-Principles Calculation of the Electronic Structure of $LaSb_2$. *J. Phys. Cond. Matter* **2003**, *15*, L511-L517.

27. Young, D. P.; Goodrich, R. G.; Ditusa, J. F.; Guo, S.; Adams, P. W.; Chan, J. Y.; Hall, D., High Magnetic Field Sensor Using $LaSb_2$. *Appl. Phys. Lett.* **2003**, *82*, 3713-3715.

28. Hartjes, K.; Jeitschko, W.; Brylak, M., Magnetic Properties of the Rare-Earth Transition Metal Antimonides $LnVSb_3$ and $LnCrSb_3$ (Ln=La-Nd, Sm). *J. Magn. Magn. Mater.* **1997**, *173*, 109-116.

29. Sefat, A. S.; Bud'ko, S. L.; Canfield, P. C., Magnetization, Resistivity, and Heat Capacity of the Anisotropic $RVSb_3$ Crystals (R=La-Nd, Sm, Gd-Dy). *J. Magn. Magn. Mater.* **2008**, *320*, 120-141.

30. Papoian, G. A.; Hoffmann, R., Hypervalent Bonding in One, Two, and Three Dimensions: Extending the Zintl-Klemm Concept to Nonclassical Electron-Rich Networks. *Angew. Chem. Int. Ed.* **2000**, *39*, 2409-2448.

31. Mills, A. M.; Lam, R.; Ferguson, M. J.; Deakin, L.; Mar, A., Chains, Planes, and Antimonides. *Coordin. Chem. Rev.* **2002**, *233-234*, 207-222.

32. Kamihara, Y.; Hiramatsu, H.; Hirano, M.; Kawamura, R.; Yanagi, H.; Kamiya, T.; Hosono, H., Iron-Based Layered Superconductor: LaOFeP. *J. Am. Chem. Soc.* **2006**, *128*, 10012-10013.

33. Takahashi, H.; Igawa, K.; Arii, K.; Kamihara, Y.; Hirano, M.; Hosono, H., Superconductivity at 43 K in an Iron-Based Layered Compound $LaO_{1-x}F_xFeAs$. *Nature* **2008**, *453*, 376-378.

34. Thomas, E. L.; Moldovan, M.; Young, D. P.; Chan, J. Y., Synthesis, structure, and magneto-transport of $LnNi_{1-x}Sb_2$ (Ln = Y, Gd-Er). *Chem. Mater.* **2005**, *17*, 5810-5816.

35. Holseth, H.; Kjekshus, A., Compounds with the Marcasite Type Crystal Structure. 4. Crystal Structure of $FeSb_2$. *Acta. Chem. Scand.* **1969**, *23*, 3043-3050.

36. Holseth, H.; Kjekshus, A.; Andresen, A. F., Compounds with Marcasite Type Crystal Structure. 6. Neutron Diffraction Studies of $CrSb_2$ and $FeSb_2$. *Acta Chem. Scand.* **1970**, *24*, 3309-3316.

37. Ramirez, A. P., Strongly Geometrically Frustrated Magnets. *Ann. Rev. Mater. Sci.* **1994**, *24*, 453-480.

38. Eisenmann, B., Sr_2Sb_3, A Zintl-Phase with a Sb6-Chain Anion. *Z. Naturforsch. B* **1979**, *34*, 1162-1164.

39. Chan, J. Y.; Wang, M. E.; Rehr, A.; Kauzlarich, S. M.; Webb, D. J., Synthesis, Structure, and Magnetic Properties of the Rare-Earth Zintl compounds $Eu_{14}MnPn_{11}$ and $Eu_{14}InPn_{11}$ (Pn = Sb, Bi). *Chem. Mater.* **1997**, *9*, 2131-2138.

40. Gersten, J. I.; Smith, F. W., *The Physics and Chemistry of Materials*. John Wiley: New York, 2001.

41. Mydosh, J. A., From Giant Moment to Kondo and Spin Glass Behavior – Electrical Resistivity of PdFe and (PdFe)H. *Phys. Rev. Lett.* **1974**, *33*, 1562-1566.

42. Rauchschwalbe, U.; Steglich, F.; Rietschel, H., Magnetoresistance of Heavy-Fermion Compounds. *Physica B & C* **1987**, *148*, 33-36.

43. Fisk, Z.; Sarrao, J. L.; Smith, J. L.; Thompson, J. D., The Physics and Chemistry of Heavy Fermions. *Proc. Natl. Acad. Sci. U.S.A.* **1995**, *92*, 6663-6667.

44. Johnston, D. C., Heavy Fermion Behaviors in LiV_2O_4. *Physica B* **2000**, *281-282*, 21-25.

45. Gschneidner, K. A.; Tang, J.; Dhar, S. K.; Goldman, A., False Heavy Fermions. *Physica B* **1990**, *163*, 507-510.

Chapter 5. Crystal Growth and Physical Properties of $LnCu_2(Al,Si)_5$ (Ln = La and Ce)*

5.1 Introduction

The search for and understanding of materials that exhibit exotic behavior derived from complex, competing, or emergent phenomena begins with identifying the unifying characteristics of these materials. When searching for materials with competing ground states, such as Kondo screening and antiferromagnetism, where heavy electron metallic behavior and unconventional superconductivity can be found, it is obviously productive to explore Ce, Yb, and U containing compounds.[1-8] Heavy fermion behavior is commonly associated with Ce compounds and is characterized by an anomalously large Sommerfeld coefficient, γ, which parameterizes the electronic contribution to the specific heat capacity which is typically of the form $C = \gamma T + \beta T^3$. The overwhelming majority of Ce compounds contain Ce in a formal +3 valence state and order antiferromagnetically at low temperatures, while Yb containing phases more commonly exist in either the + 2 and/or + 3 oxidation states.

The unconventional superconductivity associated with quantum criticality discovered in the Ce_nMIn_{3n+2} (M = Co, Rh, or Ir, n = 1 or 2) phases has generated intense interest in finding novel highly correlated electron systems.[1-2, 9] Further exploration and understanding of this system and its low temperature behavior would be enhanced if an isostructural phase could be stabilized with M = Pd to investigate how the addition of one valence electron would perturb the ground state. Such an isostructural phase was not found; instead this research led to the discovery of a new compound. The antiferromagnetic (T_N = 5 K) heavy fermion compound, $CePdGa_6$ (γ ~ 230 mJ/mol K^2as $T \rightarrow 0$ and 400 mJ/mol K^2 $T > T_N$),[4, 10] was grown from excess Ga flux and crystallizes with a variant of the $SrAu_2Ga_5$ structure type.[11] Following this work, the

*Adapted with permission from: Phelan, W. A.; Kangas, M. J.; Drake, B. L.; Zhao, L. L.; Wang, J. K.; DiTusa, J. F.; Morosan, E.; Chan, J. Y., Crystal Growth, Structure, and Physical Properties of $LnCu_2(Al,Si)_5$ (Ln = La and Ce). *Inorg. Chem.* **2011**, *51*, 920-927. Copyright (2011) American Chemical Society.

Table 5.1 Crystallographic Parameters for $LaCu_2(Al,Si)_5$ and $CeCu_2(Al,Si)_5$

Formula	$LaCu_2(Al,Si)_5$	$CeCu_2(Al,Si)_5$
a (Å)	4.221(1)	4.204(2)
c (Å)	7.916(2)	7.926(5)
V (Å^3)	141.04(6)	140.08(13)
Z	1	1
Refined Composition	$LaCu_{1.96(16)}Al_{4.04(16)}Si$	$CeCu_{1.95(10)}Al_{4.05(10)}Si$
Crystal system	tetragonal	tetragonal
Space group	*P*4/*mmm*	*P*4/*mmm*
θ range (°)	2.55-34.97	2.55-37.04
μ (mm^{-1})	15.45	16.02
Data collection		
Measured reflections	3584	3584
Independent reflections	228	226
Reflections with $I>2\sigma(I)$	227	226
R_{int}	0.020	0.017
h	-6 – 6	-6 – 6
k	-4 – 4	-4 – 4
l	-12 – 12	-12 – 10
Refinement		
[a]$R_1[F^2>2\sigma(F^2)]$	0.024	0.012
[b]$wR_2(F^2)$	0.056	0.039
Parameters	14	14
GOOF	1.32	1.21
Extinction	0.276(18)	0.192(5)
$\Delta\rho_{max}$ (eÅ^{-3})	1.98	0.76
$\Delta\rho_{min}$ (eÅ^{-3})	-2.45	-0.48

[a]$R_1=\sum \| F_o \| - \| F_c \| / \sum | F_o |$, [b]$wR_2 = [\sum[w(F_o^2 - F_c^2)]/\sum[w(F_o^2)^2]]^{1/2}$

structurally related intermetallic Ce_2PdGa_{12} was discovered and orders antiferromagnetically at 11 K, and shows moderately enhanced charge carrier mass with γ > 70 mJ/K^2 mol.[10] The discovery of these two new antiferromagnetic phases with enhanced mass behavior warranted the growth of both the Ni and Cu containing phases to investigate the effects of varying the transition metals on the structural stability and physical properties.[12-13] We found that the latter lanthanides form α – $LnNiGa_4$ (Y, Gd – Yb) and β – $LnNi_{1-x}Ga_4$ (Ln = Tb - Er),[14] $SmCu_4Ga_8$,[15] and $Ln(Cu,Ga)_{12}$ (Ln = Y, Gd – Er, and Yb).[16] In any case, the Ni or Cu analogues were not found to adopt the $SrAu_2Ga_5$ structure type.[14-15, 17-18]

Examination of related phase spaces employing an Al flux yielded the $LaNi_{1+x}Al_{6-x}$[19] and $CePd_{1-x}Al_{6-x}$ compounds.[20] The disorder of both compounds occurs on the same Wyckoff site that is observed to disorder in the parent structure, $SrAu_2Ga_5$. Density Functional Theory (DFT) calculations reveal the stabilization of $LaNi_{1+x}Al_{6-x}$ in this structure type may arise from the optimization of Al – Al and Al – Ni contacts in $LaNi_{1+x}Al_{6-x}$ and a valence electron count (VEC) of 19.68 electron/f.u.[19] This VEC value is in good agreement with the VEC values reported for $CePdGa_6$ (~ 21 e^-/f.u.),[4] $SrAu_2Ga_5$ (~ 19 e^-/f.u.),[11] and $CePd_{1-x}Al_{6-x}$ (~ 19.5 e-/f.u.)[20]

While exploring compounds in the Ln-Cu-Al phase space and searching for highly disordered Cu/Al compounds, we have serendipitously grown pseudo-ternaries of $LnCu_2(Al,Si)_5$ (Ln = La and Ce) which crystallize in the $SrAu_2Ga_5$ structure type. Herein we report the synthesis, magnetic, transport, and thermodynamic properties of the new compounds $LnCu_2(Al,Si)_5$ (Ln = La and Ce).

5.2 Experimental Section

5.2.1 Synthesis

5.2.1.1 Flux Growth Synthesis

The growth of single crystals of $LnCu_2(Al,Si)_5$ (Ln = La and Ce) from excess aluminum has been reported elsewhere.[21] It should be noted that single crystal X-ray diffraction and elemental analysis experiments confirmed that single crystals of $LaCu_2(Al,Si)_5$ and $CeCu_2(Al,Si)_5$ nucleate from the surfaces of $La(Cu,Al,Si)_4$ and $Ce(Cu,Al,Si)_4$ impurities, respectively.

5.2.1.2 Arc Melt Synthesis

Samples were prepared via arc-melting in an ultra-pure Ar atmosphere employing Zr as an oxygen getter. The Ln, Cu, and Al constituent elements (same purities as mentioned above)

Table 5.2 Selected Interatomic Distances (Å) for $LaCu_2(Al,Si)_5$ and $CeCu_2(Al,Si)_5$

	$LaCu_2(Al,Si)_5$	$CeCu_2(Al,Si)_5$
Ln – M[a] rectangular prisms		
Ln – M (x8)	3.2083(7)	3.1944(14)
M – M (x4), *c*-axis	2.3533(19)	2.338(2)
M – M (x4), *ab*-plane	4.221(1)	4.204(2)
Cu – X *rectangular prisms*		
Cu – X[a] (x8)	2.5133(8)	2.5110(11)
X – X (x4), *c*-axis	2.729(2)	2.747(2)
X – X (x4), *ab*-plane	2.9847(7)	2.9727(14)

[a]M = Cu/Al and X = Al/Si

Table 5.3 Atomic Positions and ADPs for $LnCu_2(Al,Si)_5$ (Ln = La, Ce)

Atom	Wyckoff site	*x*	*y*	*z*	Occupancy	$U_{eq}(Å^2)$[a]
La	1*a*	0	0	0	1.0	0.00656(19)
Cu	1*b*	0	0	½	1.0	0.083(2)
Cu/Al (M)	2*h*	½	½	0.14864(12)	0.482(8)/0.518(8)	0.0068(3)
Al/Si (X)	4*i*	0	½	0.32761(14)	0.75/0.25	0.0100(3)
Ce	1*a*	0	0	0	1.0	0.00615(10)
Cu	1*b*	0	0	½	1.0	0.00740(13)
Cu/Al (M)	2*h*	½	½	0.14752(8)	0.477(5)/0.523(5)	0.0064(2)
Al/Si (X)	4*i*	0	½	0.32670(10)	0.75/0.25	0.01003(16)

[a]U_{eq} is defined as 1/3 of the trace of the orthogonalized U_{ij} tensor.

Table 5.4 Crystallographic Parameters for $LnCu_2(Al,Si)_5$ (Ln = La and Ce) obtained from Rietveld Refinement

Formula	$LaCu_2(Al,Si)_5$	$CeCu_2(Al,Si)_5$
a (Å)	4.218328(4)	4.195367(3)
c (Å)	7.933527(11)	7.913732(9)Å
V ($Å^3$)	141.1720(3)	139.291(1)
Z	1	1
Refined Composition	$LaCu_{2.04(26)}Al_{3.96(26)}Si$	$CeCu_{2.06(24)}Al_{3.94(24)}Si$
[a]R_p	0.065	0.065
[b]R_{wp}	0.091	0.080
[c]R_{exp}	0.045	0.042
[d]χ^2	4.16	3.72

[a]$R_p = \sum \left| Y_o - Y_C \right| / \sum Y_o$, [b]$R_{wp} = [M/\sum w(Y_o^2)]^{1/2}$, [c]$R_{exp} = R_{wp}/(\chi^2)^{½}$, [d]$\chi^2 = M/N_{obs} - N_{va}$

were melted first, the resulting button was then turned over, and the Si pieces were then incorporated. Finally, each button was subsequently flipped and remelted three times to ensure homogeneity. Mass losses for the $LaCu_2(Al,Si)_5$ and $CeCu_2(Al,Si)_5$ buttons were calculated to be 0.17% and 0.01%, respectively. Both samples were then annealed at 750°C for 3 weeks.

5.2.2 Single Crystal X-ray Diffraction

Crystals of $LaCu_2(Al,Si)_5$ and $CeCu_2(Al,Si)_5$ obtained from flux growth were cut to suitable sizes for data collection (≤ 0.05 mm x 0.05 mm x 0.05 mm) and mounted onto separate glass fibers using epoxy. These crystals then mounted onto the goniometer of a Nonius KappaCCD X-ray diffractometer equipped with Mo K_α radiation (λ = 0.71073 Å). Crystallographic parameters for $LnCu_2(Al,Si)_5$ (Ln = La and Ce) are provided in Table 5.1. SIR97 was employed to give a starting model, SHELXL97 was used to refine the structural model, and the data were corrected using extinction coefficients and weighting schemes during the final stages of refinement.[22-23] Based on lattice parameters and the initial refinements, our starting structural model was found to be similar to $CePdGa_6$[4, 10] with $LnCu_2(Al,Si)_5$ (Ln = La and Ce) crystallizing in the $SrAu_2Ga_5$ structure type.[11] The refinement of the 2*h* Wyckoff site assuming full main group element (Al) occupancy (observed in $CePdGa_6$), yielded a model with an abnormally small anisotropic displacement parameter (ADP). Modeling the 2*h* Wyckoff site as having mixed occupancy of Cu and Al resulted in more well behaved ADP. This same type of disorder was observed for both $LnNi_{1+x}Al_{6-x}$[19] and $LnPd_{1+x}Al_{6-x}$.[20] Additionally, both Al and Si are found to be disordered on the 4*i* Wyckoff site, resulting in a structural model that converged with small final difference residual peaks and well behaved ADPs. Selected interatomic distances are presented in Table 5.2, and atomic positions and ADPs are provided in Table 5.3. These tables reflect the structural models obtained after mixing the occupancy of the 2*h* and 4*i*

sites. We note that the lattice parameter for the *c*-axis of $CeCu_2(Al,Si)_5$ is slightly larger than that of $LaCu_2(Al,Si)_5$. However, the volumes conform to the expected lanthanide contraction. Furthermore, multiple single crystal X-ray diffraction collections for both analogues showed this result was reproducible. The results for the most highly redundant data collections have been reported in Tables 5.1 – 5.3.

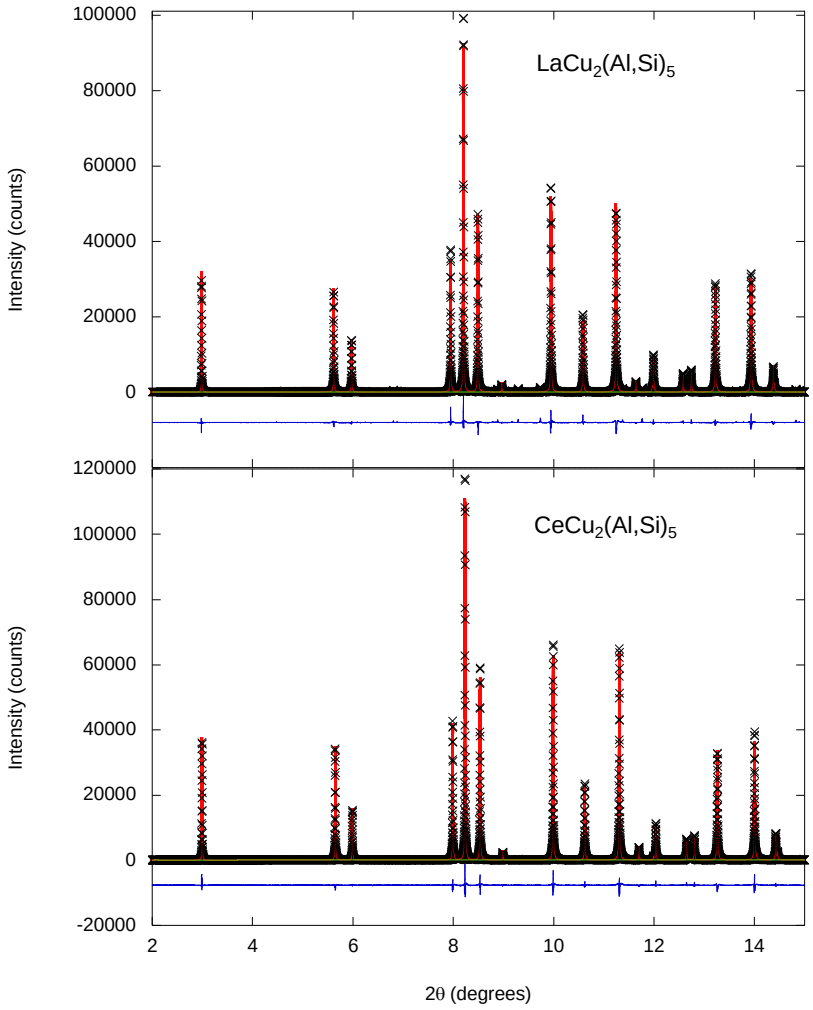

Figure 5.1 High-resolution X-ray diffraction powder patterns and Rietveld refinements of $LaCu_2(Al,Si)_5$ (above) and $CeCu_2(Al,Si)_5$ (below). The black cross, red fit line, green line, and blue line correspond to the observed data, calculated model, background fit, and difference curve, respectively.

5.2.3 Powder X-ray Diffraction

Powder X-ray diffraction patterns were obtained using a Bruker AXS D8 Advance diffractometer (Cu K_α radiation, λ = 1.54056 Å) to determine the purity of the annealed polycrystalline samples. To more fully investigate the phase purities, high-resolution synchrotron powder diffraction data were collected at ambient temperatures using the 11-BM beamline (λ = 0.413262 Å) at the Advanced Photon Source located at Argonne National Laboratory.[24] Data points were collected over a 2θ range of 2º - 50º with a step size of 0.001º. Rietveld refinements conducted using the GSAS and EXPGUI programs were employed to generate optimized models of the observed powder patterns for $LnCu_2(Al,Si)_5$ (Ln = La and Ce).[25-26] The refined models of $LaCu_2(Al,Si)_5$ and $CeCu_2(Al,Si)_5$ obtained from the single crystal X-ray diffraction experiments were employed as starting models in order to fit the data obtained from the 11-BM beamline. The histograms and the results of the Rietveld refinements are shown in Figure 5.1. For clarity, only a select 2θ range is shown. At low angles minor impurity peaks were resolved; however, attempts to model these impurity peaks were unsuccessful. The phase purity of $LaCu_2(Al,Si)_5$ was estimated to be greater than 95% by comparing the ratio of the most intense peak (~1300 counts) of the impurity phase to the most intense peak (~100,000 counts) of $LaCu_2(Al,Si)_5$. The results for phase purity of $CeCu_2(Al,Si)_5$ was determined to by roughly the same. The lattice parameters and the discrepancy factors obtained from refinement can be seen in Table 5.4. These lattice parameters are slightly different than those obtained from single crystal X-ray diffraction. Since the Cu/Al occupancies of the 2*h* Wyckoff positions for both analogues are within error when comparing the results of the single crystal and powder diffraction models, certain experimental variables such as differing growth conditions, sample manipulation, and different experimental analysis (in-house single crystal X-ray diffraction

compared with high resolution synchrotron powder diffraction) could lead to these slight changes in the lattice parameters. Attempts to grow polycrystalline $LnCu_2Al_5$ on stoichiometry resulted in the formation of $LnCuAl_3$, again indicating Si is critical to phase stabilization of $LnCu_2(Al,Si)_5$ (Ln = La and Ce).

5.2.4 Elemental Analysis

Energy Dispersive X-ray Spectroscopy (EDS) experiments were conducted using a Hitachi S-3600N Variable Pressure scanning electron microscope equipped with an energy dispersive spectrometer. The electron accelerating voltage used was 15 kV and the beam to sample distance measured 15 mm. The elemental composition for each compound were found to be $La_{1.00(2)}Cu_{1.95(6)}Al_{4.14(7)}Si_{0.97(3)}$ and $Ce_{1.00(2)}Cu_{1.96(4)}Al_{4.08(4)}Si_{0.95(3)}$. In light of these findings, the starting model obtained for single crystal X-ray diffraction for both analogues were inspected for mixed occupancy of Cu and Al in a similar fashion to the mixing observed in $EuAu_2Ga_5$ and $SrAu_2Ga_5$.[11] It is worth noting that Cu/Al and Al/Si mixing has been previously observed in $Ln(Ag,Al,Si)_2$ (Ln = Ce and Gd),[16] LnAlSi (Ln = La, Ce, Pr, Nd, Sm and Gd), $LnAl_2Si_2$ (Ln = Eu and Yb), and $Ln_2Al_3Si_2$ (Ln = Tb, Dy, Ho, Er, and Tm).[27]

5.2.5 Physical Properties

Due to the small amount of impurities ($Ln(Cu,Al,Si)_4$ (Ln = La and Ce)) which nucleate from the single crystals of $LnCu_2(Al,Si)_5$ (Ln = La and Ce), polycrystalline samples of $LaCu_2(Al,Si)_5$ and $CeCu_2(Al,Si)_5$ were used for physical property measurements. The magnetic data were collected using a Quantum Design Magnetic Property Measurement System (MPMS). The temperature-dependent magnetic susceptibility data were measured under field cooled (FC) conditions between 2.25 K to 400 K for $CeCu_2(Al,Si)_5$ under an applied field of 1 T. Field-dependent magnetization data were measured between 5 and 20 K with applied fields up to 5 T.

The electrical resistivity measurements for both samples were conducted on bar shaped polycrystalline samples using a Quantum Design Physical Property Measurement System (PPMS). Specific heat capacity data for $LnCu_2(Al,Si)_5$ (Ln = La and Ce) were obtained down to liquid ^{3}He temperatures using the PPMS.

5.3 Results and Discussion

5.3.1 Structure

A description of the structures for $LnCu_2(Al,Si)_5$ (Ln = La and Ce) have been reported elsewhere.[21]

5.3.2 Physical Properties

The temperature-dependent magnetic susceptibility of $CeCu_2(Al,Si)_5$ in a field of 1 T is shown in Figure 5.2. The modified Curie-Weiss equation was used to fit the magnetic susceptibility data from 20 K – 400 K where: $\chi(T) = \chi_0 + C/(T - \theta_W)$, C represents the Curie constant, θ_W is the Weiss temperature, and χ_0 represents the temperature independent contributions to the magnetic susceptibility due to Pauli paramagnetism and Larmor diamagnetism. The χ_0, C, and θ_W parameters obtained from this fit can be viewed in the inset table of Figure 5.2. These terms were used to generate the red line to extrapolate the Curie-Weiss form to lower temperatures for comparison to the magnetic susceptibility. The inset in Figure 5.2 shows that the data diverge from this form below 10 K. Furthermore, the magnetic susceptibility data deviate to higher values compared to the red curve, which is indicative of ferromagnetic correlations between magnetic moments. The χ_0 value obtained from the modified Curie-Weiss fit was subtracted from the raw magnetic susceptibility data and the inverse of $\chi - \chi_0$ is plotted on the right axis of Figure 5.2. A linear fit to these data from 20 K – 400 K was performed in an attempt to extract more accurate C and θ_W values. The effective

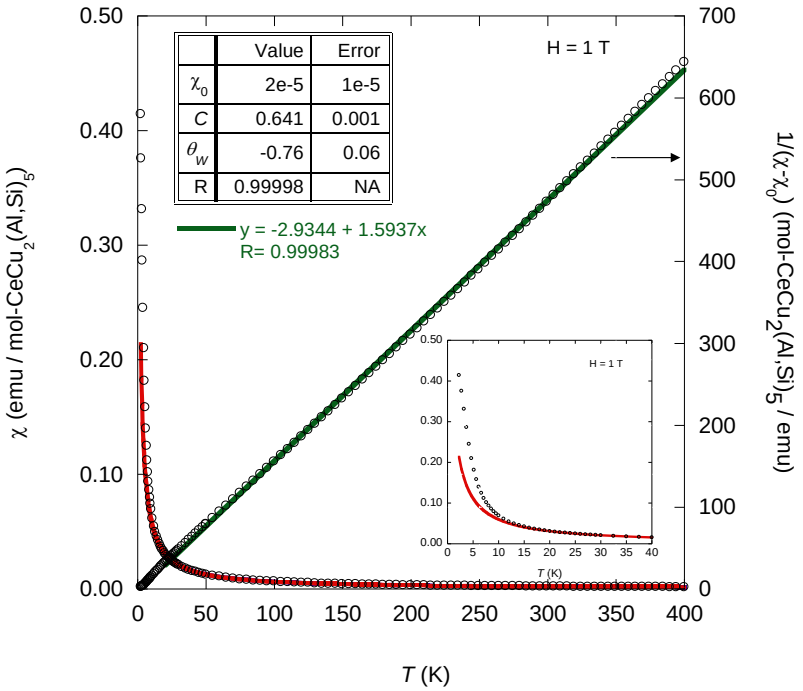

Figure 5.2 Magnetic susceptibility, χ = M/H (emu/mol), of $CeCu_2(Al,Si)_5$ as a function of temperature measured under an applied field of 1 T is shown on the left axis, and inverse magnetic susceptibility, $1/\chi$-χ_0 = H/M (mol/emu), as a function of temperature is shown on the right axis. The χ_0, C, and θ_W parameters obtained from a modified Curie-Weiss fit to the susceptibility can be viewed in the upper inset of this figure. A graph comparing the Curie-Weiss fit to magnetic susceptibility can be seen in the lower right inset.

moments obtained from C were compared to the calculated values using $\mu_{eff} = g_J[J(J+1)]^{1/2}$. We note that $CeCu_2(Al,Si)_5$ displays paramagnetic behavior down to 2.25 K and Curie-Weiss behavior above 20 K. The magnetic moment of 2.24(1) μ_B/mol Ce is somewhat lower than the expected moment of 2.54 μ_B/mol for a free Ce^{3+} ion. The observation of a somewhat smaller effective moment in $CeCu_2(Al,Si)_5$ was also observed for the related phase, $CePd_{1+x}Al_{6-5}$.[20] A positive Weiss constant, θ_W = 1.8(4) K, indicates weak ferromagnetic interactions in contrast to the Weiss temperature that results from the fitting procedure above. This indicates that the

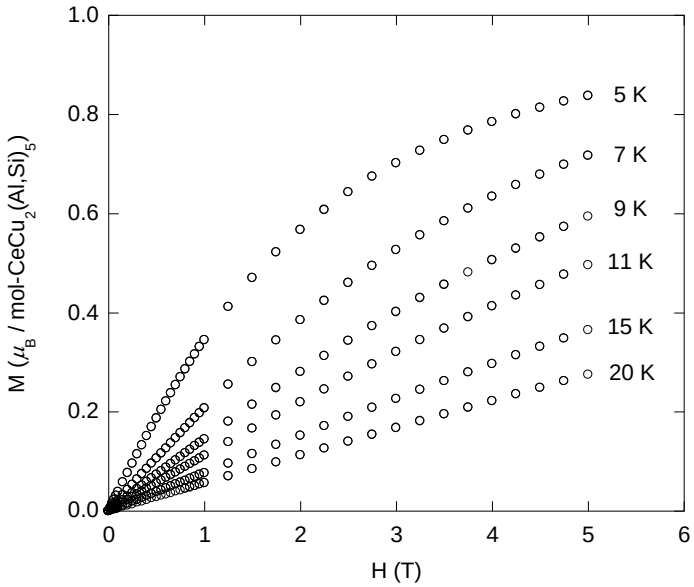

Figure 5.3 Magnetization (M) of $CeCu_2(Al,Si)_5$ as a function of applied field (H) at 5, 7, 9, 11, 15, and 20 K.

Weiss temperature is small and that our fitting of a Curie-Weiss form to the susceptibility does not result in an accurate determination of the Weiss temperature. Therefore, we have scaled the field-dependent magnetization data to more accurately determine the θ_W as presented below.

The field-dependent magnetization up to 5 T at 5, 7, 9, 11, 15, and 20 K are presented in Figure 5.3 for $CeCu_2(Al,Si)_5$. The magnetization data above 10 K is linear and shows no sign of saturation whereas the data at 5, 7, and 9 K show a tendency towards saturation at high fields as expected for a paramagnet. Figure 5.4a and 5.4b show the field-dependent magnetization curves vs. H/T and H/(T – 2 K), respectively. As can be seen in Figure 5.4b, the data overlap and scale nicely when 2 K is subtracted from the sample temperatures. This again is suggestive of weak ferromagnetic correlations between the magnetic moments and reinforces the positive Weiss temperature, $\theta_W \sim 2$ K, obtained from Curie-Weiss fits of $\chi - \chi_0$.

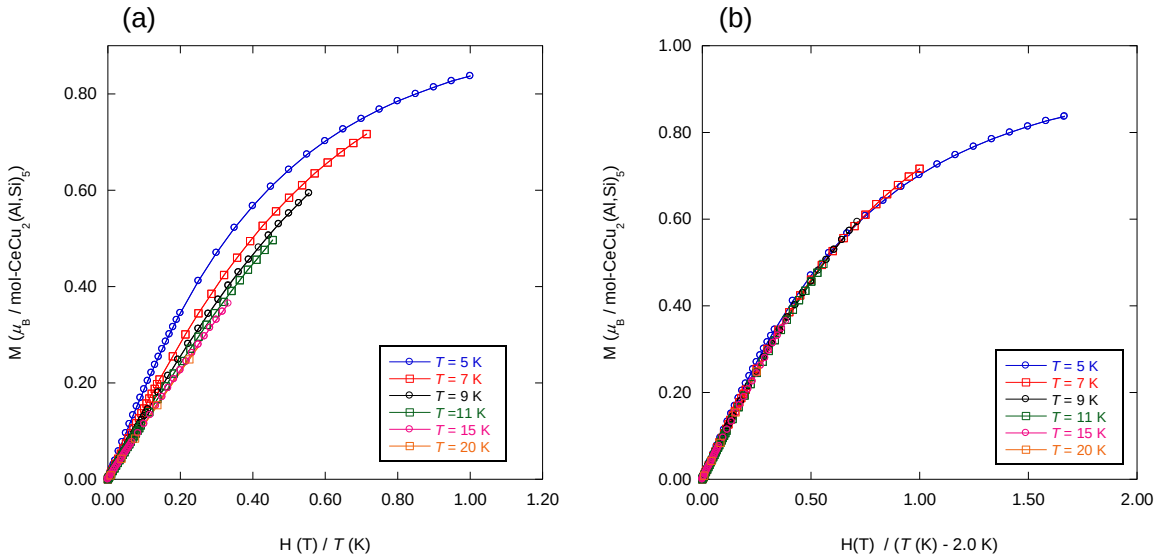

Figure 5.4 Magnetization (M) curves vs. field divided by temperature (H/*T*) **(a)** and M vs. H/(*T* – 2 K) to demonstrate scaling of the magnetization data **(b)**.

The electrical resistivity as a function of temperature for $LnCu_2(Al,Si)_5$ (Ln = La and Ce) is shown in Figure 5.5. Metallic behavior is observed down to 2 K for both analogues. The resistivity of most metals is linear in temperature for $T > \theta_D$, where θ_D is the Debye temperature and is an estimate of highest frequency phonon modes. The high temperature resistivity is roughly linear in temperature down to ~ 50 K, which is indicative of a small Debye temperature (see Below). The resistivity of $LaCu_2(Al,Si)_5$ at low *T* approaches a constant value indicating the reduction of phonon scattering and signaling the dominance of simple impurity and defect scattering. By comparison, $CeCu_2(Al,Si)_5$ displays a much more temperature dependent resistivity. The differences with the resistivity of $LaCu_2(Al,Si)_5$ indicate that conduction electron/Ce *f*-electron scattering is likely cause. The resistivity between 2 K and up is similar to the behavior observed for $CeMg_3$,[28] $Ce_3Ni_2Ge_7$,[29] $Ce_2Ni_3Ge_5$,[29] and $Ce_3Ni_7As_5$,[30] and can be attributed to the interplay between the Kondo effect and crystalline electric field effects.

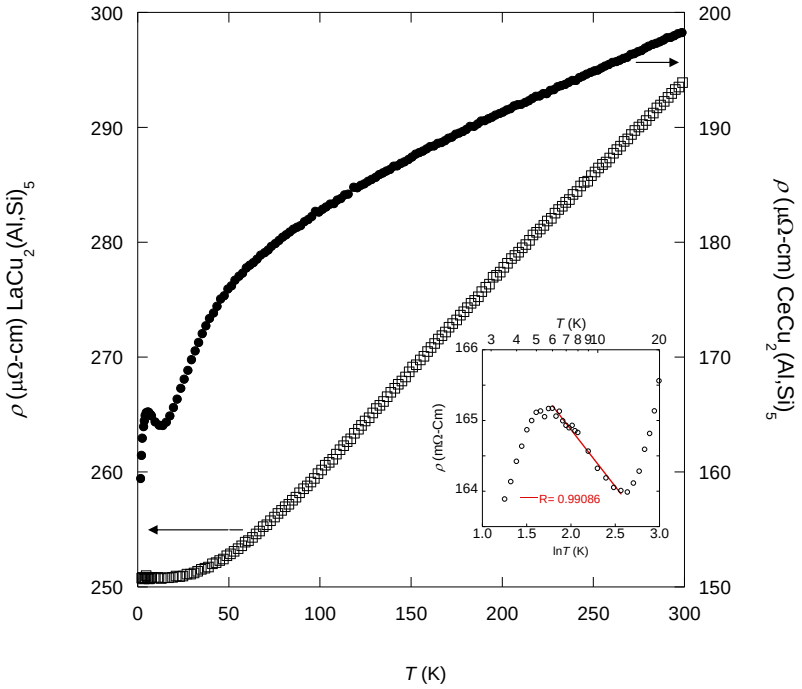

Figure 5.5 Temperature-dependent electrical resistivity (ρ) for $LnCu_2(Al,Si)_5$ (Ln = La and Ce). The inset shows a linear fit of ρ vs. ln$T$ for $CeCu_2(Al,Si)_5$ from 6 K to 13 K.

Between 5 K and 14 K a decreasing ρ with T is observed and when plotted in the inset of Figure 5.5, ρ as a function of ln$T$ displays linearity indicating a Kondo mechanism, although the T-range is limited (6 K < T < 13 K). The peak in resistivity data for $CeCu_2(Al,Si)_5$ around 5 K and a sudden drop in resistivity are likely related to the onset of a magnetic transition where the alignment of the magnetic moments reduces the spin disorder scattering.

The specific heat capacity (C_p) of $LnCu_2(Al,Si)_5$ (Ln = La and Ce) is shown in Figure 5.6. A magnetic contribution in C_p of $CeCu_2(Al,Si)_5$ as signaled by the deviation from the heat capacity of $LaCu_2(Al,Si)_5$, is observed below 10 K. This is followed by a sharp peak at 2 K signifying a phase transition that closely coincides with θ_W obtained from fits to the magnetic susceptibility data. Fits of C_p/T vs. T^2 data for $LaCu_2(Al,Si)_5$ and $CeCu_2(Al,Si)_5$ were performed

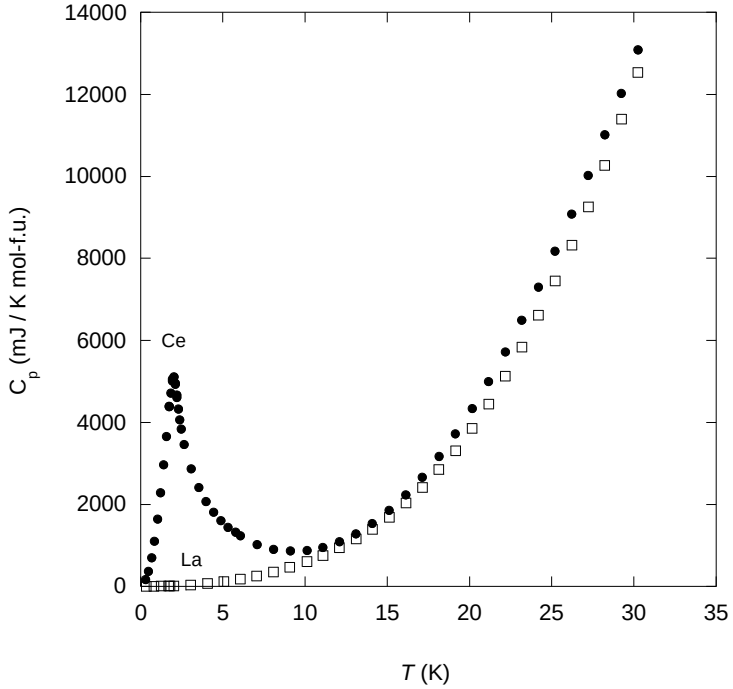

Figure 5.6 Heat capacity (C_p) for $CeCu_2(Al,Si)_5$ and $LaCu_2(Al,Si)_5$ as a function of temperature (T).

to extract the β and γ coefficients. The values for β and γ obtained from these fits for $LaCu_2(Al,Si)_5$ [$CeCu_2(Al,Si)_5$] were found to be equal 0.442 mJ/mol K^4 [0.457 mJ/mol K^4] and 12.34 mJ/mol K^2 [24.53 mJ/mol K^2]. The Debye temperature for both analogues was calculated using the formula, $\theta_D{}^3 = (234 \cdot n \cdot k_B)/\beta$ where n is the density and k_B is Boltzmann's constant. The calculated Debye temperatures for $LaCu_2(Al,Si)_5$ and $CeCu_2(Al,Si)_5$ are 163 K and 162 K, respectively. Because the Debye temperatures for $LaCu_2(Al,Si)_5$ and $CeCu_2(Al,Si)_5$ are nearly equivalent, the magnetic heat capacity divided by temperature (C_m/T) for $CeCu_2(Al,Si)_5$ (Figure 5.7) could be determined by subtraction of the phonon contribution to heat capacity by the nonmagnetic $LaCu_2(Al,Si)_5$ analogue. The magnetic entropy, S_{mag}, as a function of temperature was determined by integrating C_m/T and is shown in Figure 5.8. The expected entropy, S_{mag} =

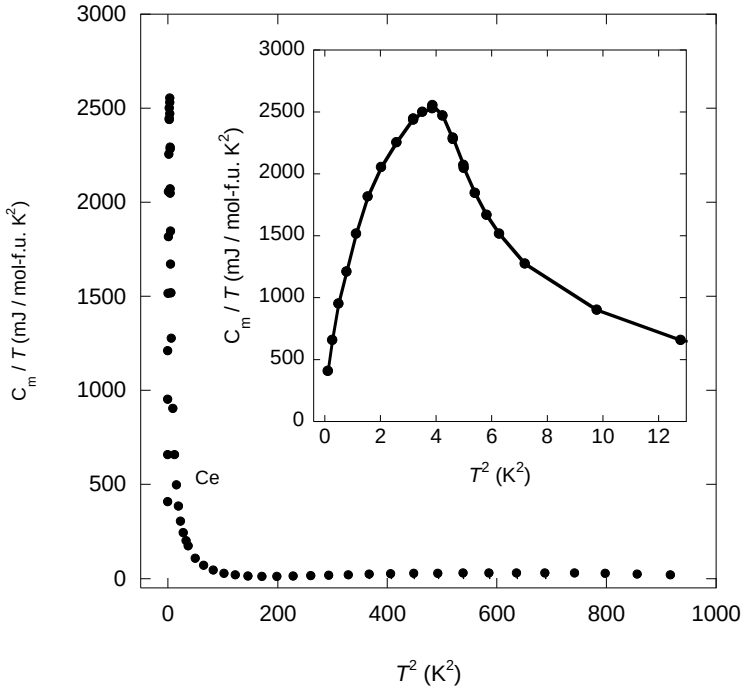

Figure 5.7 A plot of magnetic heat capacity divide by temperature (C_m/T) vs. T^2 for $CeCu_2(Al,Si)_5$. Where C_m is the magnetic contribution to the specific heat determined by subtracting the $C_p(T)$ of $LaCu_2(Al,Si)_5$. The inset serves to highlight the transition.

R*ln*(2S + 1) with S = 1/2, is completely recovered from the lowest temperatures measured to the onset of the transition, around 10 K. It is interesting to again note that the onset of the deviation of the magnetic susceptibility data for $CeCu_2(Al,Si)_5$ from Curie-Weiss behavior occurred at around 10 K (This can be seen as the red curve in Figure 5.2.). With the entropy associated with the transition in C_m being in good agreement with the entropy expected for a magnetic transition, it is reasonable to assert that the transition at 2 K is due to a magnetic ordering of Ce atoms. Furthermore, the positive θ_W and the nice scaling of the field dependent magnetization by the subtraction of 2 K to the temperature also suggest that this transition is ferromagnetic in nature (Figure 5.4a and 5.4b).

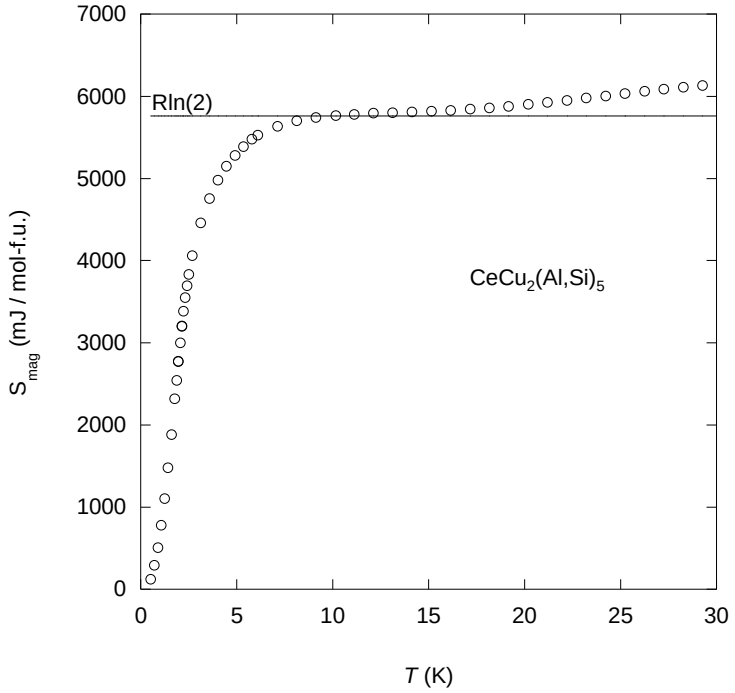

Figure 5.8 Magnetic entropy (S_{mag}) as a function of temperature (T). Rln2 is indicated by the line.

5.4 Conclusions

Single crystals of $LaCu_2(Al,Si)_5$ and $CeCu_2(Al,Si)_5$ were grown by the flux growth technique and subsequent phase pure polycrystalline samples were prepared by arc melting of the constituent elements in stoichiometric ratios and annealing. Single crystals of both $LaCu_2(Al,Si)_5$ and $CeCu_2(Al,Si)_5$ were characterized by single crystal X-ray diffraction and composition determined by EDS. The polycrystalline samples were characterized by powder X-ray diffraction, using both in-house and the synchrotron source at APS. We have shown that the magnetic susceptibility of $CeCu_2(Al,Si)_5$ is paramagnetic down to the lowest temperature measured, T = 2.25 K. The Curie-Weiss analysis and magnetization scaling suggest that

magnetic correlations for $CeCu_2(Al,Si)_5$ become relevant at 10 K and are likely ferromagnetic (θ_W = 2 K). This is supported by the heat capacity data where a transition was observed to peak at 2 K. In addition, the low temperature transport behavior of $CeCu_2(Al,Si)_5$ is consistent with incoherent Kondo scattering interactions at high temperatures. Thus, our data indicate that $CeCu_2(Al,Si)_5$ has a somewhat enhanced carrier mass, $\gamma \sim 25$ mJ/mol K^2, and likely undergoes a ferromagnetic transition at 2 K, placing it among only a handful of ferromagnetic Ce compounds.[16, 31-33] The occurrence of ferromagnetism in a Ce compound displaying distinct features of Kondo screening at higher temperatures may be indicating an underscreened or undercompensated Kondo lattice, which has been predicted and experimentally shown to result in the formation of a singular Fermi liquid. Measurements of the electrical transport of $CeCu_2(Al,Si)_5$ at lower temperature is thus of interest to explore this possibility.[34-37]

5.5 References

1. Petrovic, C.; Movshovich, R.; Jaime, M.; Pagliuso, P. G.; Hundley, M. F.; Sarrao, J. L.; Fisk, Z.; Thompson, J. D., A New Heavy-Fermion Superconductor $CeIrIn_5$: A Relative of the Cuprates? *Europhys. Lett.* **2001**, *53*, 354-359.

2. Petrovic, C.; Pagliuso, P. G.; Hundley, M. F.; Movshovich, R.; Sarrao, J. L.; Thompson, J. D.; Fisk, Z.; Monthoux, P., Heavy-Fermion Superconductivity in $CeCoIn_5$ at 2.3 K. *J. Phys.: Condens. Matter* **2001**, *13*, L337.

3. Bauer, E.; Pillmayr, N.; Gratz, E.; Gignoux, D.; Schmitt, D.; Winzer, K.; Kohlmann, J., $CeCu_4Ga$: A High γ Heavy Fermion Compound. *J. Magn. Magn. Mater* **1988**, *71*, 311-317.

4. Macaluso, R. T.; Nakatsuji, S.; Lee, H.; Fisk, Z.; Moldovan, M.; Young, D. P.; Chan, J. Y., Synthesis, Structure, and Magnetism of a New Heavy-Fermion Antiferromagnet, $CePdGa_6$. *J. Solid State Chem.* **2003**, *174*, 296-301.

5. Kishimoto, Y.; Kawasaki, Y.; Ohno, T., Mixed Valence State in Ce and Yb Compounds Studied by Magnetic Susceptibility. *Phys. Lett. A* **2003**, *317*, 308-314.

6. Fisk Z; Sarrao J L; Smith J L; Thompson J D, The Physics and Chemistry of Heavy Fermions. *P. Natl. Acad. Sci. USA* **1995**, *92*, 6663-6667.

7. Fisk, Z., A Whiff of Chemistry in Heavy Electron Physics. *Science* **2007**, *318*, 1559-1560.

8. Macaluso, R. T.; Nakatsuji, S.; Kuga, K.; Thomas, E. L.; Machida, Y.; Maeno, Y.; Fisk, Z.; Chan, J. Y., Crystal Structure and Physical Properties of Polymorphs of $LnAlB_4$ (Ln = Yb, Lu). *Chem. Mater.* **2007**, *19*, 1918-1922.

9. Hegger, H.; Petrovic, C.; Moshopoulou, E. G.; Hundley, M. F.; Sarrao, J. L.; Fisk, Z.; Thompson, J. D., Pressure-Induced Superconductivity in Quasi-2D $CeRhIn_5$. *Phys. Rev. Lett.* **2000**, *84*, 4986.

10. Macaluso, R. T.; Millican, J. N.; Nakatsuji, S.; Lee, H.-O.; Carter, B.; Moreno, N. O.; Fisk, Z.; Chan, J. Y., A Comparison of the Structure and Localized Magnetism in Ce_2PdGa_{12} with the Heavy Fermion $CePdGa_6$. *J. Solid State Chem.* **2005**, *178*, 3547-3553.

11. Cordier, G.; Dietrich, C.; Friedrich, T., Crystal Structures of Europium Digold Pentagallide, $EuAu_2Ga_5$ and Strontium Digold Pentagallide, $SrAu_2Ga_5$. *Z. Kristallogr.* **1996**, *211*, 627-628.

12. Cho, J. Y.; Millican, J. N.; Capan, C.; Sokolov, D. A.; Moldovan, M.; Karki, A. B.; Young, D. P.; Aronson, M. C.; Chan, J. Y., Crystal Growth, Structure, and Physical Properties of Ln_2MGa_{12} (Ln = La, Ce; M = Ni, Cu). *Chem. Mater.* **2008**, *20*, 6116-6123.

13. Thomas, K. R.; Cho, J. Y.; Millican, J. N.; Hembree, R. D.; Moldovan, M.; Karki, A.; Young, D. P.; Chan, J. Y., Crystal Growth and Physical Properties of Ln_2MGa_{12} (Ln = Pr, Nd, and Sm; M = Ni, Cu). *J. Cryst. Growth* **2010**, *312*, 1098-1103.

14. Menard, M. C.; Drake, B. L.; McCandless, G. T.; Thomas, K. R.; Hembree, R. D.; Haldolaarachchige, N.; DiTusa, J.; Young, D. P.; Chan, J. Y., A Tale of Two Polymorphs: Growth and Characterization of α-$LnNiGa_4$ (Ln = Y, Gd-Yb) and β–$LnNi_{1-x}Ga_4$ (Ln = Tb-Er). *Eur. J. Inorg. Chem.* **2011**, *In Press*.

15. Cho, J. Y.; Capan, C.; Young, D. P.; Chan, J. Y., Crystal Growth, Structure, and Physical Properties of $SmCu_4Ga_8$. *Inorg. Chem.* **2008**, *47*, 2472-2476.

16. Drake, B. L.; Kangas, M. J.; Capan, C.; Haldolaarachchige, N.; Xiong, Y. M.; Adams, P. W.; Young, D. P.; Chan, J. Y., Crystal Growth, Structure, and Physical Properties of $Ln(Ag,Al,Si)_2$ (Ln = Ce and Gd). *J. Phys.: Condens. Matter* **2010**, *22*, 426002.

17. Romaka, V. A.; Grin, Y. N.; Yarmolyuk, Y. P., Magnetic and Crystallographic Characteristics of Rare Earth Metal-Nickel-Gallium ($RENiGa_4$) Compounds. *Ukr. Fiz. Zh.* **1983**, *28*, 1095-1097.

18. Drake, B. L.; Capan, C.; Cho, J. Y.; Nambu, Y.; Kuga, K.; Xiong, Y. M.; Karki, A. B.; Nakatsuji, S.; Adams, P. W.; Young, D. P.; Chan, J. Y., Crystal Growth, Structure, and Physical Properties of $Ln(Cu,Al)_{12}$ (Ln = Y, Ce, Pr, Sm, and Yb) and $Ln(Cu,Ga)_{12}$ (Ln = Y, Gd-Er, and Yb). *J. Phys.: Condens. Matter* **2010**, *22*, 066001.

19. Gout, D.; Benbow, E.; Gourdon, O.; Miller, G. J., Composition-Structure Relationships in Polar Intermetallics: Experimental and Theoretical Studies of $LaNi_{1+x}Al_{6-x}$ (x = 0.44). *Inorg. Chem.* **2004**, *43*, 4604-4609.

20. Tobash, P. H.; Ronning, F.; Thompson, J. D.; Bobev, S.; Bauer, E. D., Magnetic Order and Heavy Fermion Behavior in $CePd_{1-x}Al_{6-x}$: Synthesis, Structure, and Physical Properties. *J. Solid State Chem.* **2010**, *183*, 707-711.

21. Phelan, W. A.; Kangas, M. J.; Drake, B. L.; Zhao, L. L.; Wang, J. K.; DiTusa, J. F.; Morosan, E.; Chan, J. Y., Crystal Growth, Structure, and Physical Properties of $LnCu_2(Al,Si)_5$ (Ln = La and Ce). *Inorg. Chem.* **2011**, *51*, 920-927.

22. Altomare, A.; Burla, M. C.; Camalli, M.; Luca, G. L.; Gaicovazzo, C.; Guagliardi, A.; Moliterni, A. G. G.; Polidori, G.; Spagna, R., SIR97: A New Tool for Crystal Structure Determination and Refinement. *J. Appl. Cryst.* **1999**, *32*, 115.

23. Sheldrick, G. M., A Short History of SHELX. *Acta Crystallogr. Sect. A* **2008**, *64*, 112-122.

24. Wang, J.; Toby, B. H.; Lee, P. L.; Ribaud, L.; Antao, S. M.; Kurtz, C.; Ramanathan, M.; Von Dreele, R. B.; Beno, M. A., A Dedicated Powder Diffraction Beamline at the Advanced Photon Source: Commissioning and Early Operational Results. *Rev. Sci. Instrum.* **2008**, *79*, 085105.

25. Larson, A. C.; Von Dreele, R. B., General Structure Analysis System (GSAS). *Los Alamos National Laboratory Report LAUR* **2004**, 86-748.

26. Toby, B. H., EXPGUI, A Graphical User Interface for GSAS. *J. Appl. Crystallogr.* **2001**, *34*, 210-213.

27. Bobev, S.; Tobash, P. H.; Fritsch, V.; Thompson, J. D.; Hundley, M. F.; Sarrao, J. L.; Fisk, Z., Ternary Rare-Earth Alumo-Silicides-Single-Crystal Growth from Al Flux, Structural and Physical Properties. *J. Solid State Chem.* **2005**, *178*, 2091-2103.

28. Das, P. K.; Kumar, N.; Kulkarni, R.; Thamizhavel, A., Magnetic Properties of the Heavy-fermion Antiferromagnet $CeMg_3$. *Phys. Rev. B* **2011**, *83*, 134416.

29. Pikul, A. P.; Kaczorowski, D.; Rogl, P.; Grin, Y., Kondo Effect in the Presence of Crystal-Field in Ce-Ni-Ge Compounds. *Phys. Status Solidi B-Basic Res.* **2003**, *236*, 364-367.

30. Babizhetskyy, V.; Guerin, R.; Isnard, O.; Hiebl, K., Ternary Rare-Earth Nickel Arsenides $R_3Ni_7As_5$ (R = La, Ce, Pr, Nd, Sm) with a New Variant of the $BaAl_4$-Type: Crystal Structure and Physical Properties. *J. Solid State Chem.* **2003**, *172*, 265-276.

31. Macaluso, R. T.; Wells, D. M.; Sykora, R. E.; Albrecht-Schmitt, T. E.; Mar, A.; Nakatsuji, S.; Lee, H.; Fisk, Z.; Chan, J. Y., Structure and Electrical Resistivity of $CeNiSb_3$. *J. Solid State Chem.* **2004**, *177*, 293-298.

32. Sidorov, V. A.; Bauer, E. D.; Lee, H.; Nakatsuji, S.; Thompson, J. D.; Fisk, Z., Complex Magnetic Phase Diagram of Ferromagnetic $CeNiSb_3$. *Phys. Rev. B* **2005**, *71*, 094422.

33. Thomas, E. L.; Gautreaux, D. P.; Lee, H. O.; Fisk, Z.; Chan, J. Y., Discovery of β-LnNiSb3 (Ln = La, Ce): Crystal Growth, Structure, and Magnetic and Transport Behavior. *Inorg. Chem.* **2007**, *46*, 3010-3016.

34. Sacramento, P. D.; Schlottmann, P., Thermodynamics of The N-Channel Kondo Model for General-N and Impurity Spin-S in a Magnetic-Field. *J. Phys.: Condens. Matter* **1991**, *3*, 9687-9696.

35. Gan, J.; Coleman, P.; Andrei, N., Coexistense of Fermi-Liquid and Magnetism in the Underscreened Kondo Problem. *Phys. Rev. Lett.* **1992**, *68*, 3476-3479.

36. Coleman, P.; Pepin, C., Singular Fermi Liquid Behavior in the Underscreened Kondo Model. *Phys. Rev. B* **2003**, *68*, 220405(R).

37. Manyala, N.; DiTusa, J. F.; Aeppli, G.; Ramirez, A. P., Doping a Semiconductor to Create an Unconventional Metal. *Nature* **2008**, *454*, 976-980.

Chapter 6. Synthesis and Physical Properties of $Ln(Cu,Al,Ga)_{13-x}$ (Ln = La, Ce, Pr, and Eu) and $Eu(Cu,Al)_{13-x}$

6.1 Introduction

Compounds which crystallize in the $NaZn_{13}$ structure-type display highly correlated electron behavior and interesting physical properties.[1-2] Of particular interest are those that display an enhanced electron mass. This heavy-fermion behavior is commonly associated with the valence instability of 4*f* and 5*f* electrons in Ce-, Yb-, or U compounds, and several classes of these materials have been reviewed.[1, 3-5] For example, UBe_{13} was reported to be a heavy-fermion defined by its anomalously large electronic specific-heat coefficient $\gamma \sim 1100$ mJ/mol-K^2 at low temperatures and shows an unconventional superconducting state below 0.85 K.[6-10] Enhanced effective mass ($\gamma \sim 58$ mJ/mol-K^2) has also been reported for $CeBe_{13}$.[9, 11-12]

More recently, several Pr-based heavy-fermion phases have been reported. Heavy-fermion behavior in Pr-based intermetallic compounds is uncommon, as it is well-known that the localized $4f^2$ electrons of Pr^{3+} ions are stable. The Heusler-type $PrInAg_2$ ($\gamma \sim 6500$ mJ/mol-K^2) has been reported as the first Pr-based heavy-fermion compound.[13-16] We have also reported that $Pr(Cu,Ga)_{13-x}$ shows heavy-fermion behavior with $\gamma \sim 100$ mJ/mol-K^2 and it follows the expected Kadowaki-Woods relations, $A/\gamma^2 \sim 1\times10^{-5}$ μ Ω-cm (mole K/mJ^2), where A is the coefficient of the quadratic term in the temperature dependent resistivity.[17-19]

Understanding that $Pr(Cu,Ga)_{13-x}$ exhibited enhanced mass behavior, it was of interest to study how substitution of Ga with Al would impact this structure-types physical properties. Initial attempts to prepare $Pr(Cu,Al)_{13-x}$ single crystals using the flux-growth procedure were unsuccessful. Perhaps the structural related $Ln(Cu,Al)_{12}$ phases which crystallize in $ThMn_{12}$ structure-type are more robust as we have shown that the $Ln(Cu,Al)_{12}$ (Ln = Y, Ce-Nd, Sm, Gd-Ho and Yb) compounds can be prepared *via* an Al flux.[20] However, $Ln(Cu,Al)_{13}$ (Ln = La-Nd,

Sm and Eu) have been prepared by arc melting, thus suggesting that more extreme synthetic conditions are needed to yield the $Ln(Cu,Al)_{13}$ (Ln = early lanthanide) phases.[21] Using an Al/Ga flux led to the crystallization of large cubes (> 5 × 5 × 5 mm^3) of $Ln(Cu,Al,Ga)_{13-x}$ (Ln = La, Ce, Pr, and Eu). Attempts to prepare these phases using latter lanthanides resulted in phases which adopted the $ThMn_{12}$ structure-type. This is consistent with our previous findings where it was observed that Ga flux growth led to the formation of $Ln(Cu,Ga)_{13-x}$ (Ln = La-Nd and Eu)[19] and $Ln(Cu,Ga)_{12}$ (Ln = Y, Gd-Er, Yb).[20]

In addition to enhanced mass behaviors observed in these classes of materials, certain members of this class of materials exhibit a sizable magnetocaloric effect. Specifically, $Eu(Cu,Al)_{13-x}$ was prepared to compare its magnetocaloric properties to those of $Eu(Cu,Al,Ga)_{13-x}$. Herein, physical properties of $Ln(Cu,Al,Ga)_{13-x}$ (Ln = La, Ce, Pr, and Eu) and $Eu(Cu,Al)_{13-x}$ are presented.

6.2 Experimental

6.2.1 Synthesis

Single crystals of $Ln(Cu,Al,Ga)_{13-x}$ (Ln = La – Pr and Eu) were synthesized via the flux-growth method. Ln = La – Pr, and Eu (99.9% purity), Cu (99.999% purity), Al (99.999% purity), and Ga (99.9999%) were placed into separate 2-mL alumina crucibles in a 1:9:10:10 molar ratio of Ln : Cu : Al : Ga. These filled alumina crucibles were then vacuum-sealed into separate fused silica tubes and placed into a furnace. These reaction ampoules were heated at a rate of 200 K/h to a maximum dwell temperature of 1373 K. The ampoules were allowed to dwell at this temperature for 10 hours before being cooled to 753 K at a rate of 2 K/h. The excess molten flux was then separated from cubic single crystals via centrifugation. A dilute

Table 6.1 Crystallographic Parameters for $Eu(Cu,Al)_{13-x}$ Obtained from Rietveld Refinement

	$Eu(Cu,Al)_{13-x}$
Composition	$EuCu_{6.87}Al_{5.98}$
a (Å)	11.93228(9)
V (Å^3)	1698.910(4)
Z	8
[a] R_p	0.0413
[b] R_{wp}	0.0538
[c] R_{exp}	0.0376
[d] χ	1.43

[a] $R_p = \sum \left| Y_o - Y_C \right| / \sum Y_o$; [b] $R_{wp} = [M/\sum w(Y_o^2)]^{1/2}$; [c] $R_{exp} = R_{wp}/(\chi^2)^{½}$; [d] $\chi = (M/N_{obs} - N_{va})^{1/2}$

Table 6.2 Atomic Fractional Coordinates, Site Occupancies, and U_{iso} for $Eu(Cu,Al)_{13-x}$ Obtained from Rietveld Refinement

atom	Wyckoff Site	x	y	z	Occupancy	U_{iso} (Å^2)
Eu1	8*a*	¼	¼	¼	1	0.00794(4)
Cu1	8*b*	0	0	0	0.8587(13)	0.00915(12)
Cu2	96*i*	0.117230(15)	0.177238(15)	0	0.5013(9)	0.01077(5)
Al2	96*i*	0.117230(15)	0.177238(15)	0	0.4987(9)	0.01077(5)

HNO_3 solution was used to chemically etch any remaining flux on the surface of the crystals. The crystals were observed to be slightly air and moisture sensitive over a period of months.

In order to prepare $Eu(Cu,Al)_{13-x}$, we used a similar strategy employed by Nordell and Miller.[22] A polycrystalline button of $Eu(Cu,Al)_{13-x}$ was prepared by arc-melting Eu, Cu, and Al in a 1:6.5:6.5 molar ratio in a water-cooled copper hearth under the flow of ultra-high-purity argon gas inside a purged vacuum chamber. Prior to arc melting the compound, a Zr "oxygen

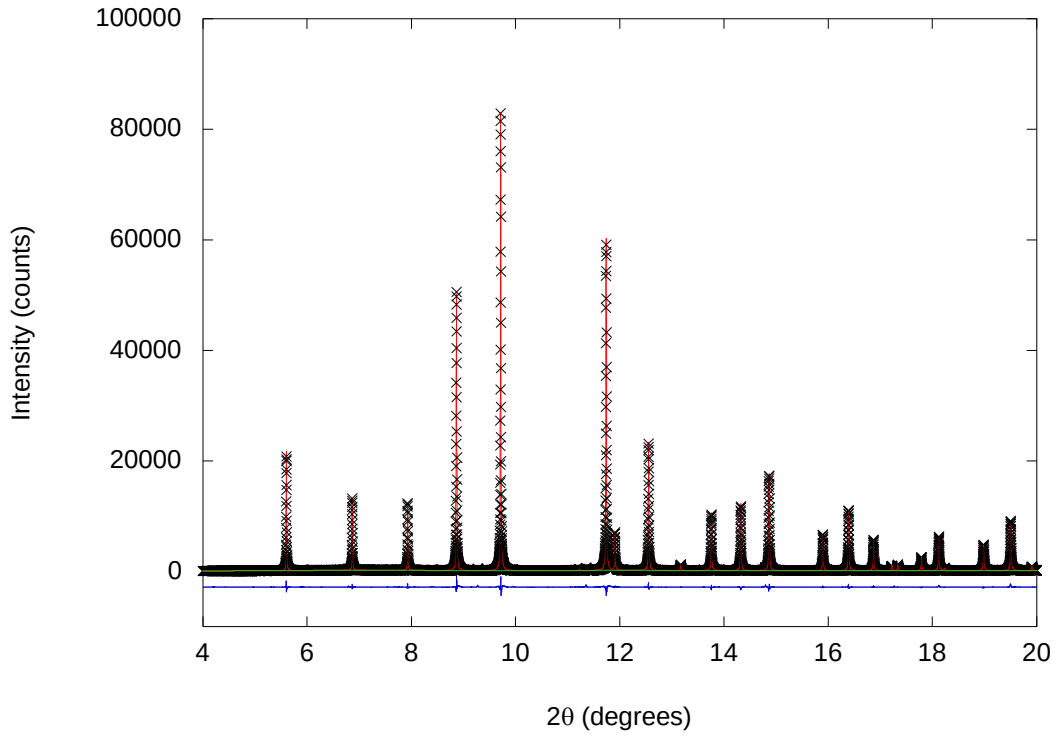

Figure 6.1 XRD powder pattern and Rietveld refinement of $Eu(Cu,Al)_{13-x}$. The black crosses, red fit line, green curve, and blue line correspond to the collected data, data fits, background, and difference curve, respectively.

getter" button was melted. The $Eu(Cu,Al)_{13-x}$ button was turned over repeatedly and remelted several times to ensure homogenization. The mass loss of the final button resulting from this procedure was nominal. The arc-melted button was then vacuum annealed in a furnace for five days at 773 K.

6.2.2 Powder X-ray Diffraction

Portions of the annealed $Eu(Cu,Al)_{13-x}$ button were ground up using a mortar and pestle. A powder X-ray diffraction pattern was obtained using a Bruker AXS D8 Advance diffractometer equipped with a Cu Kα radiation source (λ = 1.54056 Å). In order to obtain a larger signal-to-noise ratio and a larger data set, high-resolution synchrotron powder diffraction data of $Eu(Cu,Al)_{13-x}$ were obtained using the 11-BM beamline (λ = 0.412477Å) at the Advanced Photon Source at Argonne National Laboratory.[23] The data points were collected over a 2θ span

Table 6.3 Elemental Compositions as Obtained from EDS

	at.% Ln	at.% Cu	at.% Al	at.% Ga	*Composition
$La(Cu,Al,Ga)_{13-x}$	7(1)	46(4)	31(6)	16(1)	$La_{1.0}Cu_{6.3(6)}Al_{4.2(8)}Ga_{2.1(1)}$
$Ce(Cu,Al,Ga)_{13-x}$	7(1)	48(2)	32(3)	13(1)	$Ce_{1.0}Cu_{6.6(2)}Al_{4.4(5)}Ga_{1.9(1)}$
$Pr(Cu,Al,Ga)_{13-x}$	7(1)	45(2)	32(3)	15(1)	$Pr_{1.0}Cu_{6.0(3)}Al_{4.3(4)}Ga_{2.0(1)}$
$Eu(Cu,Al,Ga)_{13-x}$	7(1)	42(2)	37(4)	12(1)	$Eu_{1.0}Cu_{5.9(3)}Al_{5.2(5)}Ga_{1.7(1)}$

*These compositions were obtained by normalizing each at.% value by the corresponding at.% Ln value.

of 0.5º - 47.5º with a step size of 0.001º and step time of 0.1 seconds. Rietveld refinement was employed to generate an optimized model of $Eu(Cu,Al)_{13-x}$ using the GSAS and EXPGUI packages.[24-25] The results of the Rietveld refinements are shown in Figure 6.1. The lattice parameters and the refinement statistics are provided in Table 6.1. The atomic coordinates and the displacement parameters are listed in Table 6.2.

6.2.3 Elemental Analysis

The elemental compositions of single crystals of $Ln(Cu,Al,Ga)_{13-x}$ (Ln = La – Pr and Eu) were analyzed using a Hitachi S-3600N scanning electron microscope (SEM) equipped with an energy dispersive spectroscopy (EDS) option. An average of six scans with 60 second counting times were performed on the clean, freshly exposed surfaces of cleaved and, etched single crystals with an accelerating voltage of 15 keV and a beam-to-sample distance of 20 mm. The elemental compositions of each sample are provided in Table 6.3.

6.2.4 Physical Properties Measurements

Magnetization data for all compounds were collected using a 9-Tesla Quantum Design Physical Property Measurement System (PPMS). The temperature-dependent magnetization was obtained under zero-field cooled (ZFC) conditions from 3 K to 300 K with an applied field of 0.1

T for the $Pr(Cu,Al,Ga)_{13-x}$, $Eu(Cu,Al,Ga)_{13-x}$, and $Eu(Cu,Al)_{13-x}$ analogues and 1 T for $Ce(Cu,Al,Ga)_{13-x}$. Field-dependent measurements for $Ce(Cu,Al,Ga)_{13-x}$, $Pr(Cu,Al,Ga)_{13-x}$ and $Eu(Cu,Al,Ga)_{13-x}$ were performed at 3 K for fields ranging between 0 T and 9 T. Additionally, field-dependent measurements for $Eu(Cu,Al,Ga)_{13-x}$ and $Eu(Cu,Al)_{13-x}$ were run at 2 K, 3 K, 5 K, 7 K, 9 K, 11 K, 15 K, and 20 K for fields between 0 T and 5 T, and at 3 K, 5 K, 10 K, 15 K, 20 K, and 25 K for fields between 0 T and 5 T, respectively. The temperature-dependent electrical resistivity (3 K to 300 K) for $Ln(Cu,Al,Ga)_{13-x}$ (Ln = La – Pr and Eu) were measured using a standard four-probe ac-procedure with the PPMS. Pt wires with a diameter of 1 mil were mounted onto these samples with silver epoxy. Heat capacity measurements between 2 K – 60 K for $Ln(Cu,Al,Ga)_{13-x}$ (Ln = La – Pr and Eu) were performed using a different Quantum Design PPMS.

6.3 Results and Discussion

6.3.1 Structure Refinement

The structural models for $Ln(Cu,Al,Ga)_{13-x}$ (Ln = La – Pr and Eu) as obtained from fits to the single crystal X-ray and neutron diffraction data are not presented in this dissertation. However, these models will be discussed during the formal defense of this dissertation. For a review of the $NaZn_{13}$ structure-type please refer to reference four.[4]

The refined model for $Eu(Cu,Al,Ga)_{13-x}$ obtained from single crystal neutron diffraction was employed as a starting model for $Eu(Cu,Al)_{13-x}$. The results of the Rietveld refinements are shown in Figure 6.1. Only a select 2θ range is shown for clarity. The lattice parameters and the refinement statistics are provided in Table 6.1. The atomic coordinates and the displacement parameters are listed in Table 6.2. A few small impurity peaks were observed in the diffraction pattern *ca.* 2θ ~ 11. 5º; however, the highest intensity of these peaks was only approximately 600

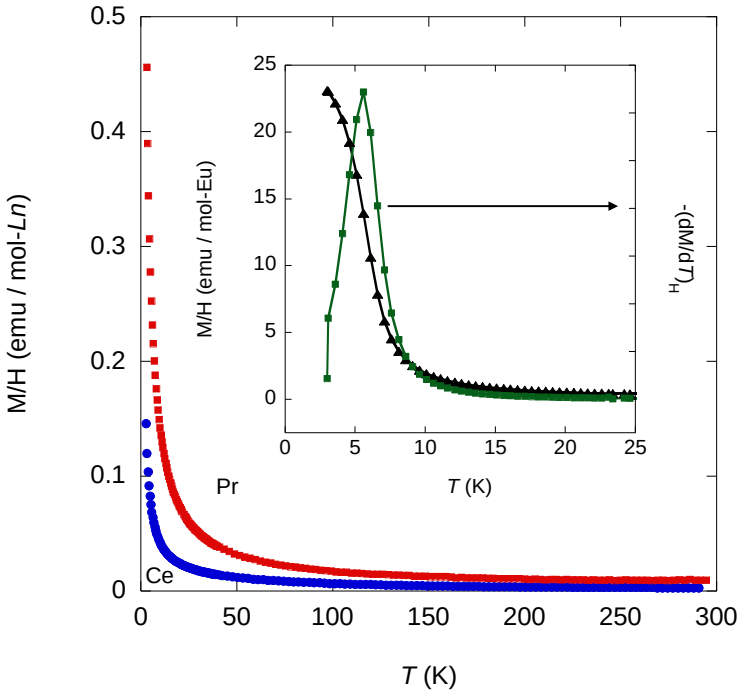

Figure 6.2 Magnetic susceptibility of $Ln(Cu,Al,Ga)_{13-x}$ (Ln = Ce and Pr). The inset shows the magnetic susceptibility and $-(dM/dT)_H$ vs. T curve for $Eu(Cu,Al,Ga)_{13-x}$.

counts above the background. The phase purity of $Eu(Cu,Al)_{13-x}$ was estimated to be greater than 95% by comparing the ratio of the most intense impurity reflection (~ 600 counts) to the most intense peak of $Eu(Cu,Al,Ga)_{13-x}$ (~ 80000 counts).

6.3.2 Physical Properties

The temperature-dependent magnetic susceptibility data for $Ln(Cu,Al,Ga)_{13-x}$ (Ln = Ce and Pr) are shown in Figure 6.2, and the $Eu(Cu,Al,Ga)_{13-x}$ data are shown in the inset of this figure. No long range magnetic order is observed down to 3 K for $Ce(Cu,Al,Ga)_{13-x}$ or $Pr(Cu,Al,Ga)_{13-x}$. From the maximum in the $-(dM/dT)_H$ vs. T curve, $Eu(Cu,Al,Ga)_{13-x}$ is observed to order ferromagnetically at around 6 K. The magnetic susceptibility data for all analogues were fit using the modified Curie-Weiss equation, $\chi(T) = \chi_0 + C/(T - \theta)$, where χ_0 represents the temperature-independent contribution to the susceptibility which can be attributed to Pauli paramagnetism and/or Larmor diamagnetism, C is the Curie constant, and θ is the Weiss

Table 6.4 Magnetic Properties of $Ln(Cu,Al,Ga)_{13-x}$ (Ln = Ce, Pr, and Eu)

	$Ce(Cu,Al,Ga)_{13-x}$	$Pr(Cu,Al,Ga)_{13-x}$	$Eu(Cu,Al,Ga)_{13-x}$
Field (H) Oe	1 T	0.1 T	0.1 T
C (emu mol^{-1} K^{-1})	0.64(1)	1.47(4)	7.77(7)
θ (K)	-3(1)	-0.52(4)	4.0(2)
χ_0 (cm^3 mol-Ln^{-1})	-0.00015(4)	0.00268(7)	0.0051(4)
μ_{calc} (μ_B)	2.54	3.58	7.94
μ_{eff} (μ_B)	2.26(4)	3.43(9)	7.88(7)
fit region (K)	80 – 255	15 – 115	31 – 287

temperature. The effective moments for each analogue obtained from these fits are 2.26(4) μ_B for $Ce(Cu,Al,Ga)_{13-x}$, 3.43(9) μ_B for $Pr(Cu,Al,Ga)_{13-x}$, and 7.88(7) μ_B for $Eu(Cu,Al,Ga)_{13-x}$. These effective moments are in good agreement but are slightly smaller compared to the calculated values for Ce^{3+} (2.54 μ_B), Pr^{3+} (3.58 μ_B), and Eu^{2+} (7.94 μ_B), suggesting the local moment magnetism in these materials is due solely to the lanthanides. The results for each fit are summarized in Table 6.4. The Weiss temperatures extrapolated for $Ln(Cu,Al,Ga)_{13-x}$ (Ln = Ce and Pr) and $Eu(Cu,Al,Ga)_{13-x}$ are suggestive of weak antiferromagnetic and ferromagnetic correlations, respectively.

The field-dependent isothermal magnetization curves at 3 K for $Ln(Cu,Al,Ga)_{13-x}$ (Ln = Ce and Pr) are shown Figure 6.3. The magnetization for both analogues is linear at low fields and begins to saturate at higher fields, below the calculated saturation moment. Knowing that the ferromagnetic material $La(Fe,Si)_{13}$ crystallizes in the $NaZn_{13}$ structure-type and exhibits a giant magnetocaloric effect (MCE) near room temperature,[26-27] it was of interest to probe the magnetocaloric properties of $Eu(Cu,Al,Ga)_{13-x}$. Furthermore, $Eu(Cu,Al)_{13-x}$ was reported to order ferromagnetically at 16 K.[28] This compound was prepared and structurally characterized (Figure 6.1 and Table 6.1) in order to compare its magnetocaloric properties to that of

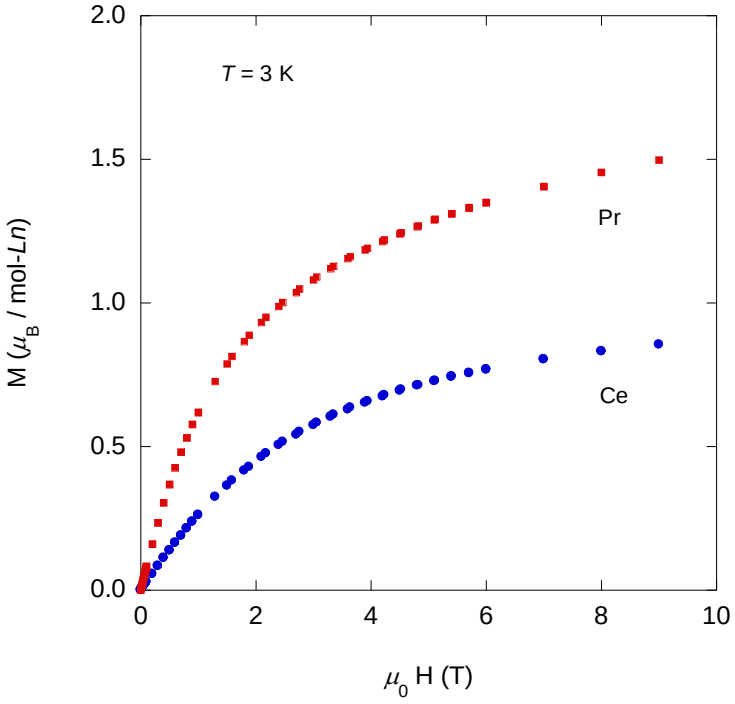

Figure 6.3 Field-dependent isothermal magnetization at 3 K for $Ln(Cu,Al,Ga)_{13-x}$ (Ln = Ce and Pr).

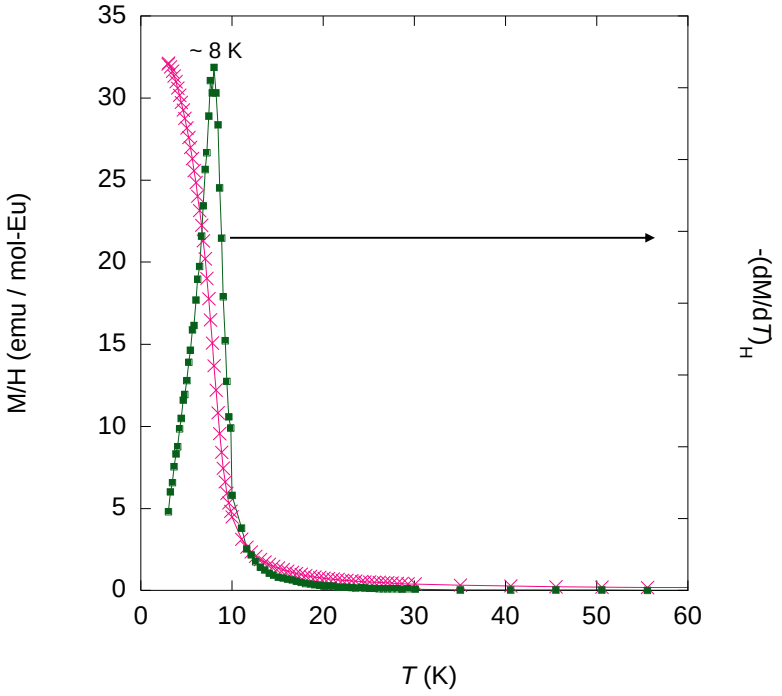

Figure 6.4 Magnetic susceptibility of $Eu(Cu,Al)_{13-x}$ (left) and the corresponding $-(dM/dT)_H$ vs. T curve (right).

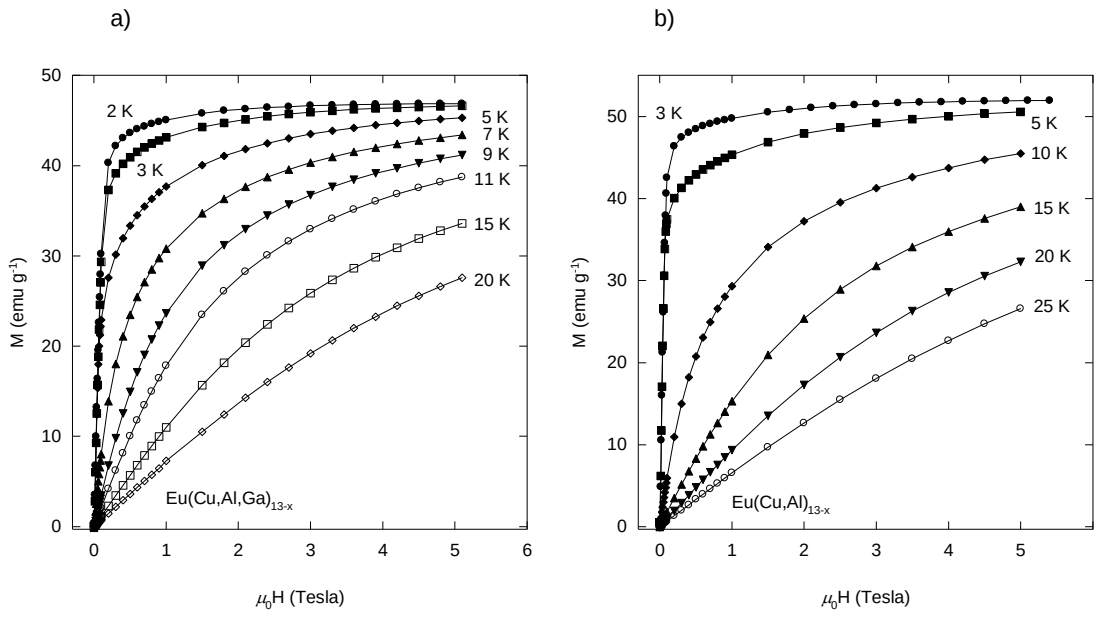

Figure 6.5 Magnetic isotherms versus field for **a)** $Eu(Cu,Al,Ga)_{13-x}$ and **b)** $Eu(Cu,Al)_{13-x}$.

$Eu(Cu,Al,Ga)_{13-x}$. However, our magnetic susceptibility data for $Eu(Cu,Al)_{13-x}$, shown in Figure 6.4, indicate that the onset of ferromagnetic order is at 8 K and not 16 K. Again, the maximum value in the $-(dM/dT)_H$ corresponds to T_C. Figure 6.5a and 6.5b show a series of magnetic isotherms for $Eu(Cu,Al,Ga)_{13-x}$ and $Eu(Cu,Al)_{13-x}$, respectively. The change in magnetic entropy, a measure of a material's MCE, can be estimated from a series of magnetic isotherms using the Maxwell relation, $\Delta S_{mag} = \sum_i (M_{i+1} - M_i)/(T_{i+1} - T_i)\cdot\Delta H_i$.[29-31] The magnetic entropy change as a function of temperature at ΔH = 2 T and ΔH = 5 T for both $Eu(Cu,Al,Ga)_{13-x}$ and $Eu(Cu,Al)_{13-x}$ are shown in Figure 6.6. The ΔS_{mag} for $Eu(Cu,Al,Ga)_{13}$ peaks around -12 J Kg^{-1} K^{-1} near its T_C under an applied magnetic field change of 5 T. This value is smaller than that previously reported for the ferromagnets $ErNi_2$ (ΔS_{mag} = -24 J Kg-1 K-1, T_C = 6.6 K)[32] and $ErAl_2$ (ΔS_{mag} = -34 J Kg-1 K-1, T_C = 11.7 K)[33] under the same field conditions. The smaller ΔS_{mag} value for

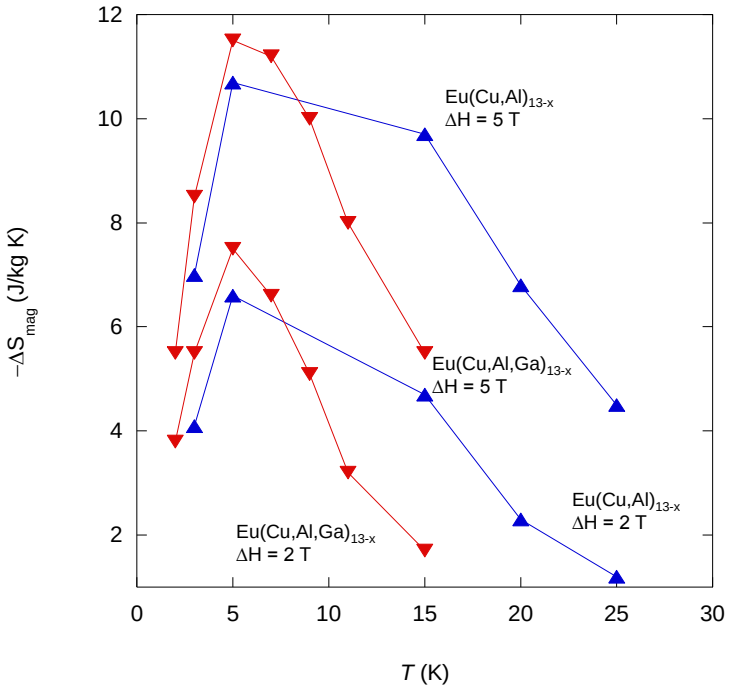

Figure 6.6 -ΔS_{mag} as a function of temperature for $Eu(Cu,Al,Ga)_{13-x}$ (red) and $Eu(Cu,Al)_{13-x}$ (blue) under the applied field changes (ΔH) of 2 T and 5 T.

$Eu(Cu,Al,Ga)_{13-x}$ is consistent with the Ln being surrounded by a more magnetically dilute matrix compared to $ErNi_2$ and $ErAl_2$.

The normalized resistance as a function of temperature is shown in Figure 6.7 for $Ln(Cu,Al,Ga)_{13-x}$ (Ln = La, Ce, Pr, and Eu). All analogues display metallic behavior. The ferromagnetic ordering in $Eu(Cu,Al,Ga)_{13-x}$ is evident in the inset of Figure 6.7, where a sharp decrease in the resistivity occurs near the Curie temperature, indicating a decrease in the spin-disorder scattering.

The specific heat capacities (C_p) of $Ln(Cu,Al,Ga)_{13-x}$ (Ln = La – Pr and Eu) are shown in Figure 6.8. The heat capacities for the Ce and Eu analogues deviate from the nonmagnetic La analogue at low temperatures, while this deviation for the Pr analogue can be seen at a much higher temperature, $T \sim 30$ K. This indicates that the magnitude of the magnetic entropy (ΔS_{mag}) is large for $Pr(Cu,Al,Ga)_{13-x}$. The thermodynamic evidence of the ferromagnetic ordering in

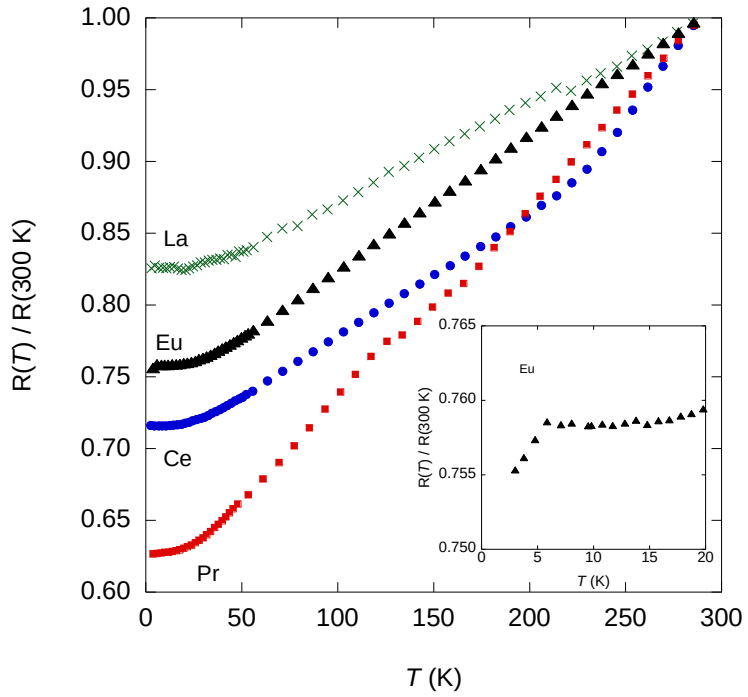

Figure 6.7 Temperature-dependent normalized resistance of $Ln(Cu,Al,Ga)_{13-x}$ (Ln = La, Ce, Pr, and Eu).

$Eu(Cu,Al,Ga)_{13-x}$ is observed as a large peak in the specific heat below ~15 k which peaks at the Curie temperature. This deviation in the C_p for $Eu(Cu,Al,Ga)_{13-x}$ coincides with the magnetic phase transition observed in the magnetic susceptibility (Figure 6.2 inset). The inset of Figure 6.8 shows the specific heat capacity divided by temperature (C_p/T) versus temperature for all analogues. The magnetic phase transition for $Eu(Cu,Al,Ga)_{13-x}$ can be seen more clearly in this inset. Additionally, upturns in the (C_p/T) vs. T curves for both $Ce(Cu,Al,Ga)_{13-x}$ and $Pr(Cu,Al,Ga)_{13-x}$ are observed at low temperature. However, no peaks in the upturns of the (C_p/T) vs. T curves for both $Ce(Cu,Al,Ga)_{13-x}$ and $Pr(Cu,Al,Ga)_{13-x}$ are observed down to the lowest temperatures measured (~ 2 K).

Fits of the standard form, $C_p/T = \gamma + \beta T^2$, to our C_p/T vs. T^2 data for $Ln(Cu,Al,Ga)_{13-x}$ (Ln = La – Pr and Eu) were performed to determine the Sommerfeld coefficients (γ) for each analogue. The best fit values for γ determined from this fitting procedure are 1.65 mJ/mol-K^2,

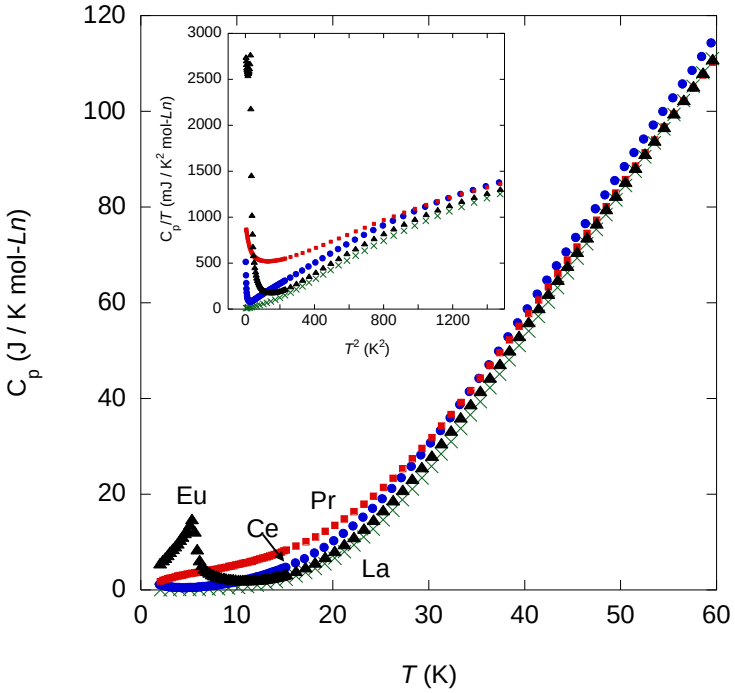

Figure 6.8 Specific heat capacities (C_p) of $Ln(Cu,Al,Ga)_{13-x}$ (Ln = La – Pr and Eu) as a function of temperature. The inset show the specific heat capacity divided by temperature (C_p/T) vs. T^2.

40.8 mJ/mol-K^2, 356 mJ/mol-K^2, and 7.08 mJ/mol-K^2 for $La(Cu,Al,Ga)_{13-x}$, $Ce(Cu,Al,Ga)_{13-x}$, $Pr(Cu,Al,Ga)_{13-x}$, and $Eu(Cu,Al,Ga)_{13-x}$, respectively. The value of γ for $Pr(Cu,Al,Ga)_{13-x}$ obtained by our fitting procedure is significantly larger than that found in simple metals such as Cu (γ ~ 1 mJ/mol-K^2). The large Sommerfeld coefficient determined for $Pr(Cu,Al,Ga)_{13-x}$ may be indicative of the formation of an enhanced electron mass state at low temperatures.[1-2, 34-36]

The magnetic contribution to the specific heat capacity (C_{mag}) for $Ln(Cu,Al,Ga)_{13-x}$ (Ln = Ce, Pr, and Eu) was estimated as the difference in the specific heats of $Ln(Cu,Al,Ga)_{13-x}$ (Ln = Ce, Pr, and Eu) and $La(Cu,Al,Ga)_{13-x}$, where it was assumed that the lattice contribution for each analogue was approximately equal to the specific heat of $La(Cu,Al,Ga)_{13-x}$. The magnetic entropy (S_{mag}) for $Ln(Cu,Al,Ga)_{13-x}$ (Ln = Ce, Pr, and Eu) was determined by integrating the magnetic heat capacity divided by temperature (C_{mag}/T) and is shown in Figure 6.9. The magnetic entropy curves for $Ce(Cu,Al,Ga)_{13-x}$ and $Eu(Cu,Al,Ga)_{13-x}$ never approach the expected

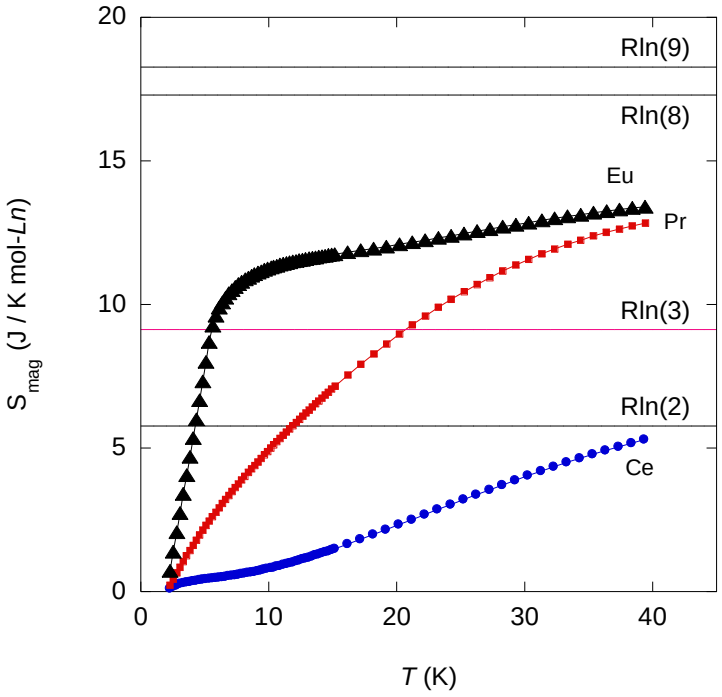

Figure 6.9 Magnetic entropy (S_{mag}) as a function of temperature for $Ln(Cu,Al,Ga)_{13-x}$ (Ln = Ce, Pr, and Eu).

entropy values of Rln(2S + 1), where S = 1/2 and S = 7/2 for the Ce and Eu analogues, respectively. This may be attributed to the lowest temperature measurements of the heat capacity, only going down to ~ 2 K. It is possible that additional magnetic entropy for $Ce(Cu,Al,Ga)_{13-x}$ and $Eu(Cu,Al,Ga)_{13-x}$ could be integrated had the heat capacity for each analogue been measured below 2 K. The magnetic entropy recovered for $Pr(Cu,Al,Ga)_{13-x}$ exceeds the expected entropy of Rln(2S + 1) where S = 1, but begins to saturate below Rln(2J +1) where J = 4.

The origins of heavy-fermion behavior in Pr-based compounds are thought to arise from two mechanisms: either (1) the quadrupolar Kondo effect[13] or (2) excitonic mass enhancement[37] associated with low energy split crystal electric field (CEF) levels. Here the conduction electrons inelastically scatter from the low lying excited CEF levels of the 4*f* electrons which results in their enhanced mass. The latter mechanism was proposed by Fulde and Jensen to account for the

low temperature mass enhancement of Pr metal.[38] These mechanisms differ from the traditional mechanism leading to the formation of heavy quasi-particles in Ce, Yb, and U compounds, where the heavy-fermion behavior is due to the complete compensation of the magnetic moments of the lanthanide ions by the conduction electrons *via* the formation of a Kondo coherent state at low temperatures.[13, 39]

The observed physical properties of $Pr(Cu,Al,Ga)_{13-x}$ bear a striking resemblance to the physical properties of other Pr-based heavy-fermion compounds, where the heavy mass state is thought to arise from the excitonic mass enhancement mechanism.[13, 39-42] The Sommerfeld coefficient determined for $Pr(Cu,Al,Ga)_{13-x}$ (356 mJ/mol-K^2) is comparable to, and in some cases larger, than the Sommerfeld coefficients of other Pr intermetallics, such as $PrOs_4Sb_{12}$ (350 mJ/mol-K^2),[39] $Pr_2Rh_3Ge_5$ (80 mJ/mol-K^2),[40] $PrIr_2B_2C$ (300 mJ/mol-K^2),[41] and $PrRh_2B_2C$ (300 mJ/mol-K^2).[42] Additionally, the magnetic entropy of $Pr(Cu,Al,Ga)_{13-x}$ exceeds Rln(3) above 20 K (Figure 6.9). Similar behavior was observed for the heavy-fermion compounds $Pr_2Rh_3Ge_5$,[40] $PrIr_2B_2C$,[41] and $PrRh_2B_2C$,[42] where the authors claimed that the increased values of the magnetic entropy above Rln(3) were due to the electronic excitations of low lying CEF levels. For $Pr(Cu,Al,Ga)_{13}$, the value of the Wilson-Sommerfeld ratio, $R_w = (\chi(0)/(\gamma(0))*(\pi^2 k_B^2/\mu_{eff})$, was calculated to be ~ 24, where χ(3 K) = 0.46 emu/mol*G, γ = 356 mJ/mol-K^2, and μ_{eff} = 3.43 erg/G. This R_w is comparable to those of $Pr_2Rh_3Ge_5$ (R_w = 17)[40] and $PrIr_2B_2C$ (R_w = 23.31)[41], where the authors attributed the large value to strong correlations and the formation of an enhanced mass state. A better understanding of the CEF levels of $Pr(Cu,Al,Ga)_{13-x}$ are needed to clarify the underlying physics which leads to the enhanced Sommerfeld coefficient. Further studies, such as inelastic neutron scattering experiments would be useful for determining the

energy differences between the excited CEF levels of $Pr(Cu,Al,Ga)_{13-x}$, as well as understanding its low temperature ground state.

6.4 Conclusions

The magnetic, transport, and thermodynamic properties of $Ln(Cu,Al,Ga)_{13-x}$ (Ln =La, Ce, Pr, and Eu) were investigated. All analogues display metallic behavior from 3 to 300 K. $Ce(Cu,Al,Ga)_{13-x}$ and $Pr(Cu,Al,Ga)_{13-x}$ displayed paramagnetic behavior over all temperatures measured in the magnetic susceptibility. $Eu(Cu,Al,Ga)_{13}$ orders ferromagnetically around 6 K. Since $La(Fe,Si)_{13}$ orders ferromagnetically, exhibits a giant magnetocaloric effect and is isostructural to $Eu(Cu,Al,Ga)_{13}$, the magnetocaloric properties of $Eu(Cu,Al,Ga)_{13}$ were examined.[43] Additionally, the magnetocaloric properties of the ferromagnet $Eu(Cu,Al)_{13}$ (T_c ~ 8 K) were studied. The ΔS_{mag} values determined for $Eu(Cu,Al,Ga)_{13}$ and $Eu(Cu,Al)_{13}$ were found to be smaller than the ΔS_{mag} values for other magnetocaloric materials ($ErNi_2$ and $ErAl_2$) which ferromagnetically order in the same temperature region. This is consistent with the Ln being surrounded by a more magnetically dilute matrix compared to $ErNi_2$ and $ErAl_2$. Additionally, the Sommerfeld coefficient for $Pr(Cu,Al,Ga)_{13}$ was found to be large with γ ~ 350 mJ/mol-K^2. Similar to the heavy fermion compound $Pr(Cu,Ga)_{13}$[19] and other Pr based heavy fermion compounds, no Kondo features were observed in the resistivity of $Pr(Cu,Al,Ga)_{13}$. Therefore, the enhancement of the Sommerfeld coefficient for $Pr(Cu,Al,Ga)_{13}$ is likely not the result of the formation of a Kondo coherent state. Further studies at low temperatures are needed to determine the origin of the large Sommerfeld coefficient of $Pr(Cu,Al,Ga)_{13}$.

6.5 References

1. Fisk, Z.; Sarrao, J. L.; Smith, J. L.; Thompson, J. D., The Physics and Chemistry of Heavy Fermions. *Proc. Natl. Acad. Sci. U.S.A.* **1995**, *92*, 6663-6667.

2. Fisk, Z.; Sarrao, J. L.; Thompson, J. D., Heavy Fermions. *Curr. Opin. Solid State Mater. Sci.* **1996**, *1*, 42-46.

3. Stewart, G. R., Heavy-Fermion Systems. *Rev. Mod. Phys.* **1984**, *56*, 755-787.

4. Phelan, W. A.; Menard, M. C.; Kangas, M. J.; McCandless, G. T.; Drake, B. L.; Chan, J. Y., Adventures in Crystal Growth: Synthesis and Characterization of Single Crystals of Complex Intermetallic Compounds. *Chem. Mater.* **2012**, *24*, 409-420.

5. Thomas, E. L.; Millican, J. N.; Okudzeto, E. K.; Chan, J. Y., Crystal Growth and the Search for Highly Correlated Intermetallics. *Comments Inorg. Chem.* **2006**, *27*, 1-39.

6. Ott, H. R.; Rudigier, H.; Fisk, Z.; Smith, J. L., UBe_{13} - An Unconventional Actinide Superconductor. *Phys. Rev. Lett.* **1983**, *50*, 1595-1598.

7. Smith, J. L.; Fisk, Z.; Willis, J. O.; Batlogg, B.; Ott, H. R., Impurities in the Heavy-Fermion Superconductor UBe_{13}. *J. Appl. Phys.* **1984**, *55*, 1996-2000.

8. Maple, M. B.; Chen, J. W.; Lambert, S. E.; Fisk, Z.; Smith, J. L.; Ott, H. R.; Brooks, J. S.; Naughton, M. J., Upper Critical Magnetic-Field of the Heavy-Fermion Superconductor UBe_{13}. *Phys. Rev. Lett.* **1985**, *54*, 477-480.

9. Cox, D. L., Quadrupolar Kondo Effect in Uranium Heavy-Electron Materials. *Phys. Rev. Lett.* **1987**, *59*, 1240-1243.

10. Kim, J. S.; Stewart, G. R., Observation of Low-Lying Levels in UBe_{13}. *Phys. Rev. B* **1995**, *51*, 16190-16193.

11. Besnus, M. J.; Kappler, J. P.; Meyer, A., On The Valence Regime in the $(Ce_xLa_{1-x})Be_{13}$ System. *Solid State Commun.* **1983**, *48*, 835-838.

12. Wilson, Z. S.; Macaluso, R. T.; Bauer, E. D.; Smith, J. L.; Thompson, J. D.; Fisk, Z.; Stanley, G. G.; Chan, J. Y., Rare Beryllium Icosahedra in the Intermediate Valence Compound $CeBe_{13}$. *J. Am. Chem. Soc.* **2004**, *126*, 13926-13927.

13. Yatskar, A.; Beyermann, W. P.; Movshovich, R.; Canfield, P. C., Possible Correlated-Electron Behavior from Quadrupolar Fluctuations in $PrInAg_2$. *Phys. Rev. Lett.* **1996**, *77*, 3637-3640.

14. Yatskar, A.; Beyermann, W. P.; Movshovich, R.; Canfield, P. C.; Panchula, A.; Budko, S. L., Unexpected Heavy-Electron Behavior at Low Temperatures in $PrInAg_2$. *Physica B* **1997**, *230*, 46-48.

15. Matsuda, T. D.; Okada, H.; Sugawara, H.; Aoki, Y.; Sato, H.; Andreev, A. V.; Shiokawa, Y.; Sechovsky, V.; Honma, T.; Yamamoto, E.; Onuki, Y., Specific-Heat Anomaly of Metamagnetism on $PrFe_4P_{12}$ and UCoAl. *Physica B* **2000**, *281*, 220-222.

16. Mitamura, H.; Takeshita, N.; Uwatoko, Y.; Mori, H.; Yamaguchi, A.; Tomita, T.; Wada, H.; Mori, N.; Ishimoto, H.; Goto, T., Precise Resistivity Measurement in $PrInAg_2$ Down to 50 mK. *Physica B* **2000**, *284*, 1341-1342.

17. Kadowaki, K.; Woods, S. B., Universal Relationship of the Resistivity and Specific-Heat in Heavy-Fermion Compounds. *Solid State Commun.* **1986**, *58*, 507-509.

18. Shimura, Y.; Sakakibara, T.; Cho, J. Y.; Chan, J. Y., *J. Phys. Conf. Ser.* **2011**, *273*, 012054.

19. Cho, J. Y.; Thomas, E. L.; Nambu, Y.; Capan, C.; Karki, A. B.; Young, D. P.; Kuga, K.; Nakatsuji, S.; Chan, J. Y., Crystal Growth, Structure, and Physical Properties of $Ln(Cu,Ga)_{13-x}$ (Ln = La-Nd, Eu; $x \approx 0.2$). *Chem. Mater.* **2009**, *21*, 3072-3078.

20. Drake, B. L.; Capan, C.; Cho, J. Y.; Nambu, Y.; Kuga, K.; Xiong, Y. M.; Karki, A. B.; Nakatsuji, S.; Adams, P. W.; Young, D. P.; Chan, J. Y., Crystal Growth, Structure, and Physical Properties of $Ln(Cu, Al)_{12}$ (Ln = Y, Ce, Pr, Sm, and Yb) and $Ln(Cu, Ga)_{12}$ (Ln = Y, Gd-Er, and Yb). *J. Phys.-Condes. Matter* **2010**, *22*, 066001.

21. Felner, I., Crystal Structures of Ternary Rare Earth-3d Transition Metal Compounds of the RT_6Al_6 Type. *J. Less-Common Met.* **1980**, *72*, 241-249.

22. Nordell, K. J.; Miller, G. J., Linking Intermetallics and Zintl Compounds: An investigation of Ternary Trielides (Al, Ga, In) Forming the $NaZn_{13}$ Structure Type. *Inorg. Chem.* **1999**, *38*, 579-590.

23. Wang, J.; Toby, B. H.; Lee, P. L.; Ribaud, L.; Antao, S. M.; Kurtz, C.; Ramanathan, M.; Von Dreele, R. B.; Beno, M. A., A Dedicated Powder Diffraction Beamline at the Advanced Photon Source: Commissioning and Early Operational Results. *Rev. Sci. Instrum.* **2008**, *79*, 085105.

24. Larson, A. C.; Von Dreele, R. B., General Structure Analysis System (GSAS). *Los Alamos National Laboratory Report LAUR 86-748* **1995-2004**, 1-224.

25. Toby, B. H., EXPGUI, A Graphical User Interface for GSAS. *J. Appl. Crystallogr.* **2001**, *34*, 210-213.

26. Shen, B. G.; Sun, J. R.; Hu, F. X.; Zhang, H. W.; Cheng, Z. H., Recent Progress in Exploring Magnetocaloric Materials. *Adv. Mater.* **2009**, *21*, 4545-4564.

27. Han, M. K.; Miller, G. J., An Application of the "Coloring Problem": Structure-Composition-Bonding Relationships in the Magnetocaloric Materials $LaFe_{13-x}Si_x$. *Inorg. Chem.* **2008**, *47*, 515-528.

28. Felner, I.; Nowik, I., Magnetic-Properties of RM_6Al_6 (R = Light Rare-Earth, M = Cu, Mn, Fe). *J. Phys. Chem. Solids* **1982**, *43*, 463-465.

29. Gschneidner, K. A.; Pecharsky, V. K., Magnetocaloric Materials. *Annu. Rev. Mater. Sci.* **2000**, *30*, 387-429.

30. Gutfleisch, O.; Willard, M. A.; Bruck, E.; Chen, C. H.; Sankar, S. G.; Liu, J. P., Magnetic Materials and Devices for the 21st Century: Stronger, Lighter, and More Energy Efficient. *Adv. Mater.* **2011**, *23*, 821-842.

31. Pecharsky, V. K.; Gschneidner, K. A., Advanced Magnetocaloric Materials: What Does the Future Hold? *Int. J. Refrig.* **2006**, *29*, 1239-1249.

32. Tomokiyo, A.; Yayama, H.; Wakabayyashi, H.; Kuzuhara, T.; Hashimoto, T.; Sahashi, M.; Inomata, K., Specific Heat and Entropy of RNi_2 (R: Rare Earth Heavy Metals) in Magnetic Field. *Adv. Cryog. Eng* **1986**, *32*, 295-301.

33. Hashimoto, T.; Matsumoto, K.; Kurihara, T.; Numazawa, T.; Tomokiyo, A.; Yayama, H.; Goto, T.; Todo, S.; Sahashi, M., Investigations of the Possibility of the RAl_2 System as a Refrigerant in an Ericsson Type Magnetic Refrigerator. *Adv. Cryog. Eng* **1986**, *32*, 279-286.

34. Fisk, Z., Physics - A Whiff of Chemistry in Heavy Electron Physics. *Science* **2007**, *318*, 1559-1560.

35. Fisk, Z.; Hess, D. W.; Pethick, C. J.; Pines, D.; Smith, J. L.; Thompson, J. D.; Willis, J. O., Heavy-Electron Metal - New Highly Correlated States of Matter. *Science* **1988**, *239*, 33-42.

36. Fisk, Z.; Ott, H. R.; Rice, T. M.; Smith, J. L., Heavy-Electron Metals. *Nature* **1986**, *320*, 124-129.

37. Goremychkin, E. A.; Osborn, R.; Bauer, E. D.; Maple, M. B.; Frederick, N. A.; Yuhasz, W. M.; Woodward, F. M.; Lynn, J. W., Crystal Field Potential of $PrOs_4Sb_{12}$: Consequences for Superconductivity. *Phys. Rev. Lett.* **2004**, *93*, 157003.

38. Fulde, P.; Jensen, J., Electronic Heat-Capacity of the Rare-Earth-Metals. *Phys. Rev. B* **1983**, *27*, 4085-4094.

39. Bauer, E. D.; Frederick, N. A.; Ho, P. C.; Zapf, V. S.; Maple, M. B., Superconductivity and Heavy Fermion Behavior in $PrOs_4Sb_{12}$. *Phys. Rev. B* **2002**, *65*, 1-5.

40. Anand, V. K.; Hossain, Z.; Geibel, C., Magnetic Order in $Pr_2Pd_3Ge_5$ and Possible Heavy-Fermion Behavior in $Pr_2Rh_3Ge_5$. *Phys. Rev. B* **2008**, *77*, 184407.

41. Anupam; Anand, V. K.; Hossain, Z.; Adroja, D. T.; Geibel, C., Signatures of Spin-Glass Behaviour in $PrIr_2B_2$ and Heavy Fermion Behaviour in $PrIr_2B_2C$. *J. Phys.: Condens. Matter* **2011**, *23*, 376001.

42. Anand, V. K.; Hossain, Z.; Chen, G.; Nicklas, M.; Geibel, C., Heavy Fermion Behavior in $PrRh_2B_2C$: Excitonic Mass Enhancement. *Phys. Rev. B* **2009**, *79*, 113107.

43. Jia, L.; Sun, J. R.; Shen, J.; Gao, B.; Zhao, T. Y.; Zhang, H. W.; Hu, F. X.; Shen, B. G., Influence of Interstitial and Substitutional Atoms on the Crystal Structure of $La(FeSi)_{13}$. *J. Alloys Compd.* **2011**, *509*, 5804-5809.

Chapter 7. Conclusion

The central objective of this dissertation was to present the crystal growth, structures, and physical properties of a select group of Ln – T – X (Ln = lanthanide; T = Fe, Co, and Cu; X = Sb, Al and Ga) intermetallics. The preparation and growth of high quality single-crystals of $LnFeSb_3$ (Ln = Pr, Nd, Sm, Gd, and Tb), $CeCo(Sb, Sn)_3$, $Ln_2Fe_4Sb_5$, (Ln = La – Nd, and Sm), and $Ln(Cu,Al,Ga)_{13}$ (Ln = La, Ce, Pr, and Eu) has allowed for the study of their structures and physical properties. In the case of $LnCu_2(Al,Si)_6$ (Ln = La and Ce), small single crystals adequate for single crystal X-ray diffraction experiments were grown. However, due to the relatively small size of these crystals and their nucleation from an impurity phase, polycrystalline powders of these compounds were prepared *via* arc-melting of the elements and subsequent annealing led to relatively phase pure compounds.

The $LnFeSb_3$ (Ln = Pr, Nd, Sm, Gd, and Tb) and $CeCo(Sb, Sn)_3$ phases were synthesized *via* an Sb and Sn flux, respectively. When the magnetic susceptibility data of $LnFeSb_3$ (Ln = Pr, Nd, Sm, and Gd) and $CeCo(Sb, Sn)_3$ were fit using the Curie-Weiss and modified Curie Weiss equations, it was determined that the observed magnetic properties of these compounds originated from within the Ln-sublattices of $LnFeSb_3$ (Ln = Pr, Nd, Sm, Gd, and Tb) and $CeCo(Sb, Sn)_3$. The observation of the variations in the magnetic properties of $LnFeSb_3$ (Ln = Pr, Nd, Sm, and Gd) with the application of an applied magnetic field along the different crystallographic directions of these compounds would not be possible to determine with polycrystalline samples. The importance of the growth of single crystals of $LnFeSb_3$ (Ln = Pr, Nd, Sm, Gd, and Tb) was made apparent when it was discovered that $LnFeSb_3$ (Ln = Pr, Nd, Sm, and Gd) displayed magnetic anisotropy. Similar magnetic behaviors were found for the

structurally related compounds $LnNiSb_3$ (Ln = Ce, Pr, Nd, and Sm),[1-2] β-$CeNiSb_3$,[3] and $LnNi(Sn,Sb)_3$ (Ln = Pr, Nd, Sm, and Gd).[4]

Neither Fe and Co carry a magnetic moment and the magnetic interactions of the abovementioned $LnFeSb_3$ (Ln = Pr, Nd, Sm, Gd, and Tb) and $CeCo(Sb, Sn)_3$ compounds are due to the localized *f*-moments. Using Fe, Ni, or Co to synthesize magnetic intermetallic compounds would seem to be a nontrivial task as they are ferromagnetic in there elemental states. However, the late transition metals (T) of Ln – T – M containing compounds often become reduced by the very electropositive lanthanide, thus quenching the transition metal's magnetic moment.[5-6] Thus it stands to reason that if the transition metal units are present in abundance with respect to the lanthanide units for a compound, then the transition metal will not contribute diamagnetically to overall magnetization.

Initially small single crystals of $Ln_2Fe_4Sb_5$ (Ln = La – Nd, and Sm) were prepared from a stoichiometric melt of their constituent elements. However, the relatively small size of the single crystals made it impossible to measure their physical properties. Based on previous experiences with using Sb as flux, it was determined that the growth of phase pure samples of $Ln_2Fe_4Sb_5$ (Ln = La – Nd, and Sm) were improbable. Therefore, binary phase diagrams were studied to find an inert flux for the synthesis of $Ln_2Fe_4Sb_5$ (Ln = La – Nd, and Sm). At high temperatures Bi does not react with these elements and reactions were conducted using the melts of Ln, Fe, Sb, and Bi with two, four, five, and ten equivalents, respectively. These reactions yielded (~ 3 mm), phase pure single crystals of $Ln_2Fe_4Sb_5$ (Ln = La – Nd, and Sm). A crystal of $Ce_2Fe_4Sb_5$ is shown above.

Spin glass behavior was observed from the magnetic susceptibility measurements of $La_2Fe_4Sb_5$, where it was seen that the zero-field cooled and field cooled magnetic susceptibility

measurements diverged below T^* ~ 30 K. Small hysteresis effects were observed in the field dependent magnetization measurements at T = 5 K, which is also a sign of spin glass behavior. A divergence of zero-field cooled and field cooled magnetic susceptibility and small hysteresis effects in the field dependent magnetization were also observed for $Ln_2Fe_4Sb_5$ (Ln = Ce, Pr, Nd, and Sm). The magnetic properties of these compounds correlate with the structure of the Fe-sublattice. The Fe-sublattice is comprised of occupational disordered Fe atoms which form bow-tie networks composed of nearly equilateral triangles. This network presents the possibility for spin glass frustration and from magnetic susceptibility data collected for $Ln_2Fe_4Sb_5$ (Ln = Ce, Pr, Nd, and Sm), it was determined that the dominant magnetic interactions originate from the Fe-sublattice.[7]

Polycrystalline buttons of $LnCu_2(Al,Si)_5$ (Ln = La and Ce) were prepared *via* arc-melting because the single crystals of these phases grown from an Al flux were small and found to nucleate from an impurity phase. Rietveld refinements were employed to model the X-ray powder diffraction data obtained from the 11-BM beamline located at the Advanced Photon Source (Argonne National Laboratory). Results from the refinements suggest that the purity of each phase was greater than 95 %. Physical property measurements were conducted on the remaining portions of the polycrystalline buttons. From the magnetic susceptibility measurements of $CeCu_2(Al,Si)_5$, paramagnetic behavior was observed down to 2 K. From Curie-Weiss fits to the magnetic susceptibility data and magnetization scaling, it was determined that magnetic correlations from $CeCu_2(Al,Si)_5$ become relevant at 10 K and are likely ferromagnetic. Additionally, Kondo features were observed in the low temperature portion of the resistivity for $CeCu_2(Al,Si)_5$. The low temperature ferromagnetic and Kondo interactions are interesting, as they could lead to the formation of a singular Fermi liquid.[8-11]

The synthesis of large single crystals of $Ln(Cu,Al,Ga)_{13}$ (Ln = La, Ce, Pr, and Eu) from a combined Al and Ga flux, allowed members of our group to collect neutron diffraction data at the Spallation Neutron Source (SNS) at Oak Ridge National Laboratory (ORNL) to better understand the disorder in these structures. The occupational disorder of the 8*b* and 96*i* Wyckoff sites of $Ln(Cu,Al,Ga)_{13}$ (Ln = La, Ce, Pr, and Eu) could not be fully elucidated due do the similar X-ray form factors and small differences of the neutron scattering lengths of Cu and Ga. However, a combined analysis of the X-ray, neutron, and EDS measurements led to the most reasonable structural models for $Ln(Cu,Al,Ga)_{13}$ (Ln = La, Ce, Pr, and Eu).

$Eu(Cu,Al,Ga)_{13}$ orders ferromagnetically around 6 K. Since $La(Fe,Si)_{13}$ orders ferromagnetically, exhibits a giant magnetocaloric effect and is isostructural to $Eu(Cu,Al,Ga)_{13}$, the magnetocaloric properties of $Eu(Cu,Al,Ga)_{13}$ were examined.[12] Additionally, the magnetocaloric properties of the ferromagnet $Eu(Cu,Al)_{13}$ ($T_c \sim 8$ K) were studied. The ΔS_{mag} values determined for $Eu(Cu,Al,Ga)_{13}$ and $Eu(Cu,Al)_{13}$ were found to be smaller than the ΔS_{mag} values for other magnetocaloric materials which ferromagnetically order in the same temperature region. Additionally, the Sommerfeld coefficient for $Pr(Cu,Al,Ga)_{13}$ was found to be large with $\gamma \sim 350$ mJ/mol-K^2. Similar to the heavy fermion compound $Pr(Cu,Ga)_{13}$[13] and other Pr based heavy fermion compounds, no Kondo features were observed in the resistivity of $Pr(Cu,Al,Ga)_{13}$. Therefore, the enhancement of the Sommerfeld coefficient for $Pr(Cu,Al,Ga)_{13}$ is likely not the result of the formation of a Kondo coherent state. Further, physical properties analysis is ongoing to determine the origin of the large Sommerfeld coefficient of $Pr(Cu,Al,Ga)_{13}$.

The research presented in this dissertation has highlighted several studies of intermetallics detailing their synthesis, structural elucidation, and physical properties. The electron-electron and electron-lattice interactions of intermetallic compounds can result in

interesting chemical and physical phenomena. Furthermore, the growth of single crystals of intermetallic compounds allows for the complete study of their structure-physical property relationships. The discovery of new intermetallic compounds and the subsequent optimization of their properties will play large roles in shaping the demands of our society. I am very much looking forward to being a part of this effort as I continue my scientific career by applying the knowledge I have learned during my tenure in the Chan group.

7.1 References

1. Macaluso, R. T.; Wells, D. M.; Sykora, R. E.; Albrecht-Schmitt, T. E.; Mar, A.; Nakatsuji, S.; Lee, H.; Fisk, Z.; Chan, J. Y., Structure and Electrical Resistivity of $CeNiSb_3$. *J. Solid State Chem.* **2004**, *177*, 293-298.

2. Thomas, E. L.; Macaluso, R. T.; Lee, H. O.; Fisk, Z.; Chan, J. Y., Crystal Growth, Characterization, and Physical Properties of $PrNiSb_3$, $NdNiSb_3$, and $SmNiSb_3$. *J. Solid State Chem.* **2004**, *177*, 4228-4236.

3. Thomas, E. L.; Gautreaux, D. P.; Lee, H. O.; Fisk, Z.; Chan, J. Y., Discovery of β-$LnNiSb_3$ (Ln = La, Ce): Crystal Growth, Structure, and Magnetic and Transport Behavior. *Inorg. Chem.* **2007**, *46*, 3010-3016.

4. Gautreaux, D. P.; Capan, C.; DiTusa, J. F.; Young, D. P.; Chan, J. Y., Synthesis, Structure, and Physical Properties of $LnNi(Sn,Sb)_3$ (Ln = Pr, Nd, Sm, Gd, Tb). *J. Solid State Chem.* **2008**, *181*, 1977-1982.

5. Francisco, M. C.; Malliakas, C. D.; Piccoli, P. M. B.; Gutmann, M. J.; Schultz, A. J.; Kanatzidis, M. G., Development and Loss of Ferromagnetism Controlled by the Interplay of Ge Concentration and Mn Vacancies in Structurally Modulated $Y_4Mn_{1-x}Ga_{12-y}Ge_y$. *J. Am. Chem. Soc.* **2010**, *132*, 8998-9006.

6. Papoian, G. A.; Hoffmann, R., Hypervalent Bonding in One, Two, and Three Dimensions: Extending the Zintl-Klemm Concept to Nonclassical Electron-Rich Networks. *Angew. Chem. Int. Ed.* **2000**, *39*, 2409-2448.

7. Ramirez, A. P., Strongly Geometrically Frustrated Magnets. *Ann. Rev. Mater. Sci.* **1994**, *24*, 453-480.

8. Sacramento, P. D.; Schlottmann, P., Thermodynamics of the N-Channel Kondo Model for General-N and Impurity Spin-S in a Magnetic Field. *J. Phys.: Condens. Matter* **1991**, *3*, 9687-9696.

9. Gan, J.; Coleman, P.; Andrei, N., Coexistence of Fermi-Liquid and Magnetism in the Underscreened Kondo Problem. *Phys. Rev. Lett.* **1992**, *68*, 3476-3479.

10. Coleman, P.; Pepin, C., Singular Fermi Liquid Behavior in the Underscreened Kondo Model. *Physical Review B* **2003**, *68*, 220405(R).

11. Manyala, N.; DiTusa, J. F.; Aeppli, G.; Ramirez, A. P., Doping a Semiconductor to Create an Unconventional Metal. *Nature* **2008**, *454*, 976-980.

12. Jia, L.; Sun, J. R.; Shen, J.; Gao, B.; Zhao, T. Y.; Zhang, H. W.; Hu, F. X.; Shen, B. G., Influence of Interstitial and Substitutional Atoms on the Crystal Structure of $La(FeSi)_{13}$. *J. Alloys Compd.* **2011**, *509*, 5804-5809.

13. Cho, J. Y.; Thomas, E. L.; Nambu, Y.; Capan, C.; Karki, A. B.; Young, D. P.; Kuga, K.; Nakatsuji, S.; Chan, J. Y., Crystal Growth, Structure, and Physical Properties of $Ln(Cu,Ga)_{13-x}$ (Ln = La-Nd, Eu; $x \approx 0.2$). *Chem. Mater.* **2009**, *21*, 3072-3078.

Appendix 1. Crystallographic Information Files (CIFs)

A1.1 $LaCo(Sb, Sn)_3$

```
data_shelxl

_audit_creation_method            SHELXL-97
_chemical_name_systematic
;
 ?
;
_chemical_name_common             ?
_chemical_melting_point           ?
_chemical_formula_moiety          'Co La
Sb3'
_chemical_formula_sum
 'Co La Sb3'
_chemical_formula_weight          563.09

loop_
 _atom_type_symbol
 _atom_type_description
 _atom_type_scat_dispersion_real
 _atom_type_scat_dispersion_imag
 _atom_type_scat_source
 'La'  'La'  -0.2871   2.4523
 'International Tables Vol C Tables 4.2.6.8
and 6.1.1.4'
 'Co'  'Co'   0.3494   0.9721
 'International Tables Vol C Tables 4.2.6.8
and 6.1.1.4'
 'Sb'  'Sb'  -0.5866   1.5461
 'International Tables Vol C Tables 4.2.6.8
and 6.1.1.4'

_symmetry_cell_setting
'Orthorhombic'
_symmetry_space_group_name_H-M    'P b c m
'

loop_
 _symmetry_equiv_pos_as_xyz
 'x, y, z'
 '-x, -y, z+1/2'
 'x, -y+1/2, -z'
 '-x, y+1/2, -z+1/2'
 '-x, -y, -z'
 'x, y, -z-1/2'
 '-x, y-1/2, z'
 'x, -y-1/2, z-1/2'

_cell_length_a                    13.019(3)
_cell_length_b                    6.162(5)
_cell_length_c                    12.159(5)
_cell_angle_alpha                 90
_cell_angle_beta                  90
_cell_angle_gamma                 90
_cell_volume                      975.5(8)
_cell_formula_units_Z             8
_cell_measurement_temperature     298(2)
_cell_measurement_reflns_used     2631
_cell_measurement_theta_min       2.55
_cell_measurement_theta_max       30.0

_exptl_crystal_description        plate
_exptl_crystal_colour             black
_exptl_crystal_size_max           0.10
_exptl_crystal_size_mid           0.05
_exptl_crystal_size_min           0.03
_exptl_crystal_density_meas       ?
_exptl_crystal_density_diffrn     7.668
_exptl_crystal_density_method     'not
measured'
_exptl_crystal_F_000              1896
_exptl_absorpt_coefficient_mu     28.103
_exptl_absorpt_correction_type    'sphere'
_exptl_absorpt_correction_T_min   0.1654
_exptl_absorpt_correction_T_max   0.5401
_exptl_absorpt_process_details    'HKL
Scalepack (Otwinowski & Minor 1997)'

_exptl_special_details
;
 ?
;

_diffrn_ambient_temperature       298(2)
_diffrn_radiation_wavelength      0.71073
_diffrn_radiation_type            MoK\a
_diffrn_radiation_source          'fine-
focus sealed tube'
_diffrn_radiation_monochromator   graphite
_diffrn_measurement_device_type   'Nonius
KappaCCD'
_diffrn_measurement_method        '\w and \f
scans'
_diffrn_detector_area_resol_mean  ?
_diffrn_standards_number          ?
_diffrn_standards_interval_count  ?
_diffrn_standards_interval_time   ?
_diffrn_standards_decay_%         ?
_diffrn_reflns_number             60223
_diffrn_reflns_av_R_equivalents   0.0000
_diffrn_reflns_av_sigmaI/netI     0.0211
_diffrn_reflns_limit_h_min        0
_diffrn_reflns_limit_h_max        18
_diffrn_reflns_limit_k_min        0
_diffrn_reflns_limit_k_max        8
_diffrn_reflns_limit_l_min        0
_diffrn_reflns_limit_l_max        16
_diffrn_reflns_theta_min          3.13
_diffrn_reflns_theta_max          30.00
_reflns_number_total              1487
_reflns_number_gt                 1242
_reflns_threshold_expression      I>2\s(I)

_computing_data_collection        ?
_computing_cell_refinement        ?
_computing_data_reduction         ?
_computing_structure_solution     ?
_computing_structure_refinement   'SHELXL-97
(Sheldrick, 2008)'
_computing_molecular_graphics     ?
_computing_publication_material   ?

_refine_special_details
;
 Refinement of F^2^ against ALL reflections.
The weighted R-factor wR and
 goodness of fit S are based on F^2^,
conventional R-factors R are based
 on F, with F set to zero for negative F^2^.
The threshold expression of
 F^2^ > 2\s(F^2^) is used only for
calculating R-factors(gt) etc. and is
 not relevant to the choice of reflections
for refinement.  R-factors based
 on F^2^ are statistically about twice as
large as those based on F, and R-
```

```
 factors based on ALL data will be even
larger.
;

_refine_ls_structure_factor_coef  Fsqd
_refine_ls_matrix_type            full
_refine_ls_weighting_scheme       calc
_refine_ls_weighting_details
 'calc
w=1/[\s^2^(Fo^2^)+(0.0285P)^2^+10.5689P]
where P=(Fo^2^+2Fc^2^)/3'
_atom_sites_solution_primary      direct
_atom_sites_solution_secondary    difmap
_atom_sites_solution_hydrogens    ?
_refine_ls_hydrogen_treatment     ?
_refine_ls_extinction_method      SHELXL
_refine_ls_extinction_coef        0.00013(3)
_refine_ls_extinction_expression
 'Fc^*^=kFc[1+0.001xFc^2^\l^3^/sin(2\q)]^-
1/4^'
_refine_ls_number_reflns          1487
_refine_ls_number_parameters      53
_refine_ls_number_restraints      0
_refine_ls_R_factor_all           0.0419
_refine_ls_R_factor_gt            0.0298
_refine_ls_wR_factor_ref          0.0701
_refine_ls_wR_factor_gt           0.0663
_refine_ls_goodness_of_fit_ref    1.161
_refine_ls_restrained_S_all       1.161
_refine_ls_shift/su_max           0.001
_refine_ls_shift/su_mean          0.000

loop_
 _atom_site_label
 _atom_site_type_symbol
 _atom_site_fract_x
 _atom_site_fract_y
 _atom_site_fract_z
 _atom_site_U_iso_or_equiv
 _atom_site_adp_type
 _atom_site_occupancy
 _atom_site_symmetry_multiplicity
 _atom_site_calc_flag
 _atom_site_refinement_flags
 _atom_site_disorder_assembly
 _atom_site_disorder_group
La1 La 0.70111(4) 0.2500 0.0000 0.00771(13)
Uani 1 2 d S . .
La2 La 0.30464(4) 0.26555(10) 0.7500
0.00745(13) Uani 1 2 d S . .
Co1 Co 0.10072(7) 0.03353(16) 0.86197(8)
0.0086(2) Uani 1 1 d . . .
Sb1 Sb 0.97354(5) 0.2500 0.0000 0.00978(16)
Uani 1 2 d S . .
Sb2 Sb 0.79094(5) 0.25641(11) 0.7500
0.00844(15) Uani 1 2 d S . .
Sb3 Sb 0.50162(4) 0.50873(8) 0.87693(3)
0.00936(12) Uani 1 1 d . . .
Sb4 Sb 0.21320(5) 0.2500 0.0000 0.00852(15)
Uani 1 2 d S . .
Sb5 Sb 0.94507(5) 0.88377(11) 0.7500
0.00938(16) Uani 1 2 d S . .

loop_
 _atom_site_aniso_label
 _atom_site_aniso_U_11
 _atom_site_aniso_U_22
 _atom_site_aniso_U_33
 _atom_site_aniso_U_23
 _atom_site_aniso_U_13
 _atom_site_aniso_U_12
La1 0.0086(2) 0.0078(3) 0.0067(3) -0.0004(2)
0.000 0.000
La2 0.0076(2) 0.0085(3) 0.0062(3) 0.000
0.000 0.0001(2)
Co1 0.0095(4) 0.0089(5) 0.0074(4) -0.0002(4)
-0.0003(4) -0.0005(4)
Sb1 0.0105(3) 0.0096(3) 0.0092(3) 0.0008(2)
0.000 0.000
Sb2 0.0101(3) 0.0080(3) 0.0072(3) 0.000
0.000 -0.0009(3)
Sb3 0.0097(2) 0.0105(2) 0.0079(2) -
0.00009(17) 0.00007(17) -0.00064(16)
Sb4 0.0101(3) 0.0085(3) 0.0070(3) -0.0010(2)
0.000 0.000
Sb5 0.0090(3) 0.0091(3) 0.0100(3) 0.000
0.000 -0.0012(3)

_geom_special_details
;
 All s.u.'s (except the s.u. in the dihedral
angle between two l.s. planes)
 are estimated using the full covariance
matrix.  The cell s.u.'s are taken
 into account individually in the estimation
of s.u.'s in distances, angles
 and torsion angles; correlations between
s.u.'s in cell parameters are only
 used when they are defined by crystal
symmetry.  An approximate (isotropic)
 treatment of cell s.u.'s is used for
estimating s.u.'s involving l.s. planes.
;

loop_
 _geom_bond_atom_site_label_1
 _geom_bond_atom_site_label_2
 _geom_bond_distance
 _geom_bond_site_symmetry_2
 _geom_bond_publ_flag
La1 Sb2 3.2572(12) 3_556 ?
La1 Sb2 3.2572(12) 1_554 ?
La1 Sb4 3.277(2) 5_665 ?
La1 Sb4 3.277(2) 5_655 ?
La1 Sb3 3.3789(9) 7_654 ?
La1 Sb3 3.3789(9) 5_666 ?
La1 Sb3 3.3952(10) 1_554 ?
La1 Sb3 3.3952(10) 3_556 ?
La1 Co1 3.5392(13) 7_664 ?
La1 Co1 3.5392(13) 5_656 ?
La1 Sb1 3.5468(11) . ?
La2 Sb4 3.2660(12) 6_556 ?
La2 Sb4 3.2660(12) 1_556 ?
La2 Sb2 3.271(2) 7_665 ?
La2 Co1 3.3086(13) 6_557 ?
La2 Co1 3.3086(13) . ?
La2 Sb5 3.3318(10) 7_655 ?
La2 Sb3 3.3473(10) . ?
La2 Sb3 3.3473(10) 6_557 ?
La2 Sb3 3.3539(10) 7_655 ?
La2 Sb3 3.3539(10) 4_646 ?
La2 Sb2 3.375(2) 7_655 ?
Co1 Sb4 2.5963(12) 1_556 ?
Co1 Sb2 2.5999(14) 7_655 ?
Co1 Sb1 2.6085(14) 5_656 ?
Co1 Sb5 2.6100(12) 1_445 ?
Co1 Sb5 2.6205(18) 7_655 ?
Co1 Sb1 2.7089(12) 1_456 ?
Co1 Co1 2.723(2) 6_557 ?
Co1 La1 3.5392(13) 5_656 ?
Sb1 Co1 2.6085(14) 7_664 ?
Sb1 Co1 2.6085(14) 5_656 ?
```

```
Sb1 Co1 2.7089(12) 3_656 ?
Sb1 Co1 2.7089(12) 1_654 ?
Sb1 Sb4 3.1203(11) 1_655 ?
Sb1 Sb1 3.157(2) 5_765 ?
Sb1 Sb1 3.157(2) 5_755 ?
Sb2 Co1 2.5999(14) 7_665 ?
Sb2 Co1 2.5999(14) 4_656 ?
Sb2 Sb5 3.0496(16) 1_545 ?
Sb2 La1 3.2572(12) 6_556 ?
Sb2 La1 3.2572(12) 1_556 ?
Sb2 La2 3.271(2) 7_655 ?
Sb2 La2 3.375(2) 7_665 ?
Sb3 Sb3 2.9950(15) 5_667 ?
Sb3 Sb3 3.081(2) 7_655 ?
Sb3 Sb3 3.081(2) 7_665 ?
Sb3 Sb3 3.0868(15) 6_557 ?
Sb3 La2 3.3539(10) 7_665 ?
Sb3 La1 3.3789(9) 5_666 ?
Sb3 La1 3.3952(10) 1_556 ?
Sb4 Co1 2.5963(12) 1_554 ?
Sb4 Co1 2.5963(12) 3_556 ?
Sb4 Sb1 3.1203(11) 1_455 ?
Sb4 La2 3.2660(12) 3_556 ?
Sb4 La2 3.2660(12) 1_554 ?
Sb4 La1 3.277(2) 5_665 ?
Sb4 La1 3.277(2) 5_655 ?
Sb5 Co1 2.6100(12) 1_665 ?
Sb5 Co1 2.6100(12) 6_667 ?
Sb5 Co1 2.6205(18) 4_656 ?
Sb5 Co1 2.6205(18) 7_665 ?
Sb5 Sb2 3.0496(16) 1_565 ?
Sb5 La2 3.3318(10) 7_665 ?

loop_
 _geom_angle_atom_site_label_1
 _geom_angle_atom_site_label_2
 _geom_angle_atom_site_label_3
 _geom_angle
 _geom_angle_site_symmetry_1
 _geom_angle_site_symmetry_3
 _geom_angle_publ_flag
Sb2 La1 Sb2 137.91(3) 3_556 1_554 ?
Sb2 La1 Sb4 83.636(15) 3_556 5_665 ?
Sb2 La1 Sb4 82.320(15) 1_554 5_665 ?
Sb2 La1 Sb4 82.320(15) 3_556 5_655 ?
Sb2 La1 Sb4 83.636(15) 1_554 5_655 ?
Sb4 La1 Sb4 140.19(4) 5_665 5_655 ?
Sb2 La1 Sb3 133.508(19) 3_556 7_654 ?
Sb2 La1 Sb3 82.68(2) 1_554 7_654 ?
Sb4 La1 Sb3 132.820(17) 5_665 7_654 ?
Sb4 La1 Sb3 81.50(3) 5_655 7_654 ?
Sb2 La1 Sb3 82.68(2) 3_556 5_666 ?
Sb2 La1 Sb3 133.508(19) 1_554 5_666 ?
Sb4 La1 Sb3 81.50(3) 5_665 5_666 ?
Sb4 La1 Sb3 132.820(17) 5_655 5_666 ?
Sb3 La1 Sb3 77.26(3) 7_654 5_666 ?
Sb2 La1 Sb3 133.764(19) 3_556 1_554 ?
Sb2 La1 Sb3 81.82(2) 1_554 1_554 ?
Sb4 La1 Sb3 79.57(3) 5_665 1_554 ?
Sb4 La1 Sb3 134.587(17) 5_655 1_554 ?
Sb3 La1 Sb3 54.12(4) 7_654 1_554 ?
Sb3 La1 Sb3 52.48(3) 5_666 1_554 ?
Sb2 La1 Sb3 81.82(2) 3_556 3_556 ?
Sb2 La1 Sb3 133.764(19) 1_554 3_556 ?
Sb4 La1 Sb3 134.587(17) 5_665 3_556 ?
Sb4 La1 Sb3 79.57(3) 5_655 3_556 ?
Sb3 La1 Sb3 52.48(3) 7_654 3_556 ?
Sb3 La1 Sb3 54.12(4) 5_666 3_556 ?
Sb3 La1 Sb3 80.19(3) 1_554 3_556 ?
Sb2 La1 Co1 100.76(3) 3_556 7_664 ?
Sb2 La1 Co1 44.74(2) 1_554 7_664 ?
Sb4 La1 Co1 44.57(2) 5_665 7_664 ?
Sb4 La1 Co1 102.48(4) 5_655 7_664 ?
Sb3 La1 Co1 125.22(3) 7_654 7_664 ?
Sb3 La1 Co1 124.21(4) 5_666 7_664 ?
Sb3 La1 Co1 96.71(3) 1_554 7_664 ?
Sb3 La1 Co1 176.86(2) 3_556 7_664 ?
Sb2 La1 Co1 44.74(2) 3_556 5_656 ?
Sb2 La1 Co1 100.76(3) 1_554 5_656 ?
Sb4 La1 Co1 102.48(4) 5_665 5_656 ?
Sb4 La1 Co1 44.57(2) 5_655 5_656 ?
Sb3 La1 Co1 124.21(4) 7_654 5_656 ?
Sb3 La1 Co1 125.22(3) 5_666 5_656 ?
Sb3 La1 Co1 176.86(2) 1_554 5_656 ?
Sb3 La1 Co1 96.71(3) 3_556 5_656 ?
Co1 La1 Co1 86.40(4) 7_664 5_656 ?
Sb2 La1 Sb1 68.957(17) 3_556 . ?
Sb2 La1 Sb1 68.957(17) 1_554 . ?
Sb4 La1 Sb1 70.10(2) 5_665 . ?
Sb4 La1 Sb1 70.10(2) 5_655 . ?
Sb3 La1 Sb1 141.369(16) 7_654 . ?
Sb3 La1 Sb1 141.369(16) 5_666 . ?
Sb3 La1 Sb1 139.907(17) 1_554 . ?
Sb3 La1 Sb1 139.907(16) 3_556 . ?
Co1 La1 Sb1 43.20(2) 7_664 . ?
Co1 La1 Sb1 43.20(2) 5_656 . ?
Sb4 La2 Sb4 137.10(3) 6_556 1_556 ?
Sb4 La2 Sb2 83.594(14) 6_556 7_665 ?
Sb4 La2 Sb2 83.594(14) 1_556 7_665 ?
Sb4 La2 Co1 46.51(2) 6_556 6_557 ?
Sb4 La2 Co1 94.46(3) 1_556 6_557 ?
Sb2 La2 Co1 95.41(4) 7_665 6_557 ?
Sb4 La2 Co1 94.46(3) 6_556 . ?
Sb4 La2 Co1 46.51(2) 1_556 . ?
Sb2 La2 Co1 95.41(4) 7_665 . ?
Co1 La2 Co1 48.60(4) 6_557 . ?
Sb4 La2 Sb5 69.555(16) 6_556 7_655 ?
Sb4 La2 Sb5 69.556(16) 1_556 7_655 ?
Sb2 La2 Sb5 55.01(2) 7_665 7_655 ?
Co1 La2 Sb5 46.48(3) 6_557 7_655 ?
Co1 La2 Sb5 46.48(3) . 7_655 ?
Sb4 La2 Sb3 136.18(2) 6_556 . ?
Sb4 La2 Sb3 82.14(2) 1_556 . ?
Sb2 La2 Sb3 82.96(4) 7_665 . ?
Co1 La2 Sb3 176.37(2) 6_557 . ?
Co1 La2 Sb3 128.21(3) . . ?
Sb5 La2 Sb3 130.52(3) 7_655 . ?
Sb4 La2 Sb3 82.14(2) 6_556 6_557 ?
Sb4 La2 Sb3 136.18(2) 1_556 6_557 ?
Sb2 La2 Sb3 82.96(4) 7_665 6_557 ?
Co1 La2 Sb3 128.21(3) 6_557 6_557 ?
Co1 La2 Sb3 176.37(2) . 6_557 ?
Sb5 La2 Sb3 130.52(3) 7_655 6_557 ?
Sb3 La2 Sb3 54.91(3) . 6_557 ?
Sb4 La2 Sb3 133.52(2) 6_556 7_655 ?
Sb4 La2 Sb3 80.33(2) 1_556 7_655 ?
Sb2 La2 Sb3 136.26(2) 7_665 7_655 ?
Co1 La2 Sb3 126.08(4) 6_557 7_655 ?
Co1 La2 Sb3 102.13(3) . 7_655 ?
Sb5 La2 Sb3 146.828(18) 7_655 7_655 ?
Sb3 La2 Sb3 54.75(4) . 7_655 ?
Sb3 La2 Sb3 81.21(3) 6_557 7_655 ?
Sb4 La2 Sb3 80.33(2) 6_556 4_646 ?
Sb4 La2 Sb3 133.52(2) 1_556 4_646 ?
Sb2 La2 Sb3 136.26(2) 7_665 4_646 ?
Co1 La2 Sb3 102.13(3) 6_557 4_646 ?
Co1 La2 Sb3 126.08(4) . 4_646 ?
Sb5 La2 Sb3 146.828(18) 7_655 4_646 ?
Sb3 La2 Sb3 81.21(3) . 4_646 ?
Sb3 La2 Sb3 54.75(4) 6_557 4_646 ?
Sb3 La2 Sb3 54.80(3) 7_655 4_646 ?
Sb4 La2 Sb2 80.696(13) 6_556 7_655 ?
```

```
Sb4 La2 Sb2 80.696(13) 1_556 7_655 ?
Sb2 La2 Sb2 136.00(4) 7_665 7_655 ?
Co1 La2 Sb2 45.77(2) 6_557 7_655 ?
Co1 La2 Sb2 45.77(2) . 7_655 ?
Sb5 La2 Sb2 80.99(3) 7_655 7_655 ?
Sb3 La2 Sb2 134.32(2) . 7_655 ?
Sb3 La2 Sb2 134.32(2) 6_557 7_655 ?
Sb3 La2 Sb2 80.72(4) 7_655 7_655 ?
Sb3 La2 Sb2 80.72(4) 4_646 7_655 ?
Sb4 Co1 Sb2 111.72(5) 1_556 7_655 ?
Sb4 Co1 Sb1 97.89(5) 1_556 5_656 ?
Sb2 Co1 Sb1 95.62(6) 7_655 5_656 ?
Sb4 Co1 Sb5 163.10(5) 1_556 1_445 ?
Sb2 Co1 Sb5 85.17(4) 7_655 1_445 ?
Sb1 Co1 Sb5 79.11(4) 5_656 1_445 ?
Sb4 Co1 Sb5 92.35(5) 1_556 7_655 ?
Sb2 Co1 Sb5 113.10(5) 7_655 7_655 ?
Sb1 Co1 Sb5 143.29(5) 5_656 7_655 ?
Sb5 Co1 Sb5 81.00(4) 1_445 7_655 ?
Sb4 Co1 Sb1 72.02(4) 1_556 1_456 ?
Sb2 Co1 Sb1 168.38(4) 7_655 1_456 ?
Sb1 Co1 Sb1 72.82(5) 5_656 1_456 ?
Sb5 Co1 Sb1 91.30(4) 1_445 1_456 ?
Sb5 Co1 Sb1 77.13(4) 7_655 1_456 ?
Sb4 Co1 Co1 130.27(3) 1_556 6_557 ?
Sb2 Co1 Co1 58.42(3) 7_655 6_557 ?
Sb1 Co1 Co1 130.05(3) 5_656 6_557 ?
Sb5 Co1 Co1 58.56(3) 1_445 6_557 ?
Sb5 Co1 Co1 58.70(3) 7_655 6_557 ?
Sb1 Co1 Co1 128.28(3) 1_456 6_557 ?
Sb4 Co1 La2 65.88(3) 1_556 . ?
Sb2 Co1 La2 68.47(5) 7_655 . ?
Sb1 Co1 La2 148.39(4) 5_656 . ?
Sb5 Co1 La2 124.14(4) 1_445 . ?
Sb5 Co1 La2 67.22(3) 7_655 . ?
Sb1 Co1 La2 122.19(5) 1_456 . ?
Co1 Co1 La2 65.701(19) 6_557 . ?
Sb4 Co1 La1 62.35(4) 1_556 5_656 ?
Sb2 Co1 La1 61.87(3) 7_655 5_656 ?
Sb1 Co1 La1 68.56(3) 5_656 5_656 ?
Sb5 Co1 La1 129.70(5) 1_445 5_656 ?
Sb5 Co1 La1 144.97(4) 7_655 5_656 ?
Sb1 Co1 La1 113.26(4) 1_456 5_656 ?
Co1 Co1 La1 118.307(19) 6_557 5_656 ?
La2 Co1 La1 79.83(3) . 5_656 ?
Co1 Sb1 Co1 136.49(5) 7_664 5_656 ?
Co1 Sb1 Co1 107.18(5) 7_664 3_656 ?
Co1 Sb1 Co1 99.08(5) 5_656 3_656 ?
Co1 Sb1 Co1 99.08(5) 7_664 1_654 ?
Co1 Sb1 Co1 107.18(5) 5_656 1_654 ?
Co1 Sb1 Co1 104.64(5) 3_656 1_654 ?
Co1 Sb1 Sb4 111.75(3) 7_664 1_655 ?
Co1 Sb1 Sb4 111.75(3) 5_656 1_655 ?
Co1 Sb1 Sb4 52.32(3) 3_656 1_655 ?
Co1 Sb1 Sb4 52.32(3) 1_654 1_655 ?
Co1 Sb1 Sb1 55.05(3) 7_664 5_765 ?
Co1 Sb1 Sb1 137.27(3) 5_656 5_765 ?
Co1 Sb1 Sb1 52.12(3) 3_656 5_765 ?
Co1 Sb1 Sb1 110.31(4) 1_654 5_765 ?
Sb4 Sb1 Sb1 77.39(2) 1_655 5_765 ?
Co1 Sb1 Sb1 137.27(3) 7_664 5_755 ?
Co1 Sb1 Sb1 55.05(3) 5_656 5_755 ?
Co1 Sb1 Sb1 110.31(4) 3_656 5_755 ?
Co1 Sb1 Sb1 52.12(3) 1_654 5_755 ?
Sb4 Sb1 Sb1 77.39(2) 1_655 5_755 ?
Sb1 Sb1 Sb1 154.79(5) 5_765 5_755 ?
Co1 Sb1 La1 68.25(3) 7_664 . ?
Co1 Sb1 La1 68.25(3) 5_656 . ?
Co1 Sb1 La1 127.68(3) 3_656 . ?
Co1 Sb1 La1 127.68(3) 1_654 . ?
Sb4 Sb1 La1 180.0 1_655 . ?
Sb1 Sb1 La1 102.61(2) 5_765 . ?
Sb1 Sb1 La1 102.61(2) 5_755 . ?
Co1 Sb2 Co1 63.16(5) 7_665 4_656 ?
Co1 Sb2 Sb5 97.91(5) 7_665 1_545 ?
Co1 Sb2 Sb5 97.91(5) 4_656 1_545 ?
Co1 Sb2 La1 133.75(3) 7_665 6_556 ?
Co1 Sb2 La1 73.38(3) 4_656 6_556 ?
Sb5 Sb2 La1 103.129(17) 1_545 6_556 ?
Co1 Sb2 La1 73.38(3) 7_665 1_556 ?
Co1 Sb2 La1 133.75(3) 4_656 1_556 ?
Sb5 Sb2 La1 103.129(17) 1_545 1_556 ?
La1 Sb2 La1 137.89(3) 6_556 1_556 ?
Co1 Sb2 La2 144.48(3) 7_665 7_655 ?
Co1 Sb2 La2 144.48(3) 4_656 7_655 ?
Sb5 Sb2 La2 63.51(4) 1_545 7_655 ?
La1 Sb2 La2 81.499(14) 6_556 7_655 ?
La1 Sb2 La2 81.499(14) 1_556 7_655 ?
Co1 Sb2 La2 65.76(4) 7_665 7_665 ?
Co1 Sb2 La2 65.76(4) 4_656 7_665 ?
Sb5 Sb2 La2 160.49(3) 1_545 7_665 ?
La1 Sb2 La2 83.043(15) 6_556 7_665 ?
La1 Sb2 La2 83.043(15) 1_556 7_665 ?
La2 Sb2 La2 136.00(4) 7_655 7_665 ?
Sb3 Sb3 Sb3 87.931(19) 5_667 7_655 ?
Sb3 Sb3 Sb3 92.047(19) 5_667 7_665 ?
Sb3 Sb3 Sb3 178.43(4) 7_655 7_665 ?
Sb3 Sb3 Sb3 177.789(19) 5_667 6_557 ?
Sb3 Sb3 Sb3 90.0 7_655 6_557 ?
Sb3 Sb3 Sb3 90.0 7_665 6_557 ?
Sb3 Sb3 La2 115.71(3) 5_667 . ?
Sb3 Sb3 La2 62.73(2) 7_655 . ?
Sb3 Sb3 La2 115.92(3) 7_665 . ?
Sb3 Sb3 La2 62.543(14) 6_557 . ?
Sb3 Sb3 La2 119.17(3) 5_667 7_665 ?
Sb3 Sb3 La2 118.82(3) 7_655 7_665 ?
Sb3 Sb3 La2 62.51(3) 7_665 7_665 ?
Sb3 Sb3 La2 62.602(14) 6_557 7_665 ?
La2 Sb3 La2 125.12(3) . 7_665 ?
Sb3 Sb3 La1 64.04(2) 5_667 5_666 ?
Sb3 Sb3 La1 115.42(3) 7_655 5_666 ?
Sb3 Sb3 La1 63.21(2) 7_665 5_666 ?
Sb3 Sb3 La1 116.287(14) 6_557 5_666 ?
La2 Sb3 La1 78.62(3) . 5_666 ?
La2 Sb3 La1 125.71(4) 7_665 5_666 ?
Sb3 Sb3 La1 63.48(2) 5_667 1_556 ?
Sb3 Sb3 La1 62.67(2) 7_655 1_556 ?
Sb3 Sb3 La1 118.69(3) 7_665 1_556 ?
Sb3 Sb3 La1 116.151(14) 6_557 1_556 ?
La2 Sb3 La1 125.39(4) . 1_556 ?
La2 Sb3 La1 81.32(3) 7_665 1_556 ?
La1 Sb3 La1 127.52(3) 5_666 1_556 ?
Co1 Sb4 Co1 111.33(5) 1_554 3_556 ?
Co1 Sb4 Sb1 55.66(3) 1_554 1_455 ?
Co1 Sb4 Sb1 55.66(3) 3_556 1_455 ?
Co1 Sb4 La2 142.39(3) 1_554 3_556 ?
Co1 Sb4 La2 67.61(3) 3_556 3_556 ?
Sb1 Sb4 La2 111.379(17) 1_455 3_556 ?
Co1 Sb4 La2 67.61(3) 1_554 1_554 ?
Co1 Sb4 La2 142.39(3) 3_556 1_554 ?
Sb1 Sb4 La2 111.379(17) 1_455 1_554 ?
La2 Sb4 La2 137.24(3) 3_556 1_554 ?
Co1 Sb4 La1 132.46(3) 1_554 5_665 ?
Co1 Sb4 La1 73.08(4) 3_556 5_665 ?
Sb1 Sb4 La1 109.90(2) 1_455 5_665 ?
La2 Sb4 La1 84.461(15) 3_556 5_665 ?
La2 Sb4 La1 81.275(14) 1_554 5_665 ?
Co1 Sb4 La1 73.08(4) 1_554 5_655 ?
Co1 Sb4 La1 132.46(3) 3_556 5_655 ?
Sb1 Sb4 La1 109.90(2) 1_455 5_655 ?
La2 Sb4 La1 81.275(14) 3_556 5_655 ?
La2 Sb4 La1 84.461(15) 1_554 5_655 ?
```

```
La1 Sb4 La1 140.19(4) 5_665 5_655 ?
Co1 Sb5 Co1 62.89(5) 1_665 6_667 ?
Co1 Sb5 Co1 137.64(4) 1_665 4_656 ?
Co1 Sb5 Co1 101.35(4) 6_667 4_656 ?
Co1 Sb5 Co1 101.35(4) 1_665 7_665 ?
Co1 Sb5 Co1 137.64(4) 6_667 7_665 ?
Co1 Sb5 Co1 62.60(6) 4_656 7_665 ?
Co1 Sb5 Sb2 104.16(4) 1_665 1_565 ?
Co1 Sb5 Sb2 104.16(4) 6_667 1_565 ?
Co1 Sb5 Sb2 118.06(4) 4_656 1_565 ?
Co1 Sb5 Sb2 118.06(4) 7_665 1_565 ?
Co1 Sb5 La2 146.61(3) 1_665 7_665 ?
Co1 Sb5 La2 146.61(3) 6_667 7_665 ?
Co1 Sb5 La2 66.29(3) 4_656 7_665 ?
Co1 Sb5 La2 66.29(3) 7_665 7_665 ?
Sb2 Sb5 La2 61.48(4) 1_565 7_665 ?

_diffrn_measured_fraction_theta_max    0.997
_diffrn_reflns_theta_full              30.00
_diffrn_measured_fraction_theta_full   0.997
_refine_diff_density_max    4.826
_refine_diff_density_min   -1.299
_refine_diff_density_rms    0.361

#===END
```

A1.2 $PrCo(Sb, Sn)_3$

```
data_shelxl

_audit_creation_method            SHELXL-97
_chemical_name_systematic
;
 ?
;
_chemical_name_common             ?
_chemical_melting_point           ?
_chemical_formula_moiety          'Co Pr
Sb3'
_chemical_formula_sum
 'Co Pr Sb3'
_chemical_formula_weight          565.09

loop_
 _atom_type_symbol
 _atom_type_description
 _atom_type_scat_dispersion_real
 _atom_type_scat_dispersion_imag
 _atom_type_scat_source
 'Pr'  'Pr'  -0.2180   2.8214
 'International Tables Vol C Tables 4.2.6.8
and 6.1.1.4'
 'Co'  'Co'   0.3494   0.9721
 'International Tables Vol C Tables 4.2.6.8
and 6.1.1.4'
 'Sb'  'Sb'  -0.5866   1.5461
 'International Tables Vol C Tables 4.2.6.8
and 6.1.1.4'

_symmetry_cell_setting
'Orthorhombic'
_symmetry_space_group_name_H-M    'P b c m
'

loop_
 _symmetry_equiv_pos_as_xyz
 'x, y, z'
 '-x, -y, z+1/2'
 'x, -y+1/2, -z'
 '-x, y+1/2, -z+1/2'
 '-x, -y, -z'
 'x, y, -z-1/2'
 '-x, y-1/2, z'
 'x, -y-1/2, z-1/2'

_cell_length_a
12.77600(10)
_cell_length_b                    6.1220(2)
_cell_length_c                    12.0820(3)
_cell_angle_alpha                 90
_cell_angle_beta                  90
_cell_angle_gamma                 90
_cell_volume                      944.99(4)
_cell_formula_units_Z             8
_cell_measurement_temperature     298(5)
_cell_measurement_reflns_used     1686
_cell_measurement_theta_min       2.546
_cell_measurement_theta_max       30.508

_exptl_crystal_description        prism
_exptl_crystal_colour             black
_exptl_crystal_size_max           0.13
_exptl_crystal_size_mid           0.05
_exptl_crystal_size_min           0.05
_exptl_crystal_density_meas       ?
_exptl_crystal_density_diffrn     7.944
_exptl_crystal_density_method     'not
measured'
_exptl_crystal_F_000              1912
_exptl_absorpt_coefficient_mu     30.282
_exptl_absorpt_correction_type    'sphere'
_exptl_absorpt_correction_T_min   0.1160
_exptl_absorpt_correction_T_max   0.3128
_exptl_absorpt_process_details    'HKL
Scalepack (Otwinowski & Minor 1997)'

_exptl_special_details
;
 ?
;

_diffrn_ambient_temperature       298(5)
_diffrn_radiation_wavelength      0.71073
_diffrn_radiation_type            MoK\a
_diffrn_radiation_source          'fine-
focus sealed tube'
_diffrn_radiation_monochromator   graphite
_diffrn_measurement_device_type   'Nonius
KappaCCD'
_diffrn_measurement_method        '\w and \f
scans'
_diffrn_detector_area_resol_mean  ?
_diffrn_standards_number          ?
_diffrn_standards_interval_count  ?
_diffrn_standards_interval_time   ?
_diffrn_standards_decay_%         ?
_diffrn_reflns_number             19199
_diffrn_reflns_av_R_equivalents   0.0292
_diffrn_reflns_av_sigmaI/netI     0.0289
_diffrn_reflns_limit_h_min        -18
_diffrn_reflns_limit_h_max        18
_diffrn_reflns_limit_k_min        -8
_diffrn_reflns_limit_k_max        8
_diffrn_reflns_limit_l_min        -17
_diffrn_reflns_limit_l_max        17
_diffrn_reflns_theta_min          3.19
_diffrn_reflns_theta_max          30.50
_reflns_number_total              1506
_reflns_number_gt                 1464
_reflns_threshold_expression      I>2\s(I)

_computing_data_collection        ?
```

```
_computing_cell_refinement        ?
_computing_data_reduction         ?
_computing_structure_solution     ?
_computing_structure_refinement   'SHELXL-97
(Sheldrick, 2008)'
_computing_molecular_graphics     ?
_computing_publication_material   ?

_refine_special_details
;
 Refinement of F^2^ against ALL reflections.
The weighted R-factor wR and
 goodness of fit S are based on F^2^,
conventional R-factors R are based
 on F, with F set to zero for negative F^2^.
The threshold expression of
 F^2^ > 2\s(F^2^) is used only for
calculating R-factors(gt) etc. and is
 not relevant to the choice of reflections
for refinement.  R-factors based
 on F^2^ are statistically about twice as
large as those based on F, and R-
 factors based on ALL data will be even
larger.
;

_refine_ls_structure_factor_coef  Fsqd
_refine_ls_matrix_type            full
_refine_ls_weighting_scheme       calc
_refine_ls_weighting_details
 'calc
w=1/[\s^2^(Fo^2^)+(0.0617P)^2^+12.9378P]
where P=(Fo^2^+2Fc^2^)/3'
_atom_sites_solution_primary      direct
_atom_sites_solution_secondary    difmap
_atom_sites_solution_hydrogens    ?
_refine_ls_hydrogen_treatment     ?
_refine_ls_extinction_method      SHELXL
_refine_ls_extinction_coef
0.00219(15)
_refine_ls_extinction_expression
 'Fc^*^=kFc[1+0.001xFc^2^\l^3^/sin(2\q)]^-
1/4^'
_refine_ls_number_reflns          1506
_refine_ls_number_parameters      53
_refine_ls_number_restraints      0
_refine_ls_R_factor_all           0.0399
_refine_ls_R_factor_gt            0.0390
_refine_ls_wR_factor_ref          0.1142
_refine_ls_wR_factor_gt           0.1134
_refine_ls_goodness_of_fit_ref    1.219
_refine_ls_restrained_S_all       1.219
_refine_ls_shift/su_max           0.001
_refine_ls_shift/su_mean          0.000

loop_
 _atom_site_label
 _atom_site_type_symbol
 _atom_site_fract_x
 _atom_site_fract_y
 _atom_site_fract_z
 _atom_site_U_iso_or_equiv
 _atom_site_adp_type
 _atom_site_occupancy
 _atom_site_symmetry_multiplicity
 _atom_site_calc_flag
 _atom_site_refinement_flags
 _atom_site_disorder_assembly
 _atom_site_disorder_group
Pr1 Pr 0.70033(5) 0.2500 0.0000 0.00779(18)
Uani 1 2 d S . .
Pr2 Pr 0.30534(4) 0.26643(8) 0.7500
0.00747(17) Uani 1 2 d S . .
Co1 Co 0.10358(7) 0.03298(15) 0.86208(7)
0.0084(2) Uani 1 1 d . . .
Sb1 Sb 0.97320(5) 0.2500 0.0000 0.00948(19)
Uani 1 2 d S . .
Sb2 Sb 0.78572(5) 0.25502(9) 0.7500
0.00813(19) Uani 1 2 d S . .
Sb3 Sb 0.50186(3) 0.50868(7) 0.87665(3)
0.00894(18) Uani 1 1 d . . .
Sb4 Sb 0.21827(6) 0.2500 0.0000 0.00816(19)
Uani 1 2 d S . .
Sb5 Sb 0.94433(5) 0.88443(10) 0.7500
0.00938(19) Uani 1 2 d S . .

loop_
 _atom_site_aniso_label
 _atom_site_aniso_U_11
 _atom_site_aniso_U_22
 _atom_site_aniso_U_33
 _atom_site_aniso_U_23
 _atom_site_aniso_U_13
 _atom_site_aniso_U_12
Pr1 0.0072(3) 0.0077(3) 0.0084(3) -
0.00013(15) 0.000 0.000
Pr2 0.0061(3) 0.0083(3) 0.0080(3) 0.000
0.000 0.00010(15)
Co1 0.0088(4) 0.0080(4) 0.0085(4) -0.0006(3)
-0.0004(3) -0.0002(3)
Sb1 0.0092(3) 0.0092(3) 0.0101(3)
0.00089(19) 0.000 0.000
Sb2 0.0082(4) 0.0080(3) 0.0082(3) 0.000
0.000 -0.00098(18)
Sb3 0.0081(3) 0.0095(3) 0.0092(3) -
0.00002(13) -0.00007(13) -0.00043(13)
Sb4 0.0087(4) 0.0078(3) 0.0080(3) -
0.00081(18) 0.000 0.000
Sb5 0.0073(3) 0.0092(3) 0.0117(3) 0.000
0.000 -0.0014(2)

_geom_special_details
;
 All s.u.'s (except the s.u. in the dihedral
angle between two l.s. planes)
 are estimated using the full covariance
matrix.  The cell s.u.'s are taken
 into account individually in the estimation
of s.u.'s in distances, angles
 and torsion angles; correlations between
s.u.'s in cell parameters are only
 used when they are defined by crystal
symmetry.  An approximate (isotropic)
 treatment of cell s.u.'s is used for
estimating s.u.'s involving l.s. planes.
;

loop_
 _geom_bond_atom_site_label_1
 _geom_bond_atom_site_label_2
 _geom_bond_distance
 _geom_bond_site_symmetry_2
 _geom_bond_publ_flag
Pr1 Sb2 3.2116(3) 3_556 ?
Pr1 Sb2 3.2116(3) 1_554 ?
Pr1 Sb4 3.2329(3) 5_665 ?
Pr1 Sb4 3.2329(3) 5_655 ?
Pr1 Sb3 3.3281(6) 7_654 ?
Pr1 Sb3 3.3281(6) 5_666 ?
Pr1 Sb3 3.3404(6) 3_556 ?
Pr1 Sb3 3.3404(6) 1_554 ?
Pr1 Co1 3.4720(10) 5_656 ?
```

```
Pr1 Co1 3.4720(10) 7_664 ?
Pr1 Sb1 3.4862(9) . ?
Pr2 Sb2 3.2094(8) 7_665 ?
Pr2 Sb4 3.2204(3) 6_556 ?
Pr2 Sb4 3.2204(3) 1_556 ?
Pr2 Co1 3.2436(10) 6_557 ?
Pr2 Co1 3.2436(10) . ?
Pr2 Sb5 3.2707(8) 7_655 ?
Pr2 Sb3 3.2931(6) . ?
Pr2 Sb3 3.2931(6) 6_557 ?
Pr2 Sb3 3.3013(6) 7_655 ?
Pr2 Sb3 3.3013(6) 4_646 ?
Pr2 Sb2 3.3400(8) 7_655 ?
Co1 Sb4 2.5863(10) 1_556 ?
Co1 Sb2 2.5942(10) 7_655 ?
Co1 Sb1 2.5962(10) 5_656 ?
Co1 Sb5 2.6077(10) 1_445 ?
Co1 Sb5 2.6149(11) 7_655 ?
Co1 Sb1 2.7049(10) 1_456 ?
Co1 Co1 2.7083(18) 6_557 ?
Co1 Pr1 3.4720(10) 5_656 ?
Sb1 Co1 2.5962(10) 5_656 ?
Sb1 Co1 2.5962(10) 7_664 ?
Sb1 Co1 2.7049(10) 3_656 ?
Sb1 Co1 2.7049(10) 1_654 ?
Sb1 Sb4 3.1310(10) 1_655 ?
Sb1 Sb1 3.1367(3) 5_765 ?
Sb1 Sb1 3.1367(3) 5_755 ?
Sb1 Sb5 3.3031(3) 5_766 ?
Sb1 Sb5 3.3031(3) 7_754 ?
Sb2 Co1 2.5942(10) 7_665 ?
Sb2 Co1 2.5942(10) 4_656 ?
Sb2 Sb5 3.0419(9) 1_545 ?
Sb2 Pr2 3.2094(8) 7_655 ?
Sb2 Pr1 3.2116(3) 6_556 ?
Sb2 Pr1 3.2116(3) 1_556 ?
Sb2 Pr2 3.3400(8) 7_665 ?
Sb3 Sb3 2.9829(8) 5_667 ?
Sb3 Sb3 3.0604(8) 6_557 ?
Sb3 Sb3 3.06137(10) 7_655 ?
Sb3 Sb3 3.06137(11) 7_665 ?
Sb3 Pr2 3.3013(6) 7_665 ?
Sb3 Pr1 3.3281(6) 5_666 ?
Sb3 Pr1 3.3404(6) 1_556 ?
Sb4 Co1 2.5863(10) 1_554 ?
Sb4 Co1 2.5863(10) 3_556 ?
Sb4 Sb1 3.1310(10) 1_455 ?
Sb4 Pr2 3.2204(3) 3_556 ?
Sb4 Pr2 3.2204(3) 1_554 ?
Sb4 Pr1 3.2329(3) 5_665 ?
Sb4 Pr1 3.2329(3) 5_655 ?
Sb5 Co1 2.6077(10) 1_665 ?
Sb5 Co1 2.6077(10) 6_667 ?
Sb5 Co1 2.6149(11) 4_656 ?
Sb5 Co1 2.6149(11) 7_665 ?
Sb5 Sb2 3.0419(9) 1_565 ?
Sb5 Pr2 3.2707(8) 7_665 ?
Sb5 Sb1 3.3031(3) 5_766 ?
Sb5 Sb1 3.3031(3) 2_765 ?

loop_
 _geom_angle_atom_site_label_1
 _geom_angle_atom_site_label_2
 _geom_angle_atom_site_label_3
 _geom_angle
 _geom_angle_site_symmetry_1
 _geom_angle_site_symmetry_3
 _geom_angle_publ_flag
Sb2 Pr1 Sb2 140.28(3) 3_556 1_554 ?
Sb2 Pr1 Sb4 84.247(13) 3_556 5_665 ?
Sb2 Pr1 Sb4 83.204(13) 1_554 5_665 ?
Sb2 Pr1 Sb4 83.204(13) 3_556 5_655 ?
Sb2 Pr1 Sb4 84.247(13) 1_554 5_655 ?
Sb4 Pr1 Sb4 142.47(3) 5_665 5_655 ?
Sb2 Pr1 Sb3 132.888(16) 3_556 7_654 ?
Sb2 Pr1 Sb3 81.186(14) 1_554 7_654 ?
Sb4 Pr1 Sb3 132.067(16) 5_665 7_654 ?
Sb4 Pr1 Sb3 80.177(13) 5_655 7_654 ?
Sb2 Pr1 Sb3 81.186(14) 3_556 5_666 ?
Sb2 Pr1 Sb3 132.888(16) 1_554 5_666 ?
Sb4 Pr1 Sb3 80.177(13) 5_665 5_666 ?
Sb4 Pr1 Sb3 132.067(16) 5_655 5_666 ?
Sb3 Pr1 Sb3 78.18(2) 7_654 5_666 ?
Sb2 Pr1 Sb3 80.430(14) 3_556 3_556 ?
Sb2 Pr1 Sb3 132.999(16) 1_554 3_556 ?
Sb4 Pr1 Sb3 133.875(15) 5_665 3_556 ?
Sb4 Pr1 Sb3 78.189(14) 5_655 3_556 ?
Sb3 Pr1 Sb3 53.142(15) 7_654 3_556 ?
Sb3 Pr1 Sb3 54.655(9) 5_666 3_556 ?
Sb2 Pr1 Sb3 132.999(16) 3_556 1_554 ?
Sb2 Pr1 Sb3 80.430(14) 1_554 1_554 ?
Sb4 Pr1 Sb3 78.189(14) 5_665 1_554 ?
Sb4 Pr1 Sb3 133.875(15) 5_655 1_554 ?
Sb3 Pr1 Sb3 54.655(9) 7_654 1_554 ?
Sb3 Pr1 Sb3 53.142(15) 5_666 1_554 ?
Sb3 Pr1 Sb3 81.235(19) 3_556 1_554 ?
Sb2 Pr1 Co1 45.471(18) 3_556 5_656 ?
Sb2 Pr1 Co1 102.18(2) 1_554 5_656 ?
Sb4 Pr1 Co1 103.90(2) 5_665 5_656 ?
Sb4 Pr1 Co1 45.204(18) 5_655 5_656 ?
Sb3 Pr1 Co1 123.607(17) 7_654 5_656 ?
Sb3 Pr1 Co1 124.517(16) 5_666 5_656 ?
Sb3 Pr1 Co1 95.570(17) 3_556 5_656 ?
Sb3 Pr1 Co1 176.78(2) 1_554 5_656 ?
Sb2 Pr1 Co1 102.18(2) 3_556 7_664 ?
Sb2 Pr1 Co1 45.471(18) 1_554 7_664 ?
Sb4 Pr1 Co1 45.204(18) 5_665 7_664 ?
Sb4 Pr1 Co1 103.90(2) 5_655 7_664 ?
Sb3 Pr1 Co1 124.517(16) 7_654 7_664 ?
Sb3 Pr1 Co1 123.607(17) 5_666 7_664 ?
Sb3 Pr1 Co1 176.78(2) 3_556 7_664 ?
Sb3 Pr1 Co1 95.570(17) 1_554 7_664 ?
Co1 Pr1 Co1 87.63(3) 5_656 7_664 ?
Sb2 Pr1 Sb1 70.141(15) 3_556 . ?
Sb2 Pr1 Sb1 70.141(15) 1_554 . ?
Sb4 Pr1 Sb1 71.234(15) 5_665 . ?
Sb4 Pr1 Sb1 71.234(15) 5_655 . ?
Sb3 Pr1 Sb1 140.911(10) 7_654 . ?
Sb3 Pr1 Sb1 140.911(10) 5_666 . ?
Sb3 Pr1 Sb1 139.383(10) 3_556 . ?
Sb3 Pr1 Sb1 139.383(10) 1_554 . ?
Co1 Pr1 Sb1 43.814(16) 5_656 . ?
Co1 Pr1 Sb1 43.814(16) 7_664 . ?
Sb2 Pr2 Sb4 84.484(12) 7_665 6_556 ?
Sb2 Pr2 Sb4 84.484(12) 7_665 1_556 ?
Sb4 Pr2 Sb4 139.41(3) 6_556 1_556 ?
Sb2 Pr2 Co1 97.04(2) 7_665 6_557 ?
Sb4 Pr2 Co1 47.168(19) 6_556 6_557 ?
Sb4 Pr2 Co1 95.93(2) 1_556 6_557 ?
Sb2 Pr2 Co1 97.04(2) 7_665 . ?
Sb4 Pr2 Co1 95.93(2) 6_556 . ?
Sb4 Pr2 Co1 47.168(19) 1_556 . ?
Co1 Pr2 Co1 49.35(3) 6_557 . ?
Sb2 Pr2 Sb5 55.985(19) 7_665 7_655 ?
Sb4 Pr2 Sb5 70.731(15) 6_556 7_655 ?
Sb4 Pr2 Sb5 70.731(15) 1_556 7_655 ?
Co1 Pr2 Sb5 47.33(2) 6_557 7_655 ?
Co1 Pr2 Sb5 47.33(2) . 7_655 ?
Sb2 Pr2 Sb3 81.758(17) 7_665 . ?
Sb4 Pr2 Sb3 135.500(18) 6_556 . ?
Sb4 Pr2 Sb3 80.886(13) 1_556 . ?
Co1 Pr2 Sb3 176.68(2) 6_557 . ?
```

```
Co1 Pr2 Sb3 127.614(17) . . ?
Sb5 Pr2 Sb3 130.098(17) 7_655 . ?
Sb2 Pr2 Sb3 81.758(17) 7_665 6_557 ?
Sb4 Pr2 Sb3 80.886(13) 6_556 6_557 ?
Sb4 Pr2 Sb3 135.500(18) 1_556 6_557 ?
Co1 Pr2 Sb3 127.614(17) 6_557 6_557 ?
Co1 Pr2 Sb3 176.68(2) . 6_557 ?
Sb5 Pr2 Sb3 130.098(17) 7_655 6_557 ?
Sb3 Pr2 Sb3 55.377(17) . 6_557 ?
Sb2 Pr2 Sb3 135.719(17) 7_665 7_655 ?
Sb4 Pr2 Sb3 132.653(17) 6_556 7_655 ?
Sb4 Pr2 Sb3 78.935(14) 1_556 7_655 ?
Co1 Pr2 Sb3 125.16(2) 6_557 7_655 ?
Co1 Pr2 Sb3 100.89(2) . 7_655 ?
Sb5 Pr2 Sb3 146.437(14) 7_655 7_655 ?
Sb3 Pr2 Sb3 55.321(9) . 7_655 ?
Sb3 Pr2 Sb3 82.055(15) 6_557 7_655 ?
Sb2 Pr2 Sb3 135.719(17) 7_665 4_646 ?
Sb4 Pr2 Sb3 78.935(14) 6_556 4_646 ?
Sb4 Pr2 Sb3 132.653(17) 1_556 4_646 ?
Co1 Pr2 Sb3 100.89(2) 6_557 4_646 ?
Co1 Pr2 Sb3 125.16(2) . 4_646 ?
Sb5 Pr2 Sb3 146.436(14) 7_655 4_646 ?
Sb3 Pr2 Sb3 82.055(15) . 4_646 ?
Sb3 Pr2 Sb3 55.321(9) 6_557 4_646 ?
Sb3 Pr2 Sb3 55.228(17) 7_655 4_646 ?
Sb2 Pr2 Sb2 138.36(3) 7_665 7_655 ?
Sb4 Pr2 Sb2 81.396(11) 6_556 7_655 ?
Sb4 Pr2 Sb2 81.396(11) 1_556 7_655 ?
Co1 Pr2 Sb2 46.38(2) 6_557 7_655 ?
Co1 Pr2 Sb2 46.38(2) . 7_655 ?
Sb5 Pr2 Sb2 82.38(2) 7_655 7_655 ?
Sb3 Pr2 Sb2 133.451(17) . 7_655 ?
Sb3 Pr2 Sb2 133.451(17) 6_557 7_655 ?
Sb3 Pr2 Sb2 79.157(16) 7_655 7_655 ?
Sb3 Pr2 Sb2 79.157(16) 4_646 7_655 ?
Sb4 Co1 Sb2 111.37(4) 1_556 7_655 ?
Sb4 Co1 Sb1 98.24(3) 1_556 5_656 ?
Sb2 Co1 Sb1 95.93(3) 7_655 5_656 ?
Sb4 Co1 Sb5 162.90(4) 1_556 1_445 ?
Sb2 Co1 Sb5 85.73(3) 7_655 1_445 ?
Sb1 Co1 Sb5 78.80(3) 5_656 1_445 ?
Sb4 Co1 Sb5 92.50(3) 1_556 7_655 ?
Sb2 Co1 Sb5 113.39(4) 7_655 7_655 ?
Sb1 Co1 Sb5 142.47(4) 5_656 7_655 ?
Sb5 Co1 Sb5 80.53(3) 1_445 7_655 ?
Sb4 Co1 Sb1 72.52(3) 1_556 1_456 ?
Sb2 Co1 Sb1 168.38(4) 7_655 1_456 ?
Sb1 Co1 Sb1 72.52(2) 5_656 1_456 ?
Sb5 Co1 Sb1 90.62(3) 1_445 1_456 ?
Sb5 Co1 Sb1 76.75(3) 7_655 1_456 ?
Sb4 Co1 Co1 130.11(2) 1_556 6_557 ?
Sb2 Co1 Co1 58.53(2) 7_655 6_557 ?
Sb1 Co1 Co1 129.93(2) 5_656 6_557 ?
Sb5 Co1 Co1 58.71(2) 1_445 6_557 ?
Sb5 Co1 Co1 58.81(2) 7_655 6_557 ?
Sb1 Co1 Co1 128.03(2) 1_456 6_557 ?
Sb4 Co1 Pr2 65.94(2) 1_556 . ?
Sb2 Co1 Pr2 68.77(3) 7_655 . ?
Sb1 Co1 Pr2 149.57(4) 5_656 . ?
Sb5 Co1 Pr2 123.84(3) 1_445 . ?
Sb5 Co1 Pr2 66.88(3) 7_655 . ?
Sb1 Co1 Pr2 122.02(3) 1_456 . ?
Co1 Co1 Pr2 65.324(16) 6_557 . ?
Sb4 Co1 Pr1 62.50(2) 1_556 5_656 ?
Sb2 Co1 Pr1 61.95(2) 7_655 5_656 ?
Sb1 Co1 Pr1 68.38(3) 5_656 5_656 ?
Sb5 Co1 Pr1 129.66(4) 1_445 5_656 ?
Sb5 Co1 Pr1 145.89(4) 7_655 5_656 ?
Sb1 Co1 Pr1 113.19(3) 1_456 5_656 ?
Co1 Co1 Pr1 118.681(15) 6_557 5_656 ?
Pr2 Co1 Pr1 81.18(2) . 5_656 ?
Co1 Sb1 Co1 135.60(5) 5_656 7_664 ?
Co1 Sb1 Co1 99.50(3) 5_656 3_656 ?
Co1 Sb1 Co1 107.48(2) 7_664 3_656 ?
Co1 Sb1 Co1 107.48(2) 5_656 1_654 ?
Co1 Sb1 Co1 99.50(3) 7_664 1_654 ?
Co1 Sb1 Co1 103.98(5) 3_656 1_654 ?
Co1 Sb1 Sb4 112.20(2) 5_656 1_655 ?
Co1 Sb1 Sb4 112.20(2) 7_664 1_655 ?
Co1 Sb1 Sb4 51.99(2) 3_656 1_655 ?
Co1 Sb1 Sb4 51.99(2) 1_654 1_655 ?
Co1 Sb1 Sb1 137.20(2) 5_656 5_765 ?
Co1 Sb1 Sb1 55.34(2) 7_664 5_765 ?
Co1 Sb1 Sb1 52.14(2) 3_656 5_765 ?
Co1 Sb1 Sb1 110.18(3) 1_654 5_765 ?
Sb4 Sb1 Sb1 77.39(2) 1_655 5_765 ?
Co1 Sb1 Sb1 55.34(2) 5_656 5_755 ?
Co1 Sb1 Sb1 137.20(2) 7_664 5_755 ?
Co1 Sb1 Sb1 110.18(3) 3_656 5_755 ?
Co1 Sb1 Sb1 52.14(2) 1_654 5_755 ?
Sb4 Sb1 Sb1 77.39(2) 1_655 5_755 ?
Sb1 Sb1 Sb1 154.78(5) 5_765 5_755 ?
Co1 Sb1 Sb5 50.75(2) 5_656 5_766 ?
Co1 Sb1 Sb5 150.89(2) 7_664 5_766 ?
Co1 Sb1 Sb5 50.40(2) 3_656 5_766 ?
Co1 Sb1 Sb5 104.15(3) 1_654 5_766 ?
Sb4 Sb1 Sb5 71.400(15) 1_655 5_766 ?
Sb1 Sb1 Sb5 99.992(16) 5_765 5_766 ?
Sb1 Sb1 Sb5 71.773(13) 5_755 5_766 ?
Co1 Sb1 Sb5 150.89(2) 5_656 7_754 ?
Co1 Sb1 Sb5 50.75(2) 7_664 7_754 ?
Co1 Sb1 Sb5 104.15(3) 3_656 7_754 ?
Co1 Sb1 Sb5 50.40(2) 1_654 7_754 ?
Sb4 Sb1 Sb5 71.400(15) 1_655 7_754 ?
Sb1 Sb1 Sb5 71.773(13) 5_765 7_754 ?
Sb1 Sb1 Sb5 99.992(16) 5_755 7_754 ?
Sb5 Sb1 Sb5 142.80(3) 5_766 7_754 ?
Co1 Sb1 Pr1 67.80(2) 5_656 . ?
Co1 Sb1 Pr1 67.80(2) 7_664 . ?
Co1 Sb1 Pr1 128.01(2) 3_656 . ?
Co1 Sb1 Pr1 128.01(2) 1_654 . ?
Sb4 Sb1 Pr1 180.0 1_655 . ?
Sb1 Sb1 Pr1 102.61(2) 5_765 . ?
Sb1 Sb1 Pr1 102.61(2) 5_755 . ?
Sb5 Sb1 Pr1 108.600(15) 5_766 . ?
Sb5 Sb1 Pr1 108.600(15) 7_754 . ?
Co1 Sb2 Co1 62.93(4) 7_665 4_656 ?
Co1 Sb2 Sb5 97.24(3) 7_665 1_545 ?
Co1 Sb2 Sb5 97.24(3) 4_656 1_545 ?
Co1 Sb2 Pr2 144.00(2) 7_665 7_655 ?
Co1 Sb2 Pr2 144.00(2) 4_656 7_655 ?
Sb5 Sb2 Pr2 63.026(18) 1_545 7_655 ?
Co1 Sb2 Pr1 133.03(3) 7_665 6_556 ?
Co1 Sb2 Pr1 72.58(2) 4_656 6_556 ?
Sb5 Sb2 Pr1 102.660(13) 1_545 6_556 ?
Pr2 Sb2 Pr1 82.412(12) 7_655 6_556 ?
Co1 Sb2 Pr1 72.58(2) 7_665 1_556 ?
Co1 Sb2 Pr1 133.03(3) 4_656 1_556 ?
Sb5 Sb2 Pr1 102.660(13) 1_545 1_556 ?
Pr2 Sb2 Pr1 82.412(12) 7_655 1_556 ?
Pr1 Sb2 Pr1 140.27(3) 6_556 1_556 ?
Co1 Sb2 Pr2 64.85(2) 7_665 7_665 ?
Co1 Sb2 Pr2 64.85(2) 4_656 7_665 ?
Sb5 Sb2 Pr2 158.61(3) 1_545 7_665 ?
Pr2 Sb2 Pr2 138.36(3) 7_655 7_665 ?
Pr1 Sb2 Pr2 83.721(12) 6_556 7_665 ?
Pr1 Sb2 Pr2 83.721(12) 1_556 7_665 ?
Sb3 Sb3 Sb3 177.762(17) 5_667 6_557 ?
Sb3 Sb3 Sb3 87.943(17) 5_667 7_655 ?
Sb3 Sb3 Sb3 90.0 6_557 7_655 ?
Sb3 Sb3 Sb3 92.029(17) 5_667 7_665 ?
```

```
Sb3 Sb3 Sb3 90.0 6_557 7_665 ?
Sb3 Sb3 Sb3 178.22(3) 7_655 7_665 ?
Sb3 Sb3 Pr2 115.86(2) 5_667 . ?
Sb3 Sb3 Pr2 62.311(8) 6_557 . ?
Sb3 Sb3 Pr2 62.475(15) 7_655 . ?
Sb3 Sb3 Pr2 116.007(19) 7_665 . ?
Sb3 Sb3 Pr2 119.48(2) 5_667 7_665 ?
Sb3 Sb3 Pr2 62.386(8) 6_557 7_665 ?
Sb3 Sb3 Pr2 119.306(19) 7_655 7_665 ?
Sb3 Sb3 Pr2 62.204(15) 7_665 7_665 ?
Pr2 Sb3 Pr2 124.661(15) . 7_665 ?
Sb3 Sb3 Pr1 63.641(15) 5_667 5_666 ?
Sb3 Sb3 Pr1 116.602(8) 6_557 5_666 ?
Sb3 Sb3 Pr1 115.582(18) 7_655 5_666 ?
Sb3 Sb3 Pr1 62.878(13) 7_665 5_666 ?
Pr2 Sb3 Pr1 79.411(15) . 5_666 ?
Pr2 Sb3 Pr1 125.065(16) 7_665 5_666 ?
Sb3 Sb3 Pr1 63.217(15) 5_667 1_556 ?
Sb3 Sb3 Pr1 116.496(8) 6_557 1_556 ?
Sb3 Sb3 Pr1 62.467(13) 7_655 1_556 ?
Sb3 Sb3 Pr1 119.066(18) 7_665 1_556 ?
Pr2 Sb3 Pr1 124.926(15) . 1_556 ?
Pr2 Sb3 Pr1 82.358(15) 7_665 1_556 ?
Pr1 Sb3 Pr1 126.858(15) 5_666 1_556 ?
Co1 Sb4 Co1 110.98(5) 1_554 3_556 ?
Co1 Sb4 Sb1 55.49(2) 1_554 1_455 ?
Co1 Sb4 Sb1 55.49(2) 3_556 1_455 ?
Co1 Sb4 Pr2 141.63(2) 1_554 3_556 ?
Co1 Sb4 Pr2 66.89(2) 3_556 3_556 ?
Sb1 Sb4 Pr2 110.209(15) 1_455 3_556 ?
Co1 Sb4 Pr2 66.89(2) 1_554 1_554 ?
Co1 Sb4 Pr2 141.63(2) 3_556 1_554 ?
Sb1 Sb4 Pr2 110.209(15) 1_455 1_554 ?
Pr2 Sb4 Pr2 139.58(3) 3_556 1_554 ?
Co1 Sb4 Pr1 131.96(2) 1_554 5_665 ?
Co1 Sb4 Pr1 72.29(2) 3_556 5_665 ?
Sb1 Sb4 Pr1 108.766(15) 1_455 5_665 ?
Pr2 Sb4 Pr1 85.321(13) 3_556 5_665 ?
Pr2 Sb4 Pr1 81.912(12) 1_554 5_665 ?
Co1 Sb4 Pr1 72.29(2) 1_554 5_655 ?
Co1 Sb4 Pr1 131.96(2) 3_556 5_655 ?
Sb1 Sb4 Pr1 108.766(15) 1_455 5_655 ?
Pr2 Sb4 Pr1 81.912(12) 3_556 5_655 ?
Pr2 Sb4 Pr1 85.322(13) 1_554 5_655 ?
Pr1 Sb4 Pr1 142.47(3) 5_665 5_655 ?
Co1 Sb5 Co1 62.57(4) 1_665 6_667 ?
Co1 Sb5 Co1 137.60(4) 1_665 4_656 ?
Co1 Sb5 Co1 101.58(3) 6_667 4_656 ?
Co1 Sb5 Co1 101.58(3) 1_665 7_665 ?
Co1 Sb5 Co1 137.60(4) 6_667 7_665 ?
Co1 Sb5 Co1 62.38(4) 4_656 7_665 ?
Co1 Sb5 Sb2 105.05(3) 1_665 1_565 ?
Co1 Sb5 Sb2 105.05(3) 6_667 1_565 ?
Co1 Sb5 Sb2 117.24(3) 4_656 1_565 ?
Co1 Sb5 Sb2 117.24(3) 7_665 1_565 ?
Co1 Sb5 Pr2 146.92(2) 1_665 7_665 ?
Co1 Sb5 Pr2 146.92(2) 6_667 7_665 ?
Co1 Sb5 Pr2 65.79(2) 4_656 7_665 ?
Co1 Sb5 Pr2 65.79(2) 7_665 7_665 ?
Sb2 Sb5 Pr2 60.990(19) 1_565 7_665 ?
Co1 Sb5 Sb1 50.44(2) 1_665 5_766 ?
Co1 Sb5 Sb1 108.23(3) 6_667 5_766 ?
Co1 Sb5 Sb1 110.07(3) 4_656 5_766 ?
Co1 Sb5 Sb1 52.85(2) 7_665 5_766 ?
Sb2 Sb5 Sb1 113.472(12) 1_565 5_766 ?
Pr2 Sb5 Sb1 104.836(16) 7_665 5_766 ?
Co1 Sb5 Sb1 108.23(3) 1_665 2_765 ?
Co1 Sb5 Sb1 50.44(2) 6_667 2_765 ?
Co1 Sb5 Sb1 52.85(2) 4_656 2_765 ?
Co1 Sb5 Sb1 110.07(3) 7_665 2_765 ?
Sb2 Sb5 Sb1 113.472(12) 1_565 2_765 ?
Pr2 Sb5 Sb1 104.836(16) 7_665 2_765 ?
Sb1 Sb5 Sb1 132.25(3) 5_766 2_765 ?

_diffrn_measured_fraction_theta_max    0.995
_diffrn_reflns_theta_full              25.00
_diffrn_measured_fraction_theta_full   0.994
_refine_diff_density_max    4.084
_refine_diff_density_min   -4.147
_refine_diff_density_rms    0.787

#===END
```

A1.3 $NdCo(Sb, Sn)_3$

```
data_shelxl

_audit_creation_method            SHELXL-97
_chemical_name_systematic
;
 ?
;
_chemical_name_common             ?
_chemical_melting_point           ?
_chemical_formula_moiety          'Co Nd
Sb3'
_chemical_formula_sum
 'Co Nd Sb3'
_chemical_formula_weight          568.42

loop_
 _atom_type_symbol
 _atom_type_description
 _atom_type_scat_dispersion_real
 _atom_type_scat_dispersion_imag
 _atom_type_scat_source
 'Nd'  'Nd'  -0.1943   3.0179
 'International Tables Vol C Tables 4.2.6.8
and 6.1.1.4'
 'Co'  'Co'   0.3494   0.9721
 'International Tables Vol C Tables 4.2.6.8
and 6.1.1.4'
 'Sb'  'Sb'  -0.5866   1.5461
 'International Tables Vol C Tables 4.2.6.8
and 6.1.1.4'

_symmetry_cell_setting
'Orthorhombic'
_symmetry_space_group_name_H-M    'P b c m
'

loop_
 _symmetry_equiv_pos_as_xyz
 'x, y, z'
 '-x, -y, z+1/2'
 'x, -y+1/2, -z'
 '-x, y+1/2, -z+1/2'
 '-x, -y, -z'
 'x, y, -z-1/2'
 '-x, y-1/2, z'
 'x, -y-1/2, z-1/2'

_cell_length_a
12.71100(10)
_cell_length_b                    6.1130(2)
_cell_length_c                    12.0630(2)
_cell_angle_alpha                 90
_cell_angle_beta                  90
_cell_angle_gamma                 90
_cell_volume                      937.32(4)
_cell_formula_units_Z             8
_cell_measurement_temperature     298(2)
_cell_measurement_reflns_used     1817
```

```
_cell_measurement_theta_min       2.546
_cell_measurement_theta_max       33.142

_exptl_crystal_description        plate
_exptl_crystal_colour             black
_exptl_crystal_size_max           0.17
_exptl_crystal_size_mid           0.13
_exptl_crystal_size_min           0.07
_exptl_crystal_density_meas       ?
_exptl_crystal_density_diffrn     8.056
_exptl_crystal_density_method     'not
measured'
_exptl_crystal_F_000              1920
_exptl_absorpt_coefficient_mu     31.212
_exptl_absorpt_correction_type    'sphere'
_exptl_absorpt_correction_T_min   0.0779
_exptl_absorpt_correction_T_max   0.2289
_exptl_absorpt_process_details    'HKL
Scalepack (Otwinowski & Minor 1997)'

_exptl_special_details
;
 ?
;

_diffrn_ambient_temperature       298(5)
_diffrn_radiation_wavelength      0.71073
_diffrn_radiation_type            MoK\a
_diffrn_radiation_source          'fine-
focus sealed tube'
_diffrn_radiation_monochromator   graphite
_diffrn_measurement_device_type   'Nonius
KappaCCD'
_diffrn_measurement_method        '\w and \f
scans'
_diffrn_detector_area_resol_mean  ?
_diffrn_standards_number          ?
_diffrn_standards_interval_count  ?
_diffrn_standards_interval_time   ?
_diffrn_standards_decay_%         ?
_diffrn_reflns_number             20926
_diffrn_reflns_av_R_equivalents   0.0195
_diffrn_reflns_av_sigmaI/netI     0.0249
_diffrn_reflns_limit_h_min        -19
_diffrn_reflns_limit_h_max        19
_diffrn_reflns_limit_k_min        -9
_diffrn_reflns_limit_k_max        9
_diffrn_reflns_limit_l_min        -17
_diffrn_reflns_limit_l_max        17
_diffrn_reflns_theta_min          3.21
_diffrn_reflns_theta_max          32.56
_reflns_number_total              1708
_reflns_number_gt                 1590
_reflns_threshold_expression      I>2\s(I)

_computing_data_collection        ?
_computing_cell_refinement        ?
_computing_data_reduction         ?
_computing_structure_solution     ?
_computing_structure_refinement   'SHELXL-97
(Sheldrick, 2008)'
_computing_molecular_graphics     ?
_computing_publication_material   ?

_refine_special_details
;
 Refinement of F^2^ against ALL reflections.
The weighted R-factor wR and
 goodness of fit S are based on F^2^,
conventional R-factors R are based
 on F, with F set to zero for negative F^2^.
The threshold expression of
 F^2^ > 2\s(F^2^) is used only for
calculating R-factors(gt) etc. and is
 not relevant to the choice of reflections
for refinement.  R-factors based
 on F^2^ are statistically about twice as
large as those based on F, and R-
 factors based on ALL data will be even
larger.
;

_refine_ls_structure_factor_coef  Fsqd
_refine_ls_matrix_type            full
_refine_ls_weighting_scheme       calc
_refine_ls_weighting_details
 'calc
w=1/[\s^2^(Fo^2^)+(0.0464P)^2^+9.3300P]
where P=(Fo^2^+2Fc^2^)/3'
_atom_sites_solution_primary      direct
_atom_sites_solution_secondary    difmap
_atom_sites_solution_hydrogens    ?
_refine_ls_hydrogen_treatment     ?
_refine_ls_extinction_method      SHELXL
_refine_ls_extinction_coef
0.00227(12)
_refine_ls_extinction_expression
 'Fc^*^=kFc[1+0.001xFc^2^\l^3^/sin(2\q)]^-
1/4^'
_refine_ls_number_reflns          1708
_refine_ls_number_parameters      53
_refine_ls_number_restraints      0
_refine_ls_R_factor_all           0.0356
_refine_ls_R_factor_gt            0.0327
_refine_ls_wR_factor_ref          0.0914
_refine_ls_wR_factor_gt           0.0897
_refine_ls_goodness_of_fit_ref    1.164
_refine_ls_restrained_S_all       1.164
_refine_ls_shift/su_max           0.001
_refine_ls_shift/su_mean          0.000

loop_
 _atom_site_label
 _atom_site_type_symbol
 _atom_site_fract_x
 _atom_site_fract_y
 _atom_site_fract_z
 _atom_site_U_iso_or_equiv
 _atom_site_adp_type
 _atom_site_occupancy
 _atom_site_symmetry_multiplicity
 _atom_site_calc_flag
 _atom_site_refinement_flags
 _atom_site_disorder_assembly
 _atom_site_disorder_group
Nd1 Nd 0.70008(4) 0.2500 0.0000 0.01129(13)
Uani 1 2 d S . .
Nd2 Nd 0.30569(3) 0.26711(7) 0.7500
0.01091(12) Uani 1 2 d S . .
Co1 Co 0.10440(6) 0.03254(13) 0.86209(6)
0.01177(17) Uani 1 1 d . . .
Sb1 Sb 0.97328(4) 0.2500 0.0000 0.01271(14)
Uani 1 2 d S . .
Sb2 Sb 0.78416(4) 0.25471(8) 0.7500
0.01160(14) Uani 1 2 d S . .
Sb3 Sb 0.50197(3) 0.50881(6) 0.87654(3)
0.01216(13) Uani 1 1 d . . .
Sb4 Sb 0.21983(4) 0.2500 0.0000 0.01156(14)
Uani 1 2 d S . .
Sb5 Sb 0.94410(4) 0.88448(9) 0.7500
0.01263(14) Uani 1 2 d S . .
```

```
loop_
 _atom_site_aniso_label
 _atom_site_aniso_U_11
 _atom_site_aniso_U_22
 _atom_site_aniso_U_33
 _atom_site_aniso_U_23
 _atom_site_aniso_U_13
 _atom_site_aniso_U_12
Nd1 0.0102(2) 0.0108(2) 0.0129(2) -
0.00002(12) 0.000 0.000
Nd2 0.0091(2) 0.0113(2) 0.0123(2) 0.000
0.000 0.00021(13)
Co1 0.0122(3) 0.0110(3) 0.0121(4) 0.0000(2)
-0.0004(3) -0.0003(2)
Sb1 0.0118(2) 0.0118(3) 0.0145(3)
0.00078(16) 0.000 0.000
Sb2 0.0114(3) 0.0109(3) 0.0125(3) 0.000
0.000 -0.00118(15)
Sb3 0.0111(2) 0.0122(2) 0.0131(2)
0.00009(11) -0.00010(12) -0.00049(11)
Sb4 0.0117(3) 0.0109(3) 0.0121(3) -
0.00078(15) 0.000 0.000
Sb5 0.0107(2) 0.0120(3) 0.0152(3) 0.000
0.000 -0.00156(17)

_geom_special_details
;
 All s.u.'s (except the s.u. in the dihedral
angle between two l.s. planes)
 are estimated using the full covariance
matrix.  The cell s.u.'s are taken
 into account individually in the estimation
of s.u.'s in distances, angles
 and torsion angles; correlations between
s.u.'s in cell parameters are only
 used when they are defined by crystal
symmetry.  An approximate (isotropic)
 treatment of cell s.u.'s is used for
estimating s.u.'s involving l.s. planes.
;

loop_
 _geom_bond_atom_site_label_1
 _geom_bond_atom_site_label_2
 _geom_bond_distance
 _geom_bond_site_symmetry_2
 _geom_bond_publ_flag
Nd1 Sb2 3.1997(2) 3_556 ?
Nd1 Sb2 3.1997(2) 1_554 ?
Nd1 Sb4 3.2216(2) 5_665 ?
Nd1 Sb4 3.2216(2) 5_655 ?
Nd1 Sb3 3.3147(5) 7_654 ?
Nd1 Sb3 3.3147(5) 5_666 ?
Nd1 Sb3 3.3260(5) 1_554 ?
Nd1 Sb3 3.3260(5) 3_556 ?
Nd1 Co1 3.4536(8) 7_664 ?
Nd1 Co1 3.4536(8) 5_656 ?
Nd1 Sb1 3.4727(7) . ?
Nd2 Sb2 3.1920(6) 7_665 ?
Nd2 Sb4 3.2088(2) 6_556 ?
Nd2 Sb4 3.2088(2) 1_556 ?
Nd2 Co1 3.2297(9) 6_557 ?
Nd2 Co1 3.2297(9) . ?
Nd2 Sb5 3.2551(6) 7_655 ?
Nd2 Sb3 3.2768(5) . ?
Nd2 Sb3 3.2768(5) 6_557 ?
Nd2 Sb3 3.2865(5) 7_655 ?
Nd2 Sb3 3.2865(5) 4_646 ?
Nd2 Sb2 3.3340(6) 7_655 ?
Co1 Sb4 2.5861(8) 1_556 ?
Co1 Sb2 2.5921(9) 7_655 ?
Co1 Sb1 2.5934(8) 5_656 ?
Co1 Sb5 2.6075(9) 1_445 ?
Co1 Sb5 2.6147(9) 7_655 ?
Co1 Sb1 2.7041(8) 1_456 ?
Co1 Co1 2.7043(15) 6_557 ?
Co1 Nd1 3.4536(8) 5_656 ?
Sb1 Co1 2.5934(8) 7_664 ?
Sb1 Co1 2.5934(8) 5_656 ?
Sb1 Co1 2.7041(8) 3_656 ?
Sb1 Co1 2.7041(8) 1_654 ?
Sb1 Sb1 3.1311(3) 5_765 ?
Sb1 Sb1 3.1311(3) 5_755 ?
Sb1 Sb4 3.1339(8) 1_655 ?
Sb1 Sb5 3.2975(3) 5_766 ?
Sb1 Sb5 3.2975(3) 7_754 ?
Sb2 Co1 2.5921(9) 7_665 ?
Sb2 Co1 2.5921(9) 4_656 ?
Sb2 Sb5 3.0422(8) 1_545 ?
Sb2 Nd2 3.1920(6) 7_655 ?
Sb2 Nd1 3.1997(2) 6_556 ?
Sb2 Nd1 3.1997(2) 1_556 ?
Sb2 Nd2 3.3340(6) 7_665 ?
Sb3 Sb3 2.9810(7) 5_667 ?
Sb3 Sb3 3.0529(7) 6_557 ?
Sb3 Sb3 3.0569 7_665 ?
Sb3 Sb3 3.0569 7_655 ?
Sb3 Nd2 3.2865(5) 7_665 ?
Sb3 Nd1 3.3147(5) 5_666 ?
Sb3 Nd1 3.3260(5) 1_556 ?
Sb4 Co1 2.5861(8) 1_554 ?
Sb4 Co1 2.5861(8) 3_556 ?
Sb4 Sb1 3.1339(8) 1_455 ?
Sb4 Nd2 3.2088(2) 3_556 ?
Sb4 Nd2 3.2088(2) 1_554 ?
Sb4 Nd1 3.2216(2) 5_665 ?
Sb4 Nd1 3.2216(2) 5_655 ?
Sb5 Co1 2.6075(9) 1_665 ?
Sb5 Co1 2.6075(9) 6_667 ?
Sb5 Co1 2.6147(9) 4_656 ?
Sb5 Co1 2.6147(9) 7_665 ?
Sb5 Sb2 3.0422(8) 1_565 ?
Sb5 Nd2 3.2551(6) 7_665 ?
Sb5 Sb1 3.2975(3) 5_766 ?
Sb5 Sb1 3.2975(3) 2_765 ?

loop_
 _geom_angle_atom_site_label_1
 _geom_angle_atom_site_label_2
 _geom_angle_atom_site_label_3
 _geom_angle
 _geom_angle_site_symmetry_1
 _geom_angle_site_symmetry_3
 _geom_angle_publ_flag
Sb2 Nd1 Sb2 140.97(2) 3_556 1_554 ?
Sb2 Nd1 Sb4 84.433(11) 3_556 5_665 ?
Sb2 Nd1 Sb4 83.449(10) 1_554 5_665 ?
Sb2 Nd1 Sb4 83.449(10) 3_556 5_655 ?
Sb2 Nd1 Sb4 84.433(11) 1_554 5_655 ?
Sb4 Nd1 Sb4 143.16(2) 5_665 5_655 ?
Sb2 Nd1 Sb3 132.709(13) 3_556 7_654 ?
Sb2 Nd1 Sb3 80.754(11) 1_554 7_654 ?
Sb4 Nd1 Sb3 131.823(13) 5_665 7_654 ?
Sb4 Nd1 Sb3 79.795(11) 5_655 7_654 ?
Sb2 Nd1 Sb3 80.754(11) 3_556 5_666 ?
Sb2 Nd1 Sb3 132.709(13) 1_554 5_666 ?
Sb4 Nd1 Sb3 79.795(11) 5_665 5_666 ?
Sb4 Nd1 Sb3 131.823(13) 5_655 5_666 ?
Sb3 Nd1 Sb3 78.430(16) 7_654 5_666 ?
Sb2 Nd1 Sb3 132.782(13) 3_556 1_554 ?
Sb2 Nd1 Sb3 80.014(11) 1_554 1_554 ?
```

```
Sb4 Nd1 Sb3 77.757(11) 5_665 1_554 ?
Sb4 Nd1 Sb3 133.674(12) 5_655 1_554 ?
Sb3 Nd1 Sb3 54.816(7) 7_654 1_554 ?
Sb3 Nd1 Sb3 53.345(12) 5_666 1_554 ?
Sb2 Nd1 Sb3 80.014(11) 3_556 3_556 ?
Sb2 Nd1 Sb3 132.782(13) 1_554 3_556 ?
Sb4 Nd1 Sb3 133.674(12) 5_665 3_556 ?
Sb4 Nd1 Sb3 77.757(11) 5_655 3_556 ?
Sb3 Nd1 Sb3 53.345(12) 7_654 3_556 ?
Sb3 Nd1 Sb3 54.816(7) 5_666 3_556 ?
Sb3 Nd1 Sb3 81.578(16) 1_554 3_556 ?
Sb2 Nd1 Co1 102.600(18) 3_556 7_664 ?
Sb2 Nd1 Co1 45.662(16) 1_554 7_664 ?
Sb4 Nd1 Co1 45.422(15) 5_665 7_664 ?
Sb4 Nd1 Co1 104.305(18) 5_655 7_664 ?
Sb3 Nd1 Co1 124.303(14) 7_654 7_664 ?
Sb3 Nd1 Co1 123.473(14) 5_666 7_664 ?
Sb3 Nd1 Co1 95.236(15) 1_554 7_664 ?
Sb3 Nd1 Co1 176.782(17) 3_556 7_664 ?
Sb2 Nd1 Co1 45.662(16) 3_556 5_656 ?
Sb2 Nd1 Co1 102.600(18) 1_554 5_656 ?
Sb4 Nd1 Co1 104.305(18) 5_665 5_656 ?
Sb4 Nd1 Co1 45.422(15) 5_655 5_656 ?
Sb3 Nd1 Co1 123.472(14) 7_654 5_656 ?
Sb3 Nd1 Co1 124.303(14) 5_666 5_656 ?
Sb3 Nd1 Co1 176.782(17) 1_554 5_656 ?
Sb3 Nd1 Co1 95.236(15) 3_556 5_656 ?
Co1 Nd1 Co1 87.95(3) 7_664 5_656 ?
Sb2 Nd1 Sb1 70.486(12) 3_556 . ?
Sb2 Nd1 Sb1 70.486(12) 1_554 . ?
Sb4 Nd1 Sb1 71.579(12) 5_665 . ?
Sb4 Nd1 Sb1 71.579(12) 5_655 . ?
Sb3 Nd1 Sb1 140.785(8) 7_654 . ?
Sb3 Nd1 Sb1 140.785(8) 5_666 . ?
Sb3 Nd1 Sb1 139.211(8) 1_554 . ?
Sb3 Nd1 Sb1 139.211(8) 3_556 . ?
Co1 Nd1 Sb1 43.977(14) 7_664 . ?
Co1 Nd1 Sb1 43.977(14) 5_656 . ?
Sb2 Nd2 Sb4 84.765(9) 7_665 6_556 ?
Sb2 Nd2 Sb4 84.765(9) 7_665 1_556 ?
Sb4 Nd2 Sb4 140.05(2) 6_556 1_556 ?
Sb2 Nd2 Co1 97.54(2) 7_665 6_557 ?
Sb4 Nd2 Co1 47.362(16) 6_556 6_557 ?
Sb4 Nd2 Co1 96.290(19) 1_556 6_557 ?
Sb2 Nd2 Co1 97.54(2) 7_665 . ?
Sb4 Nd2 Co1 96.290(19) 6_556 . ?
Sb4 Nd2 Co1 47.362(16) 1_556 . ?
Co1 Nd2 Co1 49.50(3) 6_557 . ?
Sb2 Nd2 Sb5 56.302(15) 7_665 7_655 ?
Sb4 Nd2 Sb5 71.062(12) 6_556 7_655 ?
Sb4 Nd2 Sb5 71.062(12) 1_556 7_655 ?
Co1 Nd2 Sb5 47.556(17) 6_557 7_655 ?
Co1 Nd2 Sb5 47.556(17) . 7_655 ?
Sb2 Nd2 Sb3 81.452(14) 7_665 . ?
Sb4 Nd2 Sb3 135.352(14) 6_556 . ?
Sb4 Nd2 Sb3 80.551(11) 1_556 . ?
Co1 Nd2 Sb3 176.747(17) 6_557 . ?
Co1 Nd2 Sb3 127.470(15) . . ?
Sb5 Nd2 Sb3 130.036(14) 7_655 . ?
Sb2 Nd2 Sb3 81.452(14) 7_665 6_557 ?
Sb4 Nd2 Sb3 80.551(11) 6_556 6_557 ?
Sb4 Nd2 Sb3 135.352(14) 1_556 6_557 ?
Co1 Nd2 Sb3 127.470(15) 6_557 6_557 ?
Co1 Nd2 Sb3 176.747(17) . 6_557 ?
Sb5 Nd2 Sb3 130.036(14) 7_655 6_557 ?
Sb3 Nd2 Sb3 55.528(14) . 6_557 ?
Sb2 Nd2 Sb3 135.628(14) 7_665 7_655 ?
Sb4 Nd2 Sb3 132.366(14) 6_556 7_655 ?
Sb4 Nd2 Sb3 78.511(11) 1_556 7_655 ?
Co1 Nd2 Sb3 124.784(19) 6_557 7_655 ?
Co1 Nd2 Sb3 100.462(17) . 7_655 ?
Sb5 Nd2 Sb3 146.257(12) 7_655 7_655 ?
Sb3 Nd2 Sb3 55.518(7) . 7_655 ?
Sb3 Nd2 Sb3 82.333(12) 6_557 7_655 ?
Sb2 Nd2 Sb3 135.628(14) 7_665 4_646 ?
Sb4 Nd2 Sb3 78.511(11) 6_556 4_646 ?
Sb4 Nd2 Sb3 132.366(14) 1_556 4_646 ?
Co1 Nd2 Sb3 100.462(17) 6_557 4_646 ?
Co1 Nd2 Sb3 124.784(19) . 4_646 ?
Sb5 Nd2 Sb3 146.257(12) 7_655 4_646 ?
Sb3 Nd2 Sb3 82.333(12) . 4_646 ?
Sb3 Nd2 Sb3 55.518(7) 6_557 4_646 ?
Sb3 Nd2 Sb3 55.351(14) 7_655 4_646 ?
Sb2 Nd2 Sb2 139.00(2) 7_665 7_655 ?
Sb4 Nd2 Sb2 81.540(9) 6_556 7_655 ?
Sb4 Nd2 Sb2 81.540(9) 1_556 7_655 ?
Co1 Nd2 Sb2 46.488(17) 6_557 7_655 ?
Co1 Nd2 Sb2 46.488(17) . 7_655 ?
Sb5 Nd2 Sb2 82.701(17) 7_655 7_655 ?
Sb3 Nd2 Sb2 133.191(14) . 7_655 ?
Sb3 Nd2 Sb2 133.191(14) 6_557 7_655 ?
Sb3 Nd2 Sb2 78.665(13) 7_655 7_655 ?
Sb3 Nd2 Sb2 78.665(13) 4_646 7_655 ?
Sb4 Co1 Sb2 111.24(3) 1_556 7_655 ?
Sb4 Co1 Sb1 98.38(3) 1_556 5_656 ?
Sb2 Co1 Sb1 96.10(3) 7_655 5_656 ?
Sb4 Co1 Sb5 162.82(4) 1_556 1_445 ?
Sb2 Co1 Sb5 85.93(3) 7_655 1_445 ?
Sb1 Co1 Sb5 78.69(2) 5_656 1_445 ?
Sb4 Co1 Sb5 92.49(3) 1_556 7_655 ?
Sb2 Co1 Sb5 113.47(3) 7_655 7_655 ?
Sb1 Co1 Sb5 142.18(4) 5_656 7_655 ?
Sb5 Co1 Sb5 80.40(2) 1_445 7_655 ?
Sb4 Co1 Sb1 72.62(2) 1_556 1_456 ?
Sb2 Co1 Sb1 168.46(4) 7_655 1_456 ?
Sb1 Co1 Sb1 72.43(2) 5_656 1_456 ?
Sb5 Co1 Sb1 90.46(3) 1_445 1_456 ?
Sb5 Co1 Sb1 76.61(2) 7_655 1_456 ?
Sb4 Co1 Co1 130.039(18) 1_556 6_557 ?
Sb2 Co1 Co1 58.559(18) 7_655 6_557 ?
Sb1 Co1 Co1 129.903(17) 5_656 6_557 ?
Sb5 Co1 Co1 58.765(18) 1_445 6_557 ?
Sb5 Co1 Co1 58.861(18) 7_655 6_557 ?
Sb1 Co1 Co1 127.967(18) 1_456 6_557 ?
Sb4 Co1 Nd2 65.896(19) 1_556 . ?
Sb2 Co1 Nd2 68.88(2) 7_655 . ?
Sb1 Co1 Nd2 149.98(3) 5_656 . ?
Sb5 Co1 Nd2 123.78(3) 1_445 . ?
Sb5 Co1 Nd2 66.73(2) 7_655 . ?
Sb1 Co1 Nd2 121.84(3) 1_456 . ?
Co1 Co1 Nd2 65.250(14) 6_557 . ?
Sb4 Co1 Nd1 62.541(18) 1_556 5_656 ?
Sb2 Co1 Nd1 61.989(18) 7_655 5_656 ?
Sb1 Co1 Nd1 68.40(2) 5_656 5_656 ?
Sb5 Co1 Nd1 129.68(3) 1_445 5_656 ?
Sb5 Co1 Nd1 146.12(3) 7_655 5_656 ?
Sb1 Co1 Nd1 113.14(3) 1_456 5_656 ?
Co1 Co1 Nd1 118.797(13) 6_557 5_656 ?
Nd2 Co1 Nd1 81.583(19) . 5_656 ?
Co1 Sb1 Co1 135.24(4) 7_664 5_656 ?
Co1 Sb1 Co1 107.57(2) 7_664 3_656 ?
Co1 Sb1 Co1 99.64(3) 5_656 3_656 ?
Co1 Sb1 Co1 99.64(3) 7_664 1_654 ?
Co1 Sb1 Co1 107.57(2) 5_656 1_654 ?
Co1 Sb1 Co1 103.90(4) 3_656 1_654 ?
Co1 Sb1 Sb1 55.422(18) 7_664 5_765 ?
Co1 Sb1 Sb1 137.115(19) 5_656 5_765 ?
Co1 Sb1 Sb1 52.15(2) 3_656 5_765 ?
Co1 Sb1 Sb1 110.25(3) 1_654 5_765 ?
Co1 Sb1 Sb1 137.115(19) 7_664 5_755 ?
Co1 Sb1 Sb1 55.422(18) 5_656 5_755 ?
Co1 Sb1 Sb1 110.25(3) 3_656 5_755 ?
```

```
Co1 Sb1 Sb1 52.15(2) 1_654 5_755 ?
Sb1 Sb1 Sb1 154.94(4) 5_765 5_755 ?
Co1 Sb1 Sb4 112.38(2) 7_664 1_655 ?
Co1 Sb1 Sb4 112.38(2) 5_656 1_655 ?
Co1 Sb1 Sb4 51.952(19) 3_656 1_655 ?
Co1 Sb1 Sb4 51.952(19) 1_654 1_655 ?
Sb1 Sb1 Sb4 77.472(19) 5_765 1_655 ?
Sb1 Sb1 Sb4 77.472(19) 5_755 1_655 ?
Co1 Sb1 Sb5 150.923(19) 7_664 5_766 ?
Co1 Sb1 Sb5 50.843(19) 5_656 5_766 ?
Co1 Sb1 Sb5 50.478(19) 3_656 5_766 ?
Co1 Sb1 Sb5 104.11(2) 1_654 5_766 ?
Sb1 Sb1 Sb5 100.037(13) 5_765 5_766 ?
Sb1 Sb1 Sb5 71.793(11) 5_755 5_766 ?
Sb4 Sb1 Sb5 71.429(12) 1_655 5_766 ?
Co1 Sb1 Sb5 50.843(19) 7_664 7_754 ?
Co1 Sb1 Sb5 150.923(19) 5_656 7_754 ?
Co1 Sb1 Sb5 104.11(2) 3_656 7_754 ?
Co1 Sb1 Sb5 50.478(19) 1_654 7_754 ?
Sb1 Sb1 Sb5 71.793(11) 5_765 7_754 ?
Sb1 Sb1 Sb5 100.037(13) 5_755 7_754 ?
Sb4 Sb1 Sb5 71.429(12) 1_655 7_754 ?
Sb5 Sb1 Sb5 142.86(2) 5_766 7_754 ?
Co1 Sb1 Nd1 67.62(2) 7_664 . ?
Co1 Sb1 Nd1 67.62(2) 5_656 . ?
Co1 Sb1 Nd1 128.048(19) 3_656 . ?
Co1 Sb1 Nd1 128.048(19) 1_654 . ?
Sb1 Sb1 Nd1 102.528(19) 5_765 . ?
Sb1 Sb1 Nd1 102.528(19) 5_755 . ?
Sb4 Sb1 Nd1 180.0 1_655 . ?
Sb5 Sb1 Nd1 108.571(12) 5_766 . ?
Sb5 Sb1 Nd1 108.571(12) 7_754 . ?
Co1 Sb2 Co1 62.88(4) 7_665 4_656 ?
Co1 Sb2 Sb5 97.02(3) 7_665 1_545 ?
Co1 Sb2 Sb5 97.02(3) 4_656 1_545 ?
Co1 Sb2 Nd2 143.84(2) 7_665 7_655 ?
Co1 Sb2 Nd2 143.84(2) 4_656 7_655 ?
Sb5 Sb2 Nd2 62.897(15) 1_545 7_655 ?
Co1 Sb2 Nd1 132.85(2) 7_665 6_556 ?
Co1 Sb2 Nd1 72.349(18) 4_656 6_556 ?
Sb5 Sb2 Nd1 102.505(11) 1_545 6_556 ?
Nd2 Sb2 Nd1 82.651(10) 7_655 6_556 ?
Co1 Sb2 Nd1 72.349(18) 7_665 1_556 ?
Co1 Sb2 Nd1 132.85(2) 4_656 1_556 ?
Sb5 Sb2 Nd1 102.505(11) 1_545 1_556 ?
Nd2 Sb2 Nd1 82.651(10) 7_655 1_556 ?
Nd1 Sb2 Nd1 140.96(2) 6_556 1_556 ?
Co1 Sb2 Nd2 64.64(2) 7_665 7_665 ?
Co1 Sb2 Nd2 64.64(2) 4_656 7_665 ?
Sb5 Sb2 Nd2 158.10(2) 1_545 7_665 ?
Nd2 Sb2 Nd2 139.00(2) 7_655 7_665 ?
Nd1 Sb2 Nd2 83.917(10) 6_556 7_665 ?
Nd1 Sb2 Nd2 83.917(10) 1_556 7_665 ?
Sb3 Sb3 Sb3 177.716(14) 5_667 6_557 ?
Sb3 Sb3 Sb3 92.056(14) 5_667 7_665 ?
Sb3 Sb3 Sb3 90.0 6_557 7_665 ?
Sb3 Sb3 Sb3 87.913(14) 5_667 7_655 ?
Sb3 Sb3 Sb3 90.0 6_557 7_655 ?
Sb3 Sb3 Sb3 178.13(3) 7_665 7_655 ?
Sb3 Sb3 Nd2 115.874(18) 5_667 . ?
Sb3 Sb3 Nd2 62.236(7) 6_557 . ?
Sb3 Sb3 Nd2 116.001(16) 7_665 . ?
Sb3 Sb3 Nd2 62.401(13) 7_655 . ?
Sb3 Sb3 Nd2 119.600(18) 5_667 7_665 ?
Sb3 Sb3 Nd2 62.324(7) 6_557 7_665 ?
Sb3 Sb3 Nd2 62.081(12) 7_665 7_665 ?
Sb3 Sb3 Nd2 119.508(16) 7_655 7_665 ?
Nd2 Sb3 Nd2 124.520(12) . 7_665 ?
Sb3 Sb3 Nd1 63.522(13) 5_667 5_666 ?
Sb3 Sb3 Nd1 116.699(7) 6_557 5_666 ?
Sb3 Sb3 Nd1 62.780(11) 7_665 5_666 ?
Sb3 Sb3 Nd1 115.599(15) 7_655 5_666 ?
Nd2 Sb3 Nd1 79.628(12) . 5_666 ?
Nd2 Sb3 Nd1 124.846(13) 7_665 5_666 ?
Sb3 Sb3 Nd1 63.133(13) 5_667 1_556 ?
Sb3 Sb3 Nd1 116.601(7) 6_557 1_556 ?
Sb3 Sb3 Nd1 119.209(15) 7_665 1_556 ?
Sb3 Sb3 Nd1 62.404(11) 7_655 1_556 ?
Nd2 Sb3 Nd1 124.789(13) . 1_556 ?
Nd2 Sb3 Nd1 82.719(12) 7_665 1_556 ?
Nd1 Sb3 Nd1 126.655(12) 5_666 1_556 ?
Co1 Sb4 Co1 110.86(4) 1_554 3_556 ?
Co1 Sb4 Sb1 55.43(2) 1_554 1_455 ?
Co1 Sb4 Sb1 55.43(2) 3_556 1_455 ?
Co1 Sb4 Nd2 141.33(2) 1_554 3_556 ?
Co1 Sb4 Nd2 66.742(18) 3_556 3_556 ?
Sb1 Sb4 Nd2 109.882(12) 1_455 3_556 ?
Co1 Sb4 Nd2 66.742(18) 1_554 1_554 ?
Co1 Sb4 Nd2 141.33(2) 3_556 1_554 ?
Sb1 Sb4 Nd2 109.882(12) 1_455 1_554 ?
Nd2 Sb4 Nd2 140.24(2) 3_556 1_554 ?
Co1 Sb4 Nd1 131.835(19) 1_554 5_665 ?
Co1 Sb4 Nd1 72.037(18) 3_556 5_665 ?
Sb1 Sb4 Nd1 108.421(12) 1_455 5_665 ?
Nd2 Sb4 Nd1 85.610(10) 3_556 5_665 ?
Nd2 Sb4 Nd1 82.045(10) 1_554 5_665 ?
Co1 Sb4 Nd1 72.036(18) 1_554 5_655 ?
Co1 Sb4 Nd1 131.835(19) 3_556 5_655 ?
Sb1 Sb4 Nd1 108.421(12) 1_455 5_655 ?
Nd2 Sb4 Nd1 82.045(10) 3_556 5_655 ?
Nd2 Sb4 Nd1 85.610(10) 1_554 5_655 ?
Nd1 Sb4 Nd1 143.16(2) 5_665 5_655 ?
Co1 Sb5 Co1 62.47(4) 1_665 6_667 ?
Co1 Sb5 Co1 137.56(3) 1_665 4_656 ?
Co1 Sb5 Co1 101.64(3) 6_667 4_656 ?
Co1 Sb5 Co1 101.64(3) 1_665 7_665 ?
Co1 Sb5 Co1 137.56(3) 6_667 7_665 ?
Co1 Sb5 Co1 62.28(4) 4_656 7_665 ?
Co1 Sb5 Sb2 105.31(2) 1_665 1_565 ?
Co1 Sb5 Sb2 105.31(2) 6_667 1_565 ?
Co1 Sb5 Sb2 117.04(2) 4_656 1_565 ?
Co1 Sb5 Sb2 117.04(2) 7_665 1_565 ?
Co1 Sb5 Nd2 147.005(19) 1_665 7_665 ?
Co1 Sb5 Nd2 147.005(19) 6_667 7_665 ?
Co1 Sb5 Nd2 65.71(2) 4_656 7_665 ?
Co1 Sb5 Nd2 65.71(2) 7_665 7_665 ?
Sb2 Sb5 Nd2 60.801(16) 1_565 7_665 ?
Co1 Sb5 Sb1 50.463(19) 1_665 5_766 ?
Co1 Sb5 Sb1 108.17(2) 6_667 5_766 ?
Co1 Sb5 Sb1 110.05(2) 4_656 5_766 ?
Co1 Sb5 Sb1 52.917(18) 7_665 5_766 ?
Sb2 Sb5 Sb1 113.471(10) 1_565 5_766 ?
Nd2 Sb5 Sb1 104.815(13) 7_665 5_766 ?
Co1 Sb5 Sb1 108.17(2) 1_665 2_765 ?
Co1 Sb5 Sb1 50.463(19) 6_667 2_765 ?
Co1 Sb5 Sb1 52.916(18) 4_656 2_765 ?
Co1 Sb5 Sb1 110.05(2) 7_665 2_765 ?
Sb2 Sb5 Sb1 113.471(10) 1_565 2_765 ?
Nd2 Sb5 Sb1 104.815(13) 7_665 2_765 ?
Sb1 Sb5 Sb1 132.29(2) 5_766 2_765 ?

_diffrn_measured_fraction_theta_max    0.956
_diffrn_reflns_theta_full              25.00
_diffrn_measured_fraction_theta_full   0.994
_refine_diff_density_max    2.085
_refine_diff_density_min   -2.967
_refine_diff_density_rms    0.556

#===END
```

A1.4 $SmCo(Sb, Sn)_3$

```
data_shelxl

_audit_creation_method            SHELXL-97
_chemical_name_systematic
;
 ?
;
_chemical_name_common             ?
_chemical_melting_point           ?
_chemical_formula_moiety          'Co Sb3
Sm'
_chemical_formula_sum
 'Co Sb3 Sm'
_chemical_formula_weight          574.53

loop_
 _atom_type_symbol
 _atom_type_description
 _atom_type_scat_dispersion_real
 _atom_type_scat_dispersion_imag
 _atom_type_scat_source
 'Sm'  'Sm'  -0.1638   3.4418
 'International Tables Vol C Tables 4.2.6.8
and 6.1.1.4'
 'Co'  'Co'   0.3494   0.9721
 'International Tables Vol C Tables 4.2.6.8
and 6.1.1.4'
 'Sb'  'Sb'  -0.5866   1.5461
 'International Tables Vol C Tables 4.2.6.8
and 6.1.1.4'

_symmetry_cell_setting
'Orthorhombic'
_symmetry_space_group_name_H-M    'P b c m
'

loop_
 _symmetry_equiv_pos_as_xyz
 'x, y, z'
 '-x, -y, z+1/2'
 'x, -y+1/2, -z'
 '-x, y+1/2, -z+1/2'
 '-x, -y, -z'
 'x, y, -z-1/2'
 '-x, y-1/2, z'
 'x, -y-1/2, z-1/2'

_cell_length_a
12.57500(10)
_cell_length_b                    6.0980(3)
_cell_length_c                    12.0230(3)
_cell_angle_alpha                 90
_cell_angle_beta                  90
_cell_angle_gamma                 90
_cell_volume                      921.95(5)
_cell_formula_units_Z             8
_cell_measurement_temperature     298(5)
_cell_measurement_reflns_used     1781
_cell_measurement_theta_min       2.546
_cell_measurement_theta_max       33.142

_exptl_crystal_description        rod
_exptl_crystal_colour             black
_exptl_crystal_size_max           0.08
_exptl_crystal_size_mid           0.05
_exptl_crystal_size_min           0.05
_exptl_crystal_density_meas       ?
_exptl_crystal_density_diffrn     8.278
_exptl_crystal_density_method     'not
measured'
_exptl_crystal_F_000              1936
_exptl_absorpt_coefficient_mu     33.208
_exptl_absorpt_correction_type    'sphere'
_exptl_absorpt_correction_T_min   0.1897
_exptl_absorpt_correction_T_max   0.2875
_exptl_absorpt_process_details    'HKL
Scalepack (Otwinowski & Minor 1997)'

_exptl_special_details
;
 ?
;

_diffrn_ambient_temperature       298(5)
_diffrn_radiation_wavelength      0.71073
_diffrn_radiation_type            MoK\a
_diffrn_radiation_source          'fine-
focus sealed tube'
_diffrn_radiation_monochromator   graphite
_diffrn_measurement_device_type   'Nonius
KappaCCD'
_diffrn_measurement_method        ?
_diffrn_detector_area_resol_mean  ?
_diffrn_standards_number          ?
_diffrn_standards_interval_count  ?
_diffrn_standards_interval_time   ?
_diffrn_standards_decay_%         ?
_diffrn_reflns_number             19995
_diffrn_reflns_av_R_equivalents   0.0214
_diffrn_reflns_av_sigmaI/netI     0.0254
_diffrn_reflns_limit_h_min        -18
_diffrn_reflns_limit_h_max        18
_diffrn_reflns_limit_k_min        -8
_diffrn_reflns_limit_k_max        8
_diffrn_reflns_limit_l_min        -17
_diffrn_reflns_limit_l_max        17
_diffrn_reflns_theta_min          3.24
_diffrn_reflns_theta_max          32.85
_reflns_number_total              1671
_reflns_number_gt                 1514
_reflns_threshold_expression      I>2\s(I)

_computing_data_collection        ?
_computing_cell_refinement        ?
_computing_data_reduction         ?
_computing_structure_solution     ?
_computing_structure_refinement   'SHELXL-97
(Sheldrick, 2008)'
_computing_molecular_graphics     ?
_computing_publication_material   ?

_refine_special_details
;
 Refinement of F^2^ against ALL reflections.
The weighted R-factor wR and
 goodness of fit S are based on F^2^,
conventional R-factors R are based
 on F, with F set to zero for negative F^2^.
The threshold expression of
 F^2^ > 2\s(F^2^) is used only for
calculating R-factors(gt) etc. and is
 not relevant to the choice of reflections
for refinement.  R-factors based
 on F^2^ are statistically about twice as
large as those based on F, and R-
 factors based on ALL data will be even
larger.
;

_refine_ls_structure_factor_coef  Fsqd
_refine_ls_matrix_type            full
```

```
_refine_ls_weighting_scheme       calc
_refine_ls_weighting_details
 'calc
w=1/[\s^2^(Fo^2^)+(0.0146P)^2^+12.3310P]
where P=(Fo^2^+2Fc^2^)/3'
_atom_sites_solution_primary      direct
_atom_sites_solution_secondary    difmap
_atom_sites_solution_hydrogens    ?
_refine_ls_hydrogen_treatment     ?
_refine_ls_extinction_method      SHELXL
_refine_ls_extinction_coef        0.00082(4)
_refine_ls_extinction_expression
 'Fc^*^=kFc[1+0.001xFc^2^\l^3^/sin(2\q)]^-
1/4^'
_refine_ls_number_reflns          1671
_refine_ls_number_parameters      53
_refine_ls_number_restraints      0
_refine_ls_R_factor_all           0.0331
_refine_ls_R_factor_gt            0.0278
_refine_ls_wR_factor_ref          0.0616
_refine_ls_wR_factor_gt           0.0600
_refine_ls_goodness_of_fit_ref    1.244
_refine_ls_restrained_S_all       1.244
_refine_ls_shift/su_max           0.001
_refine_ls_shift/su_mean          0.000

loop_
 _atom_site_label
 _atom_site_type_symbol
 _atom_site_fract_x
 _atom_site_fract_y
 _atom_site_fract_z
 _atom_site_U_iso_or_equiv
 _atom_site_adp_type
 _atom_site_occupancy
 _atom_site_symmetry_multiplicity
 _atom_site_calc_flag
 _atom_site_refinement_flags
 _atom_site_disorder_assembly
 _atom_site_disorder_group
Sm1 Sm 0.69969(3) 0.2500 0.0000 0.00784(10)
Uani 1 2 d S . .
Sm2 Sm 0.30611(3) 0.26858(7) 0.7500
0.00750(10) Uani 1 2 d S . .
Co1 Co 0.10566(6) 0.03281(13) 0.86214(7)
0.00809(16) Uani 1 1 d . . .
Sb1 Sb 0.97314(4) 0.2500 0.0000 0.00887(12)
Uani 1 2 d S . .
Sb2 Sb 0.78140(4) 0.25460(8) 0.7500
0.00814(12) Uani 1 2 d S . .
Sb3 Sb 0.50227(3) 0.50899(6) 0.87630(3)
0.00861(10) Uani 1 1 d . . .
Sb4 Sb 0.22290(4) 0.2500 0.0000 0.00806(12)
Uani 1 2 d S . .
Sb5 Sb 0.94353(4) 0.88538(9) 0.7500
0.00899(12) Uani 1 2 d S . .

loop_
 _atom_site_aniso_label
 _atom_site_aniso_U_11
 _atom_site_aniso_U_22
 _atom_site_aniso_U_33
 _atom_site_aniso_U_23
 _atom_site_aniso_U_13
 _atom_site_aniso_U_12
Sm1 0.00801(18) 0.00757(18) 0.0079(2) -
0.00013(13) 0.000 0.000
Sm2 0.00661(18) 0.00821(18) 0.0077(2) 0.000
0.000 0.00016(13)
Co1 0.0096(3) 0.0074(3) 0.0073(4) -0.0005(3)
-0.0006(3) -0.0005(3)
Sb1 0.0091(2) 0.0080(2) 0.0094(3)
0.00064(17) 0.000 0.000
Sb2 0.0090(2) 0.0076(2) 0.0078(3) 0.000
0.000 -0.00121(17)
Sb3 0.00861(18) 0.00881(18) 0.0084(2)
0.00004(12) -0.00012(13) -0.00032(11)
Sb4 0.0087(2) 0.0078(2) 0.0077(3) -
0.00085(17) 0.000 0.000
Sb5 0.0081(2) 0.0084(2) 0.0105(2) 0.000
0.000 -0.00140(18)

_geom_special_details
;
 All s.u.'s (except the s.u. in the dihedral
angle between two l.s. planes)
 are estimated using the full covariance
matrix.  The cell s.u.'s are taken
 into account individually in the estimation
of s.u.'s in distances, angles
 and torsion angles; correlations between
s.u.'s in cell parameters are only
 used when they are defined by crystal
symmetry.  An approximate (isotropic)
 treatment of cell s.u.'s is used for
estimating s.u.'s involving l.s. planes.
;

loop_
 _geom_bond_atom_site_label_1
 _geom_bond_atom_site_label_2
 _geom_bond_distance
 _geom_bond_site_symmetry_2
 _geom_bond_publ_flag
Sm1 Sb2 3.1767(2) 3_556 ?
Sm1 Sb2 3.1767(2) 1_554 ?
Sm1 Sb4 3.2006(2) 5_665 ?
Sm1 Sb4 3.2006(2) 5_655 ?
Sm1 Sb3 3.2896(5) 7_654 ?
Sm1 Sb3 3.2896(5) 5_666 ?
Sm1 Sb3 3.2968(5) 3_556 ?
Sm1 Sb3 3.2968(5) 1_554 ?
Sm1 Co1 3.4224(8) 5_656 ?
Sm1 Co1 3.4224(8) 7_664 ?
Sm1 Sb1 3.4387(6) . ?
Sm2 Sb2 3.1615(7) 7_665 ?
Sm2 Sb4 3.1847(2) 6_556 ?
Sm2 Sb4 3.1847(2) 1_556 ?
Sm2 Co1 3.1997(8) 6_557 ?
Sm2 Co1 3.1997(8) . ?
Sm2 Sb5 3.2190(6) 7_655 ?
Sm2 Sb3 3.2465(5) . ?
Sm2 Sb3 3.2465(5) 6_557 ?
Sm2 Sb3 3.2585(5) 7_655 ?
Sm2 Sb3 3.2585(5) 4_646 ?
Sm2 Sb2 3.3218(7) 7_655 ?
Co1 Sb4 2.5836(8) 1_556 ?
Co1 Sb1 2.5891(8) 5_656 ?
Co1 Sb2 2.5909(9) 7_655 ?
Co1 Sb5 2.6044(9) 1_445 ?
Co1 Sb5 2.6121(9) 7_655 ?
Co1 Co1 2.6964(16) 6_557 ?
Co1 Sb1 2.6979(8) 1_456 ?
Co1 Sm1 3.4224(8) 5_656 ?
Sb1 Co1 2.5891(8) 5_656 ?
Sb1 Co1 2.5891(8) 7_664 ?
Sb1 Co1 2.6979(8) 3_656 ?
Sb1 Co1 2.6979(8) 1_654 ?
Sb1 Sb1 3.1229(3) 5_765 ?
Sb1 Sb1 3.1229(3) 5_755 ?
Sb1 Sb4 3.1407(7) 1_655 ?
Sb1 Sb5 3.2885(3) 5_766 ?
```

```
Sb1 Sb5 3.2885(3) 7_754 ?
Sb2 Co1 2.5909(9) 7_665 ?
Sb2 Co1 2.5909(9) 4_656 ?
Sb2 Sb5 3.0374(7) 1_545 ?
Sb2 Sm2 3.1615(7) 7_655 ?
Sb2 Sm1 3.1767(2) 6_556 ?
Sb2 Sm1 3.1767(2) 1_556 ?
Sb2 Sm2 3.3218(7) 7_665 ?
Sb3 Sb3 2.9771(7) 5_667 ?
Sb3 Sb3 3.0369(7) 6_557 ?
Sb3 Sb3 3.04953(15) 7_655 ?
Sb3 Sb3 3.04953(16) 7_665 ?
Sb3 Sm2 3.2585(5) 7_665 ?
Sb3 Sm1 3.2896(5) 5_666 ?
Sb3 Sm1 3.2968(5) 1_556 ?
Sb4 Co1 2.5836(8) 1_554 ?
Sb4 Co1 2.5836(8) 3_556 ?
Sb4 Sb1 3.1407(7) 1_455 ?
Sb4 Sm2 3.1847(2) 3_556 ?
Sb4 Sm2 3.1847(2) 1_554 ?
Sb4 Sm1 3.2006(2) 5_665 ?
Sb4 Sm1 3.2006(2) 5_655 ?
Sb5 Co1 2.6044(9) 1_665 ?
Sb5 Co1 2.6044(9) 6_667 ?
Sb5 Co1 2.6121(9) 4_656 ?
Sb5 Co1 2.6121(9) 7_665 ?
Sb5 Sb2 3.0374(7) 1_565 ?
Sb5 Sm2 3.2190(6) 7_665 ?
Sb5 Sb1 3.2885(3) 5_766 ?
Sb5 Sb1 3.2885(3) 2_765 ?

loop_
 _geom_angle_atom_site_label_1
 _geom_angle_atom_site_label_2
 _geom_angle_atom_site_label_3
 _geom_angle
 _geom_angle_site_symmetry_1
 _geom_angle_site_symmetry_3
 _geom_angle_publ_flag
Sb2 Sm1 Sb2 142.25(2) 3_556 1_554 ?
Sb2 Sm1 Sb4 84.838(11) 3_556 5_665 ?
Sb2 Sm1 Sb4 83.869(10) 1_554 5_665 ?
Sb2 Sm1 Sb4 83.869(10) 3_556 5_655 ?
Sb2 Sm1 Sb4 84.838(11) 1_554 5_655 ?
Sb4 Sm1 Sb4 144.58(2) 5_665 5_655 ?
Sb2 Sm1 Sb3 132.343(13) 3_556 7_654 ?
Sb2 Sm1 Sb3 79.972(11) 1_554 7_654 ?
Sb4 Sm1 Sb3 131.331(12) 5_665 7_654 ?
Sb4 Sm1 Sb3 79.002(11) 5_655 7_654 ?
Sb2 Sm1 Sb3 79.972(11) 3_556 5_666 ?
Sb2 Sm1 Sb3 132.343(13) 1_554 5_666 ?
Sb4 Sm1 Sb3 79.002(11) 5_665 5_666 ?
Sb4 Sm1 Sb3 131.331(12) 5_655 5_666 ?
Sb3 Sm1 Sb3 78.931(16) 7_654 5_666 ?
Sb2 Sm1 Sb3 79.193(11) 3_556 3_556 ?
Sb2 Sm1 Sb3 132.427(13) 1_554 3_556 ?
Sb4 Sm1 Sb3 133.266(12) 5_665 3_556 ?
Sb4 Sm1 Sb3 76.861(11) 5_655 3_556 ?
Sb3 Sm1 Sb3 53.745(12) 7_654 3_556 ?
Sb3 Sm1 Sb3 55.162(7) 5_666 3_556 ?
Sb2 Sm1 Sb3 132.427(13) 3_556 1_554 ?
Sb2 Sm1 Sb3 79.193(11) 1_554 1_554 ?
Sb4 Sm1 Sb3 76.861(11) 5_665 1_554 ?
Sb4 Sm1 Sb3 133.266(12) 5_655 1_554 ?
Sb3 Sm1 Sb3 55.162(7) 7_654 1_554 ?
Sb3 Sm1 Sb3 53.745(12) 5_666 1_554 ?
Sb3 Sm1 Sb3 82.299(16) 3_556 1_554 ?
Sb2 Sm1 Co1 46.048(16) 3_556 5_656 ?
Sb2 Sm1 Co1 103.377(18) 1_554 5_656 ?
Sb4 Sm1 Co1 105.218(18) 5_665 5_656 ?
Sb4 Sm1 Co1 45.768(15) 5_655 5_656 ?
Sb3 Sm1 Co1 123.092(14) 7_654 5_656 ?
Sb3 Sm1 Co1 123.939(15) 5_666 5_656 ?
Sb3 Sm1 Co1 94.512(15) 3_556 5_656 ?
Sb3 Sm1 Co1 176.785(17) 1_554 5_656 ?
Sb2 Sm1 Co1 103.377(18) 3_556 7_664 ?
Sb2 Sm1 Co1 46.048(16) 1_554 7_664 ?
Sb4 Sm1 Co1 45.768(15) 5_665 7_664 ?
Sb4 Sm1 Co1 105.218(18) 5_655 7_664 ?
Sb3 Sm1 Co1 123.939(15) 7_654 7_664 ?
Sb3 Sm1 Co1 123.092(14) 5_666 7_664 ?
Sb3 Sm1 Co1 176.785(17) 3_556 7_664 ?
Sb3 Sm1 Co1 94.512(15) 1_554 7_664 ?
Co1 Sm1 Co1 88.68(3) 5_656 7_664 ?
Sb2 Sm1 Sb1 71.127(11) 3_556 . ?
Sb2 Sm1 Sb1 71.127(11) 1_554 . ?
Sb4 Sm1 Sb1 72.292(11) 5_665 . ?
Sb4 Sm1 Sb1 72.292(11) 5_655 . ?
Sb3 Sm1 Sb1 140.534(8) 7_654 . ?
Sb3 Sm1 Sb1 140.534(8) 5_666 . ?
Sb3 Sm1 Sb1 138.851(8) 3_556 . ?
Sb3 Sm1 Sb1 138.851(8) 1_554 . ?
Co1 Sm1 Sb1 44.340(14) 5_656 . ?
Co1 Sm1 Sb1 44.340(14) 7_664 . ?
Sb2 Sm2 Sb4 85.353(9) 7_665 6_556 ?
Sb2 Sm2 Sb4 85.353(9) 7_665 1_556 ?
Sb4 Sm2 Sb4 141.40(2) 6_556 1_556 ?
Sb2 Sm2 Co1 98.455(19) 7_665 6_557 ?
Sb4 Sm2 Co1 47.740(16) 6_556 6_557 ?
Sb4 Sm2 Co1 97.058(19) 1_556 6_557 ?
Sb2 Sm2 Co1 98.455(19) 7_665 . ?
Sb4 Sm2 Co1 97.058(19) 6_556 . ?
Sb4 Sm2 Co1 47.740(16) 1_556 . ?
Co1 Sm2 Co1 49.84(3) 6_557 . ?
Sb2 Sm2 Sb5 56.846(15) 7_665 7_655 ?
Sb4 Sm2 Sb5 71.787(11) 6_556 7_655 ?
Sb4 Sm2 Sb5 71.788(11) 1_556 7_655 ?
Co1 Sm2 Sb5 48.025(17) 6_557 7_655 ?
Co1 Sm2 Sb5 48.025(17) . 7_655 ?
Sb2 Sm2 Sb3 80.859(14) 7_665 . ?
Sb4 Sm2 Sb3 135.003(14) 6_556 . ?
Sb4 Sm2 Sb3 79.878(11) 1_556 . ?
Co1 Sm2 Sb3 176.895(17) 6_557 . ?
Co1 Sm2 Sb3 127.184(15) . . ?
Sb5 Sm2 Sb3 129.870(15) 7_655 . ?
Sb2 Sm2 Sb3 80.859(14) 7_665 6_557 ?
Sb4 Sm2 Sb3 79.878(11) 6_556 6_557 ?
Sb4 Sm2 Sb3 135.003(14) 1_556 6_557 ?
Co1 Sm2 Sb3 127.184(15) 6_557 6_557 ?
Co1 Sm2 Sb3 176.895(17) . 6_557 ?
Sb5 Sm2 Sb3 129.870(15) 7_655 6_557 ?
Sb3 Sm2 Sb3 55.773(14) . 6_557 ?
Sb2 Sm2 Sb3 135.464(14) 7_665 7_655 ?
Sb4 Sm2 Sb3 131.721(14) 6_556 7_655 ?
Sb4 Sm2 Sb3 77.635(11) 1_556 7_655 ?
Co1 Sm2 Sb3 124.10(2) 6_557 7_655 ?
Co1 Sm2 Sb3 99.666(17) . 7_655 ?
Sb5 Sm2 Sb3 145.961(12) 7_655 7_655 ?
Sb3 Sm2 Sb3 55.912(7) . 7_655 ?
Sb3 Sm2 Sb3 82.846(11) 6_557 7_655 ?
Sb2 Sm2 Sb3 135.464(14) 7_665 4_646 ?
Sb4 Sm2 Sb3 77.635(11) 6_556 4_646 ?
Sb4 Sm2 Sb3 131.721(14) 1_556 4_646 ?
Co1 Sm2 Sb3 99.666(17) 6_557 4_646 ?
Co1 Sm2 Sb3 124.10(2) . 4_646 ?
Sb5 Sm2 Sb3 145.961(12) 7_655 4_646 ?
Sb3 Sm2 Sb3 82.846(11) . 4_646 ?
Sb3 Sm2 Sb3 55.912(7) 6_557 4_646 ?
Sb3 Sm2 Sb3 55.550(14) 7_655 4_646 ?
Sb2 Sm2 Sb2 140.28(2) 7_665 7_655 ?
Sb4 Sm2 Sb2 81.813(8) 6_556 7_655 ?
Sb4 Sm2 Sb2 81.813(8) 1_556 7_655 ?
```

```
Co1 Sm2 Sb2 46.771(16) 6_557 7_655 ?
Co1 Sm2 Sb2 46.771(16) . 7_655 ?
Sb5 Sm2 Sb2 83.438(16) 7_655 7_655 ?
Sb3 Sm2 Sb2 132.671(14) . 7_655 ?
Sb3 Sm2 Sb2 132.671(14) 6_557 7_655 ?
Sb3 Sm2 Sb2 77.679(13) 7_655 7_655 ?
Sb3 Sm2 Sb2 77.679(13) 4_646 7_655 ?
Sb4 Co1 Sb1 98.58(3) 1_556 5_656 ?
Sb4 Co1 Sb2 110.90(3) 1_556 7_655 ?
Sb1 Co1 Sb2 96.13(3) 5_656 7_655 ?
Sb4 Co1 Sb5 162.90(4) 1_556 1_445 ?
Sb1 Co1 Sb5 78.57(2) 5_656 1_445 ?
Sb2 Co1 Sb5 86.20(3) 7_655 1_445 ?
Sb4 Co1 Sb5 92.54(3) 1_556 7_655 ?
Sb1 Co1 Sb5 142.00(4) 5_656 7_655 ?
Sb2 Co1 Sb5 113.59(3) 7_655 7_655 ?
Sb5 Co1 Sb5 80.30(2) 1_445 7_655 ?
Sb4 Co1 Co1 129.908(18) 1_556 6_557 ?
Sb1 Co1 Co1 129.806(17) 5_656 6_557 ?
Sb2 Co1 Co1 58.643(19) 7_655 6_557 ?
Sb5 Co1 Co1 58.823(19) 1_445 6_557 ?
Sb5 Co1 Co1 58.926(18) 7_655 6_557 ?
Sb4 Co1 Sb1 72.94(2) 1_556 1_456 ?
Sb1 Co1 Sb1 72.38(2) 5_656 1_456 ?
Sb2 Co1 Sb1 168.45(4) 7_655 1_456 ?
Sb5 Co1 Sb1 90.23(3) 1_445 1_456 ?
Sb5 Co1 Sb1 76.51(2) 7_655 1_456 ?
Co1 Co1 Sb1 127.907(18) 6_557 1_456 ?
Sb4 Co1 Sm2 65.825(18) 1_556 . ?
Sb1 Co1 Sm2 150.52(3) 5_656 . ?
Sb2 Co1 Sm2 69.09(2) 7_655 . ?
Sb5 Co1 Sm2 123.62(3) 1_445 . ?
Sb5 Co1 Sm2 66.37(2) 7_655 . ?
Co1 Co1 Sm2 65.080(14) 6_557 . ?
Sb1 Co1 Sm2 121.66(3) 1_456 . ?
Sb4 Co1 Sm1 62.580(17) 1_556 5_656 ?
Sb1 Co1 Sm1 68.16(2) 5_656 5_656 ?
Sb2 Co1 Sm1 61.968(17) 7_655 5_656 ?
Sb5 Co1 Sm1 129.55(3) 1_445 5_656 ?
Sb5 Co1 Sm1 146.52(3) 7_655 5_656 ?
Co1 Co1 Sm1 118.967(13) 6_557 5_656 ?
Sb1 Co1 Sm1 113.05(3) 1_456 5_656 ?
Sm2 Co1 Sm1 82.361(19) . 5_656 ?
Co1 Sb1 Co1 134.99(4) 5_656 7_664 ?
Co1 Sb1 Co1 99.79(3) 5_656 3_656 ?
Co1 Sb1 Co1 107.62(2) 7_664 3_656 ?
Co1 Sb1 Co1 107.62(2) 5_656 1_654 ?
Co1 Sb1 Co1 99.79(3) 7_664 1_654 ?
Co1 Sb1 Co1 103.71(4) 3_656 1_654 ?
Co1 Sb1 Sb1 137.147(18) 5_656 5_765 ?
Co1 Sb1 Sb1 55.422(18) 7_664 5_765 ?
Co1 Sb1 Sb1 52.200(19) 3_656 5_765 ?
Co1 Sb1 Sb1 110.22(3) 1_654 5_765 ?
Co1 Sb1 Sb1 55.422(18) 5_656 5_755 ?
Co1 Sb1 Sb1 137.147(18) 7_664 5_755 ?
Co1 Sb1 Sb1 110.22(3) 3_656 5_755 ?
Co1 Sb1 Sb1 52.200(19) 1_654 5_755 ?
Sb1 Sb1 Sb1 155.02(4) 5_765 5_755 ?
Co1 Sb1 Sb4 112.50(2) 5_656 1_655 ?
Co1 Sb1 Sb4 112.50(2) 7_664 1_655 ?
Co1 Sb1 Sb4 51.853(18) 3_656 1_655 ?
Co1 Sb1 Sb4 51.853(18) 1_654 1_655 ?
Sb1 Sb1 Sb4 77.508(18) 5_765 1_655 ?
Sb1 Sb1 Sb4 77.508(18) 5_755 1_655 ?
Co1 Sb1 Sb5 50.920(19) 5_656 5_766 ?
Co1 Sb1 Sb5 150.966(19) 7_664 5_766 ?
Co1 Sb1 Sb5 50.57(2) 3_656 5_766 ?
Co1 Sb1 Sb5 103.97(2) 1_654 5_766 ?
Sb1 Sb1 Sb5 100.148(13) 5_765 5_766 ?
Sb1 Sb1 Sb5 71.698(11) 5_755 5_766 ?
Sb4 Sb1 Sb5 71.419(12) 1_655 5_766 ?
Co1 Sb1 Sb5 150.966(19) 5_656 7_754 ?
Co1 Sb1 Sb5 50.920(19) 7_664 7_754 ?
Co1 Sb1 Sb5 103.97(2) 3_656 7_754 ?
Co1 Sb1 Sb5 50.57(2) 1_654 7_754 ?
Sb1 Sb1 Sb5 71.698(11) 5_765 7_754 ?
Sb1 Sb1 Sb5 100.148(13) 5_755 7_754 ?
Sb4 Sb1 Sb5 71.419(12) 1_655 7_754 ?
Sb5 Sb1 Sb5 142.84(2) 5_766 7_754 ?
Co1 Sb1 Sm1 67.50(2) 5_656 . ?
Co1 Sb1 Sm1 67.50(2) 7_664 . ?
Co1 Sb1 Sm1 128.147(18) 3_656 . ?
Co1 Sb1 Sm1 128.147(18) 1_654 . ?
Sb1 Sb1 Sm1 102.492(18) 5_765 . ?
Sb1 Sb1 Sm1 102.492(18) 5_755 . ?
Sb4 Sb1 Sm1 180.0 1_655 . ?
Sb5 Sb1 Sm1 108.581(12) 5_766 . ?
Sb5 Sb1 Sm1 108.581(12) 7_754 . ?
Co1 Sb2 Co1 62.71(4) 7_665 4_656 ?
Co1 Sb2 Sb5 96.74(2) 7_665 1_545 ?
Co1 Sb2 Sb5 96.74(2) 4_656 1_545 ?
Co1 Sb2 Sm2 143.58(2) 7_665 7_655 ?
Co1 Sb2 Sm2 143.58(2) 4_656 7_655 ?
Sb5 Sb2 Sm2 62.531(16) 1_545 7_655 ?
Co1 Sb2 Sm1 132.49(2) 7_665 6_556 ?
Co1 Sb2 Sm1 71.984(18) 4_656 6_556 ?
Sb5 Sb2 Sm1 102.156(11) 1_545 6_556 ?
Sm2 Sb2 Sm1 83.058(10) 7_655 6_556 ?
Co1 Sb2 Sm1 71.984(18) 7_665 1_556 ?
Co1 Sb2 Sm1 132.49(2) 4_656 1_556 ?
Sb5 Sb2 Sm1 102.156(11) 1_545 1_556 ?
Sm2 Sb2 Sm1 83.058(10) 7_655 1_556 ?
Sm1 Sb2 Sm1 142.24(2) 6_556 1_556 ?
Co1 Sb2 Sm2 64.14(2) 7_665 7_665 ?
Co1 Sb2 Sm2 64.14(2) 4_656 7_665 ?
Sb5 Sb2 Sm2 157.18(2) 1_545 7_665 ?
Sm2 Sb2 Sm2 140.28(2) 7_655 7_665 ?
Sm1 Sb2 Sm2 84.328(10) 6_556 7_665 ?
Sm1 Sb2 Sm2 84.328(10) 1_556 7_665 ?
Sb3 Sb3 Sb3 177.620(14) 5_667 6_557 ?
Sb3 Sb3 Sb3 87.869(14) 5_667 7_655 ?
Sb3 Sb3 Sb3 90.0 6_557 7_655 ?
Sb3 Sb3 Sb3 92.090(14) 5_667 7_665 ?
Sb3 Sb3 Sb3 90.0 6_557 7_665 ?
Sb3 Sb3 Sb3 177.85(3) 7_655 7_665 ?
Sb3 Sb3 Sm2 115.856(18) 5_667 . ?
Sb3 Sb3 Sm2 62.113(7) 6_557 . ?
Sb3 Sb3 Sm2 62.243(13) 7_655 . ?
Sb3 Sb3 Sm2 115.930(17) 7_665 . ?
Sb3 Sb3 Sm2 119.846(19) 5_667 7_665 ?
Sb3 Sb3 Sm2 62.225(7) 6_557 7_665 ?
Sb3 Sb3 Sm2 119.970(17) 7_655 7_665 ?
Sb3 Sb3 Sm2 61.845(13) 7_665 7_665 ?
Sm2 Sb3 Sm2 124.283(12) . 7_665 ?
Sb3 Sb3 Sm1 63.252(13) 5_667 5_666 ?
Sb3 Sb3 Sm1 116.880(7) 6_557 5_666 ?
Sb3 Sb3 Sm1 115.609(16) 7_655 5_666 ?
Sb3 Sb3 Sm1 62.540(12) 7_665 5_666 ?
Sm2 Sb3 Sm1 80.017(12) . 5_666 ?
Sm2 Sb3 Sm1 124.371(14) 7_665 5_666 ?
Sb3 Sb3 Sm1 63.003(13) 5_667 1_556 ?
Sb3 Sb3 Sm1 116.816(7) 6_557 1_556 ?
Sb3 Sb3 Sm1 62.298(11) 7_655 1_556 ?
Sb3 Sb3 Sm1 119.542(16) 7_665 1_556 ?
Sm2 Sb3 Sm1 124.528(14) . 1_556 ?
Sm2 Sb3 Sm1 83.460(12) 7_665 1_556 ?
Sm1 Sb3 Sm1 126.255(12) 5_666 1_556 ?
Co1 Sb4 Co1 110.41(4) 1_554 3_556 ?
Co1 Sb4 Sb1 55.207(19) 1_554 1_455 ?
Co1 Sb4 Sb1 55.207(19) 3_556 1_455 ?
Co1 Sb4 Sm2 140.78(2) 1_554 3_556 ?
Co1 Sb4 Sm2 66.435(18) 3_556 3_556 ?
```

```
Sb1 Sb4 Sm2 109.181(11) 1_455 3_556 ?
Co1 Sb4 Sm2 66.435(19) 1_554 1_554 ?
Co1 Sb4 Sm2 140.78(2) 3_556 1_554 ?
Sb1 Sb4 Sm2 109.181(11) 1_455 1_554 ?
Sm2 Sb4 Sm2 141.64(2) 3_556 1_554 ?
Co1 Sb4 Sm1 131.445(19) 1_554 5_665 ?
Co1 Sb4 Sm1 71.652(18) 3_556 5_665 ?
Sb1 Sb4 Sm1 107.708(11) 1_455 5_665 ?
Sm2 Sb4 Sm1 86.213(10) 3_556 5_665 ?
Sm2 Sb4 Sm1 82.310(9) 1_554 5_665 ?
Co1 Sb4 Sm1 71.652(18) 1_554 5_655 ?
Co1 Sb4 Sm1 131.445(19) 3_556 5_655 ?
Sb1 Sb4 Sm1 107.708(11) 1_455 5_655 ?
Sm2 Sb4 Sm1 82.310(9) 3_556 5_655 ?
Sm2 Sb4 Sm1 86.213(10) 1_554 5_655 ?
Sm1 Sb4 Sm1 144.58(2) 5_665 5_655 ?
Co1 Sb5 Co1 62.35(4) 1_665 6_667 ?
Co1 Sb5 Co1 137.45(3) 1_665 4_656 ?
Co1 Sb5 Co1 101.67(3) 6_667 4_656 ?
Co1 Sb5 Co1 101.67(3) 1_665 7_665 ?
Co1 Sb5 Co1 137.45(3) 6_667 7_665 ?
Co1 Sb5 Co1 62.15(4) 4_656 7_665 ?
Co1 Sb5 Sb2 105.64(2) 1_665 1_565 ?
Co1 Sb5 Sb2 105.64(2) 6_667 1_565 ?
Co1 Sb5 Sb2 116.82(2) 4_656 1_565 ?
Co1 Sb5 Sb2 116.82(2) 7_665 1_565 ?
Co1 Sb5 Sm2 147.122(19) 1_665 7_665 ?
Co1 Sb5 Sm2 147.122(19) 6_667 7_665 ?
Co1 Sb5 Sm2 65.60(2) 4_656 7_665 ?
Co1 Sb5 Sm2 65.60(2) 7_665 7_665 ?
Sb2 Sb5 Sm2 60.623(16) 1_565 7_665 ?
Co1 Sb5 Sb1 50.508(19) 1_665 5_766 ?
Co1 Sb5 Sb1 108.08(2) 6_667 5_766 ?
Co1 Sb5 Sb1 109.91(2) 4_656 5_766 ?
Co1 Sb5 Sb1 52.918(18) 7_665 5_766 ?
Sb2 Sb5 Sb1 113.577(10) 1_565 5_766 ?
Sm2 Sb5 Sb1 104.785(13) 7_665 5_766 ?
Co1 Sb5 Sb1 108.08(2) 1_665 2_765 ?
Co1 Sb5 Sb1 50.508(19) 6_667 2_765 ?
Co1 Sb5 Sb1 52.918(18) 4_656 2_765 ?
Co1 Sb5 Sb1 109.91(2) 7_665 2_765 ?
Sb2 Sb5 Sb1 113.577(10) 1_565 2_765 ?
Sm2 Sb5 Sb1 104.785(13) 7_665 2_765 ?
Sb1 Sb5 Sb1 132.13(2) 5_766 2_765 ?

_diffrn_measured_fraction_theta_max    0.930
_diffrn_reflns_theta_full              25.00
_diffrn_measured_fraction_theta_full   0.994
_refine_diff_density_max    2.060
_refine_diff_density_min   -1.571
_refine_diff_density_rms    0.417

#===END
```

A1.5 $La_2Fe_4Sb_5$

```
data_shelxl

_audit_creation_method            SHELXL-97
_chemical_name_systematic
;
 ?
;
_chemical_name_common             ?
_chemical_melting_point           ?
_chemical_formula_moiety          'Fe4.03
La2 Sb4.94'
_chemical_formula_sum
 'Fe4.03 La2 Sb4.94'
_chemical_formula_weight          1104.62

loop_
 _atom_type_symbol
 _atom_type_description
 _atom_type_scat_dispersion_real
 _atom_type_scat_dispersion_imag
 _atom_type_scat_source
 'La'  'La'  -0.2871   2.4523
 'International Tables Vol C Tables 4.2.6.8
and 6.1.1.4'
 'Fe'  'Fe'   0.3463   0.8444
 'International Tables Vol C Tables 4.2.6.8
and 6.1.1.4'
 'Sb'  'Sb'  -0.5866   1.5461
 'International Tables Vol C Tables 4.2.6.8
and 6.1.1.4'

_symmetry_cell_setting
'Tetragonal'
_symmetry_space_group_name_H-M    'I 4/m m m
'

loop_
 _symmetry_equiv_pos_as_xyz
 'x, y, z'
 '-x, -y, z'
 'x, -y, -z'
 '-x, y, -z'
 '-y, -x, -z'
 'y, x, -z'
 'y, -x, z'
 '-y, x, z'
 'x+1/2, y+1/2, z+1/2'
 '-x+1/2, -y+1/2, z+1/2'
 'x+1/2, -y+1/2, -z+1/2'
 '-x+1/2, y+1/2, -z+1/2'
 '-y+1/2, -x+1/2, -z+1/2'
 'y+1/2, x+1/2, -z+1/2'
 'y+1/2, -x+1/2, z+1/2'
 '-y+1/2, x+1/2, z+1/2'
 '-x, -y, -z'
 'x, y, -z'
 '-x, y, z'
 'x, -y, z'
 'y, x, z'
 '-y, -x, z'
 '-y, x, -z'
 'y, -x, -z'
 '-x+1/2, -y+1/2, -z+1/2'
 'x+1/2, y+1/2, -z+1/2'
 '-x+1/2, y+1/2, z+1/2'
 'x+1/2, -y+1/2, z+1/2'
 'y+1/2, x+1/2, z+1/2'
 '-y+1/2, -x+1/2, z+1/2'
 '-y+1/2, x+1/2, -z+1/2'
 'y+1/2, -x+1/2, -z+1/2'

_cell_length_a                    4.3522(15)
_cell_length_b                    4.3522(15)
_cell_length_c                    26.201(8)
_cell_angle_alpha                 90
_cell_angle_beta                  90
_cell_angle_gamma                 90
_cell_volume                      496.3(3)
_cell_formula_units_Z             2
_cell_measurement_temperature     298(2)
_cell_measurement_reflns_used     603
_cell_measurement_theta_min       31
_cell_measurement_theta_max       36.5

_exptl_crystal_description        plate
_exptl_crystal_colour             black
_exptl_crystal_size_max           0.10
```

```
_exptl_crystal_size_mid           0.08
_exptl_crystal_size_min           0.01
_exptl_crystal_density_meas       ?
_exptl_crystal_density_diffrn     7.392
_exptl_crystal_density_method     'not
measured'
_exptl_crystal_F_000              942
_exptl_absorpt_coefficient_mu     27.236
_exptl_absorpt_correction_type    'multi-
scan'
_exptl_absorpt_correction_T_min   0.1715
_exptl_absorpt_correction_T_max   0.7271
_exptl_absorpt_process_details    'HKL
Scalepack (Otwinowski & Minor 1997)'

_exptl_special_details
;
 ?
;

_diffrn_ambient_temperature       298(2)
_diffrn_radiation_wavelength      0.71073
_diffrn_radiation_type            MoK\a
_diffrn_radiation_source          'fine-
focus sealed tube'
_diffrn_radiation_monochromator   graphite
_diffrn_measurement_device_type   'Nonius
KappaCCD'
_diffrn_measurement_method        '\w and \f
scans'
_diffrn_detector_area_resol_mean  ?
_diffrn_standards_number          ?
_diffrn_standards_interval_count  ?
_diffrn_standards_interval_time   ?
_diffrn_standards_decay_%         ?
_diffrn_reflns_number             6672
_diffrn_reflns_av_R_equivalents   0.0276
_diffrn_reflns_av_sigmaI/netI     0.0205
_diffrn_reflns_limit_h_min        0
_diffrn_reflns_limit_h_max        7
_diffrn_reflns_limit_k_min        -4
_diffrn_reflns_limit_k_max        5
_diffrn_reflns_limit_l_min        0
_diffrn_reflns_limit_l_max        42
_diffrn_reflns_theta_min          3.11
_diffrn_reflns_theta_max          36.47
_reflns_number_total              424
_reflns_number_gt                 398
_reflns_threshold_expression      I>2\s(I)

_computing_data_collection        ?
_computing_cell_refinement        ?
_computing_data_reduction         ?
_computing_structure_solution     ?
_computing_structure_refinement   'SHELXL-97
(Sheldrick, 2008)'
_computing_molecular_graphics     ?
_computing_publication_material   ?

_refine_special_details
;
 Refinement of F^2^ against ALL reflections.
The weighted R-factor wR and
 goodness of fit S are based on F^2^,
conventional R-factors R are based
 on F, with F set to zero for negative F^2^.
The threshold expression of
 F^2^ > 2\s(F^2^) is used only for
calculating R-factors(gt) etc. and is
 not relevant to the choice of reflections
for refinement.  R-factors based
 on F^2^ are statistically about twice as
large as those based on F, and R-
 factors based on ALL data will be even
larger.
;

_refine_ls_structure_factor_coef  Fsqd
_refine_ls_matrix_type            full
_refine_ls_weighting_scheme       calc
_refine_ls_weighting_details
 'calc
w=1/[\s^2^(Fo^2^)+(0.0595P)^2^+38.9398P]
where P=(Fo^2^+2Fc^2^)/3'
_atom_sites_solution_primary      direct
_atom_sites_solution_secondary    difmap
_atom_sites_solution_hydrogens    ?
_refine_ls_hydrogen_treatment     ?
_refine_ls_extinction_method      SHELXL
_refine_ls_extinction_coef        0.0019(4)
_refine_ls_extinction_expression
 'Fc^*^=kFc[1+0.001xFc^2^\l^3^/sin(2\q)]^-
1/4^'
_refine_ls_number_reflns          424
_refine_ls_number_parameters      22
_refine_ls_number_restraints      0
_refine_ls_R_factor_all           0.0491
_refine_ls_R_factor_gt            0.0457
_refine_ls_wR_factor_ref          0.1210
_refine_ls_wR_factor_gt           0.1183
_refine_ls_goodness_of_fit_ref    1.139
_refine_ls_restrained_S_all       1.139
_refine_ls_shift/su_max           0.000
_refine_ls_shift/su_mean          0.000

loop_
 _atom_site_label
 _atom_site_type_symbol
 _atom_site_fract_x
 _atom_site_fract_y
 _atom_site_fract_z
 _atom_site_U_iso_or_equiv
 _atom_site_adp_type
 _atom_site_occupancy
 _atom_site_symmetry_multiplicity
 _atom_site_calc_flag
 _atom_site_refinement_flags
 _atom_site_disorder_assembly
 _atom_site_disorder_group
La1 La 0.0000 0.0000 0.34800(4) 0.0102(3)
Uani 1 8 d S . .
Fe1 Fe 0.0000 0.0000 0.0000 0.0150(7) Uani 1
16 d S . .
Fe2 Fe 0.0000 0.5000 0.45039(10) 0.0291(12)
Uani 0.759(14) 4 d SP . .
Sb1 Sb 0.0000 0.5000 0.2500 0.0088(3) Uani 1
8 d S . .
Sb2 Sb 0.0000 0.0000 0.10768(4) 0.0104(3)
Uani 1 8 d S . .
Sb3 Sb 0.0000 0.0788(11) 0.5000 0.0298(17)
Uani 0.235(5) 4 d SP . .

loop_
 _atom_site_aniso_label
 _atom_site_aniso_U_11
 _atom_site_aniso_U_22
 _atom_site_aniso_U_33
 _atom_site_aniso_U_23
 _atom_site_aniso_U_13
 _atom_site_aniso_U_12
La1 0.0108(3) 0.0108(3) 0.0091(4) 0.000
0.000 0.000
```

```
Fe1 0.0178(11) 0.0178(11) 0.0092(13) 0.000
0.000 0.000
Fe2 0.0144(14) 0.064(3) 0.0088(11) 0.000
0.000 0.000
Sb1 0.0099(3) 0.0099(3) 0.0066(4) 0.000
0.000 0.000
Sb2 0.0105(3) 0.0105(3) 0.0100(5) 0.000
0.000 0.000
Sb3 0.021(2) 0.023(3) 0.046(2) 0.000 0.000
0.000

_geom_special_details
;
 All s.u.'s (except the s.u. in the dihedral
angle between two l.s. planes)
 are estimated using the full covariance
matrix.  The cell s.u.'s are taken
 into account individually in the estimation
of s.u.'s in distances, angles
 and torsion angles; correlations between
s.u.'s in cell parameters are only
 used when they are defined by crystal
symmetry.  An approximate (isotropic)
 treatment of cell s.u.'s is used for
estimating s.u.'s involving l.s. planes.
;

loop_
 _geom_bond_atom_site_label_1
 _geom_bond_atom_site_label_2
 _geom_bond_distance
 _geom_bond_site_symmetry_2
 _geom_bond_publ_flag
La1 Sb2 3.2893(11) 25 ?
La1 Sb2 3.2893(11) 25_445 ?
La1 Sb2 3.2893(11) 25_455 ?
La1 Sb2 3.2893(11) 25_545 ?
La1 Sb1 3.3657(10) 25_455 ?
La1 Sb1 3.3657(10) 1_545 ?
La1 Sb1 3.3657(11) . ?
La1 Sb1 3.3657(11) 25 ?
La1 Fe2 3.454(2) . ?
La1 Fe2 3.454(2) 21 ?
La1 Fe2 3.454(2) 21_455 ?
La1 Fe2 3.454(2) 1_545 ?
Fe1 Fe2 2.5348(15) 29_444 ?
Fe1 Fe2 2.5348(15) 13 ?
Fe1 Fe2 2.5348(15) 9_444 ?
Fe1 Fe2 2.5348(15) 25 ?
Fe1 Fe2 2.5348(15) 29_454 ?
Fe1 Fe2 2.5348(15) 25_455 ?
Fe1 Fe2 2.5348(15) 13_545 ?
Fe1 Fe2 2.5348(15) 9_544 ?
Fe1 Sb2 2.8215(14) 17 ?
Fe1 Sb2 2.8215(14) . ?
Fe1 Sb3 2.845(3) 13 ?
Fe1 Sb3 2.845(3) 25 ?
Fe2 Sb3 2.247(4) 17_566 ?
Fe2 Sb3 2.247(4) . ?
Fe2 Fe1 2.5348(15) 9 ?
Fe2 Fe1 2.5348(15) 9_455 ?
Fe2 Sb3 2.5579(17) 21_565 ?
Fe2 Sb3 2.5579(17) 5_566 ?
Fe2 Sb3 2.5579(17) 5_556 ?
Fe2 Sb3 2.5579(16) 21 ?
Fe2 Fe2 2.600(5) 17_566 ?
Fe2 Sb2 2.6553(18) 25_455 ?
Fe2 Sb2 2.6553(18) 25 ?
Fe2 Sb3 2.835(5) 1_565 ?
Sb1 Sb1 3.0775(11) 25_565 ?
Sb1 Sb1 3.0775(11) 25_455 ?
Sb1 Sb1 3.0775(11) 25_465 ?
Sb1 Sb1 3.0775(11) 25 ?
Sb1 La1 3.3657(10) 25_455 ?
Sb1 La1 3.3657(10) 1_565 ?
Sb1 La1 3.3657(10) 25 ?
Sb2 Fe2 2.6553(18) 13_545 ?
Sb2 Fe2 2.6553(18) 25_455 ?
Sb2 Fe2 2.6553(18) 13 ?
Sb2 Fe2 2.6553(18) 25 ?
Sb2 La1 3.2893(11) 25 ?
Sb2 La1 3.2893(11) 25_445 ?
Sb2 La1 3.2893(11) 25_545 ?
Sb2 La1 3.2893(11) 25_455 ?
Sb3 Sb3 0.485(7) 5_556 ?
Sb3 Sb3 0.485(7) 21 ?
Sb3 Sb3 0.686(10) 17_556 ?
Sb3 Fe2 2.247(4) 17_566 ?
Sb3 Fe2 2.5579(16) 21_455 ?
Sb3 Fe2 2.5579(16) 5_656 ?
Sb3 Fe2 2.5579(16) 5_556 ?
Sb3 Fe2 2.5579(16) 21 ?
Sb3 Fe2 2.835(5) 1_545 ?
Sb3 Fe2 2.835(5) 17_556 ?
Sb3 Fe1 2.845(3) 9 ?

loop_
 _geom_angle_atom_site_label_1
 _geom_angle_atom_site_label_2
 _geom_angle_atom_site_label_3
 _geom_angle
 _geom_angle_site_symmetry_1
 _geom_angle_site_symmetry_3
 _geom_angle_publ_flag
Sb2 La1 Sb2 138.65(5) 25 25_445 ?
Sb2 La1 Sb2 82.840(16) 25 25_455 ?
Sb2 La1 Sb2 82.840(16) 25_445 25_455 ?
Sb2 La1 Sb2 82.840(16) 25 25_545 ?
Sb2 La1 Sb2 82.840(16) 25_445 25_545 ?
Sb2 La1 Sb2 138.65(5) 25_455 25_545 ?
Sb2 La1 Sb1 134.19(2) 25 25_455 ?
Sb2 La1 Sb1 80.89(2) 25_445 25_455 ?
Sb2 La1 Sb1 80.89(2) 25_455 25_455 ?
Sb2 La1 Sb1 134.19(2) 25_545 25_455 ?
Sb2 La1 Sb1 134.19(2) 25 1_545 ?
Sb2 La1 Sb1 80.89(2) 25_445 1_545 ?
Sb2 La1 Sb1 134.19(2) 25_455 1_545 ?
Sb2 La1 Sb1 80.89(2) 25_545 1_545 ?
Sb1 La1 Sb1 54.41(2) 25_455 1_545 ?
Sb2 La1 Sb1 80.89(2) 25 . ?
Sb2 La1 Sb1 134.19(2) 25_445 . ?
Sb2 La1 Sb1 80.89(2) 25_455 . ?
Sb2 La1 Sb1 134.19(2) 25_545 . ?
Sb1 La1 Sb1 54.41(2) 25_455 . ?
Sb1 La1 Sb1 80.56(3) 1_545 . ?
Sb2 La1 Sb1 80.89(2) 25 25 ?
Sb2 La1 Sb1 134.19(2) 25_445 25 ?
Sb2 La1 Sb1 134.19(2) 25_455 25 ?
Sb2 La1 Sb1 80.89(2) 25_545 25 ?
Sb1 La1 Sb1 80.56(3) 25_455 25 ?
Sb1 La1 Sb1 54.41(2) 1_545 25 ?
Sb1 La1 Sb1 54.41(2) . 25 ?
Sb2 La1 Fe2 46.30(2) 25 . ?
Sb2 La1 Fe2 98.20(4) 25_445 . ?
Sb2 La1 Fe2 46.30(2) 25_455 . ?
Sb2 La1 Fe2 98.20(4) 25_545 . ?
Sb1 La1 Fe2 126.33(2) 25_455 . ?
Sb1 La1 Fe2 178.77(3) 1_545 . ?
Sb1 La1 Fe2 100.67(4) . . ?
Sb1 La1 Fe2 126.33(2) 25 . ?
Sb2 La1 Fe2 46.30(2) 25 21 ?
Sb2 La1 Fe2 98.20(4) 25_445 21 ?
```

```
Sb2 La1 Fe2 98.20(4) 25_455 21 ?
Sb2 La1 Fe2 46.30(2) 25_545 21 ?
Sb1 La1 Fe2 178.77(3) 25_455 21 ?
Sb1 La1 Fe2 126.33(2) 1_545 21 ?
Sb1 La1 Fe2 126.33(2) . 21 ?
Sb1 La1 Fe2 100.67(4) 25 21 ?
Fe2 La1 Fe2 52.90(4) . 21 ?
Sb2 La1 Fe2 98.20(4) 25 21_455 ?
Sb2 La1 Fe2 46.30(2) 25_445 21_455 ?
Sb2 La1 Fe2 46.30(2) 25_455 21_455 ?
Sb2 La1 Fe2 98.20(4) 25_545 21_455 ?
Sb1 La1 Fe2 100.67(4) 25_455 21_455 ?
Sb1 La1 Fe2 126.33(2) 1_545 21_455 ?
Sb1 La1 Fe2 126.33(2) . 21_455 ?
Sb1 La1 Fe2 178.77(3) 25 21_455 ?
Fe2 La1 Fe2 52.90(4) . 21_455 ?
Fe2 La1 Fe2 78.09(6) 21 21_455 ?
Sb2 La1 Fe2 98.20(4) 25 1_545 ?
Sb2 La1 Fe2 46.30(2) 25_445 1_545 ?
Sb2 La1 Fe2 98.20(4) 25_455 1_545 ?
Sb2 La1 Fe2 46.30(2) 25_545 1_545 ?
Sb1 La1 Fe2 126.33(2) 25_455 1_545 ?
Sb1 La1 Fe2 100.67(4) 1_545 1_545 ?
Sb1 La1 Fe2 178.77(3) . 1_545 ?
Sb1 La1 Fe2 126.33(2) 25 1_545 ?
Fe2 La1 Fe2 78.09(6) . 1_545 ?
Fe2 La1 Fe2 52.90(4) 21 1_545 ?
Fe2 La1 Fe2 52.90(4) 21_455 1_545 ?
Fe2 Fe1 Fe2 180.00(10) 29_444 13 ?
Fe2 Fe1 Fe2 74.75(5) 29_444 9_444 ?
Fe2 Fe1 Fe2 105.25(5) 13 9_444 ?
Fe2 Fe1 Fe2 105.25(5) 29_444 25 ?
Fe2 Fe1 Fe2 74.75(5) 13 25 ?
Fe2 Fe1 Fe2 180.00(10) 9_444 25 ?
Fe2 Fe1 Fe2 118.29(10) 29_444 29_454 ?
Fe2 Fe1 Fe2 61.71(10) 13 29_454 ?
Fe2 Fe1 Fe2 74.75(5) 9_444 29_454 ?
Fe2 Fe1 Fe2 105.25(5) 25 29_454 ?
Fe2 Fe1 Fe2 105.25(5) 29_444 25_455 ?
Fe2 Fe1 Fe2 74.75(5) 13 25_455 ?
Fe2 Fe1 Fe2 61.71(10) 9_444 25_455 ?
Fe2 Fe1 Fe2 118.29(10) 25 25_455 ?
Fe2 Fe1 Fe2 105.25(5) 29_454 25_455 ?
Fe2 Fe1 Fe2 61.71(10) 29_444 13_545 ?
Fe2 Fe1 Fe2 118.29(10) 13 13_545 ?
Fe2 Fe1 Fe2 105.25(5) 9_444 13_545 ?
Fe2 Fe1 Fe2 74.75(5) 25 13_545 ?
Fe2 Fe1 Fe2 180.00(10) 29_454 13_545 ?
Fe2 Fe1 Fe2 74.75(5) 25_455 13_545 ?
Fe2 Fe1 Fe2 74.75(5) 29_444 9_544 ?
Fe2 Fe1 Fe2 105.25(5) 13 9_544 ?
Fe2 Fe1 Fe2 118.29(10) 9_444 9_544 ?
Fe2 Fe1 Fe2 61.71(10) 25 9_544 ?
Fe2 Fe1 Fe2 74.75(5) 29_454 9_544 ?
Fe2 Fe1 Fe2 180.00(10) 25_455 9_544 ?
Fe2 Fe1 Fe2 105.25(5) 13_545 9_544 ?
Fe2 Fe1 Sb2 59.15(5) 29_444 17 ?
Fe2 Fe1 Sb2 120.85(5) 13 17 ?
Fe2 Fe1 Sb2 59.15(5) 9_444 17 ?
Fe2 Fe1 Sb2 120.85(5) 25 17 ?
Fe2 Fe1 Sb2 59.15(5) 29_454 17 ?
Fe2 Fe1 Sb2 120.85(5) 25_455 17 ?
Fe2 Fe1 Sb2 120.85(5) 13_545 17 ?
Fe2 Fe1 Sb2 59.15(5) 9_544 17 ?
Fe2 Fe1 Sb2 120.85(5) 29_444 . ?
Fe2 Fe1 Sb2 59.15(5) 13 . ?
Fe2 Fe1 Sb2 120.85(5) 9_444 . ?
Fe2 Fe1 Sb2 59.15(5) 25 . ?
Fe2 Fe1 Sb2 120.85(5) 29_454 . ?
Fe2 Fe1 Sb2 59.15(5) 25_455 . ?
Fe2 Fe1 Sb2 59.15(5) 13_545 . ?
Fe2 Fe1 Sb2 120.85(5) 9_544 . ?
Sb2 Fe1 Sb2 180.0 17 . ?
Fe2 Fe1 Sb3 131.04(6) 29_444 13 ?
Fe2 Fe1 Sb3 48.96(6) 13 13 ?
Fe2 Fe1 Sb3 123.58(6) 9_444 13 ?
Fe2 Fe1 Sb3 56.42(6) 25 13 ?
Fe2 Fe1 Sb3 48.96(6) 29_454 13 ?
Fe2 Fe1 Sb3 123.58(6) 25_455 13 ?
Fe2 Fe1 Sb3 131.04(6) 13_545 13 ?
Fe2 Fe1 Sb3 56.42(6) 9_544 13 ?
Sb2 Fe1 Sb3 90.0 17 13 ?
Sb2 Fe1 Sb3 90.0 . 13 ?
Fe2 Fe1 Sb3 123.58(6) 29_444 25 ?
Fe2 Fe1 Sb3 56.42(6) 13 25 ?
Fe2 Fe1 Sb3 131.04(6) 9_444 25 ?
Fe2 Fe1 Sb3 48.96(6) 25 25 ?
Fe2 Fe1 Sb3 56.42(6) 29_454 25 ?
Fe2 Fe1 Sb3 131.04(6) 25_455 25 ?
Fe2 Fe1 Sb3 123.58(6) 13_545 25 ?
Fe2 Fe1 Sb3 48.96(6) 9_544 25 ?
Sb2 Fe1 Sb3 90.0 17 25 ?
Sb2 Fe1 Sb3 90.0 . 25 ?
Sb3 Fe1 Sb3 9.78(15) 13 25 ?
Sb3 Fe2 Sb3 109.32(18) 17_566 . ?
Sb3 Fe2 Fe1 72.74(6) 17_566 9 ?
Sb3 Fe2 Fe1 72.74(6) . 9 ?
Sb3 Fe2 Fe1 72.74(6) 17_566 9_455 ?
Sb3 Fe2 Fe1 72.74(6) . 9_455 ?
Fe1 Fe2 Fe1 118.29(10) 9 9_455 ?
Sb3 Fe2 Sb3 8.91(13) 17_566 21_565 ?
Sb3 Fe2 Sb3 113.58(13) . 21_565 ?
Fe1 Fe2 Sb3 67.93(11) 9 21_565 ?
Fe1 Fe2 Sb3 81.63(11) 9_455 21_565 ?
Sb3 Fe2 Sb3 8.91(13) 17_566 5_566 ?
Sb3 Fe2 Sb3 113.58(13) . 5_566 ?
Fe1 Fe2 Sb3 81.63(11) 9 5_566 ?
Fe1 Fe2 Sb3 67.93(10) 9_455 5_566 ?
Sb3 Fe2 Sb3 15.4(2) 21_565 5_566 ?
Sb3 Fe2 Sb3 113.58(13) 17_566 5_556 ?
Sb3 Fe2 Sb3 8.91(13) . 5_556 ?
Fe1 Fe2 Sb3 81.63(11) 9 5_556 ?
Fe1 Fe2 Sb3 67.93(11) 9_455 5_556 ?
Sb3 Fe2 Sb3 118.91(10) 21_565 5_556 ?
Sb3 Fe2 Sb3 116.58(11) 5_566 5_556 ?
Sb3 Fe2 Sb3 113.58(13) 17_566 21 ?
Sb3 Fe2 Sb3 8.91(13) . 21 ?
Fe1 Fe2 Sb3 67.93(10) 9 21 ?
Fe1 Fe2 Sb3 81.63(11) 9_455 21 ?
Sb3 Fe2 Sb3 116.58(11) 21_565 21 ?
Sb3 Fe2 Sb3 118.91(10) 5_566 21 ?
Sb3 Fe2 Sb3 15.4(2) 5_556 21 ?
Sb3 Fe2 Fe2 54.66(9) 17_566 17_566 ?
Sb3 Fe2 Fe2 54.66(9) . 17_566 ?
Fe1 Fe2 Fe2 59.15(5) 9 17_566 ?
Fe1 Fe2 Fe2 59.15(5) 9_455 17_566 ?
Sb3 Fe2 Fe2 59.46(5) 21_565 17_566 ?
Sb3 Fe2 Fe2 59.46(5) 5_566 17_566 ?
Sb3 Fe2 Fe2 59.46(5) 5_556 17_566 ?
Sb3 Fe2 Fe2 59.46(5) 21 17_566 ?
Sb3 Fe2 Sb2 109.36(4) 17_566 25_455 ?
Sb3 Fe2 Sb2 109.36(4) . 25_455 ?
Fe1 Fe2 Sb2 175.89(10) 9 25_455 ?
Fe1 Fe2 Sb2 65.81(3) 9_455 25_455 ?
Sb3 Fe2 Sb2 113.65(9) 21_565 25_455 ?
Sb3 Fe2 Sb2 100.45(10) 5_566 25_455 ?
Sb3 Fe2 Sb2 100.45(10) 5_556 25_455 ?
Sb3 Fe2 Sb2 113.65(9) 21 25_455 ?
Fe2 Fe2 Sb2 124.96(5) 17_566 25_455 ?
Sb3 Fe2 Sb2 109.36(4) 17_566 25 ?
Sb3 Fe2 Sb2 109.36(4) . 25 ?
Fe1 Fe2 Sb2 65.81(3) 9 25 ?
```

```
Fe1 Fe2 Sb2 175.89(10) 9_455 25 ?
Sb3 Fe2 Sb2 100.45(10) 21_565 25 ?
Sb3 Fe2 Sb2 113.65(9) 5_566 25 ?
Sb3 Fe2 Sb2 113.65(9) 5_556 25 ?
Sb3 Fe2 Sb2 100.45(10) 21 25 ?
Fe2 Fe2 Sb2 124.96(5) 17_566 25 ?
Sb2 Fe2 Sb2 110.08(10) 25_455 25 ?
Sb3 Fe2 Sb3 8.05(12) 17_566 1_565 ?
Sb3 Fe2 Sb3 117.36(11) . 1_565 ?
Fe1 Fe2 Sb3 76.40(5) 9 1_565 ?
Fe1 Fe2 Sb3 76.40(5) 9_455 1_565 ?
Sb3 Fe2 Sb3 8.48(12) 21_565 1_565 ?
Sb3 Fe2 Sb3 8.48(12) 5_566 1_565 ?
Sb3 Fe2 Sb3 121.53(10) 5_556 1_565 ?
Sb3 Fe2 Sb3 121.53(10) 21 1_565 ?
Fe2 Fe2 Sb3 62.70(7) 17_566 1_565 ?
Sb2 Fe2 Sb3 105.23(3) 25_455 1_565 ?
Sb2 Fe2 Sb3 105.23(3) 25 1_565 ?
Sb1 Sb1 Sb1 180.0 25_565 25_455 ?
Sb1 Sb1 Sb1 90.0 25_565 25_465 ?
Sb1 Sb1 Sb1 90.0 25_455 25_465 ?
Sb1 Sb1 Sb1 90.0 25_565 25 ?
Sb1 Sb1 Sb1 90.0 25_455 25 ?
Sb1 Sb1 Sb1 180.0 25_465 25 ?
Sb1 Sb1 La1 117.205(10) 25_565 25_455 ?
Sb1 Sb1 La1 62.795(10) 25_455 25_455 ?
Sb1 Sb1 La1 62.795(10) 25_465 25_455 ?
Sb1 Sb1 La1 117.205(10) 25 25_455 ?
Sb1 Sb1 La1 62.795(10) 25_565 1_565 ?
Sb1 Sb1 La1 117.205(10) 25_455 1_565 ?
Sb1 Sb1 La1 62.795(10) 25_465 1_565 ?
Sb1 Sb1 La1 117.205(10) 25 1_565 ?
La1 Sb1 La1 125.59(2) 25_455 1_565 ?
Sb1 Sb1 La1 62.795(10) 25_565 25 ?
Sb1 Sb1 La1 117.205(10) 25_455 25 ?
Sb1 Sb1 La1 117.205(10) 25_465 25 ?
Sb1 Sb1 La1 62.795(10) 25 25 ?
La1 Sb1 La1 80.56(3) 25_455 25 ?
La1 Sb1 La1 125.59(2) 1_565 25 ?
Sb1 Sb1 La1 117.205(10) 25_565 . ?
Sb1 Sb1 La1 62.795(10) 25_455 . ?
Sb1 Sb1 La1 117.205(10) 25_465 . ?
Sb1 Sb1 La1 62.795(10) 25 . ?
La1 Sb1 La1 125.59(2) 25_455 . ?
La1 Sb1 La1 80.56(3) 1_565 . ?
La1 Sb1 La1 125.59(2) 25 . ?
Fe2 Sb2 Fe2 70.83(5) 13_545 25_455 ?
Fe2 Sb2 Fe2 110.08(10) 13_545 13 ?
Fe2 Sb2 Fe2 70.83(5) 25_455 13 ?
Fe2 Sb2 Fe2 70.83(5) 13_545 25 ?
Fe2 Sb2 Fe2 110.08(10) 25_455 25 ?
Fe2 Sb2 Fe2 70.83(5) 13 25 ?
Fe2 Sb2 Fe1 55.04(5) 13_545 . ?
Fe2 Sb2 Fe1 55.04(5) 25_455 . ?
Fe2 Sb2 Fe1 55.04(5) 13 . ?
Fe2 Sb2 Fe1 55.04(5) 25 . ?
Fe2 Sb2 La1 138.115(16) 13_545 25 ?
Fe2 Sb2 La1 138.115(16) 25_455 25 ?
Fe2 Sb2 La1 70.13(4) 13 25 ?
Fe2 Sb2 La1 70.13(4) 25 25 ?
Fe1 Sb2 La1 110.67(2) . 25 ?
Fe2 Sb2 La1 70.13(4) 13_545 25_445 ?
Fe2 Sb2 La1 70.13(4) 25_455 25_445 ?
Fe2 Sb2 La1 138.115(16) 13 25_445 ?
Fe2 Sb2 La1 138.115(16) 25 25_445 ?
Fe1 Sb2 La1 110.67(2) . 25_445 ?
La1 Sb2 La1 138.65(5) 25 25_445 ?
Fe2 Sb2 La1 70.13(4) 13_545 25_545 ?
Fe2 Sb2 La1 138.115(16) 25_455 25_545 ?
Fe2 Sb2 La1 138.115(16) 13 25_545 ?
Fe2 Sb2 La1 70.13(4) 25 25_545 ?
Fe1 Sb2 La1 110.67(2) . 25_545 ?
La1 Sb2 La1 82.840(16) 25 25_545 ?
La1 Sb2 La1 82.840(16) 25_445 25_545 ?
Fe2 Sb2 La1 138.115(16) 13_545 25_455 ?
Fe2 Sb2 La1 70.13(4) 25_455 25_455 ?
Fe2 Sb2 La1 70.13(4) 13 25_455 ?
Fe2 Sb2 La1 138.115(16) 25 25_455 ?
Fe1 Sb2 La1 110.67(2) . 25_455 ?
La1 Sb2 La1 82.840(16) 25 25_455 ?
La1 Sb2 La1 82.840(16) 25_445 25_455 ?
La1 Sb2 La1 138.65(5) 25_545 25_455 ?
Sb3 Sb3 Sb3 90.000(7) 5_556 21 ?
Sb3 Sb3 Sb3 45.000(4) 5_556 17_556 ?
Sb3 Sb3 Sb3 45.000(11) 21 17_556 ?
Sb3 Sb3 Fe2 125.23(5) 5_556 17_566 ?
Sb3 Sb3 Fe2 125.23(5) 21 17_566 ?
Sb3 Sb3 Fe2 144.66(9) 17_556 17_566 ?
Sb3 Sb3 Fe2 125.23(5) 5_556 . ?
Sb3 Sb3 Fe2 125.23(5) 21 . ?
Sb3 Sb3 Fe2 144.66(9) 17_556 . ?
Fe2 Sb3 Fe2 70.68(18) 17_566 . ?
Sb3 Sb3 Fe2 45.86(10) 5_556 21_455 ?
Sb3 Sb3 Fe2 120.45(9) 21 21_455 ?
Sb3 Sb3 Fe2 82.29(11) 17_556 21_455 ?
Fe2 Sb3 Fe2 113.79(13) 17_566 21_455 ?
Fe2 Sb3 Fe2 79.36(8) . 21_455 ?
Sb3 Sb3 Fe2 120.45(10) 5_556 5_656 ?
Sb3 Sb3 Fe2 45.86(10) 21 5_656 ?
Sb3 Sb3 Fe2 82.29(10) 17_556 5_656 ?
Fe2 Sb3 Fe2 79.36(8) 17_566 5_656 ?
Fe2 Sb3 Fe2 113.79(13) . 5_656 ?
Fe2 Sb3 Fe2 164.6(2) 21_455 5_656 ?
Sb3 Sb3 Fe2 45.86(10) 5_556 5_556 ?
Sb3 Sb3 Fe2 120.45(9) 21 5_556 ?
Sb3 Sb3 Fe2 82.29(11) 17_556 5_556 ?
Fe2 Sb3 Fe2 79.36(8) 17_566 5_556 ?
Fe2 Sb3 Fe2 113.79(13) . 5_556 ?
Fe2 Sb3 Fe2 61.09(10) 21_455 5_556 ?
Fe2 Sb3 Fe2 116.58(11) 5_656 5_556 ?
Sb3 Sb3 Fe2 120.45(10) 5_556 21 ?
Sb3 Sb3 Fe2 45.86(10) 21 21 ?
Sb3 Sb3 Fe2 82.29(10) 17_556 21 ?
Fe2 Sb3 Fe2 113.79(13) 17_566 21 ?
Fe2 Sb3 Fe2 79.36(8) . 21 ?
Fe2 Sb3 Fe2 116.58(11) 21_455 21 ?
Fe2 Sb3 Fe2 61.09(10) 5_656 21 ?
Fe2 Sb3 Fe2 164.6(2) 5_556 21 ?
Sb3 Sb3 Fe2 51.07(3) 5_556 1_545 ?
Sb3 Sb3 Fe2 51.07(2) 21 1_545 ?
Sb3 Sb3 Fe2 27.30(7) 17_556 1_545 ?
Fe2 Sb3 Fe2 171.95(12) 17_566 1_545 ?
Fe2 Sb3 Fe2 117.36(11) . 1_545 ?
Fe2 Sb3 Fe2 69.38(9) 21_455 1_545 ?
Fe2 Sb3 Fe2 96.54(13) 5_656 1_545 ?
Fe2 Sb3 Fe2 96.54(13) 5_556 1_545 ?
Fe2 Sb3 Fe2 69.38(9) 21 1_545 ?
Sb3 Sb3 Fe2 51.07(3) 5_556 17_556 ?
Sb3 Sb3 Fe2 51.07(2) 21 17_556 ?
Sb3 Sb3 Fe2 27.30(7) 17_556 17_556 ?
Fe2 Sb3 Fe2 117.36(11) 17_566 17_556 ?
Fe2 Sb3 Fe2 171.95(12) . 17_556 ?
Fe2 Sb3 Fe2 96.54(13) 21_455 17_556 ?
Fe2 Sb3 Fe2 69.38(9) 5_656 17_556 ?
Fe2 Sb3 Fe2 69.38(9) 5_556 17_556 ?
Fe2 Sb3 Fe2 96.54(13) 21 17_556 ?
Fe2 Sb3 Fe2 54.59(13) 1_545 17_556 ?
Sb3 Sb3 Fe1 175.11(8) 5_556 9 ?
Sb3 Sb3 Fe1 85.11(8) 21 9 ?
Sb3 Sb3 Fe1 130.11(7) 17_556 9 ?
Fe2 Sb3 Fe1 58.30(9) 17_566 9 ?
Fe2 Sb3 Fe1 58.30(9) . 9 ?
```

```
Fe2 Sb3 Fe1 137.48(14) 21_455 9 ?
Fe2 Sb3 Fe1 55.65(4) 5_656 9 ?
Fe2 Sb3 Fe1 137.48(14) 5_556 9 ?
Fe2 Sb3 Fe1 55.65(4) 21 9 ?
Fe2 Sb3 Fe1 124.93(5) 1_545 9 ?
Fe2 Sb3 Fe1 124.93(5) 17_556 9 ?

_diffrn_measured_fraction_theta_max    0.988
_diffrn_reflns_theta_full              36.47
_diffrn_measured_fraction_theta_full   0.988
_refine_diff_density_max    6.319
_refine_diff_density_min   -2.706
_refine_diff_density_rms    0.637

#===END
```

A1.6 $Ce_2Fe_4Sb_5$

```
data_shelxl

_audit_creation_method            SHELXL-97
_chemical_name_systematic
;
 ?
;
_chemical_name_common             ?
_chemical_melting_point           ?
_chemical_formula_moiety          'Ce2
Fe3.98 Sb4.93'
_chemical_formula_sum
 'Ce2 Fe3.98 Sb4.93'
_chemical_formula_weight          1101.86

loop_
 _atom_type_symbol
 _atom_type_description
 _atom_type_scat_dispersion_real
 _atom_type_scat_dispersion_imag
 _atom_type_scat_source
 'Ce'  'Ce'  -0.2486   2.6331
 'International Tables Vol C Tables 4.2.6.8
and 6.1.1.4'
 'Fe'  'Fe'   0.3463   0.8444
 'International Tables Vol C Tables 4.2.6.8
and 6.1.1.4'
 'Sb'  'Sb'  -0.5866   1.5461
 'International Tables Vol C Tables 4.2.6.8
and 6.1.1.4'

_symmetry_cell_setting
'Tetragonal'
_symmetry_space_group_name_H-M    'I 4/m m m
'

loop_
 _symmetry_equiv_pos_as_xyz
 'x, y, z'
 '-x, -y, z'
 'x, -y, -z'
 '-x, y, -z'
 '-y, -x, -z'
 'y, x, -z'
 'y, -x, z'
 '-y, x, z'
 'x+1/2, y+1/2, z+1/2'
 '-x+1/2, -y+1/2, z+1/2'
 'x+1/2, -y+1/2, -z+1/2'
 '-x+1/2, y+1/2, -z+1/2'
 '-y+1/2, -x+1/2, -z+1/2'
 'y+1/2, x+1/2, -z+1/2'
 'y+1/2, -x+1/2, z+1/2'
 '-y+1/2, x+1/2, z+1/2'
 '-x, -y, -z'
 'x, y, -z'
 '-x, y, z'
 'x, -y, z'
 'y, x, z'
 '-y, -x, z'
 '-y, x, -z'
 'y, -x, -z'
 '-x+1/2, -y+1/2, -z+1/2'
 'x+1/2, y+1/2, -z+1/2'
 '-x+1/2, y+1/2, z+1/2'
 'x+1/2, -y+1/2, z+1/2'
 'y+1/2, x+1/2, z+1/2'
 '-y+1/2, -x+1/2, z+1/2'
 '-y+1/2, x+1/2, -z+1/2'
 'y+1/2, -x+1/2, -z+1/2'

_cell_length_a                    4.3237(15)
_cell_length_b                    4.3237(15)
_cell_length_c                    25.998(2)
_cell_angle_alpha                 90
_cell_angle_beta                  90
_cell_angle_gamma                 90
_cell_volume                      486.0(2)
_cell_formula_units_Z             2
_cell_measurement_temperature     298(2)
_cell_measurement_reflns_used     585
_cell_measurement_theta_min       2.6
_cell_measurement_theta_max       37.0

_exptl_crystal_description        plate
_exptl_crystal_colour             black
_exptl_crystal_size_max           0.08
_exptl_crystal_size_mid           0.05
_exptl_crystal_size_min           0.03
_exptl_crystal_density_meas       ?
_exptl_crystal_density_diffrn     7.529
_exptl_crystal_density_method     'not
measured'
_exptl_crystal_F_000              941
_exptl_absorpt_coefficient_mu     28.261
_exptl_absorpt_correction_type    'multi-
scan'
_exptl_absorpt_correction_T_min   0.2257
_exptl_absorpt_correction_T_max   0.5385
_exptl_absorpt_process_details    'HKL
Scalepack (Otwinowski & Minor 1997)'
_exptl_special_details
;
 ?
;

_diffrn_ambient_temperature       298(2)
_diffrn_radiation_wavelength      0.71073
_diffrn_radiation_type            MoK\a
_diffrn_radiation_source          'fine-
focus sealed tube'
_diffrn_radiation_monochromator   graphite
_diffrn_measurement_device_type   'Nonius
KappaCCD'
_diffrn_measurement_method        '\w and \f
scans'
_diffrn_detector_area_resol_mean  ?
_diffrn_standards_number          ?
_diffrn_standards_interval_count  ?
_diffrn_standards_interval_time   ?
_diffrn_standards_decay_%         ?
_diffrn_reflns_number             6745
_diffrn_reflns_av_R_equivalents   0.0245
_diffrn_reflns_av_sigmaI/netI     0.0225
```

```
_diffrn_reflns_limit_h_min        0
_diffrn_reflns_limit_h_max        7
_diffrn_reflns_limit_k_min        -4
_diffrn_reflns_limit_k_max        5
_diffrn_reflns_limit_l_min        0
_diffrn_reflns_limit_l_max        43
_diffrn_reflns_theta_min          3.13
_diffrn_reflns_theta_max          36.83
_reflns_number_total              418
_reflns_number_gt                 375
_reflns_threshold_expression      I>2\s(I)

_computing_data_collection        ?
_computing_cell_refinement        ?
_computing_data_reduction         ?
_computing_structure_solution     ?
_computing_structure_refinement   'SHELXL-97
(Sheldrick, 2008)'
_computing_molecular_graphics     ?
_computing_publication_material   ?

_refine_special_details
;
 Refinement of F^2^ against ALL reflections.
The weighted R-factor wR and
 goodness of fit S are based on F^2^,
conventional R-factors R are based
 on F, with F set to zero for negative F^2^.
The threshold expression of
 F^2^ > 2\s(F^2^) is used only for
calculating R-factors(gt) etc. and is
 not relevant to the choice of reflections
for refinement.  R-factors based
 on F^2^ are statistically about twice as
large as those based on F, and R-
 factors based on ALL data will be even
larger.
;

_refine_ls_structure_factor_coef  Fsqd
_refine_ls_matrix_type            full
_refine_ls_weighting_scheme       calc
_refine_ls_weighting_details
 'calc
w=1/[\s^2^(Fo^2^)+(0.0491P)^2^+25.9981P]
where P=(Fo^2^+2Fc^2^)/3'
_atom_sites_solution_primary      direct
_atom_sites_solution_secondary    difmap
_atom_sites_solution_hydrogens    ?
_refine_ls_hydrogen_treatment     ?
_refine_ls_extinction_method      SHELXL
_refine_ls_extinction_coef        0.0021(4)
_refine_ls_extinction_expression
 'Fc^*^=kFc[1+0.001xFc^2^\l^3^/sin(2\q)]^-
1/4^'
_refine_ls_number_reflns          418
_refine_ls_number_parameters      21
_refine_ls_number_restraints      0
_refine_ls_R_factor_all           0.0455
_refine_ls_R_factor_gt            0.0376
_refine_ls_wR_factor_ref          0.1037
_refine_ls_wR_factor_gt           0.0981
_refine_ls_goodness_of_fit_ref    1.159
_refine_ls_restrained_S_all       1.159
_refine_ls_shift/su_max           0.000
_refine_ls_shift/su_mean          0.000

loop_
 _atom_site_label
 _atom_site_type_symbol
 _atom_site_fract_x
 _atom_site_fract_y
 _atom_site_fract_z
 _atom_site_U_iso_or_equiv
 _atom_site_adp_type
 _atom_site_occupancy
 _atom_site_symmetry_multiplicity
 _atom_site_calc_flag
 _atom_site_refinement_flags
 _atom_site_disorder_assembly
 _atom_site_disorder_group
Ce1 Ce 0.0000 0.0000 0.34751(3) 0.0090(2)
Uani 1 8 d S . .
Fe1 Fe 0.0000 0.0000 0.0000 0.0129(6) Uani 1
16 d S . .
Fe2 Fe 0.0000 0.5000 0.44922(10) 0.0316(12)
Uani 0.744(12) 4 d SP . .
Sb1 Sb 0.0000 0.5000 0.2500 0.0070(2) Uani 1
8 d S . .
Sb2 Sb 0.0000 0.0000 0.10983(4) 0.0091(2)
Uani 1 8 d S . .
Sb3 Sb 0.0000 0.0000 0.48595(15) 0.0412(13)
Uani 0.462(8) 8 d SP . .

loop_
 _atom_site_aniso_label
 _atom_site_aniso_U_11
 _atom_site_aniso_U_22
 _atom_site_aniso_U_33
 _atom_site_aniso_U_23
 _atom_site_aniso_U_13
 _atom_site_aniso_U_12
Ce1 0.0079(3) 0.0079(3) 0.0112(4) 0.000
0.000 0.000
Fe1 0.0135(9) 0.0135(9) 0.0115(12) 0.000
0.000 0.000
Fe2 0.0087(12) 0.076(3) 0.0101(11) 0.000
0.000 0.000
Sb1 0.0067(3) 0.0067(3) 0.0075(4) 0.000
0.000 0.000
Sb2 0.0082(3) 0.0082(3) 0.0109(4) 0.000
0.000 0.000
Sb3 0.0461(18) 0.0461(18) 0.0315(18) 0.000
0.000 0.000

_geom_special_details
;
 All s.u.'s (except the s.u. in the dihedral
angle between two l.s. planes)
 are estimated using the full covariance
matrix.  The cell s.u.'s are taken
 into account individually in the estimation
of s.u.'s in distances, angles
 and torsion angles; correlations between
s.u.'s in cell parameters are only
 used when they are defined by crystal
symmetry.  An approximate (isotropic)
 treatment of cell s.u.'s is used for
estimating s.u.'s involving l.s. planes.
;

loop_
 _geom_bond_atom_site_label_1
 _geom_bond_atom_site_label_2
 _geom_bond_distance
 _geom_bond_site_symmetry_2
 _geom_bond_publ_flag
Ce1 Sb2 3.2522(11) 25 ?
Ce1 Sb2 3.2522(11) 25_445 ?
Ce1 Sb2 3.2522(11) 25_455 ?
Ce1 Sb2 3.2522(11) 25_545 ?
Ce1 Sb1 3.3318(8) 25_455 ?
```

```
Ce1 Sb1 3.3318(8) 1_545 ?
Ce1 Sb1 3.3318(8) . ?
Ce1 Sb1 3.3318(8) 25 ?
Ce1 Fe2 3.415(2) . ?
Ce1 Fe2 3.415(2) 21 ?
Ce1 Fe2 3.415(2) 21_455 ?
Ce1 Fe2 3.415(2) 1_545 ?
Fe1 Fe2 2.5331(15) 13 ?
Fe1 Fe2 2.5331(15) 25 ?
Fe1 Fe2 2.5331(15) 13_545 ?
Fe1 Fe2 2.5331(15) 25_455 ?
Fe1 Fe2 2.5331(15) 29_444 ?
Fe1 Fe2 2.5331(15) 9_444 ?
Fe1 Fe2 2.5331(15) 29_454 ?
Fe1 Fe2 2.5331(15) 9_544 ?
Fe1 Sb2 2.8553(11) 17 ?
Fe1 Sb2 2.8553(11) . ?
Fe1 Sb3 3.0791(12) 9_444 ?
Fe1 Sb3 3.0791(12) 25 ?
Fe2 Sb3 2.3634(19) 1_565 ?
Fe2 Sb3 2.3634(19) . ?
Fe2 Fe1 2.5331(15) 9 ?
Fe2 Fe1 2.5331(15) 9_455 ?
Fe2 Fe2 2.641(5) 17_566 ?
Fe2 Sb2 2.6514(18) 25_455 ?
Fe2 Sb2 2.6514(18) 25 ?
Fe2 Sb3 2.741(3) 17_566 ?
Fe2 Sb3 2.741(3) 17_556 ?
Fe2 Ce1 3.415(2) 1_565 ?
Sb1 Sb1 3.0573(11) 25_565 ?
Sb1 Sb1 3.0573(11) 25_455 ?
Sb1 Sb1 3.0573(11) 25_465 ?
Sb1 Sb1 3.0573(11) 25 ?
Sb1 Ce1 3.3318(8) 25_455 ?
Sb1 Ce1 3.3318(8) 1_565 ?
Sb1 Ce1 3.3318(8) 25 ?
Sb2 Fe2 2.6514(18) 13_545 ?
Sb2 Fe2 2.6514(18) 25_455 ?
Sb2 Fe2 2.6514(18) 13 ?
Sb2 Fe2 2.6514(18) 25 ?
Sb2 Ce1 3.2522(11) 25 ?
Sb2 Ce1 3.2522(11) 25_445 ?
Sb2 Ce1 3.2522(11) 25_545 ?
Sb2 Ce1 3.2522(11) 25_455 ?
Sb3 Sb3 0.731(8) 17_556 ?
Sb3 Fe2 2.3634(19) 21_455 ?
Sb3 Fe2 2.3634(19) 1_545 ?
Sb3 Fe2 2.3634(19) 21 ?
Sb3 Fe2 2.741(3) 5_656 ?
Sb3 Fe2 2.741(3) 17_566 ?
Sb3 Fe2 2.741(3) 5_556 ?
Sb3 Fe2 2.741(3) 17_556 ?
Sb3 Fe1 3.0791(12) 9 ?
Sb3 Fe1 3.0791(12) 9_445 ?
Sb3 Fe1 3.0791(12) 9_545 ?

loop_
 _geom_angle_atom_site_label_1
 _geom_angle_atom_site_label_2
 _geom_angle_atom_site_label_3
 _geom_angle
 _geom_angle_site_symmetry_1
 _geom_angle_site_symmetry_3
 _geom_angle_publ_flag
Sb2 Ce1 Sb2 140.13(5) 25 25_445 ?
Sb2 Ce1 Sb2 83.323(15) 25 25_455 ?
Sb2 Ce1 Sb2 83.323(15) 25_445 25_455 ?
Sb2 Ce1 Sb2 83.323(15) 25 25_545 ?
Sb2 Ce1 Sb2 83.323(15) 25_445 25_545 ?
Sb2 Ce1 Sb2 140.13(5) 25_455 25_545 ?
Sb2 Ce1 Sb1 133.692(19) 25 25_455 ?
Sb2 Ce1 Sb1 80.10(2) 25_445 25_455 ?
Sb2 Ce1 Sb1 80.10(2) 25_455 25_455 ?
Sb2 Ce1 Sb1 133.692(19) 25_545 25_455 ?
Sb2 Ce1 Sb1 133.692(19) 25 1_545 ?
Sb2 Ce1 Sb1 80.10(2) 25_445 1_545 ?
Sb2 Ce1 Sb1 133.692(19) 25_455 1_545 ?
Sb2 Ce1 Sb1 80.10(2) 25_545 1_545 ?
Sb1 Ce1 Sb1 54.621(17) 25_455 1_545 ?
Sb2 Ce1 Sb1 80.10(2) 25 . ?
Sb2 Ce1 Sb1 133.692(19) 25_445 . ?
Sb2 Ce1 Sb1 80.10(2) 25_455 . ?
Sb2 Ce1 Sb1 133.692(19) 25_545 . ?
Sb1 Ce1 Sb1 54.621(17) 25_455 . ?
Sb1 Ce1 Sb1 80.91(3) 1_545 . ?
Sb2 Ce1 Sb1 80.10(2) 25 25 ?
Sb2 Ce1 Sb1 133.692(19) 25_445 25 ?
Sb2 Ce1 Sb1 133.692(19) 25_455 25 ?
Sb2 Ce1 Sb1 80.10(2) 25_545 25 ?
Sb1 Ce1 Sb1 80.91(3) 25_455 25 ?
Sb1 Ce1 Sb1 54.621(17) 1_545 25 ?
Sb1 Ce1 Sb1 54.621(17) . 25 ?
Sb2 Ce1 Fe2 46.78(2) 25 . ?
Sb2 Ce1 Fe2 99.02(3) 25_445 . ?
Sb2 Ce1 Fe2 46.78(2) 25_455 . ?
Sb2 Ce1 Fe2 99.02(3) 25_545 . ?
Sb1 Ce1 Fe2 126.09(2) 25_455 . ?
Sb1 Ce1 Fe2 178.82(3) 1_545 . ?
Sb1 Ce1 Fe2 100.27(3) . . ?
Sb1 Ce1 Fe2 126.09(2) 25 . ?
Sb2 Ce1 Fe2 46.78(2) 25 21 ?
Sb2 Ce1 Fe2 99.02(3) 25_445 21 ?
Sb2 Ce1 Fe2 99.02(3) 25_455 21 ?
Sb2 Ce1 Fe2 46.78(2) 25_545 21 ?
Sb1 Ce1 Fe2 178.82(3) 25_455 21 ?
Sb1 Ce1 Fe2 126.09(2) 1_545 21 ?
Sb1 Ce1 Fe2 126.09(2) . 21 ?
Sb1 Ce1 Fe2 100.27(3) 25 21 ?
Fe2 Ce1 Fe2 53.18(4) . 21 ?
Sb2 Ce1 Fe2 99.02(3) 25 21_455 ?
Sb2 Ce1 Fe2 46.78(2) 25_445 21_455 ?
Sb2 Ce1 Fe2 46.78(2) 25_455 21_455 ?
Sb2 Ce1 Fe2 99.02(3) 25_545 21_455 ?
Sb1 Ce1 Fe2 100.27(3) 25_455 21_455 ?
Sb1 Ce1 Fe2 126.09(2) 1_545 21_455 ?
Sb1 Ce1 Fe2 126.09(2) . 21_455 ?
Sb1 Ce1 Fe2 178.82(3) 25 21_455 ?
Fe2 Ce1 Fe2 53.18(4) . 21_455 ?
Fe2 Ce1 Fe2 78.54(6) 21 21_455 ?
Sb2 Ce1 Fe2 99.02(3) 25 1_545 ?
Sb2 Ce1 Fe2 46.78(2) 25_445 1_545 ?
Sb2 Ce1 Fe2 99.02(3) 25_455 1_545 ?
Sb2 Ce1 Fe2 46.78(2) 25_545 1_545 ?
Sb1 Ce1 Fe2 126.09(2) 25_455 1_545 ?
Sb1 Ce1 Fe2 100.27(3) 1_545 1_545 ?
Sb1 Ce1 Fe2 178.82(3) . 1_545 ?
Sb1 Ce1 Fe2 126.09(2) 25 1_545 ?
Fe2 Ce1 Fe2 78.54(6) . 1_545 ?
Fe2 Ce1 Fe2 53.18(4) 21 1_545 ?
Fe2 Ce1 Fe2 53.18(4) 21_455 1_545 ?
Fe2 Fe1 Fe2 74.24(5) 13 25 ?
Fe2 Fe1 Fe2 117.17(10) 13 13_545 ?
Fe2 Fe1 Fe2 74.24(5) 25 13_545 ?
Fe2 Fe1 Fe2 74.24(5) 13 25_455 ?
Fe2 Fe1 Fe2 117.17(10) 25 25_455 ?
Fe2 Fe1 Fe2 74.24(5) 13_545 25_455 ?
Fe2 Fe1 Fe2 180.00(10) 13 29_444 ?
Fe2 Fe1 Fe2 105.76(5) 25 29_444 ?
Fe2 Fe1 Fe2 62.83(10) 13_545 29_444 ?
Fe2 Fe1 Fe2 105.76(5) 25_455 29_444 ?
Fe2 Fe1 Fe2 105.76(5) 13 9_444 ?
Fe2 Fe1 Fe2 180.00(10) 25 9_444 ?
```

```
Fe2 Fe1 Fe2 105.76(5) 13_545 9_444 ?
Fe2 Fe1 Fe2 62.83(10) 25_455 9_444 ?
Fe2 Fe1 Fe2 74.24(5) 29_444 9_444 ?
Fe2 Fe1 Fe2 62.83(10) 13 29_454 ?
Fe2 Fe1 Fe2 105.76(5) 25 29_454 ?
Fe2 Fe1 Fe2 180.00(10) 13_545 29_454 ?
Fe2 Fe1 Fe2 105.76(5) 25_455 29_454 ?
Fe2 Fe1 Fe2 117.17(10) 29_444 29_454 ?
Fe2 Fe1 Fe2 74.24(5) 9_444 29_454 ?
Fe2 Fe1 Fe2 105.76(5) 13 9_544 ?
Fe2 Fe1 Fe2 62.83(10) 25 9_544 ?
Fe2 Fe1 Fe2 105.76(5) 13_545 9_544 ?
Fe2 Fe1 Fe2 180.00(10) 25_455 9_544 ?
Fe2 Fe1 Fe2 74.24(5) 29_444 9_544 ?
Fe2 Fe1 Fe2 117.17(10) 9_444 9_544 ?
Fe2 Fe1 Fe2 74.24(5) 29_454 9_544 ?
Fe2 Fe1 Sb2 121.41(5) 13 17 ?
Fe2 Fe1 Sb2 121.41(5) 25 17 ?
Fe2 Fe1 Sb2 121.41(5) 13_545 17 ?
Fe2 Fe1 Sb2 121.41(5) 25_455 17 ?
Fe2 Fe1 Sb2 58.59(5) 29_444 17 ?
Fe2 Fe1 Sb2 58.59(5) 9_444 17 ?
Fe2 Fe1 Sb2 58.59(5) 29_454 17 ?
Fe2 Fe1 Sb2 58.59(5) 9_544 17 ?
Fe2 Fe1 Sb2 58.59(5) 13 . ?
Fe2 Fe1 Sb2 58.59(5) 25 . ?
Fe2 Fe1 Sb2 58.59(5) 13_545 . ?
Fe2 Fe1 Sb2 58.59(5) 25_455 . ?
Fe2 Fe1 Sb2 121.41(5) 29_444 . ?
Fe2 Fe1 Sb2 121.41(5) 9_444 . ?
Fe2 Fe1 Sb2 121.41(5) 29_454 . ?
Fe2 Fe1 Sb2 121.41(5) 9_544 . ?
Sb2 Fe1 Sb2 180.0 17 . ?
Fe2 Fe1 Sb3 131.38(5) 13 9_444 ?
Fe2 Fe1 Sb3 131.38(5) 25 9_444 ?
Fe2 Fe1 Sb3 57.50(6) 13_545 9_444 ?
Fe2 Fe1 Sb3 57.50(6) 25_455 9_444 ?
Fe2 Fe1 Sb3 48.62(5) 29_444 9_444 ?
Fe2 Fe1 Sb3 48.62(5) 9_444 9_444 ?
Fe2 Fe1 Sb3 122.50(6) 29_454 9_444 ?
Fe2 Fe1 Sb3 122.50(6) 9_544 9_444 ?
Sb2 Fe1 Sb3 83.19(7) 17 9_444 ?
Sb2 Fe1 Sb3 96.81(7) . 9_444 ?
Fe2 Fe1 Sb3 48.62(5) 13 25 ?
Fe2 Fe1 Sb3 48.62(5) 25 25 ?
Fe2 Fe1 Sb3 122.50(6) 13_545 25 ?
Fe2 Fe1 Sb3 122.50(6) 25_455 25 ?
Fe2 Fe1 Sb3 131.38(5) 29_444 25 ?
Fe2 Fe1 Sb3 131.38(5) 9_444 25 ?
Fe2 Fe1 Sb3 57.50(6) 29_454 25 ?
Fe2 Fe1 Sb3 57.50(6) 9_544 25 ?
Sb2 Fe1 Sb3 96.81(7) 17 25 ?
Sb2 Fe1 Sb3 83.19(7) . 25 ?
Sb3 Fe1 Sb3 180.0 9_444 25 ?
Sb3 Fe2 Sb3 132.3(2) 1_565 . ?
Sb3 Fe2 Fe1 77.84(6) 1_565 9 ?
Sb3 Fe2 Fe1 77.84(6) . 9 ?
Sb3 Fe2 Fe1 77.84(6) 1_565 9_455 ?
Sb3 Fe2 Fe1 77.84(6) . 9_455 ?
Fe1 Fe2 Fe1 117.17(10) 9 9_455 ?
Sb3 Fe2 Fe2 66.17(10) 1_565 17_566 ?
Sb3 Fe2 Fe2 66.17(10) . 17_566 ?
Fe1 Fe2 Fe2 58.59(5) 9 17_566 ?
Fe1 Fe2 Fe2 58.59(5) 9_455 17_566 ?
Sb3 Fe2 Sb2 103.53(5) 1_565 25_455 ?
Sb3 Fe2 Sb2 103.53(5) . 25_455 ?
Fe1 Fe2 Sb2 176.04(10) 9 25_455 ?
Fe1 Fe2 Sb2 66.79(3) 9_455 25_455 ?
Fe2 Fe2 Sb2 125.38(5) 17_566 25_455 ?
Sb3 Fe2 Sb2 103.53(5) 1_565 25 ?
Sb3 Fe2 Sb2 103.53(5) . 25 ?
Fe1 Fe2 Sb2 66.79(3) 9 25 ?
Fe1 Fe2 Sb2 176.04(10) 9_455 25 ?
Fe2 Fe2 Sb2 125.38(5) 17_566 25 ?
Sb2 Fe2 Sb2 109.25(10) 25_455 25 ?
Sb3 Fe2 Sb3 14.11(15) 1_565 17_566 ?
Sb3 Fe2 Sb3 118.22(10) . 17_566 ?
Fe1 Fe2 Sb3 71.31(6) 9 17_566 ?
Fe1 Fe2 Sb3 71.31(6) 9_455 17_566 ?
Fe2 Fe2 Sb3 52.06(8) 17_566 17_566 ?
Sb2 Fe2 Sb3 110.85(4) 25_455 17_566 ?
Sb2 Fe2 Sb3 110.85(4) 25 17_566 ?
Sb3 Fe2 Sb3 118.22(10) 1_565 17_556 ?
Sb3 Fe2 Sb3 14.11(15) . 17_556 ?
Fe1 Fe2 Sb3 71.31(6) 9 17_556 ?
Fe1 Fe2 Sb3 71.31(6) 9_455 17_556 ?
Fe2 Fe2 Sb3 52.06(8) 17_566 17_556 ?
Sb2 Fe2 Sb3 110.85(4) 25_455 17_556 ?
Sb2 Fe2 Sb3 110.85(4) 25 17_556 ?
Sb3 Fe2 Sb3 104.11(17) 17_566 17_556 ?
Sb3 Fe2 Ce1 153.10(12) 1_565 . ?
Sb3 Fe2 Ce1 74.56(9) . . ?
Fe1 Fe2 Ce1 113.80(3) 9 . ?
Fe1 Fe2 Ce1 113.80(3) 9_455 . ?
Fe2 Fe2 Ce1 140.73(3) 17_566 . ?
Sb2 Fe2 Ce1 63.37(5) 25_455 . ?
Sb2 Fe2 Ce1 63.37(5) 25 . ?
Sb3 Fe2 Ce1 167.22(10) 17_566 . ?
Sb3 Fe2 Ce1 88.67(7) 17_556 . ?
Sb3 Fe2 Ce1 74.56(9) 1_565 1_565 ?
Sb3 Fe2 Ce1 153.10(11) . 1_565 ?
Fe1 Fe2 Ce1 113.80(3) 9 1_565 ?
Fe1 Fe2 Ce1 113.80(3) 9_455 1_565 ?
Fe2 Fe2 Ce1 140.73(3) 17_566 1_565 ?
Sb2 Fe2 Ce1 63.37(5) 25_455 1_565 ?
Sb2 Fe2 Ce1 63.37(5) 25 1_565 ?
Sb3 Fe2 Ce1 88.67(7) 17_566 1_565 ?
Sb3 Fe2 Ce1 167.22(10) 17_556 1_565 ?
Ce1 Fe2 Ce1 78.54(6) . 1_565 ?
Sb1 Sb1 Sb1 180.0 25_565 25_455 ?
Sb1 Sb1 Sb1 90.0 25_565 25_465 ?
Sb1 Sb1 Sb1 90.0 25_455 25_465 ?
Sb1 Sb1 Sb1 90.0 25_565 25 ?
Sb1 Sb1 Sb1 90.0 25_455 25 ?
Sb1 Sb1 Sb1 180.0 25_465 25 ?
Sb1 Sb1 Ce1 117.310(8) 25_565 25_455 ?
Sb1 Sb1 Ce1 62.690(8) 25_455 25_455 ?
Sb1 Sb1 Ce1 62.690(8) 25_465 25_455 ?
Sb1 Sb1 Ce1 117.310(8) 25 25_455 ?
Sb1 Sb1 Ce1 62.690(8) 25_565 1_565 ?
Sb1 Sb1 Ce1 117.310(9) 25_455 1_565 ?
Sb1 Sb1 Ce1 62.690(8) 25_465 1_565 ?
Sb1 Sb1 Ce1 117.310(8) 25 1_565 ?
Ce1 Sb1 Ce1 125.379(17) 25_455 1_565 ?
Sb1 Sb1 Ce1 62.690(8) 25_565 25 ?
Sb1 Sb1 Ce1 117.310(8) 25_455 25 ?
Sb1 Sb1 Ce1 117.310(8) 25_465 25 ?
Sb1 Sb1 Ce1 62.690(8) 25 25 ?
Ce1 Sb1 Ce1 80.91(3) 25_455 25 ?
Ce1 Sb1 Ce1 125.379(17) 1_565 25 ?
Sb1 Sb1 Ce1 117.310(8) 25_565 . ?
Sb1 Sb1 Ce1 62.690(8) 25_455 . ?
Sb1 Sb1 Ce1 117.310(9) 25_465 . ?
Sb1 Sb1 Ce1 62.690(8) 25 . ?
Ce1 Sb1 Ce1 125.379(17) 25_455 . ?
Ce1 Sb1 Ce1 80.91(3) 1_565 . ?
Ce1 Sb1 Ce1 125.379(17) 25 . ?
Fe2 Sb2 Fe2 70.42(5) 13_545 25_455 ?
Fe2 Sb2 Fe2 109.25(10) 13_545 13 ?
Fe2 Sb2 Fe2 70.42(5) 25_455 13 ?
Fe2 Sb2 Fe2 70.42(5) 13_545 25 ?
Fe2 Sb2 Fe2 109.25(10) 25_455 25 ?
```

```
Fe2 Sb2 Fe2 70.42(5) 13 25 ?
Fe2 Sb2 Fe1 54.62(5) 13_545 . ?
Fe2 Sb2 Fe1 54.62(5) 25_455 . ?
Fe2 Sb2 Fe1 54.62(5) 13 . ?
Fe2 Sb2 Fe1 54.62(5) 25 . ?
Fe2 Sb2 Ce1 137.681(16) 13_545 25 ?
Fe2 Sb2 Ce1 137.681(16) 25_455 25 ?
Fe2 Sb2 Ce1 69.84(4) 13 25 ?
Fe2 Sb2 Ce1 69.84(4) 25 25 ?
Fe1 Sb2 Ce1 109.94(2) . 25 ?
Fe2 Sb2 Ce1 69.84(4) 13_545 25_445 ?
Fe2 Sb2 Ce1 69.84(4) 25_455 25_445 ?
Fe2 Sb2 Ce1 137.681(16) 13 25_445 ?
Fe2 Sb2 Ce1 137.681(16) 25 25_445 ?
Fe1 Sb2 Ce1 109.94(2) . 25_445 ?
Ce1 Sb2 Ce1 140.13(5) 25 25_445 ?
Fe2 Sb2 Ce1 69.84(4) 13_545 25_545 ?
Fe2 Sb2 Ce1 137.681(16) 25_455 25_545 ?
Fe2 Sb2 Ce1 137.681(16) 13 25_545 ?
Fe2 Sb2 Ce1 69.84(4) 25 25_545 ?
Fe1 Sb2 Ce1 109.94(2) . 25_545 ?
Ce1 Sb2 Ce1 83.323(15) 25 25_545 ?
Ce1 Sb2 Ce1 83.323(15) 25_445 25_545 ?
Fe2 Sb2 Ce1 137.681(16) 13_545 25_455 ?
Fe2 Sb2 Ce1 69.84(4) 25_455 25_455 ?
Fe2 Sb2 Ce1 69.84(4) 13 25_455 ?
Fe2 Sb2 Ce1 137.681(16) 25 25_455 ?
Fe1 Sb2 Ce1 109.94(2) . 25_455 ?
Ce1 Sb2 Ce1 83.323(15) 25 25_455 ?
Ce1 Sb2 Ce1 83.323(15) 25_445 25_455 ?
Ce1 Sb2 Ce1 140.13(5) 25_545 25_455 ?
Sb3 Sb3 Fe2 113.83(10) 17_556 21_455 ?
Sb3 Sb3 Fe2 113.83(10) 17_556 1_545 ?
Fe2 Sb3 Fe2 80.60(8) 21_455 1_545 ?
Sb3 Sb3 Fe2 113.83(10) 17_556 21 ?
Fe2 Sb3 Fe2 132.3(2) 21_455 21 ?
Fe2 Sb3 Fe2 80.60(7) 1_545 21 ?
Sb3 Sb3 Fe2 113.83(10) 17_556 . ?
Fe2 Sb3 Fe2 80.60(7) 21_455 . ?
Fe2 Sb3 Fe2 132.3(2) 1_545 . ?
Fe2 Sb3 Fe2 80.60(7) 21 . ?
Sb3 Sb3 Fe2 52.06(8) 17_556 5_656 ?
Fe2 Sb3 Fe2 165.89(15) 21_455 5_656 ?
Fe2 Sb3 Fe2 104.39(5) 1_545 5_656 ?
Fe2 Sb3 Fe2 61.78(10) 21 5_656 ?
Fe2 Sb3 Fe2 104.39(5) . 5_656 ?
Sb3 Sb3 Fe2 52.06(8) 17_556 17_566 ?
Fe2 Sb3 Fe2 104.39(5) 21_455 17_566 ?
Fe2 Sb3 Fe2 165.89(15) 1_545 17_566 ?
Fe2 Sb3 Fe2 104.39(5) 21 17_566 ?
Fe2 Sb3 Fe2 61.78(10) . 17_566 ?
Fe2 Sb3 Fe2 67.78(9) 5_656 17_566 ?
Sb3 Sb3 Fe2 52.06(8) 17_556 5_556 ?
Fe2 Sb3 Fe2 61.78(10) 21_455 5_556 ?
Fe2 Sb3 Fe2 104.39(5) 1_545 5_556 ?
Fe2 Sb3 Fe2 165.89(15) 21 5_556 ?
Fe2 Sb3 Fe2 104.39(5) . 5_556 ?
Fe2 Sb3 Fe2 104.11(17) 5_656 5_556 ?
Fe2 Sb3 Fe2 67.78(9) 17_566 5_556 ?
Sb3 Sb3 Fe2 52.06(8) 17_556 17_556 ?
Fe2 Sb3 Fe2 104.39(5) 21_455 17_556 ?
Fe2 Sb3 Fe2 61.78(10) 1_545 17_556 ?
Fe2 Sb3 Fe2 104.39(5) 21 17_556 ?
Fe2 Sb3 Fe2 165.89(15) . 17_556 ?
Fe2 Sb3 Fe2 67.78(9) 5_656 17_556 ?
Fe2 Sb3 Fe2 104.11(17) 17_566 17_556 ?
Fe2 Sb3 Fe2 67.78(9) 5_556 17_556 ?
Sb3 Sb3 Fe1 83.19(7) 17_556 9 ?
Fe2 Sb3 Fe1 133.64(5) 21_455 9 ?
Fe2 Sb3 Fe1 133.64(5) 1_545 9 ?
Fe2 Sb3 Fe1 53.54(3) 21 9 ?
Fe2 Sb3 Fe1 53.54(3) . 9 ?
Fe2 Sb3 Fe1 51.20(3) 5_656 9 ?
Fe2 Sb3 Fe1 51.20(3) 17_566 9 ?
Fe2 Sb3 Fe1 118.73(10) 5_556 9 ?
Fe2 Sb3 Fe1 118.73(10) 17_556 9 ?
Sb3 Sb3 Fe1 83.19(7) 17_556 9_445 ?
Fe2 Sb3 Fe1 53.54(3) 21_455 9_445 ?
Fe2 Sb3 Fe1 53.54(3) 1_545 9_445 ?
Fe2 Sb3 Fe1 133.64(5) 21 9_445 ?
Fe2 Sb3 Fe1 133.64(5) . 9_445 ?
Fe2 Sb3 Fe1 118.73(10) 5_656 9_445 ?
Fe2 Sb3 Fe1 118.73(10) 17_566 9_445 ?
Fe2 Sb3 Fe1 51.20(3) 5_556 9_445 ?
Fe2 Sb3 Fe1 51.20(3) 17_556 9_445 ?
Fe1 Sb3 Fe1 166.37(15) 9 9_445 ?
Sb3 Sb3 Fe1 83.19(7) 17_556 9_545 ?
Fe2 Sb3 Fe1 133.64(5) 21_455 9_545 ?
Fe2 Sb3 Fe1 53.54(3) 1_545 9_545 ?
Fe2 Sb3 Fe1 53.54(3) 21 9_545 ?
Fe2 Sb3 Fe1 133.64(5) . 9_545 ?
Fe2 Sb3 Fe1 51.20(3) 5_656 9_545 ?
Fe2 Sb3 Fe1 118.73(10) 17_566 9_545 ?
Fe2 Sb3 Fe1 118.73(10) 5_556 9_545 ?
Fe2 Sb3 Fe1 51.20(3) 17_556 9_545 ?
Fe1 Sb3 Fe1 89.193(18) 9 9_545 ?
Fe1 Sb3 Fe1 89.193(18) 9_445 9_545 ?

_diffrn_measured_fraction_theta_max    0.970
_diffrn_reflns_theta_full              36.83
_diffrn_measured_fraction_theta_full   0.970
_refine_diff_density_max    5.448
_refine_diff_density_min   -3.993
_refine_diff_density_rms    0.695

#===END
```

A1.7 $Pr_2Fe_4Sb_5$

```
data_shelxl

_audit_creation_method            SHELXL-97
_chemical_name_systematic
;
 ?
;
_chemical_name_common             ?
_chemical_melting_point           ?
_chemical_formula_moiety          'Fe4.02
Pr2 Sb4.93'
_chemical_formula_sum
 'Fe4.02 Pr2 Sb4.93'
_chemical_formula_weight          1105.96

loop_
 _atom_type_symbol
 _atom_type_description
 _atom_type_scat_dispersion_real
 _atom_type_scat_dispersion_imag
 _atom_type_scat_source
 'Pr'  'Pr'  -0.2180   2.8214
 'International Tables Vol C Tables 4.2.6.8
and 6.1.1.4'
 'Fe'  'Fe'   0.3463   0.8444
 'International Tables Vol C Tables 4.2.6.8
and 6.1.1.4'
 'Sb'  'Sb'  -0.5866   1.5461
 'International Tables Vol C Tables 4.2.6.8
and 6.1.1.4'

_symmetry_cell_setting
'Tetragonal'
```

```
_symmetry_space_group_name_H-M    'I 4/m m m
'

loop_
 _symmetry_equiv_pos_as_xyz
 'x, y, z'
 '-x, -y, z'
 'x, -y, -z'
 '-x, y, -z'
 '-y, -x, -z'
 'y, x, -z'
 'y, -x, z'
 '-y, x, z'
 'x+1/2, y+1/2, z+1/2'
 '-x+1/2, -y+1/2, z+1/2'
 'x+1/2, -y+1/2, -z+1/2'
 '-x+1/2, y+1/2, -z+1/2'
 '-y+1/2, -x+1/2, -z+1/2'
 'y+1/2, x+1/2, -z+1/2'
 'y+1/2, -x+1/2, z+1/2'
 '-y+1/2, x+1/2, z+1/2'
 '-x, -y, -z'
 'x, y, -z'
 '-x, y, z'
 'x, -y, z'
 'y, x, z'
 '-y, -x, z'
 '-y, x, -z'
 'y, -x, -z'
 '-x+1/2, -y+1/2, -z+1/2'
 'x+1/2, y+1/2, -z+1/2'
 '-x+1/2, y+1/2, z+1/2'
 'x+1/2, -y+1/2, z+1/2'
 'y+1/2, x+1/2, z+1/2'
 '-y+1/2, -x+1/2, z+1/2'
 '-y+1/2, x+1/2, -z+1/2'
 'y+1/2, -x+1/2, -z+1/2'

_cell_length_a                    4.3133(15)
_cell_length_b                    4.3133(15)
_cell_length_c                    25.976(15)
_cell_angle_alpha                 90
_cell_angle_beta                  90
_cell_angle_gamma                 90
_cell_volume                      483.3(4)
_cell_formula_units_Z             2
_cell_measurement_temperature     298(2)
_cell_measurement_reflns_used     587
_cell_measurement_theta_min       2.6
_cell_measurement_theta_max       37.0

_exptl_crystal_description        plate
_exptl_crystal_colour             black
_exptl_crystal_size_max           0.10
_exptl_crystal_size_mid           0.08
_exptl_crystal_size_min           0.03
_exptl_crystal_density_meas       ?
_exptl_crystal_density_diffrn     7.600
_exptl_crystal_density_method     'not
measured'
_exptl_crystal_F_000              947
_exptl_absorpt_coefficient_mu     29.149
_exptl_absorpt_correction_type    'multi-
scan'
_exptl_absorpt_correction_T_min   0.1586
_exptl_absorpt_correction_T_max   0.5294
_exptl_absorpt_process_details    'HKL
Scalepack (Otwinowski & Minor 1997)'

_exptl_special_details
;
 ?
;

_diffrn_ambient_temperature       298(2)
_diffrn_radiation_wavelength      0.71073
_diffrn_radiation_type            MoK\a
_diffrn_radiation_source          'fine-
focus sealed tube'
_diffrn_radiation_monochromator   graphite
_diffrn_measurement_device_type   'Nonius
KappaCCD'
_diffrn_measurement_method        '\w and \f
scans'
_diffrn_detector_area_resol_mean  ?
_diffrn_standards_number          ?
_diffrn_standards_interval_count  ?
_diffrn_standards_interval_time   ?
_diffrn_standards_decay_%         ?
_diffrn_reflns_number             6743
_diffrn_reflns_av_R_equivalents   0.0299
_diffrn_reflns_av_sigmaI/netI     0.0208
_diffrn_reflns_limit_h_min        0
_diffrn_reflns_limit_h_max        7
_diffrn_reflns_limit_k_min        -4
_diffrn_reflns_limit_k_max        5
_diffrn_reflns_limit_l_min        0
_diffrn_reflns_limit_l_max        43
_diffrn_reflns_theta_min          3.14
_diffrn_reflns_theta_max          36.84
_reflns_number_total              422
_reflns_number_gt                 392
_reflns_threshold_expression      I>2\s(I)

_computing_data_collection        ?
_computing_cell_refinement        ?
_computing_data_reduction         ?
_computing_structure_solution     ?
_computing_structure_refinement   'SHELXL-97
(Sheldrick, 2008)'
_computing_molecular_graphics     ?
_computing_publication_material   ?

_refine_special_details
;
 Refinement of F^2^ against ALL reflections.
The weighted R-factor wR and
 goodness of fit S are based on F^2^,
conventional R-factors R are based
 on F, with F set to zero for negative F^2^.
The threshold expression of
 F^2^ > 2\s(F^2^) is used only for
calculating R-factors(gt) etc. and is
 not relevant to the choice of reflections
for refinement.  R-factors based
 on F^2^ are statistically about twice as
large as those based on F, and R-
 factors based on ALL data will be even
larger.
;

_refine_ls_structure_factor_coef  Fsqd
_refine_ls_matrix_type            full
_refine_ls_weighting_scheme       calc
_refine_ls_weighting_details
 'calc
w=1/[\s^2^(Fo^2^)+(0.0789P)^2^+47.6839P]
where P=(Fo^2^+2Fc^2^)/3'
_atom_sites_solution_primary      direct
_atom_sites_solution_secondary    difmap
_atom_sites_solution_hydrogens    ?
_refine_ls_hydrogen_treatment     ?
```

```
_refine_ls_extinction_method      SHELXL
_refine_ls_extinction_coef        0.0070(10)
_refine_ls_extinction_expression
 'Fc^*^=kFc[1+0.001xFc^2^\l^3^/sin(2\q)]^-
1/4^'
_refine_ls_number_reflns          422
_refine_ls_number_parameters      21
_refine_ls_number_restraints      0
_refine_ls_R_factor_all           0.0510
_refine_ls_R_factor_gt            0.0488
_refine_ls_wR_factor_ref          0.1494
_refine_ls_wR_factor_gt           0.1476
_refine_ls_goodness_of_fit_ref    1.152
_refine_ls_restrained_S_all       1.152
_refine_ls_shift/su_max           0.000
_refine_ls_shift/su_mean          0.000

loop_
 _atom_site_label
 _atom_site_type_symbol
 _atom_site_fract_x
 _atom_site_fract_y
 _atom_site_fract_z
 _atom_site_U_iso_or_equiv
 _atom_site_adp_type
 _atom_site_occupancy
 _atom_site_symmetry_multiplicity
 _atom_site_calc_flag
 _atom_site_refinement_flags
 _atom_site_disorder_assembly
 _atom_site_disorder_group
Pr1 Pr 0.0000 0.0000 0.34716(4) 0.0104(3)
Uani 1 8 d S . .
Fe1 Fe 0.0000 0.0000 0.0000 0.0146(8) Uani 1
16 d S . .
Fe2 Fe 0.0000 0.5000 0.44894(13) 0.0344(16)
Uani 0.755(19) 4 d SP . .
Sb1 Sb 0.0000 0.5000 0.2500 0.0085(3) Uani 1
8 d S . .
Sb2 Sb 0.0000 0.0000 0.11072(5) 0.0100(4)
Uani 1 8 d S . .
Sb3 Sb 0.0000 0.0000 0.48405(18) 0.0318(13)
Uani 0.464(11) 8 d SP . .

loop_
 _atom_site_aniso_label
 _atom_site_aniso_U_11
 _atom_site_aniso_U_22
 _atom_site_aniso_U_33
 _atom_site_aniso_U_23
 _atom_site_aniso_U_13
 _atom_site_aniso_U_12
Pr1 0.0100(4) 0.0100(4) 0.0111(5) 0.000
0.000 0.000
Fe1 0.0161(12) 0.0161(12) 0.0115(16) 0.000
0.000 0.000
Fe2 0.0101(15) 0.083(4) 0.0103(14) 0.000
0.000 0.000
Sb1 0.0091(4) 0.0091(4) 0.0073(5) 0.000
0.000 0.000
Sb2 0.0096(4) 0.0096(4) 0.0109(5) 0.000
0.000 0.000
Sb3 0.0369(18) 0.0369(18) 0.0216(15) 0.000
0.000 0.000

_geom_special_details
;
 All s.u.'s (except the s.u. in the dihedral
angle between two l.s. planes)
 are estimated using the full covariance
matrix.  The cell s.u.'s are taken
 into account individually in the estimation
of s.u.'s in distances, angles
 and torsion angles; correlations between
s.u.'s in cell parameters are only
 used when they are defined by crystal
symmetry.  An approximate (isotropic)
 treatment of cell s.u.'s is used for
estimating s.u.'s involving l.s. planes.
;

loop_
 _geom_bond_atom_site_label_1
 _geom_bond_atom_site_label_2
 _geom_bond_distance
 _geom_bond_site_symmetry_2
 _geom_bond_publ_flag
Pr1 Sb2 3.2403(12) 25 ?
Pr1 Sb2 3.2403(12) 25_445 ?
Pr1 Sb2 3.2403(12) 25_455 ?
Pr1 Sb2 3.2403(12) 25_545 ?
Pr1 Sb1 3.3197(15) 25_455 ?
Pr1 Sb1 3.3197(15) 1_545 ?
Pr1 Sb1 3.3197(15) . ?
Pr1 Sb1 3.3197(15) 25 ?
Pr1 Fe2 3.412(3) . ?
Pr1 Fe2 3.412(3) 21 ?
Pr1 Fe2 3.412(3) 21_455 ?
Pr1 Fe2 3.412(3) 1_545 ?
Fe1 Fe2 2.5318(19) 29_444 ?
Fe1 Fe2 2.5318(19) 9_444 ?
Fe1 Fe2 2.5318(19) 29_454 ?
Fe1 Fe2 2.5318(19) 9_544 ?
Fe1 Fe2 2.5318(19) 13 ?
Fe1 Fe2 2.5318(19) 25 ?
Fe1 Fe2 2.5318(19) 25_455 ?
Fe1 Fe2 2.5318(19) 13_545 ?
Fe1 Sb2 2.876(2) 17 ?
Fe1 Sb2 2.876(2) . ?
Fe1 Sb3 3.0780(12) 25 ?
Fe1 Sb3 3.0780(12) 9_444 ?
Fe2 Sb3 2.342(2) 1_565 ?
Fe2 Sb3 2.342(2) . ?
Fe2 Fe1 2.5318(19) 9 ?
Fe2 Fe1 2.5318(19) 9_455 ?
Fe2 Fe2 2.652(7) 17_566 ?
Fe2 Sb2 2.656(2) 25_455 ?
Fe2 Sb2 2.656(2) 25 ?
Fe2 Sb3 2.771(4) 17_566 ?
Fe2 Sb3 2.771(4) 17_556 ?
Fe2 Pr1 3.412(3) 1_565 ?
Sb1 Sb1 3.0500(11) 25_565 ?
Sb1 Sb1 3.0500(11) 25_455 ?
Sb1 Sb1 3.0500(11) 25_465 ?
Sb1 Sb1 3.0500(11) 25 ?
Sb1 Pr1 3.3197(15) 25_455 ?
Sb1 Pr1 3.3197(15) 1_565 ?
Sb1 Pr1 3.3197(15) 25 ?
Sb2 Fe2 2.656(2) 13_545 ?
Sb2 Fe2 2.656(2) 25_455 ?
Sb2 Fe2 2.656(2) 13 ?
Sb2 Fe2 2.656(2) 25 ?
Sb2 Pr1 3.2403(12) 25 ?
Sb2 Pr1 3.2403(12) 25_445 ?
Sb2 Pr1 3.2403(12) 25_545 ?
Sb2 Pr1 3.2403(12) 25_455 ?
Sb3 Sb3 0.828(10) 17_556 ?
Sb3 Fe2 2.342(2) 21_455 ?
Sb3 Fe2 2.342(2) 1_545 ?
Sb3 Fe2 2.342(2) 21 ?
Sb3 Fe2 2.771(4) 5_656 ?
Sb3 Fe2 2.771(4) 17_566 ?
```

```
Sb3 Fe2 2.771(4) 5_556 ?
Sb3 Fe2 2.771(4) 17_556 ?
Sb3 Fe1 3.0780(12) 9 ?
Sb3 Fe1 3.0780(12) 9_445 ?
Sb3 Fe1 3.0780(12) 9_545 ?

loop_
 _geom_angle_atom_site_label_1
 _geom_angle_atom_site_label_2
 _geom_angle_atom_site_label_3
 _geom_angle
 _geom_angle_site_symmetry_1
 _geom_angle_site_symmetry_3
 _geom_angle_publ_flag
Sb2 Pr1 Sb2 140.53(6) 25 25_445 ?
Sb2 Pr1 Sb2 83.45(2) 25 25_455 ?
Sb2 Pr1 Sb2 83.45(2) 25_445 25_455 ?
Sb2 Pr1 Sb2 83.45(2) 25 25_545 ?
Sb2 Pr1 Sb2 83.45(2) 25_445 25_545 ?
Sb2 Pr1 Sb2 140.53(6) 25_455 25_545 ?
Sb2 Pr1 Sb1 133.56(3) 25 25_455 ?
Sb2 Pr1 Sb1 79.88(3) 25_445 25_455 ?
Sb2 Pr1 Sb1 79.88(3) 25_455 25_455 ?
Sb2 Pr1 Sb1 133.56(3) 25_545 25_455 ?
Sb2 Pr1 Sb1 133.56(3) 25 1_545 ?
Sb2 Pr1 Sb1 79.88(3) 25_445 1_545 ?
Sb2 Pr1 Sb1 133.56(3) 25_455 1_545 ?
Sb2 Pr1 Sb1 79.88(3) 25_545 1_545 ?
Sb1 Pr1 Sb1 54.69(3) 25_455 1_545 ?
Sb2 Pr1 Sb1 79.88(3) 25 . ?
Sb2 Pr1 Sb1 133.56(3) 25_445 . ?
Sb2 Pr1 Sb1 79.88(3) 25_455 . ?
Sb2 Pr1 Sb1 133.56(3) 25_545 . ?
Sb1 Pr1 Sb1 54.69(3) 25_455 . ?
Sb1 Pr1 Sb1 81.03(5) 1_545 . ?
Sb2 Pr1 Sb1 79.88(3) 25 25 ?
Sb2 Pr1 Sb1 133.56(3) 25_445 25 ?
Sb2 Pr1 Sb1 133.56(3) 25_455 25 ?
Sb2 Pr1 Sb1 79.88(3) 25_545 25 ?
Sb1 Pr1 Sb1 81.03(5) 25_455 25 ?
Sb1 Pr1 Sb1 54.69(3) 1_545 25 ?
Sb1 Pr1 Sb1 54.69(3) . 25 ?
Sb2 Pr1 Fe2 46.97(3) 25 . ?
Sb2 Pr1 Fe2 99.15(5) 25_445 . ?
Sb2 Pr1 Fe2 46.97(3) 25_455 . ?
Sb2 Pr1 Fe2 99.15(5) 25_545 . ?
Sb1 Pr1 Fe2 126.09(3) 25_455 . ?
Sb1 Pr1 Fe2 178.69(4) 1_545 . ?
Sb1 Pr1 Fe2 100.28(5) . . ?
Sb1 Pr1 Fe2 126.09(3) 25 . ?
Sb2 Pr1 Fe2 46.97(3) 25 21 ?
Sb2 Pr1 Fe2 99.15(5) 25_445 21 ?
Sb2 Pr1 Fe2 99.15(5) 25_455 21 ?
Sb2 Pr1 Fe2 46.97(3) 25_545 21 ?
Sb1 Pr1 Fe2 178.69(4) 25_455 21 ?
Sb1 Pr1 Fe2 126.09(3) 1_545 21 ?
Sb1 Pr1 Fe2 126.09(3) . 21 ?
Sb1 Pr1 Fe2 100.28(5) 25 21 ?
Fe2 Pr1 Fe2 53.10(5) . 21 ?
Sb2 Pr1 Fe2 99.15(5) 25 21_455 ?
Sb2 Pr1 Fe2 46.97(3) 25_445 21_455 ?
Sb2 Pr1 Fe2 46.97(3) 25_455 21_455 ?
Sb2 Pr1 Fe2 99.15(5) 25_545 21_455 ?
Sb1 Pr1 Fe2 100.28(5) 25_455 21_455 ?
Sb1 Pr1 Fe2 126.09(3) 1_545 21_455 ?
Sb1 Pr1 Fe2 126.09(3) . 21_455 ?
Sb1 Pr1 Fe2 178.69(4) 25 21_455 ?
Fe2 Pr1 Fe2 53.10(5) . 21_455 ?
Fe2 Pr1 Fe2 78.41(8) 21 21_455 ?
Sb2 Pr1 Fe2 99.15(5) 25 1_545 ?
Sb2 Pr1 Fe2 46.97(3) 25_445 1_545 ?
Sb2 Pr1 Fe2 99.15(5) 25_455 1_545 ?
Sb2 Pr1 Fe2 46.97(3) 25_545 1_545 ?
Sb1 Pr1 Fe2 126.09(3) 25_455 1_545 ?
Sb1 Pr1 Fe2 100.28(5) 1_545 1_545 ?
Sb1 Pr1 Fe2 178.69(4) . 1_545 ?
Sb1 Pr1 Fe2 126.09(3) 25 1_545 ?
Fe2 Pr1 Fe2 78.41(8) . 1_545 ?
Fe2 Pr1 Fe2 53.10(5) 21 1_545 ?
Fe2 Pr1 Fe2 53.10(5) 21_455 1_545 ?
Fe2 Fe1 Fe2 74.07(6) 29_444 9_444 ?
Fe2 Fe1 Fe2 116.82(13) 29_444 29_454 ?
Fe2 Fe1 Fe2 74.07(6) 9_444 29_454 ?
Fe2 Fe1 Fe2 74.07(6) 29_444 9_544 ?
Fe2 Fe1 Fe2 116.82(13) 9_444 9_544 ?
Fe2 Fe1 Fe2 74.07(6) 29_454 9_544 ?
Fe2 Fe1 Fe2 180.00(13) 29_444 13 ?
Fe2 Fe1 Fe2 105.93(6) 9_444 13 ?
Fe2 Fe1 Fe2 63.18(13) 29_454 13 ?
Fe2 Fe1 Fe2 105.93(6) 9_544 13 ?
Fe2 Fe1 Fe2 105.93(6) 29_444 25 ?
Fe2 Fe1 Fe2 180.00(13) 9_444 25 ?
Fe2 Fe1 Fe2 105.93(6) 29_454 25 ?
Fe2 Fe1 Fe2 63.18(13) 9_544 25 ?
Fe2 Fe1 Fe2 74.07(6) 13 25 ?
Fe2 Fe1 Fe2 105.93(6) 29_444 25_455 ?
Fe2 Fe1 Fe2 63.18(13) 9_444 25_455 ?
Fe2 Fe1 Fe2 105.93(6) 29_454 25_455 ?
Fe2 Fe1 Fe2 180.00(13) 9_544 25_455 ?
Fe2 Fe1 Fe2 74.07(6) 13 25_455 ?
Fe2 Fe1 Fe2 116.82(13) 25 25_455 ?
Fe2 Fe1 Fe2 63.18(13) 29_444 13_545 ?
Fe2 Fe1 Fe2 105.93(6) 9_444 13_545 ?
Fe2 Fe1 Fe2 180.00(13) 29_454 13_545 ?
Fe2 Fe1 Fe2 105.93(6) 9_544 13_545 ?
Fe2 Fe1 Fe2 116.82(13) 13 13_545 ?
Fe2 Fe1 Fe2 74.07(6) 25 13_545 ?
Fe2 Fe1 Fe2 74.07(6) 25_455 13_545 ?
Fe2 Fe1 Sb2 58.41(7) 29_444 17 ?
Fe2 Fe1 Sb2 58.41(7) 9_444 17 ?
Fe2 Fe1 Sb2 58.41(7) 29_454 17 ?
Fe2 Fe1 Sb2 58.41(7) 9_544 17 ?
Fe2 Fe1 Sb2 121.59(7) 13 17 ?
Fe2 Fe1 Sb2 121.59(7) 25 17 ?
Fe2 Fe1 Sb2 121.59(7) 25_455 17 ?
Fe2 Fe1 Sb2 121.59(7) 13_545 17 ?
Fe2 Fe1 Sb2 121.59(7) 29_444 . ?
Fe2 Fe1 Sb2 121.59(7) 9_444 . ?
Fe2 Fe1 Sb2 121.59(7) 29_454 . ?
Fe2 Fe1 Sb2 121.59(7) 9_544 . ?
Fe2 Fe1 Sb2 58.41(7) 13 . ?
Fe2 Fe1 Sb2 58.41(7) 25 . ?
Fe2 Fe1 Sb2 58.41(7) 25_455 . ?
Fe2 Fe1 Sb2 58.41(7) 13_545 . ?
Sb2 Fe1 Sb2 180.0 17 . ?
Fe2 Fe1 Sb3 131.86(5) 29_444 25 ?
Fe2 Fe1 Sb3 131.86(5) 9_444 25 ?
Fe2 Fe1 Sb3 58.24(7) 29_454 25 ?
Fe2 Fe1 Sb3 58.24(7) 9_544 25 ?
Fe2 Fe1 Sb3 48.14(5) 13 25 ?
Fe2 Fe1 Sb3 48.14(5) 25 25 ?
Fe2 Fe1 Sb3 121.76(7) 25_455 25 ?
Fe2 Fe1 Sb3 121.76(7) 13_545 25 ?
Sb2 Fe1 Sb3 97.73(9) 17 25 ?
Sb2 Fe1 Sb3 82.27(9) . 25 ?
Fe2 Fe1 Sb3 48.14(5) 29_444 9_444 ?
Fe2 Fe1 Sb3 48.14(5) 9_444 9_444 ?
Fe2 Fe1 Sb3 121.76(7) 29_454 9_444 ?
Fe2 Fe1 Sb3 121.76(7) 9_544 9_444 ?
Fe2 Fe1 Sb3 131.86(5) 13 9_444 ?
Fe2 Fe1 Sb3 131.86(5) 25 9_444 ?
Fe2 Fe1 Sb3 58.24(7) 25_455 9_444 ?
```

```
Fe2 Fe1 Sb3 58.24(7) 13_545 9_444 ?
Sb2 Fe1 Sb3 82.27(9) 17 9_444 ?
Sb2 Fe1 Sb3 97.73(9) . 9_444 ?
Sb3 Fe1 Sb3 180.00(18) 25 9_444 ?
Sb3 Fe2 Sb3 134.2(3) 1_565 . ?
Sb3 Fe2 Fe1 78.23(8) 1_565 9 ?
Sb3 Fe2 Fe1 78.23(8) . 9 ?
Sb3 Fe2 Fe1 78.23(8) 1_565 9_455 ?
Sb3 Fe2 Fe1 78.23(8) . 9_455 ?
Fe1 Fe2 Fe1 116.82(13) 9 9_455 ?
Sb3 Fe2 Fe2 67.08(13) 1_565 17_566 ?
Sb3 Fe2 Fe2 67.08(13) . 17_566 ?
Fe1 Fe2 Fe2 58.41(7) 9 17_566 ?
Fe1 Fe2 Fe2 58.41(7) 9_455 17_566 ?
Sb3 Fe2 Sb2 103.14(6) 1_565 25_455 ?
Sb3 Fe2 Sb2 103.14(6) . 25_455 ?
Fe1 Fe2 Sb2 175.89(13) 9 25_455 ?
Fe1 Fe2 Sb2 67.29(4) 9_455 25_455 ?
Fe2 Fe2 Sb2 125.70(7) 17_566 25_455 ?
Sb3 Fe2 Sb2 103.14(6) 1_565 25 ?
Sb3 Fe2 Sb2 103.14(6) . 25 ?
Fe1 Fe2 Sb2 67.29(4) 9 25 ?
Fe1 Fe2 Sb2 175.89(13) 9_455 25 ?
Fe2 Fe2 Sb2 125.70(7) 17_566 25 ?
Sb2 Fe2 Sb2 108.60(13) 25_455 25 ?
Sb3 Fe2 Sb3 15.98(18) 1_565 17_566 ?
Sb3 Fe2 Sb3 118.17(13) . 17_566 ?
Fe1 Fe2 Sb3 70.79(7) 9 17_566 ?
Fe1 Fe2 Sb3 70.79(7) 9_455 17_566 ?
Fe2 Fe2 Sb3 51.10(10) 17_566 17_566 ?
Sb2 Fe2 Sb3 111.50(5) 25_455 17_566 ?
Sb2 Fe2 Sb3 111.50(5) 25 17_566 ?
Sb3 Fe2 Sb3 118.17(13) 1_565 17_556 ?
Sb3 Fe2 Sb3 15.98(18) . 17_556 ?
Fe1 Fe2 Sb3 70.79(7) 9 17_556 ?
Fe1 Fe2 Sb3 70.79(7) 9_455 17_556 ?
Fe2 Fe2 Sb3 51.10(10) 17_566 17_556 ?
Sb2 Fe2 Sb3 111.50(5) 25_455 17_556 ?
Sb2 Fe2 Sb3 111.50(5) 25 17_556 ?
Sb3 Fe2 Sb3 102.2(2) 17_566 17_556 ?
Sb3 Fe2 Pr1 152.13(15) 1_565 . ?
Sb3 Fe2 Pr1 73.72(12) . . ?
Fe1 Fe2 Pr1 113.95(4) 9 . ?
Fe1 Fe2 Pr1 113.95(4) 9_455 . ?
Fe2 Fe2 Pr1 140.80(4) 17_566 . ?
Sb2 Fe2 Pr1 63.12(6) 25_455 . ?
Sb2 Fe2 Pr1 63.12(6) 25 . ?
Sb3 Fe2 Pr1 168.11(12) 17_566 . ?
Sb3 Fe2 Pr1 89.70(9) 17_556 . ?
Sb3 Fe2 Pr1 73.72(12) 1_565 1_565 ?
Sb3 Fe2 Pr1 152.13(15) . 1_565 ?
Fe1 Fe2 Pr1 113.95(4) 9 1_565 ?
Fe1 Fe2 Pr1 113.95(4) 9_455 1_565 ?
Fe2 Fe2 Pr1 140.80(4) 17_566 1_565 ?
Sb2 Fe2 Pr1 63.12(6) 25_455 1_565 ?
Sb2 Fe2 Pr1 63.12(6) 25 1_565 ?
Sb3 Fe2 Pr1 89.70(9) 17_566 1_565 ?
Sb3 Fe2 Pr1 168.11(12) 17_556 1_565 ?
Pr1 Fe2 Pr1 78.41(8) . 1_565 ?
Sb1 Sb1 Sb1 180.0 25_565 25_455 ?
Sb1 Sb1 Sb1 90.0 25_565 25_465 ?
Sb1 Sb1 Sb1 90.0 25_455 25_465 ?
Sb1 Sb1 Sb1 90.0 25_565 25 ?
Sb1 Sb1 Sb1 90.0 25_455 25 ?
Sb1 Sb1 Sb1 180.0 25_465 25 ?
Sb1 Sb1 Pr1 117.346(14) 25_565 25_455 ?
Sb1 Sb1 Pr1 62.654(14) 25_455 25_455 ?
Sb1 Sb1 Pr1 62.654(14) 25_465 25_455 ?
Sb1 Sb1 Pr1 117.346(14) 25 25_455 ?
Sb1 Sb1 Pr1 62.654(14) 25_565 1_565 ?
Sb1 Sb1 Pr1 117.346(14) 25_455 1_565 ?
Sb1 Sb1 Pr1 62.654(14) 25_465 1_565 ?
Sb1 Sb1 Pr1 117.346(14) 25 1_565 ?
Pr1 Sb1 Pr1 125.31(3) 25_455 1_565 ?
Sb1 Sb1 Pr1 62.654(14) 25_565 25 ?
Sb1 Sb1 Pr1 117.346(14) 25_455 25 ?
Sb1 Sb1 Pr1 117.346(14) 25_465 25 ?
Sb1 Sb1 Pr1 62.654(14) 25 25 ?
Pr1 Sb1 Pr1 81.03(5) 25_455 25 ?
Pr1 Sb1 Pr1 125.31(3) 1_565 25 ?
Sb1 Sb1 Pr1 117.346(14) 25_565 . ?
Sb1 Sb1 Pr1 62.654(14) 25_455 . ?
Sb1 Sb1 Pr1 117.346(14) 25_465 . ?
Sb1 Sb1 Pr1 62.654(14) 25 . ?
Pr1 Sb1 Pr1 125.31(3) 25_455 . ?
Pr1 Sb1 Pr1 81.03(5) 1_565 . ?
Pr1 Sb1 Pr1 125.31(3) 25 . ?
Fe2 Sb2 Fe2 70.09(7) 13_545 25_455 ?
Fe2 Sb2 Fe2 108.60(13) 13_545 13 ?
Fe2 Sb2 Fe2 70.09(7) 25_455 13 ?
Fe2 Sb2 Fe2 70.09(7) 13_545 25 ?
Fe2 Sb2 Fe2 108.60(13) 25_455 25 ?
Fe2 Sb2 Fe2 70.09(7) 13 25 ?
Fe2 Sb2 Fe1 54.30(7) 13_545 . ?
Fe2 Sb2 Fe1 54.30(7) 25_455 . ?
Fe2 Sb2 Fe1 54.30(7) 13 . ?
Fe2 Sb2 Fe1 54.30(7) 25 . ?
Fe2 Sb2 Pr1 137.52(2) 13_545 25 ?
Fe2 Sb2 Pr1 137.52(2) 25_455 25 ?
Fe2 Sb2 Pr1 69.91(5) 13 25 ?
Fe2 Sb2 Pr1 69.91(5) 25 25 ?
Fe1 Sb2 Pr1 109.74(3) . 25 ?
Fe2 Sb2 Pr1 69.91(5) 13_545 25_445 ?
Fe2 Sb2 Pr1 69.91(5) 25_455 25_445 ?
Fe2 Sb2 Pr1 137.52(2) 13 25_445 ?
Fe2 Sb2 Pr1 137.52(2) 25 25_445 ?
Fe1 Sb2 Pr1 109.74(3) . 25_445 ?
Pr1 Sb2 Pr1 140.53(6) 25 25_445 ?
Fe2 Sb2 Pr1 69.91(5) 13_545 25_545 ?
Fe2 Sb2 Pr1 137.52(2) 25_455 25_545 ?
Fe2 Sb2 Pr1 137.52(2) 13 25_545 ?
Fe2 Sb2 Pr1 69.91(5) 25 25_545 ?
Fe1 Sb2 Pr1 109.74(3) . 25_545 ?
Pr1 Sb2 Pr1 83.45(2) 25 25_545 ?
Pr1 Sb2 Pr1 83.45(2) 25_445 25_545 ?
Fe2 Sb2 Pr1 137.52(2) 13_545 25_455 ?
Fe2 Sb2 Pr1 69.91(5) 25_455 25_455 ?
Fe2 Sb2 Pr1 69.91(5) 13 25_455 ?
Fe2 Sb2 Pr1 137.52(2) 25 25_455 ?
Fe1 Sb2 Pr1 109.74(3) . 25_455 ?
Pr1 Sb2 Pr1 83.45(2) 25 25_455 ?
Pr1 Sb2 Pr1 83.45(2) 25_445 25_455 ?
Pr1 Sb2 Pr1 140.53(6) 25_545 25_455 ?
Sb3 Sb3 Fe2 112.92(13) 17_556 21_455 ?
Sb3 Sb3 Fe2 112.92(13) 17_556 1_545 ?
Fe2 Sb3 Fe2 81.27(9) 21_455 1_545 ?
Sb3 Sb3 Fe2 112.92(13) 17_556 21 ?
Fe2 Sb3 Fe2 134.2(3) 21_455 21 ?
Fe2 Sb3 Fe2 81.27(9) 1_545 21 ?
Sb3 Sb3 Fe2 112.92(13) 17_556 . ?
Fe2 Sb3 Fe2 81.27(9) 21_455 . ?
Fe2 Sb3 Fe2 134.2(3) 1_545 . ?
Fe2 Sb3 Fe2 81.27(9) 21 . ?
Sb3 Sb3 Fe2 51.10(10) 17_556 5_656 ?
Fe2 Sb3 Fe2 164.02(18) 21_455 5_656 ?
Fe2 Sb3 Fe2 104.16(7) 1_545 5_656 ?
Fe2 Sb3 Fe2 61.83(13) 21 5_656 ?
Fe2 Sb3 Fe2 104.16(7) . 5_656 ?
Sb3 Sb3 Fe2 51.10(10) 17_556 17_566 ?
Fe2 Sb3 Fe2 104.16(7) 21_455 17_566 ?
Fe2 Sb3 Fe2 164.02(18) 1_545 17_566 ?
Fe2 Sb3 Fe2 104.16(7) 21 17_566 ?
```

```
Fe2 Sb3 Fe2 61.83(13) . 17_566 ?
Fe2 Sb3 Fe2 66.77(10) 5_656 17_566 ?
Sb3 Sb3 Fe2 51.10(10) 17_556 5_556 ?
Fe2 Sb3 Fe2 61.83(13) 21_455 5_556 ?
Fe2 Sb3 Fe2 104.16(7) 1_545 5_556 ?
Fe2 Sb3 Fe2 164.02(18) 21 5_556 ?
Fe2 Sb3 Fe2 104.16(7) . 5_556 ?
Fe2 Sb3 Fe2 102.19(19) 5_656 5_556 ?
Fe2 Sb3 Fe2 66.77(10) 17_566 5_556 ?
Sb3 Sb3 Fe2 51.10(10) 17_556 17_556 ?
Fe2 Sb3 Fe2 104.16(7) 21_455 17_556 ?
Fe2 Sb3 Fe2 61.83(13) 1_545 17_556 ?
Fe2 Sb3 Fe2 104.16(7) 21 17_556 ?
Fe2 Sb3 Fe2 164.02(18) . 17_556 ?
Fe2 Sb3 Fe2 66.77(10) 5_656 17_556 ?
Fe2 Sb3 Fe2 102.19(19) 17_566 17_556 ?
Fe2 Sb3 Fe2 66.77(10) 5_556 17_556 ?
Sb3 Sb3 Fe1 82.27(9) 17_556 9 ?
Fe2 Sb3 Fe1 134.25(6) 21_455 9 ?
Fe2 Sb3 Fe1 134.25(6) 1_545 9 ?
Fe2 Sb3 Fe1 53.64(4) 21 9 ?
Fe2 Sb3 Fe1 53.64(4) . 9 ?
Fe2 Sb3 Fe1 50.97(4) 5_656 9 ?
Fe2 Sb3 Fe1 50.97(4) 17_566 9 ?
Fe2 Sb3 Fe1 117.44(12) 5_556 9 ?
Fe2 Sb3 Fe1 117.44(12) 17_556 9 ?
Sb3 Sb3 Fe1 82.27(9) 17_556 9_445 ?
Fe2 Sb3 Fe1 53.64(4) 21_455 9_445 ?
Fe2 Sb3 Fe1 53.64(4) 1_545 9_445 ?
Fe2 Sb3 Fe1 134.25(6) 21 9_445 ?
Fe2 Sb3 Fe1 134.25(6) . 9_445 ?
Fe2 Sb3 Fe1 117.44(12) 5_656 9_445 ?
Fe2 Sb3 Fe1 117.44(12) 17_566 9_445 ?
Fe2 Sb3 Fe1 50.97(4) 5_556 9_445 ?
Fe2 Sb3 Fe1 50.97(4) 17_556 9_445 ?
Fe1 Sb3 Fe1 164.53(18) 9 9_445 ?
Sb3 Sb3 Fe1 82.27(9) 17_556 9_545 ?
Fe2 Sb3 Fe1 134.25(6) 21_455 9_545 ?
Fe2 Sb3 Fe1 53.64(4) 1_545 9_545 ?
Fe2 Sb3 Fe1 53.64(4) 21 9_545 ?
Fe2 Sb3 Fe1 134.25(6) . 9_545 ?
Fe2 Sb3 Fe1 50.97(4) 5_656 9_545 ?
Fe2 Sb3 Fe1 117.44(12) 17_566 9_545 ?
Fe2 Sb3 Fe1 117.44(12) 5_556 9_545 ?
Fe2 Sb3 Fe1 50.97(4) 17_556 9_545 ?
Fe1 Sb3 Fe1 88.96(2) 9 9_545 ?
Fe1 Sb3 Fe1 88.96(2) 9_445 9_545 ?

_diffrn_measured_fraction_theta_max    0.986
_diffrn_reflns_theta_full              36.84
_diffrn_measured_fraction_theta_full   0.986
_refine_diff_density_max    5.106
_refine_diff_density_min   -3.280
_refine_diff_density_rms    0.743

#===END
```

A1.8 $Nd_2Fe_4Sb_5$

```
data_shelxl

_audit_creation_method            SHELXL-97
_chemical_name_systematic
;
 ?
;
_chemical_name_common             ?
_chemical_melting_point           ?
_chemical_formula_moiety          'Fe3.96
Nd2 Sb4.91'
_chemical_formula_sum
 'Fe3.96 Nd2 Sb4.91'
_chemical_formula_weight          1107.16

loop_
 _atom_type_symbol
 _atom_type_description
 _atom_type_scat_dispersion_real
 _atom_type_scat_dispersion_imag
 _atom_type_scat_source
 'Nd'  'Nd'  -0.1943   3.0179
 'International Tables Vol C Tables 4.2.6.8
and 6.1.1.4'
 'Fe'  'Fe'   0.3463   0.8444
 'International Tables Vol C Tables 4.2.6.8
and 6.1.1.4'
 'Sb'  'Sb'  -0.5866   1.5461
 'International Tables Vol C Tables 4.2.6.8
and 6.1.1.4'

_symmetry_cell_setting
'Tetragonal'
_symmetry_space_group_name_H-M    'I 4/m m m
'

loop_
 _symmetry_equiv_pos_as_xyz
 'x, y, z'
 '-x, -y, z'
 'x, -y, -z'
 '-x, y, -z'
 '-y, -x, -z'
 'y, x, -z'
 'y, -x, z'
 '-y, x, z'
 'x+1/2, y+1/2, z+1/2'
 '-x+1/2, -y+1/2, z+1/2'
 'x+1/2, -y+1/2, -z+1/2'
 '-x+1/2, y+1/2, -z+1/2'
 '-y+1/2, -x+1/2, -z+1/2'
 'y+1/2, x+1/2, -z+1/2'
 'y+1/2, -x+1/2, z+1/2'
 '-y+1/2, x+1/2, z+1/2'
 '-x, -y, -z'
 'x, y, -z'
 '-x, y, z'
 'x, -y, z'
 'y, x, z'
 '-y, -x, z'
 '-y, x, -z'
 'y, -x, -z'
 '-x+1/2, -y+1/2, -z+1/2'
 'x+1/2, y+1/2, -z+1/2'
 '-x+1/2, y+1/2, z+1/2'
 'x+1/2, -y+1/2, z+1/2'
 'y+1/2, x+1/2, z+1/2'
 '-y+1/2, -x+1/2, z+1/2'
 '-y+1/2, x+1/2, -z+1/2'
 'y+1/2, -x+1/2, -z+1/2'

_cell_length_a                    4.3051(15)
_cell_length_b                    4.3051(15)
_cell_length_c
25.9080(15)
_cell_angle_alpha                 90
_cell_angle_beta                  90
_cell_angle_gamma                 90
_cell_volume                      480.2(2)
_cell_formula_units_Z             2
_cell_measurement_temperature     298(2)
_cell_measurement_reflns_used     419
_cell_measurement_theta_min       2.6
_cell_measurement_theta_max       33.1
```

```
_exptl_crystal_description        plate
_exptl_crystal_colour             black
_exptl_crystal_size_max           0.13
_exptl_crystal_size_mid           0.08
_exptl_crystal_size_min           0.01
_exptl_crystal_density_meas       ?
_exptl_crystal_density_diffrn     7.658
_exptl_crystal_density_method     'not
measured'
_exptl_crystal_F_000              946
_exptl_absorpt_coefficient_mu     29.867
_exptl_absorpt_correction_type    'multi-
scan'
_exptl_absorpt_correction_T_min   0.1180
_exptl_absorpt_correction_T_max   0.7065
_exptl_absorpt_process_details    'HKL
Scalepack (Otwinowski & Minor 1997)'

_exptl_special_details
;
 ?
;

_diffrn_ambient_temperature       298(2)
_diffrn_radiation_wavelength      0.71073
_diffrn_radiation_type            MoK\a
_diffrn_radiation_source          'fine-
focus sealed tube'
_diffrn_radiation_monochromator   graphite
_diffrn_measurement_device_type   'Nonius
KappaCCD'
_diffrn_measurement_method        '\w and \f
scans'
_diffrn_detector_area_resol_mean  ?
_diffrn_standards_number          ?
_diffrn_standards_interval_count  ?
_diffrn_standards_interval_time   ?
_diffrn_standards_decay_%         ?
_diffrn_reflns_number             5198
_diffrn_reflns_av_R_equivalents   0.0259
_diffrn_reflns_av_sigmaI/netI     0.0179
_diffrn_reflns_limit_h_min        0
_diffrn_reflns_limit_h_max        6
_diffrn_reflns_limit_k_min        -3
_diffrn_reflns_limit_k_max        4
_diffrn_reflns_limit_l_min        0
_diffrn_reflns_limit_l_max        38
_diffrn_reflns_theta_min          3.15
_diffrn_reflns_theta_max          32.75
_reflns_number_total              311
_reflns_number_gt                 298
_reflns_threshold_expression      I>2\s(I)

_computing_data_collection        ?
_computing_cell_refinement        ?
_computing_data_reduction         ?
_computing_structure_solution     ?
_computing_structure_refinement   'SHELXL-97
(Sheldrick, 2008)'
_computing_molecular_graphics     ?
_computing_publication_material   ?

_refine_special_details
;
 Refinement of F^2^ against ALL reflections.
The weighted R-factor wR and
 goodness of fit S are based on F^2^,
conventional R-factors R are based
 on F, with F set to zero for negative F^2^.
The threshold expression of
 F^2^ > 2\s(F^2^) is used only for
calculating R-factors(gt) etc. and is
 not relevant to the choice of reflections
for refinement.  R-factors based
 on F^2^ are statistically about twice as
large as those based on F, and R-
 factors based on ALL data will be even
larger.
;

_refine_ls_structure_factor_coef  Fsqd
_refine_ls_matrix_type            full
_refine_ls_weighting_scheme       calc
_refine_ls_weighting_details
 'calc
w=1/[\s^2^(Fo^2^)+(0.0551P)^2^+42.6505P]
where P=(Fo^2^+2Fc^2^)/3'
_atom_sites_solution_primary      direct
_atom_sites_solution_secondary    difmap
_atom_sites_solution_hydrogens    ?
_refine_ls_hydrogen_treatment     ?
_refine_ls_extinction_method      SHELXL
_refine_ls_extinction_coef        0.0041(6)
_refine_ls_extinction_expression
 'Fc^*^=kFc[1+0.001xFc^2^\l^3^/sin(2\q)]^-
1/4^'
_refine_ls_number_reflns          311
_refine_ls_number_parameters      21
_refine_ls_number_restraints      0
_refine_ls_R_factor_all           0.0450
_refine_ls_R_factor_gt            0.0437
_refine_ls_wR_factor_ref          0.1177
_refine_ls_wR_factor_gt           0.1167
_refine_ls_goodness_of_fit_ref    1.211
_refine_ls_restrained_S_all       1.211
_refine_ls_shift/su_max           0.000
_refine_ls_shift/su_mean          0.000

loop_
 _atom_site_label
 _atom_site_type_symbol
 _atom_site_fract_x
 _atom_site_fract_y
 _atom_site_fract_z
 _atom_site_U_iso_or_equiv
 _atom_site_adp_type
 _atom_site_occupancy
 _atom_site_symmetry_multiplicity
 _atom_site_calc_flag
 _atom_site_refinement_flags
 _atom_site_disorder_assembly
 _atom_site_disorder_group
Nd1 Nd 0.0000 0.0000 0.34686(4) 0.0103(4)
Uani 1 8 d S . .
Fe1 Fe 0.0000 0.0000 0.0000 0.0117(9) Uani 1
16 d S . .
Fe2 Fe 0.0000 0.5000 0.44849(13) 0.0328(17)
Uani 0.739(17) 4 d SP . .
Sb1 Sb 0.0000 0.5000 0.2500 0.0080(4) Uani 1
8 d S . .
Sb2 Sb 0.0000 0.0000 0.11160(5) 0.0100(4)
Uani 1 8 d S . .
Sb3 Sb 0.0000 0.0000 0.48338(16) 0.0247(13)
Uani 0.456(10) 8 d SP . .

loop_
 _atom_site_aniso_label
 _atom_site_aniso_U_11
 _atom_site_aniso_U_22
 _atom_site_aniso_U_33
 _atom_site_aniso_U_23
```

```
 _atom_site_aniso_U_13
 _atom_site_aniso_U_12
Nd1 0.0103(4) 0.0103(4) 0.0102(6) 0.000
0.000 0.000
Fe1 0.0133(13) 0.0133(13) 0.0085(17) 0.000
0.000 0.000
Fe2 0.0089(17) 0.081(4) 0.0083(16) 0.000
0.000 0.000
Sb1 0.0087(5) 0.0087(5) 0.0065(6) 0.000
0.000 0.000
Sb2 0.0103(5) 0.0103(5) 0.0093(6) 0.000
0.000 0.000
Sb3 0.0293(17) 0.0293(17) 0.0157(14) 0.000
0.000 0.000

_geom_special_details
;
 All s.u.'s (except the s.u. in the dihedral
angle between two l.s. planes)
 are estimated using the full covariance
matrix.  The cell s.u.'s are taken
 into account individually in the estimation
of s.u.'s in distances, angles
 and torsion angles; correlations between
s.u.'s in cell parameters are only
 used when they are defined by crystal
symmetry.  An approximate (isotropic)
 treatment of cell s.u.'s is used for
estimating s.u.'s involving l.s. planes.
;

loop_
 _geom_bond_atom_site_label_1
 _geom_bond_atom_site_label_2
 _geom_bond_distance
 _geom_bond_site_symmetry_2
 _geom_bond_publ_flag
Nd1 Sb2 3.2288(12) 25 ?
Nd1 Sb2 3.2288(12) 25_445 ?
Nd1 Sb2 3.2288(12) 25_455 ?
Nd1 Sb2 3.2288(12) 25_545 ?
Nd1 Sb1 3.3062(10) 25_455 ?
Nd1 Sb1 3.3062(10) 1_545 ?
Nd1 Sb1 3.3062(10) . ?
Nd1 Sb1 3.3062(10) 25 ?
Nd1 Fe2 3.401(3) . ?
Nd1 Fe2 3.401(3) 21 ?
Nd1 Fe2 3.401(3) 21_455 ?
Nd1 Fe2 3.401(3) 1_545 ?
Fe1 Fe2 2.5326(18) 29_444 ?
Fe1 Fe2 2.5326(18) 13 ?
Fe1 Fe2 2.5326(18) 9_444 ?
Fe1 Fe2 2.5326(18) 25 ?
Fe1 Fe2 2.5326(18) 29_454 ?
Fe1 Fe2 2.5326(18) 25_455 ?
Fe1 Fe2 2.5326(18) 13_545 ?
Fe1 Fe2 2.5326(18) 9_544 ?
Fe1 Sb2 2.8913(14) . ?
Fe1 Sb2 2.8913(14) 17 ?
Fe1 Sb3 3.0745(12) 25 ?
Fe1 Sb3 3.0745(12) 9_444 ?
Fe2 Sb3 2.335(2) 1_565 ?
Fe2 Sb3 2.335(2) . ?
Fe2 Fe1 2.5326(18) 9 ?
Fe2 Fe1 2.5326(18) 9_455 ?
Fe2 Sb2 2.657(2) 25_455 ?
Fe2 Sb2 2.657(2) 25 ?
Fe2 Fe2 2.669(6) 17_566 ?
Fe2 Sb3 2.784(3) 17_566 ?
Fe2 Sb3 2.784(3) 17_556 ?
Fe2 Nd1 3.401(3) 1_565 ?
Sb1 Sb1 3.0442(11) 25_565 ?
Sb1 Sb1 3.0442(11) 25_455 ?
Sb1 Sb1 3.0442(11) 25_465 ?
Sb1 Sb1 3.0442(11) 25 ?
Sb1 Nd1 3.3062(10) 25_455 ?
Sb1 Nd1 3.3062(10) 1_565 ?
Sb1 Nd1 3.3062(10) 25 ?
Sb2 Fe2 2.657(2) 13_545 ?
Sb2 Fe2 2.657(2) 25_455 ?
Sb2 Fe2 2.657(2) 13 ?
Sb2 Fe2 2.657(2) 25 ?
Sb2 Nd1 3.2288(12) 25 ?
Sb2 Nd1 3.2288(12) 25_445 ?
Sb2 Nd1 3.2288(12) 25_545 ?
Sb2 Nd1 3.2288(12) 25_455 ?
Sb3 Sb3 0.861(8) 17_556 ?
Sb3 Fe2 2.335(2) 21_455 ?
Sb3 Fe2 2.335(2) 1_545 ?
Sb3 Fe2 2.335(2) 21 ?
Sb3 Fe2 2.784(3) 5_656 ?
Sb3 Fe2 2.784(3) 17_566 ?
Sb3 Fe2 2.784(3) 5_556 ?
Sb3 Fe2 2.784(3) 17_556 ?
Sb3 Fe1 3.0745(12) 9 ?
Sb3 Fe1 3.0745(12) 9_445 ?
Sb3 Fe1 3.0745(12) 9_545 ?

loop_
 _geom_angle_atom_site_label_1
 _geom_angle_atom_site_label_2
 _geom_angle_atom_site_label_3
 _geom_angle
 _geom_angle_site_symmetry_1
 _geom_angle_site_symmetry_3
 _geom_angle_publ_flag
Sb2 Nd1 Sb2 141.06(6) 25 25_445 ?
Sb2 Nd1 Sb2 83.621(19) 25 25_455 ?
Sb2 Nd1 Sb2 83.621(19) 25_445 25_455 ?
Sb2 Nd1 Sb2 83.621(19) 25 25_545 ?
Sb2 Nd1 Sb2 83.621(19) 25_445 25_545 ?
Sb2 Nd1 Sb2 141.06(6) 25_455 25_545 ?
Sb2 Nd1 Sb1 133.40(3) 25 25_455 ?
Sb2 Nd1 Sb1 79.57(3) 25_445 25_455 ?
Sb2 Nd1 Sb1 79.57(3) 25_455 25_455 ?
Sb2 Nd1 Sb1 133.40(3) 25_545 25_455 ?
Sb2 Nd1 Sb1 133.40(3) 25 1_545 ?
Sb2 Nd1 Sb1 79.57(3) 25_445 1_545 ?
Sb2 Nd1 Sb1 133.40(3) 25_455 1_545 ?
Sb2 Nd1 Sb1 79.57(3) 25_545 1_545 ?
Sb1 Nd1 Sb1 54.823(19) 25_455 1_545 ?
Sb2 Nd1 Sb1 79.57(3) 25 . ?
Sb2 Nd1 Sb1 133.40(3) 25_445 . ?
Sb2 Nd1 Sb1 79.57(3) 25_455 . ?
Sb2 Nd1 Sb1 133.40(3) 25_545 . ?
Sb1 Nd1 Sb1 54.823(19) 25_455 . ?
Sb1 Nd1 Sb1 81.24(3) 1_545 . ?
Sb2 Nd1 Sb1 79.57(3) 25 25 ?
Sb2 Nd1 Sb1 133.40(3) 25_445 25 ?
Sb2 Nd1 Sb1 133.40(3) 25_455 25 ?
Sb2 Nd1 Sb1 79.57(3) 25_545 25 ?
Sb1 Nd1 Sb1 81.24(3) 25_455 25 ?
Sb1 Nd1 Sb1 54.823(19) 1_545 25 ?
Sb1 Nd1 Sb1 54.823(19) . 25 ?
Sb2 Nd1 Fe2 47.15(3) 25 . ?
Sb2 Nd1 Fe2 99.43(4) 25_445 . ?
Sb2 Nd1 Fe2 47.15(3) 25_455 . ?
Sb2 Nd1 Fe2 99.43(4) 25_545 . ?
Sb1 Nd1 Fe2 125.99(2) 25_455 . ?
Sb1 Nd1 Fe2 178.64(4) 1_545 . ?
Sb1 Nd1 Fe2 100.11(4) . . ?
Sb1 Nd1 Fe2 125.99(2) 25 . ?
```

```
Sb2 Nd1 Fe2 47.15(3) 25 21 ?
Sb2 Nd1 Fe2 99.43(4) 25_445 21 ?
Sb2 Nd1 Fe2 99.43(4) 25_455 21 ?
Sb2 Nd1 Fe2 47.15(3) 25_545 21 ?
Sb1 Nd1 Fe2 178.64(4) 25_455 21 ?
Sb1 Nd1 Fe2 125.99(2) 1_545 21 ?
Sb1 Nd1 Fe2 125.99(2) . 21 ?
Sb1 Nd1 Fe2 100.11(4) 25 21 ?
Fe2 Nd1 Fe2 53.17(5) . 21 ?
Sb2 Nd1 Fe2 99.43(4) 25 21_455 ?
Sb2 Nd1 Fe2 47.15(3) 25_445 21_455 ?
Sb2 Nd1 Fe2 47.15(3) 25_455 21_455 ?
Sb2 Nd1 Fe2 99.43(4) 25_545 21_455 ?
Sb1 Nd1 Fe2 100.11(4) 25_455 21_455 ?
Sb1 Nd1 Fe2 125.99(2) 1_545 21_455 ?
Sb1 Nd1 Fe2 125.99(2) . 21_455 ?
Sb1 Nd1 Fe2 178.64(4) 25 21_455 ?
Fe2 Nd1 Fe2 53.17(5) . 21_455 ?
Fe2 Nd1 Fe2 78.53(7) 21 21_455 ?
Sb2 Nd1 Fe2 99.43(4) 25 1_545 ?
Sb2 Nd1 Fe2 47.15(3) 25_445 1_545 ?
Sb2 Nd1 Fe2 99.43(4) 25_455 1_545 ?
Sb2 Nd1 Fe2 47.15(3) 25_545 1_545 ?
Sb1 Nd1 Fe2 125.99(2) 25_455 1_545 ?
Sb1 Nd1 Fe2 100.11(4) 1_545 1_545 ?
Sb1 Nd1 Fe2 178.64(4) . 1_545 ?
Sb1 Nd1 Fe2 125.99(2) 25 1_545 ?
Fe2 Nd1 Fe2 78.53(7) . 1_545 ?
Fe2 Nd1 Fe2 53.17(5) 21 1_545 ?
Fe2 Nd1 Fe2 53.17(5) 21_455 1_545 ?
Fe2 Fe1 Fe2 180.00(12) 29_444 13 ?
Fe2 Fe1 Fe2 73.88(6) 29_444 9_444 ?
Fe2 Fe1 Fe2 106.12(6) 13 9_444 ?
Fe2 Fe1 Fe2 106.12(6) 29_444 25 ?
Fe2 Fe1 Fe2 73.88(6) 13 25 ?
Fe2 Fe1 Fe2 180.00(12) 9_444 25 ?
Fe2 Fe1 Fe2 116.41(13) 29_444 29_454 ?
Fe2 Fe1 Fe2 63.59(13) 13 29_454 ?
Fe2 Fe1 Fe2 73.88(6) 9_444 29_454 ?
Fe2 Fe1 Fe2 106.12(6) 25 29_454 ?
Fe2 Fe1 Fe2 106.12(6) 29_444 25_455 ?
Fe2 Fe1 Fe2 73.88(6) 13 25_455 ?
Fe2 Fe1 Fe2 63.59(13) 9_444 25_455 ?
Fe2 Fe1 Fe2 116.41(13) 25 25_455 ?
Fe2 Fe1 Fe2 106.12(6) 29_454 25_455 ?
Fe2 Fe1 Fe2 63.59(13) 29_444 13_545 ?
Fe2 Fe1 Fe2 116.41(13) 13 13_545 ?
Fe2 Fe1 Fe2 106.12(6) 9_444 13_545 ?
Fe2 Fe1 Fe2 73.88(6) 25 13_545 ?
Fe2 Fe1 Fe2 180.00(12) 29_454 13_545 ?
Fe2 Fe1 Fe2 73.88(6) 25_455 13_545 ?
Fe2 Fe1 Fe2 73.88(6) 29_444 9_544 ?
Fe2 Fe1 Fe2 106.12(6) 13 9_544 ?
Fe2 Fe1 Fe2 116.41(13) 9_444 9_544 ?
Fe2 Fe1 Fe2 63.59(13) 25 9_544 ?
Fe2 Fe1 Fe2 73.88(6) 29_454 9_544 ?
Fe2 Fe1 Fe2 180.00(12) 25_455 9_544 ?
Fe2 Fe1 Fe2 106.12(6) 13_545 9_544 ?
Fe2 Fe1 Sb2 121.80(6) 29_444 . ?
Fe2 Fe1 Sb2 58.20(6) 13 . ?
Fe2 Fe1 Sb2 121.80(6) 9_444 . ?
Fe2 Fe1 Sb2 58.20(6) 25 . ?
Fe2 Fe1 Sb2 121.80(6) 29_454 . ?
Fe2 Fe1 Sb2 58.20(6) 25_455 . ?
Fe2 Fe1 Sb2 58.20(6) 13_545 . ?
Fe2 Fe1 Sb2 121.80(6) 9_544 . ?
Fe2 Fe1 Sb2 58.20(6) 29_444 17 ?
Fe2 Fe1 Sb2 121.80(6) 13 17 ?
Fe2 Fe1 Sb2 58.20(6) 9_444 17 ?
Fe2 Fe1 Sb2 121.80(6) 25 17 ?
Fe2 Fe1 Sb2 58.20(6) 29_454 17 ?
Fe2 Fe1 Sb2 121.80(6) 25_455 17 ?
Fe2 Fe1 Sb2 121.80(6) 13_545 17 ?
Fe2 Fe1 Sb2 58.20(6) 9_544 17 ?
Sb2 Fe1 Sb2 180.0 . 17 ?
Fe2 Fe1 Sb3 131.98(5) 29_444 25 ?
Fe2 Fe1 Sb3 48.02(5) 13 25 ?
Fe2 Fe1 Sb3 131.98(5) 9_444 25 ?
Fe2 Fe1 Sb3 48.02(5) 25 25 ?
Fe2 Fe1 Sb3 58.58(7) 29_454 25 ?
Fe2 Fe1 Sb3 121.42(7) 25_455 25 ?
Fe2 Fe1 Sb3 121.42(7) 13_545 25 ?
Fe2 Fe1 Sb3 58.58(7) 9_544 25 ?
Sb2 Fe1 Sb3 81.95(7) . 25 ?
Sb2 Fe1 Sb3 98.05(7) 17 25 ?
Fe2 Fe1 Sb3 48.02(5) 29_444 9_444 ?
Fe2 Fe1 Sb3 131.98(5) 13 9_444 ?
Fe2 Fe1 Sb3 48.02(5) 9_444 9_444 ?
Fe2 Fe1 Sb3 131.98(5) 25 9_444 ?
Fe2 Fe1 Sb3 121.42(7) 29_454 9_444 ?
Fe2 Fe1 Sb3 58.58(7) 25_455 9_444 ?
Fe2 Fe1 Sb3 58.58(7) 13_545 9_444 ?
Fe2 Fe1 Sb3 121.42(7) 9_544 9_444 ?
Sb2 Fe1 Sb3 98.05(7) . 9_444 ?
Sb2 Fe1 Sb3 81.95(7) 17 9_444 ?
Sb3 Fe1 Sb3 180.00(15) 25 9_444 ?
Sb3 Fe2 Sb3 134.4(2) 1_565 . ?
Sb3 Fe2 Fe1 78.23(7) 1_565 9 ?
Sb3 Fe2 Fe1 78.23(7) . 9 ?
Sb3 Fe2 Fe1 78.23(7) 1_565 9_455 ?
Sb3 Fe2 Fe1 78.23(7) . 9_455 ?
Fe1 Fe2 Fe1 116.41(13) 9 9_455 ?
Sb3 Fe2 Sb2 103.11(6) 1_565 25_455 ?
Sb3 Fe2 Sb2 103.11(6) . 25_455 ?
Fe1 Fe2 Sb2 175.92(12) 9 25_455 ?
Fe1 Fe2 Sb2 67.67(3) 9_455 25_455 ?
Sb3 Fe2 Sb2 103.11(6) 1_565 25 ?
Sb3 Fe2 Sb2 103.11(6) . 25 ?
Fe1 Fe2 Sb2 67.67(3) 9 25 ?
Fe1 Fe2 Sb2 175.92(12) 9_455 25 ?
Sb2 Fe2 Sb2 108.25(13) 25_455 25 ?
Sb3 Fe2 Fe2 67.22(12) 1_565 17_566 ?
Sb3 Fe2 Fe2 67.22(11) . 17_566 ?
Fe1 Fe2 Fe2 58.20(6) 9 17_566 ?
Fe1 Fe2 Fe2 58.20(6) 9_455 17_566 ?
Sb2 Fe2 Fe2 125.88(6) 25_455 17_566 ?
Sb2 Fe2 Fe2 125.88(6) 25 17_566 ?
Sb3 Fe2 Sb3 16.57(16) 1_565 17_566 ?
Sb3 Fe2 Sb3 117.87(13) . 17_566 ?
Fe1 Fe2 Sb3 70.48(7) 9 17_566 ?
Fe1 Fe2 Sb3 70.48(7) 9_455 17_566 ?
Sb2 Fe2 Sb3 111.81(4) 25_455 17_566 ?
Sb2 Fe2 Sb3 111.81(4) 25 17_566 ?
Fe2 Fe2 Sb3 50.65(8) 17_566 17_566 ?
Sb3 Fe2 Sb3 117.87(13) 1_565 17_556 ?
Sb3 Fe2 Sb3 16.57(16) . 17_556 ?
Fe1 Fe2 Sb3 70.48(7) 9 17_556 ?
Fe1 Fe2 Sb3 70.48(7) 9_455 17_556 ?
Sb2 Fe2 Sb3 111.81(4) 25_455 17_556 ?
Sb2 Fe2 Sb3 111.81(4) 25 17_556 ?
Fe2 Fe2 Sb3 50.65(8) 17_566 17_556 ?
Sb3 Fe2 Sb3 101.30(17) 17_566 17_556 ?
Sb3 Fe2 Nd1 152.04(14) 1_565 . ?
Sb3 Fe2 Nd1 73.51(10) . . ?
Fe1 Fe2 Nd1 114.08(3) 9 . ?
Fe1 Fe2 Nd1 114.08(3) 9_455 . ?
Sb2 Fe2 Nd1 63.02(6) 25_455 . ?
Sb2 Fe2 Nd1 63.02(6) 25 . ?
Fe2 Fe2 Nd1 140.73(4) 17_566 . ?
Sb3 Fe2 Nd1 168.62(11) 17_566 . ?
Sb3 Fe2 Nd1 90.08(7) 17_556 . ?
Sb3 Fe2 Nd1 73.51(10) 1_565 1_565 ?
```

```
Sb3 Fe2 Nd1 152.04(14) . 1_565 ?
Fe1 Fe2 Nd1 114.08(3) 9 1_565 ?
Fe1 Fe2 Nd1 114.08(3) 9_455 1_565 ?
Sb2 Fe2 Nd1 63.02(6) 25_455 1_565 ?
Sb2 Fe2 Nd1 63.02(6) 25 1_565 ?
Fe2 Fe2 Nd1 140.73(4) 17_566 1_565 ?
Sb3 Fe2 Nd1 90.08(7) 17_566 1_565 ?
Sb3 Fe2 Nd1 168.62(11) 17_556 1_565 ?
Nd1 Fe2 Nd1 78.53(7) . 1_565 ?
Sb1 Sb1 Sb1 180.0 25_565 25_455 ?
Sb1 Sb1 Sb1 90.0 25_565 25_465 ?
Sb1 Sb1 Sb1 90.0 25_455 25_465 ?
Sb1 Sb1 Sb1 90.0 25_565 25 ?
Sb1 Sb1 Sb1 90.0 25_455 25 ?
Sb1 Sb1 Sb1 180.0 25_465 25 ?
Sb1 Sb1 Nd1 117.411(10) 25_565 25_455 ?
Sb1 Sb1 Nd1 62.589(10) 25_455 25_455 ?
Sb1 Sb1 Nd1 62.589(10) 25_465 25_455 ?
Sb1 Sb1 Nd1 117.411(10) 25 25_455 ?
Sb1 Sb1 Nd1 62.589(10) 25_565 1_565 ?
Sb1 Sb1 Nd1 117.411(10) 25_455 1_565 ?
Sb1 Sb1 Nd1 62.589(10) 25_465 1_565 ?
Sb1 Sb1 Nd1 117.411(10) 25 1_565 ?
Nd1 Sb1 Nd1 125.178(19) 25_455 1_565 ?
Sb1 Sb1 Nd1 117.411(10) 25_565 . ?
Sb1 Sb1 Nd1 62.589(10) 25_455 . ?
Sb1 Sb1 Nd1 117.411(10) 25_465 . ?
Sb1 Sb1 Nd1 62.589(10) 25 . ?
Nd1 Sb1 Nd1 125.177(19) 25_455 . ?
Nd1 Sb1 Nd1 81.24(3) 1_565 . ?
Sb1 Sb1 Nd1 62.589(10) 25_565 25 ?
Sb1 Sb1 Nd1 117.411(10) 25_455 25 ?
Sb1 Sb1 Nd1 117.411(10) 25_465 25 ?
Sb1 Sb1 Nd1 62.589(10) 25 25 ?
Nd1 Sb1 Nd1 81.24(3) 25_455 25 ?
Nd1 Sb1 Nd1 125.177(19) 1_565 25 ?
Nd1 Sb1 Nd1 125.177(19) . 25 ?
Fe2 Sb2 Fe2 69.91(6) 13_545 25_455 ?
Fe2 Sb2 Fe2 108.25(13) 13_545 13 ?
Fe2 Sb2 Fe2 69.91(6) 25_455 13 ?
Fe2 Sb2 Fe2 69.91(6) 13_545 25 ?
Fe2 Sb2 Fe2 108.25(13) 25_455 25 ?
Fe2 Sb2 Fe2 69.91(6) 13 25 ?
Fe2 Sb2 Fe1 54.12(6) 13_545 . ?
Fe2 Sb2 Fe1 54.12(6) 25_455 . ?
Fe2 Sb2 Fe1 54.12(6) 13 . ?
Fe2 Sb2 Fe1 54.12(6) 25 . ?
Fe2 Sb2 Nd1 137.35(2) 13_545 25 ?
Fe2 Sb2 Nd1 137.35(2) 25_455 25 ?
Fe2 Sb2 Nd1 69.83(4) 13 25 ?
Fe2 Sb2 Nd1 69.83(4) 25 25 ?
Fe1 Sb2 Nd1 109.47(3) . 25 ?
Fe2 Sb2 Nd1 69.83(4) 13_545 25_445 ?
Fe2 Sb2 Nd1 69.83(4) 25_455 25_445 ?
Fe2 Sb2 Nd1 137.35(2) 13 25_445 ?
Fe2 Sb2 Nd1 137.35(2) 25 25_445 ?
Fe1 Sb2 Nd1 109.47(3) . 25_445 ?
Nd1 Sb2 Nd1 141.06(6) 25 25_445 ?
Fe2 Sb2 Nd1 69.83(4) 13_545 25_545 ?
Fe2 Sb2 Nd1 137.35(2) 25_455 25_545 ?
Fe2 Sb2 Nd1 137.35(2) 13 25_545 ?
Fe2 Sb2 Nd1 69.83(4) 25 25_545 ?
Fe1 Sb2 Nd1 109.47(3) . 25_545 ?
Nd1 Sb2 Nd1 83.621(19) 25 25_545 ?
Nd1 Sb2 Nd1 83.621(19) 25_445 25_545 ?
Fe2 Sb2 Nd1 137.35(2) 13_545 25_455 ?
Fe2 Sb2 Nd1 69.83(4) 25_455 25_455 ?
Fe2 Sb2 Nd1 69.83(4) 13 25_455 ?
Fe2 Sb2 Nd1 137.35(2) 25 25_455 ?
Fe1 Sb2 Nd1 109.47(3) . 25_455 ?
Nd1 Sb2 Nd1 83.621(19) 25 25_455 ?
Nd1 Sb2 Nd1 83.621(19) 25_445 25_455 ?
Nd1 Sb2 Nd1 141.06(6) 25_545 25_455 ?
Sb3 Sb3 Fe2 112.78(12) 17_556 21_455 ?
Sb3 Sb3 Fe2 112.78(12) 17_556 1_545 ?
Fe2 Sb3 Fe2 81.38(8) 21_455 1_545 ?
Sb3 Sb3 Fe2 112.78(11) 17_556 21 ?
Fe2 Sb3 Fe2 134.4(2) 21_455 21 ?
Fe2 Sb3 Fe2 81.38(8) 1_545 21 ?
Sb3 Sb3 Fe2 112.78(11) 17_556 . ?
Fe2 Sb3 Fe2 81.38(8) 21_455 . ?
Fe2 Sb3 Fe2 134.4(2) 1_545 . ?
Fe2 Sb3 Fe2 81.38(8) 21 . ?
Sb3 Sb3 Fe2 50.65(8) 17_556 5_656 ?
Fe2 Sb3 Fe2 163.43(16) 21_455 5_656 ?
Fe2 Sb3 Fe2 104.21(7) 1_545 5_656 ?
Fe2 Sb3 Fe2 62.13(13) 21 5_656 ?
Fe2 Sb3 Fe2 104.21(7) . 5_656 ?
Sb3 Sb3 Fe2 50.65(8) 17_556 17_566 ?
Fe2 Sb3 Fe2 104.21(7) 21_455 17_566 ?
Fe2 Sb3 Fe2 163.43(16) 1_545 17_566 ?
Fe2 Sb3 Fe2 104.21(7) 21 17_566 ?
Fe2 Sb3 Fe2 62.13(13) . 17_566 ?
Fe2 Sb3 Fe2 66.29(9) 5_656 17_566 ?
Sb3 Sb3 Fe2 50.65(9) 17_556 5_556 ?
Fe2 Sb3 Fe2 62.13(13) 21_455 5_556 ?
Fe2 Sb3 Fe2 104.21(7) 1_545 5_556 ?
Fe2 Sb3 Fe2 163.43(16) 21 5_556 ?
Fe2 Sb3 Fe2 104.21(7) . 5_556 ?
Fe2 Sb3 Fe2 101.30(17) 5_656 5_556 ?
Fe2 Sb3 Fe2 66.29(9) 17_566 5_556 ?
Sb3 Sb3 Fe2 50.65(9) 17_556 17_556 ?
Fe2 Sb3 Fe2 104.21(7) 21_455 17_556 ?
Fe2 Sb3 Fe2 62.13(13) 1_545 17_556 ?
Fe2 Sb3 Fe2 104.21(7) 21 17_556 ?
Fe2 Sb3 Fe2 163.43(16) . 17_556 ?
Fe2 Sb3 Fe2 66.29(9) 5_656 17_556 ?
Fe2 Sb3 Fe2 101.30(17) 17_566 17_556 ?
Fe2 Sb3 Fe2 66.29(9) 5_556 17_556 ?
Sb3 Sb3 Fe1 81.95(7) 17_556 9 ?
Fe2 Sb3 Fe1 134.41(5) 21_455 9 ?
Fe2 Sb3 Fe1 134.41(5) 1_545 9 ?
Fe2 Sb3 Fe1 53.75(4) 21 9 ?
Fe2 Sb3 Fe1 53.75(4) . 9 ?
Fe2 Sb3 Fe1 50.94(3) 5_656 9 ?
Fe2 Sb3 Fe1 50.94(3) 17_566 9 ?
Fe2 Sb3 Fe1 116.91(11) 5_556 9 ?
Fe2 Sb3 Fe1 116.91(11) 17_556 9 ?
Sb3 Sb3 Fe1 81.95(8) 17_556 9_445 ?
Fe2 Sb3 Fe1 53.75(4) 21_455 9_445 ?
Fe2 Sb3 Fe1 53.75(4) 1_545 9_445 ?
Fe2 Sb3 Fe1 134.41(5) 21 9_445 ?
Fe2 Sb3 Fe1 134.41(5) . 9_445 ?
Fe2 Sb3 Fe1 116.91(11) 5_656 9_445 ?
Fe2 Sb3 Fe1 116.91(11) 17_566 9_445 ?
Fe2 Sb3 Fe1 50.94(3) 5_556 9_445 ?
Fe2 Sb3 Fe1 50.94(3) 17_556 9_445 ?
Fe1 Sb3 Fe1 163.90(15) 9 9_445 ?
Sb3 Sb3 Fe1 81.95(7) 17_556 9_545 ?
Fe2 Sb3 Fe1 134.41(5) 21_455 9_545 ?
Fe2 Sb3 Fe1 53.75(4) 1_545 9_545 ?
Fe2 Sb3 Fe1 53.75(4) 21 9_545 ?
Fe2 Sb3 Fe1 134.41(5) . 9_545 ?
Fe2 Sb3 Fe1 50.94(3) 5_656 9_545 ?
Fe2 Sb3 Fe1 116.91(11) 17_566 9_545 ?
Fe2 Sb3 Fe1 116.91(11) 5_556 9_545 ?
Fe2 Sb3 Fe1 50.94(3) 17_556 9_545 ?
Fe1 Sb3 Fe1 88.88(2) 9 9_545 ?
Fe1 Sb3 Fe1 88.88(2) 9_445 9_545 ?

_diffrn_measured_fraction_theta_max    0.963
_diffrn_reflns_theta_full              32.75
```

```
_diffrn_measured_fraction_theta_full   0.963
_refine_diff_density_max    3.905
_refine_diff_density_min   -2.640
_refine_diff_density_rms    0.628

#===END
```

A1.9 $Sm_2Fe_4Sb_5$

```
data_shelxl

_audit_creation_method            SHELXL-97
_chemical_name_systematic
;
 ?
;
_chemical_name_common             ?
_chemical_melting_point           ?
_chemical_formula_moiety          'Fe3.95
Sb4.93 Sm2'
_chemical_formula_sum
 'Fe3.95 Sb4.93 Sm2'
_chemical_formula_weight          1120.65

loop_
 _atom_type_symbol
 _atom_type_description
 _atom_type_scat_dispersion_real
 _atom_type_scat_dispersion_imag
 _atom_type_scat_source
 'Sm'  'Sm'  -0.1638   3.4418
 'International Tables Vol C Tables 4.2.6.8
and 6.1.1.4'
 'Fe'  'Fe'   0.3463   0.8444
 'International Tables Vol C Tables 4.2.6.8
and 6.1.1.4'
 'Sb'  'Sb'  -0.5866   1.5461
 'International Tables Vol C Tables 4.2.6.8
and 6.1.1.4'

_symmetry_cell_setting
'Tetragonal'
_symmetry_space_group_name_H-M    'I 4/m m m
'

loop_
 _symmetry_equiv_pos_as_xyz
 'x, y, z'
 '-x, -y, z'
 'x, -y, -z'
 '-x, y, -z'
 '-y, -x, -z'
 'y, x, -z'
 'y, -x, z'
 '-y, x, z'
 'x+1/2, y+1/2, z+1/2'
 '-x+1/2, -y+1/2, z+1/2'
 'x+1/2, -y+1/2, -z+1/2'
 '-x+1/2, y+1/2, -z+1/2'
 '-y+1/2, -x+1/2, -z+1/2'
 'y+1/2, x+1/2, -z+1/2'
 'y+1/2, -x+1/2, z+1/2'
 '-y+1/2, x+1/2, z+1/2'
 '-x, -y, -z'
 'x, y, -z'
 '-x, y, z'
 'x, -y, z'
 'y, x, z'
 '-y, -x, z'
 '-y, x, -z'
 'y, -x, -z'
 '-x+1/2, -y+1/2, -z+1/2'
 'x+1/2, y+1/2, -z+1/2'
 '-x+1/2, y+1/2, z+1/2'
 'x+1/2, -y+1/2, z+1/2'
 'y+1/2, x+1/2, z+1/2'
 '-y+1/2, -x+1/2, z+1/2'
 '-y+1/2, x+1/2, -z+1/2'
 'y+1/2, -x+1/2, -z+1/2'

_cell_length_a                    4.2723(15)
_cell_length_b                    4.2723(15)
_cell_length_c                    25.558(9)
_cell_angle_alpha                 90
_cell_angle_beta                  90
_cell_angle_gamma                 90
_cell_volume                      466.5(3)
_cell_formula_units_Z             2
_cell_measurement_temperature     298(2)
_cell_measurement_reflns_used     573
_cell_measurement_theta_min       2.6
_cell_measurement_theta_max       37

_exptl_crystal_description        plate
_exptl_crystal_colour             black
_exptl_crystal_size_max           0.13
_exptl_crystal_size_mid           0.10
_exptl_crystal_size_min           0.03
_exptl_crystal_density_meas       ?
_exptl_crystal_density_diffrn     7.978
_exptl_crystal_density_method     'not
measured'
_exptl_crystal_F_000              955
_exptl_absorpt_coefficient_mu     32.228
_exptl_absorpt_correction_type    'multi-
scan'
_exptl_absorpt_correction_T_min   0.1074
_exptl_absorpt_correction_T_max   0.4996
_exptl_absorpt_process_details    'HKL
Scalepack (Otwinowski & Minor 1997)'

_exptl_special_details
;
 ?
;

_diffrn_ambient_temperature       298(2)
_diffrn_radiation_wavelength      0.71073
_diffrn_radiation_type            MoK\a
_diffrn_radiation_source          'fine-
focus sealed tube'
_diffrn_radiation_monochromator   graphite
_diffrn_measurement_device_type   'Nonius
KappaCCD'
_diffrn_measurement_method        '\w and \f
scans'
_diffrn_detector_area_resol_mean  ?
_diffrn_standards_number          ?
_diffrn_standards_interval_count  ?
_diffrn_standards_interval_time   ?
_diffrn_standards_decay_%         ?
_diffrn_reflns_number             6413
_diffrn_reflns_av_R_equivalents   0.0314
_diffrn_reflns_av_sigmaI/netI     0.0199
_diffrn_reflns_limit_h_min        0
_diffrn_reflns_limit_h_max        7
_diffrn_reflns_limit_k_min        -4
_diffrn_reflns_limit_k_max        5
_diffrn_reflns_limit_l_min        0
_diffrn_reflns_limit_l_max        42
_diffrn_reflns_theta_min          3.19
_diffrn_reflns_theta_max          36.56
```

```
_reflns_number_total              401
_reflns_number_gt                 384
_reflns_threshold_expression      I>2\s(I)

_computing_data_collection        ?
_computing_cell_refinement        ?
_computing_data_reduction         ?
_computing_structure_solution     ?
_computing_structure_refinement   'SHELXL-97
(Sheldrick, 2008)'
_computing_molecular_graphics     ?
_computing_publication_material   ?

_refine_special_details
;
 Refinement of F^2^ against ALL reflections.
The weighted R-factor wR and
 goodness of fit S are based on F^2^,
conventional R-factors R are based
 on F, with F set to zero for negative F^2^.
The threshold expression of
 F^2^ > 2\s(F^2^) is used only for
calculating R-factors(gt) etc. and is
 not relevant to the choice of reflections
for refinement.  R-factors based
 on F^2^ are statistically about twice as
large as those based on F, and R-
 factors based on ALL data will be even
larger.
;

_refine_ls_structure_factor_coef  Fsqd
_refine_ls_matrix_type            full
_refine_ls_weighting_scheme       calc
_refine_ls_weighting_details
 'calc
w=1/[\s^2^(Fo^2^)+(0.0538P)^2^+24.2299P]
where P=(Fo^2^+2Fc^2^)/3'
_atom_sites_solution_primary      direct
_atom_sites_solution_secondary    difmap
_atom_sites_solution_hydrogens    ?
_refine_ls_hydrogen_treatment     ?
_refine_ls_extinction_method      SHELXL
_refine_ls_extinction_coef        0.0011(3)
_refine_ls_extinction_expression
 'Fc^*^=kFc[1+0.001xFc^2^\l^3^/sin(2\q)]^-
1/4^'
_refine_ls_number_reflns          401
_refine_ls_number_parameters      21
_refine_ls_number_restraints      0
_refine_ls_R_factor_all           0.0427
_refine_ls_R_factor_gt            0.0399
_refine_ls_wR_factor_ref          0.1108
_refine_ls_wR_factor_gt           0.1083
_refine_ls_goodness_of_fit_ref    1.197
_refine_ls_restrained_S_all       1.197
_refine_ls_shift/su_max           0.000
_refine_ls_shift/su_mean          0.000

loop_
 _atom_site_label
 _atom_site_type_symbol
 _atom_site_fract_x
 _atom_site_fract_y
 _atom_site_fract_z
 _atom_site_U_iso_or_equiv
 _atom_site_adp_type
 _atom_site_occupancy
 _atom_site_symmetry_multiplicity
 _atom_site_calc_flag
 _atom_site_refinement_flags
 _atom_site_disorder_assembly
 _atom_site_disorder_group
Sm1 Sm 0.0000 0.0000 0.34659(3) 0.0113(2)
Uani 1 8 d S . .
Fe1 Fe 0.0000 0.0000 0.0000 0.0145(6) Uani 1
16 d S . .
Fe2 Fe 0.0000 0.5000 0.44755(10) 0.0338(13)
Uani 0.737(13) 4 d SP . .
Sb1 Sb 0.0000 0.5000 0.2500 0.0097(2) Uani 1
8 d S . .
Sb2 Sb 0.0000 0.0000 0.11287(4) 0.0109(3)
Uani 1 8 d S . .
Sb3 Sb 0.0000 0.0000 0.48335(12) 0.0240(9)
Uani 0.461(8) 8 d SP . .

loop_
 _atom_site_aniso_label
 _atom_site_aniso_U_11
 _atom_site_aniso_U_22
 _atom_site_aniso_U_33
 _atom_site_aniso_U_23
 _atom_site_aniso_U_13
 _atom_site_aniso_U_12
Sm1 0.0107(3) 0.0107(3) 0.0125(3) 0.000
0.000 0.000
Fe1 0.0151(10) 0.0151(10) 0.0132(12) 0.000
0.000 0.000
Fe2 0.0097(12) 0.081(3) 0.0108(10) 0.000
0.000 0.000
Sb1 0.0099(3) 0.0099(3) 0.0094(4) 0.000
0.000 0.000
Sb2 0.0105(3) 0.0105(3) 0.0116(4) 0.000
0.000 0.000
Sb3 0.0274(12) 0.0274(12) 0.0171(10) 0.000
0.000 0.000

_geom_special_details
;
 All s.u.'s (except the s.u. in the dihedral
angle between two l.s. planes)
 are estimated using the full covariance
matrix.  The cell s.u.'s are taken
 into account individually in the estimation
of s.u.'s in distances, angles
 and torsion angles; correlations between
s.u.'s in cell parameters are only
 used when they are defined by crystal
symmetry.  An approximate (isotropic)
 treatment of cell s.u.'s is used for
estimating s.u.'s involving l.s. planes.
;

loop_
 _geom_bond_atom_site_label_1
 _geom_bond_atom_site_label_2
 _geom_bond_distance
 _geom_bond_site_symmetry_2
 _geom_bond_publ_flag
Sm1 Sb2 3.1937(11) 25 ?
Sm1 Sb2 3.1937(11) 25_445 ?
Sm1 Sb2 3.1937(11) 25_455 ?
Sm1 Sb2 3.1937(11) 25_545 ?
Sm1 Sb1 3.2645(10) 25_455 ?
Sm1 Sb1 3.2645(10) 1_545 ?
Sm1 Sb1 3.2645(10) . ?
Sm1 Sb1 3.2645(10) 25 ?
Sm1 Fe2 3.350(2) . ?
Sm1 Fe2 3.350(2) 21 ?
Sm1 Fe2 3.350(2) 21_455 ?
Sm1 Fe2 3.350(2) 1_545 ?
Fe1 Fe2 2.5219(15) 29_444 ?
```

```
Fe1 Fe2 2.5219(15) 9_444 ?
Fe1 Fe2 2.5219(15) 29_454 ?
Fe1 Fe2 2.5219(15) 9_544 ?
Fe1 Fe2 2.5219(15) 13 ?
Fe1 Fe2 2.5219(15) 25 ?
Fe1 Fe2 2.5219(15) 25_455 ?
Fe1 Fe2 2.5219(15) 13_545 ?
Fe1 Sb2 2.8848(14) . ?
Fe1 Sb2 2.8848(14) 17 ?
Fe1 Sb3 3.0508(11) 9_444 ?
Fe1 Sb3 3.0508(11) 25 ?
Fe2 Sb3 2.3239(17) 1_565 ?
Fe2 Sb3 2.3239(17) . ?
Fe2 Fe1 2.5219(15) 9 ?
Fe2 Fe1 2.5219(15) 9_455 ?
Fe2 Sb2 2.6360(17) 25_455 ?
Fe2 Sb2 2.6360(17) 25 ?
Fe2 Fe2 2.681(5) 17_566 ?
Fe2 Sb3 2.772(3) 17_566 ?
Fe2 Sb3 2.772(3) 17_556 ?
Fe2 Sm1 3.350(2) 1_565 ?
Sb1 Sb1 3.0210(11) 25_565 ?
Sb1 Sb1 3.0210(11) 25_455 ?
Sb1 Sb1 3.0210(11) 25_465 ?
Sb1 Sb1 3.0210(11) 25 ?
Sb1 Sm1 3.2645(10) 25_455 ?
Sb1 Sm1 3.2645(10) 1_565 ?
Sb1 Sm1 3.2645(10) 25 ?
Sb2 Fe2 2.6360(17) 13_545 ?
Sb2 Fe2 2.6360(17) 25_455 ?
Sb2 Fe2 2.6360(17) 13 ?
Sb2 Fe2 2.6360(17) 25 ?
Sb2 Sm1 3.1937(11) 25 ?
Sb2 Sm1 3.1937(11) 25_445 ?
Sb2 Sm1 3.1937(11) 25_545 ?
Sb2 Sm1 3.1937(11) 25_455 ?
Sb3 Sb3 0.851(6) 17_556 ?
Sb3 Fe2 2.3239(17) 21_455 ?
Sb3 Fe2 2.3239(17) 1_545 ?
Sb3 Fe2 2.3239(17) 21 ?
Sb3 Fe2 2.772(3) 5_656 ?
Sb3 Fe2 2.772(3) 17_566 ?
Sb3 Fe2 2.772(3) 5_556 ?
Sb3 Fe2 2.772(3) 17_556 ?
Sb3 Fe1 3.0508(11) 9 ?
Sb3 Fe1 3.0508(11) 9_445 ?
Sb3 Fe1 3.0508(11) 9_545 ?

loop_
 _geom_angle_atom_site_label_1
 _geom_angle_atom_site_label_2
 _geom_angle_atom_site_label_3
 _geom_angle
 _geom_angle_site_symmetry_1
 _geom_angle_site_symmetry_3
 _geom_angle_publ_flag
Sb2 Sm1 Sb2 142.14(5) 25 25_445 ?
Sb2 Sm1 Sb2 83.958(14) 25 25_455 ?
Sb2 Sm1 Sb2 83.958(14) 25_445 25_455 ?
Sb2 Sm1 Sb2 83.958(14) 25 25_545 ?
Sb2 Sm1 Sb2 83.958(14) 25_445 25_545 ?
Sb2 Sm1 Sb2 142.14(5) 25_455 25_545 ?
Sb2 Sm1 Sb1 133.079(19) 25 25_455 ?
Sb2 Sm1 Sb1 78.91(2) 25_445 25_455 ?
Sb2 Sm1 Sb1 78.91(2) 25_455 25_455 ?
Sb2 Sm1 Sb1 133.079(19) 25_545 25_455 ?
Sb2 Sm1 Sb1 133.079(19) 25 1_545 ?
Sb2 Sm1 Sb1 78.91(2) 25_445 1_545 ?
Sb2 Sm1 Sb1 133.079(19) 25_455 1_545 ?
Sb2 Sm1 Sb1 78.91(2) 25_545 1_545 ?
Sb1 Sm1 Sb1 55.12(2) 25_455 1_545 ?
Sb2 Sm1 Sb1 78.91(2) 25 . ?
Sb2 Sm1 Sb1 133.079(19) 25_445 . ?
Sb2 Sm1 Sb1 78.91(2) 25_455 . ?
Sb2 Sm1 Sb1 133.079(19) 25_545 . ?
Sb1 Sm1 Sb1 55.12(2) 25_455 . ?
Sb1 Sm1 Sb1 81.74(3) 1_545 . ?
Sb2 Sm1 Sb1 78.91(2) 25 25 ?
Sb2 Sm1 Sb1 133.079(19) 25_445 25 ?
Sb2 Sm1 Sb1 133.079(19) 25_455 25 ?
Sb2 Sm1 Sb1 78.91(2) 25_545 25 ?
Sb1 Sm1 Sb1 81.74(3) 25_455 25 ?
Sb1 Sm1 Sb1 55.12(2) 1_545 25 ?
Sb1 Sm1 Sb1 55.12(2) . 25 ?
Sb2 Sm1 Fe2 47.435(19) 25 . ?
Sb2 Sm1 Fe2 100.17(3) 25_445 . ?
Sb2 Sm1 Fe2 47.435(19) 25_455 . ?
Sb2 Sm1 Fe2 100.17(3) 25_545 . ?
Sb1 Sm1 Fe2 125.63(2) 25_455 . ?
Sb1 Sm1 Fe2 178.75(3) 1_545 . ?
Sb1 Sm1 Fe2 99.51(4) . . ?
Sb1 Sm1 Fe2 125.63(2) 25 . ?
Sb2 Sm1 Fe2 47.435(19) 25 21 ?
Sb2 Sm1 Fe2 100.17(3) 25_445 21 ?
Sb2 Sm1 Fe2 100.17(3) 25_455 21 ?
Sb2 Sm1 Fe2 47.435(19) 25_545 21 ?
Sb1 Sm1 Fe2 178.75(3) 25_455 21 ?
Sb1 Sm1 Fe2 125.63(2) 1_545 21 ?
Sb1 Sm1 Fe2 125.63(2) . 21 ?
Sb1 Sm1 Fe2 99.51(4) 25 21 ?
Fe2 Sm1 Fe2 53.60(4) . 21 ?
Sb2 Sm1 Fe2 100.17(3) 25 21_455 ?
Sb2 Sm1 Fe2 47.435(19) 25_445 21_455 ?
Sb2 Sm1 Fe2 47.435(19) 25_455 21_455 ?
Sb2 Sm1 Fe2 100.17(3) 25_545 21_455 ?
Sb1 Sm1 Fe2 99.51(4) 25_455 21_455 ?
Sb1 Sm1 Fe2 125.63(2) 1_545 21_455 ?
Sb1 Sm1 Fe2 125.63(2) . 21_455 ?
Sb1 Sm1 Fe2 178.75(3) 25 21_455 ?
Fe2 Sm1 Fe2 53.60(4) . 21_455 ?
Fe2 Sm1 Fe2 79.24(6) 21 21_455 ?
Sb2 Sm1 Fe2 100.17(3) 25 1_545 ?
Sb2 Sm1 Fe2 47.435(19) 25_445 1_545 ?
Sb2 Sm1 Fe2 100.17(3) 25_455 1_545 ?
Sb2 Sm1 Fe2 47.435(19) 25_545 1_545 ?
Sb1 Sm1 Fe2 125.63(2) 25_455 1_545 ?
Sb1 Sm1 Fe2 99.51(4) 1_545 1_545 ?
Sb1 Sm1 Fe2 178.75(3) . 1_545 ?
Sb1 Sm1 Fe2 125.63(2) 25 1_545 ?
Fe2 Sm1 Fe2 79.24(6) . 1_545 ?
Fe2 Sm1 Fe2 53.60(4) 21 1_545 ?
Fe2 Sm1 Fe2 53.60(4) 21_455 1_545 ?
Fe2 Fe1 Fe2 73.59(5) 29_444 9_444 ?
Fe2 Fe1 Fe2 115.78(10) 29_444 29_454 ?
Fe2 Fe1 Fe2 73.59(5) 9_444 29_454 ?
Fe2 Fe1 Fe2 73.59(5) 29_444 9_544 ?
Fe2 Fe1 Fe2 115.78(10) 9_444 9_544 ?
Fe2 Fe1 Fe2 73.59(5) 29_454 9_544 ?
Fe2 Fe1 Fe2 180.00(10) 29_444 13 ?
Fe2 Fe1 Fe2 106.41(5) 9_444 13 ?
Fe2 Fe1 Fe2 64.22(10) 29_454 13 ?
Fe2 Fe1 Fe2 106.41(5) 9_544 13 ?
Fe2 Fe1 Fe2 106.41(5) 29_444 25 ?
Fe2 Fe1 Fe2 180.00(10) 9_444 25 ?
Fe2 Fe1 Fe2 106.41(5) 29_454 25 ?
Fe2 Fe1 Fe2 64.22(10) 9_544 25 ?
Fe2 Fe1 Fe2 73.59(5) 13 25 ?
Fe2 Fe1 Fe2 106.41(5) 29_444 25_455 ?
Fe2 Fe1 Fe2 64.22(10) 9_444 25_455 ?
Fe2 Fe1 Fe2 106.41(5) 29_454 25_455 ?
Fe2 Fe1 Fe2 180.00(10) 9_544 25_455 ?
Fe2 Fe1 Fe2 73.59(5) 13 25_455 ?
```

```
Fe2 Fe1 Fe2 115.78(10) 25 25_455 ?
Fe2 Fe1 Fe2 64.22(10) 29_444 13_545 ?
Fe2 Fe1 Fe2 106.41(5) 9_444 13_545 ?
Fe2 Fe1 Fe2 180.00(10) 29_454 13_545 ?
Fe2 Fe1 Fe2 106.41(5) 9_544 13_545 ?
Fe2 Fe1 Fe2 115.78(10) 13 13_545 ?
Fe2 Fe1 Fe2 73.59(5) 25 13_545 ?
Fe2 Fe1 Fe2 73.59(5) 25_455 13_545 ?
Fe2 Fe1 Sb2 122.11(5) 29_444 . ?
Fe2 Fe1 Sb2 122.11(5) 9_444 . ?
Fe2 Fe1 Sb2 122.11(5) 29_454 . ?
Fe2 Fe1 Sb2 122.11(5) 9_544 . ?
Fe2 Fe1 Sb2 57.89(5) 13 . ?
Fe2 Fe1 Sb2 57.89(5) 25 . ?
Fe2 Fe1 Sb2 57.89(5) 25_455 . ?
Fe2 Fe1 Sb2 57.89(5) 13_545 . ?
Fe2 Fe1 Sb2 57.89(5) 29_444 17 ?
Fe2 Fe1 Sb2 57.89(5) 9_444 17 ?
Fe2 Fe1 Sb2 57.89(5) 29_454 17 ?
Fe2 Fe1 Sb2 57.89(5) 9_544 17 ?
Fe2 Fe1 Sb2 122.11(5) 13 17 ?
Fe2 Fe1 Sb2 122.11(5) 25 17 ?
Fe2 Fe1 Sb2 122.11(5) 25_455 17 ?
Fe2 Fe1 Sb2 122.11(5) 13_545 17 ?
Sb2 Fe1 Sb2 180.0 . 17 ?
Fe2 Fe1 Sb3 48.15(4) 29_444 9_444 ?
Fe2 Fe1 Sb3 48.15(4) 9_444 9_444 ?
Fe2 Fe1 Sb3 121.26(5) 29_454 9_444 ?
Fe2 Fe1 Sb3 121.26(5) 9_544 9_444 ?
Fe2 Fe1 Sb3 131.85(4) 13 9_444 ?
Fe2 Fe1 Sb3 131.85(4) 25 9_444 ?
Fe2 Fe1 Sb3 58.74(5) 25_455 9_444 ?
Fe2 Fe1 Sb3 58.74(5) 13_545 9_444 ?
Sb2 Fe1 Sb3 98.02(6) . 9_444 ?
Sb2 Fe1 Sb3 81.98(6) 17 9_444 ?
Fe2 Fe1 Sb3 131.85(4) 29_444 25 ?
Fe2 Fe1 Sb3 131.85(4) 9_444 25 ?
Fe2 Fe1 Sb3 58.74(5) 29_454 25 ?
Fe2 Fe1 Sb3 58.74(5) 9_544 25 ?
Fe2 Fe1 Sb3 48.15(4) 13 25 ?
Fe2 Fe1 Sb3 48.15(4) 25 25 ?
Fe2 Fe1 Sb3 121.26(5) 25_455 25 ?
Fe2 Fe1 Sb3 121.26(5) 13_545 25 ?
Sb2 Fe1 Sb3 81.98(6) . 25 ?
Sb2 Fe1 Sb3 98.02(6) 17 25 ?
Sb3 Fe1 Sb3 180.0 9_444 25 ?
Sb3 Fe2 Sb3 133.63(18) 1_565 . ?
Sb3 Fe2 Fe1 77.92(6) 1_565 9 ?
Sb3 Fe2 Fe1 77.92(6) . 9 ?
Sb3 Fe2 Fe1 77.92(6) 1_565 9_455 ?
Sb3 Fe2 Fe1 77.92(6) . 9_455 ?
Fe1 Fe2 Fe1 115.78(10) 9 9_455 ?
Sb3 Fe2 Sb2 103.34(4) 1_565 25_455 ?
Sb3 Fe2 Sb2 103.34(4) . 25_455 ?
Fe1 Fe2 Sb2 176.24(9) 9 25_455 ?
Fe1 Fe2 Sb2 67.97(3) 9_455 25_455 ?
Sb3 Fe2 Sb2 103.34(4) 1_565 25 ?
Sb3 Fe2 Sb2 103.34(4) . 25 ?
Fe1 Fe2 Sb2 67.97(3) 9 25 ?
Fe1 Fe2 Sb2 176.24(9) 9_455 25 ?
Sb2 Fe2 Sb2 108.27(10) 25_455 25 ?
Sb3 Fe2 Fe2 66.81(9) 1_565 17_566 ?
Sb3 Fe2 Fe2 66.81(9) . 17_566 ?
Fe1 Fe2 Fe2 57.89(5) 9 17_566 ?
Fe1 Fe2 Fe2 57.89(5) 9_455 17_566 ?
Sb2 Fe2 Fe2 125.87(5) 25_455 17_566 ?
Sb2 Fe2 Fe2 125.87(5) 25 17_566 ?
Sb3 Fe2 Sb3 16.39(12) 1_565 17_566 ?
Sb3 Fe2 Sb3 117.23(10) . 17_566 ?
Fe1 Fe2 Sb3 70.20(5) 9 17_566 ?
Fe1 Fe2 Sb3 70.20(5) 9_455 17_566 ?
Sb2 Fe2 Sb3 111.92(3) 25_455 17_566 ?
Sb2 Fe2 Sb3 111.92(3) 25 17_566 ?
Fe2 Fe2 Sb3 50.42(6) 17_566 17_566 ?
Sb3 Fe2 Sb3 117.23(10) 1_565 17_556 ?
Sb3 Fe2 Sb3 16.39(12) . 17_556 ?
Fe1 Fe2 Sb3 70.20(5) 9 17_556 ?
Fe1 Fe2 Sb3 70.20(5) 9_455 17_556 ?
Sb2 Fe2 Sb3 111.92(3) 25_455 17_556 ?
Sb2 Fe2 Sb3 111.92(3) 25 17_556 ?
Fe2 Fe2 Sb3 50.42(6) 17_566 17_556 ?
Sb3 Fe2 Sb3 100.84(13) 17_566 17_556 ?
Sb3 Fe2 Sm1 152.80(11) 1_565 . ?
Sb3 Fe2 Sm1 73.57(8) . . ?
Fe1 Fe2 Sm1 114.17(3) 9 . ?
Fe1 Fe2 Sm1 114.17(3) 9_455 . ?
Sb2 Fe2 Sm1 63.17(5) 25_455 . ?
Sb2 Fe2 Sm1 63.17(5) 25 . ?
Fe2 Fe2 Sm1 140.38(3) 17_566 . ?
Sb3 Fe2 Sm1 169.20(8) 17_566 . ?
Sb3 Fe2 Sm1 89.96(6) 17_556 . ?
Sb3 Fe2 Sm1 73.57(8) 1_565 1_565 ?
Sb3 Fe2 Sm1 152.80(11) . 1_565 ?
Fe1 Fe2 Sm1 114.17(3) 9 1_565 ?
Fe1 Fe2 Sm1 114.17(3) 9_455 1_565 ?
Sb2 Fe2 Sm1 63.17(5) 25_455 1_565 ?
Sb2 Fe2 Sm1 63.17(5) 25 1_565 ?
Fe2 Fe2 Sm1 140.38(3) 17_566 1_565 ?
Sb3 Fe2 Sm1 89.96(6) 17_566 1_565 ?
Sb3 Fe2 Sm1 169.20(8) 17_556 1_565 ?
Sm1 Fe2 Sm1 79.24(6) . 1_565 ?
Sb1 Sb1 Sb1 180.0 25_565 25_455 ?
Sb1 Sb1 Sb1 90.0 25_565 25_465 ?
Sb1 Sb1 Sb1 90.0 25_455 25_465 ?
Sb1 Sb1 Sb1 90.0 25_565 25 ?
Sb1 Sb1 Sb1 90.0 25_455 25 ?
Sb1 Sb1 Sb1 180.0 25_465 25 ?
Sb1 Sb1 Sm1 117.561(10) 25_565 25_455 ?
Sb1 Sb1 Sm1 62.439(10) 25_455 25_455 ?
Sb1 Sb1 Sm1 62.439(10) 25_465 25_455 ?
Sb1 Sb1 Sm1 117.561(10) 25 25_455 ?
Sb1 Sb1 Sm1 62.439(10) 25_565 1_565 ?
Sb1 Sb1 Sm1 117.561(10) 25_455 1_565 ?
Sb1 Sb1 Sm1 62.439(10) 25_465 1_565 ?
Sb1 Sb1 Sm1 117.561(10) 25 1_565 ?
Sm1 Sb1 Sm1 124.88(2) 25_455 1_565 ?
Sb1 Sb1 Sm1 117.561(10) 25_565 . ?
Sb1 Sb1 Sm1 62.439(10) 25_455 . ?
Sb1 Sb1 Sm1 117.561(10) 25_465 . ?
Sb1 Sb1 Sm1 62.439(10) 25 . ?
Sm1 Sb1 Sm1 124.88(2) 25_455 . ?
Sm1 Sb1 Sm1 81.74(3) 1_565 . ?
Sb1 Sb1 Sm1 62.439(10) 25_565 25 ?
Sb1 Sb1 Sm1 117.561(10) 25_455 25 ?
Sb1 Sb1 Sm1 117.561(10) 25_465 25 ?
Sb1 Sb1 Sm1 62.439(10) 25 25 ?
Sm1 Sb1 Sm1 81.74(3) 25_455 25 ?
Sm1 Sb1 Sm1 124.88(2) 1_565 25 ?
Sm1 Sb1 Sm1 124.88(2) . 25 ?
Fe2 Sb2 Fe2 69.92(5) 13_545 25_455 ?
Fe2 Sb2 Fe2 108.27(10) 13_545 13 ?
Fe2 Sb2 Fe2 69.92(5) 25_455 13 ?
Fe2 Sb2 Fe2 69.92(5) 13_545 25 ?
Fe2 Sb2 Fe2 108.27(10) 25_455 25 ?
Fe2 Sb2 Fe2 69.92(5) 13 25 ?
Fe2 Sb2 Fe1 54.13(5) 13_545 . ?
Fe2 Sb2 Fe1 54.13(5) 25_455 . ?
Fe2 Sb2 Fe1 54.13(5) 13 . ?
Fe2 Sb2 Fe1 54.13(5) 25 . ?
Fe2 Sb2 Sm1 137.064(17) 13_545 25 ?
Fe2 Sb2 Sm1 137.064(17) 25_455 25 ?
Fe2 Sb2 Sm1 69.39(4) 13 25 ?
```

```
Fe2 Sb2 Sm1 69.39(4) 25 25 ?
Fe1 Sb2 Sm1 108.93(2) . 25 ?
Fe2 Sb2 Sm1 69.39(4) 13_545 25_445 ?
Fe2 Sb2 Sm1 69.39(4) 25_455 25_445 ?
Fe2 Sb2 Sm1 137.064(17) 13 25_445 ?
Fe2 Sb2 Sm1 137.064(17) 25 25_445 ?
Fe1 Sb2 Sm1 108.93(2) . 25_445 ?
Sm1 Sb2 Sm1 142.14(5) 25 25_445 ?
Fe2 Sb2 Sm1 69.39(4) 13_545 25_545 ?
Fe2 Sb2 Sm1 137.064(17) 25_455 25_545 ?
Fe2 Sb2 Sm1 137.064(17) 13 25_545 ?
Fe2 Sb2 Sm1 69.39(4) 25 25_545 ?
Fe1 Sb2 Sm1 108.93(2) . 25_545 ?
Sm1 Sb2 Sm1 83.958(14) 25 25_545 ?
Sm1 Sb2 Sm1 83.958(14) 25_445 25_545 ?
Fe2 Sb2 Sm1 137.064(17) 13_545 25_455 ?
Fe2 Sb2 Sm1 69.39(4) 25_455 25_455 ?
Fe2 Sb2 Sm1 69.39(4) 13 25_455 ?
Fe2 Sb2 Sm1 137.064(17) 25 25_455 ?
Fe1 Sb2 Sm1 108.93(2) . 25_455 ?
Sm1 Sb2 Sm1 83.958(14) 25 25_455 ?
Sm1 Sb2 Sm1 83.958(14) 25_445 25_455 ?
Sm1 Sb2 Sm1 142.14(5) 25_545 25_455 ?
Sb3 Sb3 Fe2 113.19(9) 17_556 21_455 ?
Sb3 Sb3 Fe2 113.19(9) 17_556 1_545 ?
Fe2 Sb3 Fe2 81.08(6) 21_455 1_545 ?
Sb3 Sb3 Fe2 113.19(9) 17_556 21 ?
Fe2 Sb3 Fe2 133.63(18) 21_455 21 ?
Fe2 Sb3 Fe2 81.08(6) 1_545 21 ?
Sb3 Sb3 Fe2 113.19(9) 17_556 . ?
Fe2 Sb3 Fe2 81.08(6) 21_455 . ?
Fe2 Sb3 Fe2 133.63(18) 1_545 . ?
Fe2 Sb3 Fe2 81.08(6) 21 . ?
Sb3 Sb3 Fe2 50.42(6) 17_556 5_656 ?
Fe2 Sb3 Fe2 163.61(12) 21_455 5_656 ?
Fe2 Sb3 Fe2 104.53(5) 1_545 5_656 ?
Fe2 Sb3 Fe2 62.77(10) 21 5_656 ?
Fe2 Sb3 Fe2 104.53(5) . 5_656 ?
Sb3 Sb3 Fe2 50.42(6) 17_556 17_566 ?
Fe2 Sb3 Fe2 104.53(5) 21_455 17_566 ?
Fe2 Sb3 Fe2 163.61(12) 1_545 17_566 ?
Fe2 Sb3 Fe2 104.53(5) 21 17_566 ?
Fe2 Sb3 Fe2 62.77(10) . 17_566 ?
Fe2 Sb3 Fe2 66.05(7) 5_656 17_566 ?
Sb3 Sb3 Fe2 50.42(6) 17_556 5_556 ?
Fe2 Sb3 Fe2 62.77(10) 21_455 5_556 ?
Fe2 Sb3 Fe2 104.53(5) 1_545 5_556 ?
Fe2 Sb3 Fe2 163.61(12) 21 5_556 ?
Fe2 Sb3 Fe2 104.53(5) . 5_556 ?
Fe2 Sb3 Fe2 100.84(13) 5_656 5_556 ?
Fe2 Sb3 Fe2 66.05(7) 17_566 5_556 ?
Sb3 Sb3 Fe2 50.42(6) 17_556 17_556 ?
Fe2 Sb3 Fe2 104.53(5) 21_455 17_556 ?
Fe2 Sb3 Fe2 62.77(10) 1_545 17_556 ?
Fe2 Sb3 Fe2 104.53(5) 21 17_556 ?
Fe2 Sb3 Fe2 163.61(12) . 17_556 ?
Fe2 Sb3 Fe2 66.05(7) 5_656 17_556 ?
Fe2 Sb3 Fe2 100.84(13) 17_566 17_556 ?
Fe2 Sb3 Fe2 66.05(7) 5_556 17_556 ?
Sb3 Sb3 Fe1 81.98(6) 17_556 9 ?
Fe2 Sb3 Fe1 134.31(4) 21_455 9 ?
Fe2 Sb3 Fe1 134.31(4) 1_545 9 ?
Fe2 Sb3 Fe1 53.93(3) 21 9 ?
Fe2 Sb3 Fe1 53.93(3) . 9 ?
Fe2 Sb3 Fe1 51.06(3) 5_656 9 ?
Fe2 Sb3 Fe1 51.06(3) 17_566 9 ?
Fe2 Sb3 Fe1 116.80(8) 5_556 9 ?
Fe2 Sb3 Fe1 116.80(8) 17_556 9 ?
Sb3 Sb3 Fe1 81.98(6) 17_556 9_445 ?
Fe2 Sb3 Fe1 53.93(3) 21_455 9_445 ?
Fe2 Sb3 Fe1 53.93(3) 1_545 9_445 ?
Fe2 Sb3 Fe1 134.31(4) 21 9_445 ?
Fe2 Sb3 Fe1 134.31(4) . 9_445 ?
Fe2 Sb3 Fe1 116.80(8) 5_656 9_445 ?
Fe2 Sb3 Fe1 116.80(8) 17_566 9_445 ?
Fe2 Sb3 Fe1 51.06(3) 5_556 9_445 ?
Fe2 Sb3 Fe1 51.06(3) 17_556 9_445 ?
Fe1 Sb3 Fe1 163.97(11) 9 9_445 ?
Sb3 Sb3 Fe1 81.98(6) 17_556 9_545 ?
Fe2 Sb3 Fe1 134.31(4) 21_455 9_545 ?
Fe2 Sb3 Fe1 53.93(3) 1_545 9_545 ?
Fe2 Sb3 Fe1 53.93(3) 21 9_545 ?
Fe2 Sb3 Fe1 134.31(4) . 9_545 ?
Fe2 Sb3 Fe1 51.06(3) 5_656 9_545 ?
Fe2 Sb3 Fe1 116.80(8) 17_566 9_545 ?
Fe2 Sb3 Fe1 116.80(8) 5_556 9_545 ?
Fe2 Sb3 Fe1 51.06(3) 17_556 9_545 ?
Fe1 Sb3 Fe1 88.886(16) 9 9_545 ?
Fe1 Sb3 Fe1 88.886(16) 9_445 9_545 ?

_diffrn_measured_fraction_theta_max    0.990
_diffrn_reflns_theta_full              36.56
_diffrn_measured_fraction_theta_full   0.990
_refine_diff_density_max    4.476
_refine_diff_density_min   -5.697
_refine_diff_density_rms    0.761

#===END
```

Appendix 2. Letters of Permission

A2.1

Adapted with permission from: Phelan, W. A.; Menard, M. C.; Kangas, M. J.; McCandless, G. T.; Drake, B. L.; Chan, J. Y., Adventures in Crystal Growth: Synthesis and Characterization of Single Crystals of Complex Intermetallic Compounds. *Chem. Mater.* **2012**, *24*, 409-420. Copyright (2012) American Chemical Society. (Please see page 203.)

A2.2

Adapted with permission of The Royal Society of Chemistry: Phelan, W. A.; Nguyen, G. V.; Karki, A. B.; Young, D. P.; Chan, J. Y., Synthesis, Structure, Magnetic and Transport Properties of *Ln*$FeSb_3$ (*Ln* = Pr, Nd, Sm, Gd, and Tb) -Tuning of Anisotropic Long-Range Magnetic Order as a Function of *Ln*. *Dalton Trans.* **2010**, *39*, 6403-6409. (Please see pages 204-205.)

A2.3

Adapted with Permission from Elsevier: Phelan, W. A.; Nguyen, G. V.; DiTusa, J. F.; Chan, J. Y., Synthesis, Magnetic, Transport, and Thermodynamic Investigation of $CeCo(Sb, Sn)_3$. *J. Alloys Compd.* **2012**, 523, 171-181. (Please see pages 206-210.)

A2.4

Adapted with permission from: Phelan, W. A.; Kangas, M. J.; Drake, B. L.; Zhao, L. L.; Wang, J. K.; DiTusa, J. F.; Morosan, E.; Chan, J. Y., Crystal Growth, Structure, and Physical Properties of $LnCu_2(Al,Si)_5$ (Ln = La and Ce). *Inorg. Chem.* **2011**, *51*, 920-927. Copyright (2011) American Chemical Society. (Please see page 211.)

William Adam Phelan

From: CONTRACTS-COPYRIGHT (shared) <Contracts-Copyright@rsc.org>
Sent: Tuesday, February 21, 2012 7:04 AM
To: 'wphela1@tigers.lsu.edu'
Subject: RE: Permission Request Form: William Adam Phelan

Dear William

The Royal Society of Chemistry (RSC) hereby grants permission for the use of your paper(s) specified below in the printed and microfilm version of your thesis. You may also make available the PDF version of your paper(s) that the RSC sent to the corresponding author(s) of your paper(s) upon publication of the paper(s) in the following ways: in your thesis via any website that your university may have for the deposition of theses, via your university's Intranet or via your own personal website. We are however unable to grant you permission to include the PDF version of the paper(s) on its own in your institutional repository. The Royal Society of Chemistry is a signatory to the STM Guidelines on Permissions (available on request).

Please note that if the material specified below or any part of it appears with credit or acknowledgement to a third party then you must also secure permission from that third party before reproducing that material.

Please ensure that the thesis states the following:

Reproduced by permission of The Royal Society of Chemistry

and include a link to the paper on the Royal Society of Chemistry's website.

Please ensure that your co-authors are aware that you are including the paper in your thesis.

Regards

Gill Cockhead
Publishing Contracts & Copyright Executive

Gill Cockhead (Mrs), Publishing Contracts & Copyright Executive
Royal Society of Chemistry, Thomas Graham House
Science Park, Milton Road, Cambridge CB4 0WF, UK
Tel +44 (0) 1223 432134, Fax +44 (0) 1223 423623
http://www.rsc.org

-----Original Message-----
From: wphela1@tigers.lsu.edu [mailto:wphela1@tigers.lsu.edu]
Sent: 20 February 2012 22:56
To: CONTRACTS-COPYRIGHT (shared)
Subject: Permission Request Form: William Adam Phelan

Name : William Adam Phelan
Address :

Louisiana State University
Department of Chemistry
232 Choppin Hall
Baton Rouge, LA, 70803

Tel : 2256630920
Fax :
Email : wphela1@tigers.lsu.edu

I am preparing the following work for publication:

Article/Chapter Title : Dissertation Chapter
Journal/Book Title :
Editor/Author(s) : William Adam Phelan
Publisher : Louisiana State University

I would very much appreciate your permission to use the following material:

Journal/Book Title : Synthesis, Structure, Magnetic and Transport Properties of LnFeSb3 (Ln = Pr, Nd, Sm, Gd, and Tb) - Tuning of Anisotropic Long-Range Magnetic Order as a Function of Ln
Editor/Author(s) : Phelan, W. A.; Nguyen, G. V.; Karki, A. B.; Young, D. P.; Chan, J. Y.
Volume Number : 39
Year of Publication : 2010
Description of Material : Dalton Transactions
Page(s) : 6403-6409

Any Additional Comments :

ELSEVIER LICENSE TERMS AND CONDITIONS

Feb 28, 2012

This is a License Agreement between William A Phelan ("You") and Elsevier ("Elsevier") provided by Copyright Clearance Center ("CCC"). The license consists of your order details, the terms and conditions provided by Elsevier, and the payment terms and conditions.

All payments must be made in full to CCC. For payment instructions, please see information listed at the bottom of this form.

Supplier	Elsevier Limited The Boulevard,Langford Lane Kidlington,Oxford,OX5 1GB,UK
Registered Company Number	1982084
Customer name	William A Phelan
Customer address	Louisiana State University Baton Rouge, LA 70803-0001
License number	2857690365929
License date	Feb 28, 2012
Licensed content publisher	Elsevier
Licensed content publication	Journal of Alloys and Compounds
Licensed content title	Synthesis, Magnetic, Transport, and Thermodynamic Investigation of CeCo(Sb,Sn)3
Licensed content author	W. Adam. Phelan,Giang V. Nguyen,J.F. DiTusa,Julia Y. Chan
Licensed content date	9 February 2012
Licensed content volume number	
Licensed content issue number	
Number of pages	1
Start Page	
End Page	
Type of Use	reuse in a thesis/dissertation
Portion	full article
Format	both print and electronic
Are you the author of this Elsevier article?	Yes
Will you be translating?	No
Order reference number	
Title of your	Synthesis and Physical Properties of Ln – M – X Intermetallics (Ln

thesis/dissertation	= Lanthanide; M = Fe, Co, and Cu; and X = Sb, Al, and Ga)
Expected completion date	Mar 2012
Estimated size (number of pages)	200
Elsevier VAT number	GB 494 6272 12
Permissions price	0.00 USD
VAT/Local Sales Tax	0.00 USD / GBP
Total	0.00 USD
Terms and Conditions	

INTRODUCTION

1. The publisher for this copyrighted material is Elsevier. By clicking "accept" in connection with completing this licensing transaction, you agree that the following terms and conditions apply to this transaction (along with the Billing and Payment terms and conditions established by Copyright Clearance Center, Inc. ("CCC"), at the time that you opened your Rightslink account and that are available at any time at http://myaccount.copyright.com).

GENERAL TERMS

2. Elsevier hereby grants you permission to reproduce the aforementioned material subject to the terms and conditions indicated.

3. Acknowledgement: If any part of the material to be used (for example, figures) has appeared in our publication with credit or acknowledgement to another source, permission must also be sought from that source. If such permission is not obtained then that material may not be included in your publication/copies. Suitable acknowledgement to the source must be made, either as a footnote or in a reference list at the end of your publication, as follows:

"Reprinted from Publication title, Vol /edition number, Author(s), Title of article / title of chapter, Pages No., Copyright (Year), with permission from Elsevier [OR APPLICABLE SOCIETY COPYRIGHT OWNER]." Also Lancet special credit - "Reprinted from The Lancet, Vol. number, Author(s), Title of article, Pages No., Copyright (Year), with permission from Elsevier."

4. Reproduction of this material is confined to the purpose and/or media for which permission is hereby given.

5. Altering/Modifying Material: Not Permitted. However figures and illustrations may be altered/adapted minimally to serve your work. Any other abbreviations, additions, deletions and/or any other alterations shall be made only with prior written authorization of Elsevier Ltd. (Please contact Elsevier at permissions@elsevier.com)

6. If the permission fee for the requested use of our material is waived in this instance, please be advised that your future requests for Elsevier materials may attract a fee.

7. Reservation of Rights: Publisher reserves all rights not specifically granted in the combination of (i) the license details provided by you and accepted in the course of this licensing transaction, (ii)

these terms and conditions and (iii) CCC's Billing and Payment terms and conditions.

8. License Contingent Upon Payment: While you may exercise the rights licensed immediately upon issuance of the license at the end of the licensing process for the transaction, provided that you have disclosed complete and accurate details of your proposed use, no license is finally effective unless and until full payment is received from you (either by publisher or by CCC) as provided in CCC's Billing and Payment terms and conditions. If full payment is not received on a timely basis, then any license preliminarily granted shall be deemed automatically revoked and shall be void as if never granted. Further, in the event that you breach any of these terms and conditions or any of CCC's Billing and Payment terms and conditions, the license is automatically revoked and shall be void as if never granted. Use of materials as described in a revoked license, as well as any use of the materials beyond the scope of an unrevoked license, may constitute copyright infringement and publisher reserves the right to take any and all action to protect its copyright in the materials.

9. Warranties: Publisher makes no representations or warranties with respect to the licensed material.

10. Indemnity: You hereby indemnify and agree to hold harmless publisher and CCC, and their respective officers, directors, employees and agents, from and against any and all claims arising out of your use of the licensed material other than as specifically authorized pursuant to this license.

11. No Transfer of License: This license is personal to you and may not be sublicensed, assigned, or transferred by you to any other person without publisher's written permission.

12. No Amendment Except in Writing: This license may not be amended except in a writing signed by both parties (or, in the case of publisher, by CCC on publisher's behalf).

13. Objection to Contrary Terms: Publisher hereby objects to any terms contained in any purchase order, acknowledgment, check endorsement or other writing prepared by you, which terms are inconsistent with these terms and conditions or CCC's Billing and Payment terms and conditions. These terms and conditions, together with CCC's Billing and Payment terms and conditions (which are incorporated herein), comprise the entire agreement between you and publisher (and CCC) concerning this licensing transaction. In the event of any conflict between your obligations established by these terms and conditions and those established by CCC's Billing and Payment terms and conditions, these terms and conditions shall control.

14. Revocation: Elsevier or Copyright Clearance Center may deny the permissions described in this License at their sole discretion, for any reason or no reason, with a full refund payable to you. Notice of such denial will be made using the contact information provided by you. Failure to receive such notice will not alter or invalidate the denial. In no event will Elsevier or Copyright Clearance Center be responsible or liable for any costs, expenses or damage incurred by you as a result of a denial of your permission request, other than a refund of the amount(s) paid by you to Elsevier and/or Copyright Clearance Center for denied permissions.

LIMITED LICENSE

The following terms and conditions apply only to specific license types:

15. **Translation**: This permission is granted for non-exclusive world **English** rights only unless your license was granted for translation rights. If you licensed translation rights you may only translate this content into the languages you requested. A professional translator must perform all translations and reproduce the content word for word preserving the integrity of the article. If this license is to re-use 1 or 2 figures then permission is granted for non-exclusive world rights in all languages.

16. **Website**: The following terms and conditions apply to electronic reserve and author websites:
Electronic reserve: If licensed material is to be posted to website, the web site is to be password-protected and made available only to bona fide students registered on a relevant course if:
This license was made in connection with a course,
This permission is granted for 1 year only. You may obtain a license for future website posting,
All content posted to the web site must maintain the copyright information line on the bottom of each image,
A hyper-text must be included to the Homepage of the journal from which you are licensing at http://www.sciencedirect.com/science/journal/xxxxx or the Elsevier homepage for books at http://www.elsevier.com , and
Central Storage: This license does not include permission for a scanned version of the material to be stored in a central repository such as that provided by Heron/XanEdu.

17. **Author website** for journals with the following additional clauses:

All content posted to the web site must maintain the copyright information line on the bottom of each image, and
he permission granted is limited to the personal version of your paper. You are not allowed to download and post the published electronic version of your article (whether PDF or HTML, proof or final version), nor may you scan the printed edition to create an electronic version,
A hyper-text must be included to the Homepage of the journal from which you are licensing at http://www.sciencedirect.com/science/journal/xxxxx , As part of our normal production process, you will receive an e-mail notice when your article appears on Elsevier's online service ScienceDirect (www.sciencedirect.com). That e-mail will include the article's Digital Object Identifier (DOI). This number provides the electronic link to the published article and should be included in the posting of your personal version. We ask that you wait until you receive this e-mail and have the DOI to do any posting.
Central Storage: This license does not include permission for a scanned version of the material to be stored in a central repository such as that provided by Heron/XanEdu.

18. **Author website** for books with the following additional clauses:
Authors are permitted to place a brief summary of their work online only.
A hyper-text must be included to the Elsevier homepage at http://www.elsevier.com

All content posted to the web site must maintain the copyright information line on the bottom of each image
You are not allowed to download and post the published electronic version of your chapter, nor may you scan the printed edition to create an electronic version.

Central Storage: This license does not include permission for a scanned version of the material to be stored in a central repository such as that provided by Heron/XanEdu.

19. **Website** (regular and for author): A hyper-text must be included to the Homepage of the journal from which you are licensing at http://www.sciencedirect.com/science/journal/xxxxx. or for books to the Elsevier homepage at http://www.elsevier.com

20. **Thesis/Dissertation**: If your license is for use in a thesis/dissertation your thesis may be submitted to your institution in either print or electronic form. Should your thesis be published commercially, please reapply for permission. These requirements include permission for the Library and Archives of Canada to supply single copies, on demand, of the complete thesis and include permission for UMI to supply single copies, on demand, of the complete thesis. Should your thesis be published commercially, please reapply for permission.

21. **Other Conditions**: Please accept this as confirmation that, as part of your author rights, you have the right to include the journal article, in full or in part, in a thesis or dissertation. For more information on the rights you retain as a journal author, please see http://www.elsevier.com/wps/find/authorsview.authors/copyright#whatrights

v1.6

If you would like to pay for this license now, please remit this license along with your payment made payable to "COPYRIGHT CLEARANCE CENTER" otherwise you will be invoiced within 48 hours of the license date. Payment should be in the form of a check or money order referencing your account number and this invoice number RLNK500728789. Once you receive your invoice for this order, you may pay your invoice by credit card. Please follow instructions provided at that time.

Make Payment To:
Copyright Clearance Center
Dept 001
P.O. Box 843006
Boston, MA 02284-3006

For suggestions or comments regarding this order, contact RightsLink Customer Support: customercare@copyright.com or +1-877-622-5543 (toll free in the US) or +1-978-646-2777.

Gratis licenses (referencing $0 in the Total field) are free. Please retain this printable license for your reference. No payment is required.

Appendix 3. Supplemental Information for Chapter 3

Table A3.1 Crystallographic Parameters for $LnCo(Sb, Sn)_3$ (Ln = La, Pr, Nd, and Sm)

Formula	$LaCo(Sb, Sn)_3$	$PrCo(Sb, Sn)_3$	$NdCo(Sb, Sn)_3$	$SmCo(Sb, Sn)_3$
a (Å)	13.019(3)	12.7760(10)	12.71100(10)	12.57500(10)
b (Å)	6.152(5)	6.1220(2)	6.1130(2)	6.0980(3)
c (Å)	12.159(8)	12.0820(3)	12.06030(2)	12.0230(3)
V (Å^3)	975.5	944.99(4)	937.32(4)	
Z	8	8	8	8
Crystal system	Orthorhombic	Orthorhombic	Orthorhombic	Orthorhombic
Space group	*Pbcm*	*Pbcm*	*Pbcm*	*Pbcm*
θ range (°)	26-30	2.6-30.5	2.6-33.1	2.6-33.1
μ (mm^{-1})	28.10	30.28	31.21	33.21
Data collection				
Measured reflections	60223	19199	20926	19995
Independent reflections	1487	1506	1708	1671
Reflections with $I>2\sigma(I)$	1242	1464	1590	1514
R_{int}	0.0000	0.029	0.020	0.21
h	0-18	-18-18	-19-19	-18-18
k	0-8	-8-8	-9-9	-8-8
l	0-16	-17-17	-17-17	-17-17
Refinement				
[a]$R_1[F^2>2\sigma(F^2)]$	0.030	0.039	0.33	0.028
[b]$wR_2(F^2)$	0.070	0.114	0.091	0.062
Parameters	53	53	53	53
GOOF	1.16	1.22	1.16	1.24
$\Delta\rho_{max}$ (e Å^{-3})	4.83	4.08	2.09	2.06
$\Delta\rho_{min}$ (e Å^{-3})	-1.30	-4.15	-2.97	-1.57

[a]$R_1=\sum \| F_o | - | F_c \| / \sum | F_o |$, [b]$wR_2 = [\sum[w(F_o^2 - F_c^2)]/\sum[w(F_o^2)^2]]^{1/2}$

Table A3.2 Atomic Positions and Anisotropic Displacement Parameters for $LnCo(Sb, Sn)_3$ (Ln = La, Pr, Nd, and Sm) where X = Sb and Sn

Atom	x	y	z	$U_{eq}(Å^2)^a$
La1	0.70111(4)	¼	0	0.00771(13)
La2	0.30464(4)	0.26555(10)	¾	0.00745(13)
Co1	0.10072(7)	0.3353(16)	0.86197(8)	0.0086(2)
X1	0.97354(5)	¼	0	0.00978(16)
X2	0.79094(5)	0.25641(11)	¾	0.00844(15)
X3	0.50162(4)	0.50873(8)	0.87693(3)	0.00936(12)
X4	0.21320(5)	¼	0	0.00852(15)
X5	0.94507(5)	0.88377(11)	¾	0.00938(16)
Pr1	0.70033(5)	¼	0	0.00779(18)
Pr2	0.30534(4)	0.26643(8)	¾	0.00747(17)
Co1	0.10358(7)	0.03298(15)	0.86208(7)	0.0084(2)
X1	0.97320(5)	¼	0	0.00948(19)
X2	0.78572(5)	0.25502(9)	¾	0.00813(19)
X3	0.50186(3)	0.50868(7)	0.87665(3)	0.00894(18)
X4	0.21827(6)	¼	0	0.00816(19)
X5	0.94433(5)	0.88443(10)	¾	0.00938(19)
Nd1	0.70008(4)	¼	0	0.01129(13)
Nd2	0.30569(3)	0.26711(7)	¾	0.01091(12)
Co1	0.10440(6)	0.03254(13)	0.86209(6)	0.01177(17)
X1	0.97328(4)	¼	0	0.01271(14)
X2	0.78416(4)	0.25471(8)	¾	0.01160(14)
X3	0.50197(3)	0.50881(6)	0.87654(3)	0.01216(13)
X4	0.21983(4)	¼	0	0.01156(14)
X5	0.94410(4)	0.88448(9)	¾	0.01263(14)
Sm1	0.69969(3)	¼	0	0.00784(10)
Sm2	0.30611(3)	0.26858(7)	¾	0.00750(10)
Co1	0.10566(6)	0.03281(13)	0.86214(7)	0.00809(16)
X1	0.97314(4)	¼	0	0.00887(12)
X2	0.78140(4)	0.25460(8)	¾	0.00814(12)
X3	0.50227(3)	0.50899(6)	0.87630(3)	0.00861(10)
X4	0.22290(4)	¼	0	0.00806(12)
X5	0.94353(4)	0.88538(9)	¾	0.00899(12)

[a] U_{eq} is defined as 1/3 of the trace of the orthogonalized U_{ij} tensor.

Table A3.3 Selected Interatomic Distances and Angles for $LnCo(Sb, Sn)_3$ (Ln = La, Pr, Nd, and Sm) where X = Sb and Sn

	$LaCo(Sb, Sn)_3$	$PrCo(Sb, Sn)_3$	$NdCo(Sb, Sn)_3$	$SmCo(Sb, Sn)_3$
Distances (Å)				
Ln1 – X1	3.5468(11)	3.4862(9)	3.4727(7)	3.4387(6)
Ln1 – X2 (x 2)	3.2572(12)	3.2116(3)	3.1997(2)	3.1767(2)
Ln1 – X3 (x 2)	3.3789(9)	3.3281(6)	3.3147(5)	3.2896(5)
Ln1 – X3 (x 2)	3.3789(9)	3.3404(6)	3.3260(5)	3.2968(5)
Ln1 – X4 (x 2)	3.277(2)	3.2329(3)	3.2216(2)	3.2006(2)
Ln2 – X2	3.271(2)	3.2094(8)	3.1920(6)	3.1615(7)
Ln2 – X2	3.375(2)	3.3400(8)	3.3340(6)	3.3218(7)
Ln2 – X3 (x 2)	3.3473(10)	3.2931(6)	3.2768(5)	3.2465(5)
Ln2 – X3 (x 2)	3.3539(10)	3.3013(6)	3.2865(5)	3.2585(5)
Ln2 – X4 (x 2)	3.2660(12)	3.2204(3)	3.2088(2)	3.1847(2)
Ln2 – X5	3.3318(10)	3.2707(8)	3.2551(6)	3.2190(6)
X3 – X3	2.9950(15)	2.9829(8)	2.9810(7)	2.9771(7)
X3 – X3	3.081(2)	3.0604(8)	3.0529(7)	3.0369(7)
X3 – X3	3.0868(15)	3.06137(10)	3.0569	3.04953(15)
Co – X1	2.6085(14)	2.5962(10)	2.5934(8)	2.5891(8)
Co – X1	2.7089(12)	2.7049(10)	2.7041(8)	2.6979(8)
Co – X2	2.5999(14)	2.5942(10)	2.5921(9)	2.5909(9)
Co – X4	2.5963(12)	2.5863(10)	2.5861(8)	2.5836(8)
Co – X5	2.6100(12)	2.6077(10)	2.6075(9)	2.6044(9)
Co – X5	2.6205(18)	2.6149(11)	2.6147(9)	2.6121(9)
Co – Co	2.723(2)	2.7049(10)	2.7043(15)	2.6964(16)
Angles (º)				
X3 – X3 – X3	87.931(19)	87.943(17)	87.913(14)	87.869(14)
X3 – X3 – X3	90.0	90.0	90.0	90.0
X3 – X3 – X3	90.0	90.0	90.0	90.0
X3 – X3 – X3	92.047(19)	92.029(17)	92.056(14)	92.090(14)
X5 – Co – X1	79.11(4)	78.80(3)	78.69(2)	78.57(2)
X5 – Co – X5	81.00(4)	80.53(3)	80.40(2)	80.30(2)
X5 – Co – X2	85.17(4)	85.73(3)	85.93(3)	86.20(3)
X5 – Co – X4	92.35(5)	92.50(3)	92.49(3)	92.54(3)
X1 – Co – X2	95.62(6)	95.93(3)	96.10(3)	96.13(3)
X1 – Co – X4	97.89(5)	98.24(3)	98.38(3)	98.58(3)
X2 – Co – X4	111.72(5)	111.37(4)	111.24(3)	110.90(3)
X2 – Co – X5	113.10(5)	113.39(4)	113.47(3)	113.59(3)
X1 – Co – X5	143.29(5)	142.47(4)	142.18(4)	142.00(4)
X5 – Co – X4	163.10(5)	162.90(4)	162.82(4)	162.90(4)

Vita

William Adam Phelan was born in June of 1984, at what is now St. Edward Mercy Medical Center in Fort Smith, Arkansas, to his parents Jim Patrick Phelan and Cynthia Anne Phelan (Page). He is the older brother by four years to James Hunter Phelan. He and his best friend and high school sweetheart Sarah Caitlin Phelan (Schirmer), daughter to Roy Edmond Schirmer and Cheryl Ann Schirmer (Gregg) and sister to Richard Edmond Schirmer, were married in May of 2008.

Adam graduated with honors in the spring of 2003 from Southside High School in Fort Smith. Upon graduation, he attended the University of Arkansas-Fort Smith from 2003 through 2005 with the support of a University Scholarship. While at the University of Arkansas-Fort Smith, Adam concentrated his studies on chemistry under the mentorship of Charles Todd Watson, who opened his eyes to the field of graduate studies and was the model teacher Adam one day hopes to become.

Seeking a more challenging college atmosphere and with a desire to conduct research Adam transferred to the University of Central Arkansas in Conway, Arkansas, in the fall of 2005 with the support of a University Transfer Scholarship. There he conducted research in Richard Tarkka's laboratory. In the spring of 2007 Adam graduated with his Bachelors of Science degree in Chemistry.

Adam then began his graduate studies in the fall of 2007 at Louisiana State University where he was awarded a Board of Regents fellowship. He joined Julia Y. Chan's research group in the spring of 2008, and since has devoted his time to discovering and characterizing new intermetallic compounds. Under Julia Y Chan, Adam has exceeded the expectations set forward by himself. If successful, he will be the first member of his family to graduate with a Doctor of Philosophy degree.